On the Origins of the Karnali Channel Shift

Assessment of 2D hydro-morphological processes at the Karnali river bifurcation, Nepal

Marijn Wolf

Technische Universiteit Delft

TU Delft

On the Origins of the Karnali Channel Shift

Assessment of 2D hydro-morphological processes at the Karnali river bifurcation, Nepal

by

Marijn Wolf

to obtain the degree of Master of Science
at the Delft University of Technology,
to be defended publicly on Friday June 28, 2024 at 13:00 PM.

Student number:	4680197	
Project duration:	September 1, 2023 – May 29, 2024	
Thesis committee:	Prof. Dr. T. A. Bogaard,	TU Delft, main supervisor
	Dr. ir. A. Blom,	TU Delft, supervisor
	Dr. ir. C. J. Sloff,	TU Delft, supervisor
	K. Gautam,	TU Delft, supervisor

TU Delft Delft University of Technology

SAVE THE TIGER THE GRASSLANDS THE WATER

Preface

> *"No man ever steps in the same river twice, for it's not the same river and he's not the same man."*
> **— Heraclitus, 5th century BCE**

This document is the final product of the Master Water Management at TU Delft. It marks the end of three wonderful years. Water management and, in particular, river engineering combine all my interests: Nature, fieldwork, societal impact, and what I love the most is its universal character. With a few exceptions, each country has its rivers and associated problems, likely increasing since climate extremes are becoming more extreme. Having the chance to solve river and flood-related issues makes me very enthusiastic; this study has given me the capability to work on relevant issues.

This thesis subject was a genuinely fantastic opportunity, and I have enjoyed most aspects of it. I have had the chance to visit the study area in Nepal and get to know the country and its people well. I want to thank Kshitiz Gautam for giving me such a lovely time in his home country. It was a pleasure working together on this project. Our trip to the EGU conference in Vienna was another highlight. I am very grateful to have had the supervision of Thom, Astrid and Kees, all exceptional people with great knowledge. Their insights and guidance made my understanding of bifurcating rivers and research in general a whole lot greater. Furthermore, this study and their guidance make me more passionate about research, and I would love to continue doing such projects in the future.

Patience is not my strongest character trait, and this thesis tested it. Staying focused on one subject for over 10 months was not always easy. I want to deeply thank Svenja and my family for tolerating and encouraging me during this period. I would also like to thank Diana, Bart, Ole Sergio, Job, Max, Ezekiel, and Bruno for all the wonderful study and coffee sessions. Without their support and shared struggles, this process would have been a whole lot harder.

All that is left to say is that I am really excited about the future. The world will always face (water-related) challenges, and I am eager to contribute to finding their solutions. I reflect on the quote by Heraclitus as I and the Karnali river are in constant development, for the better and the worse, everything will find its way.

Marijn Wolf
Delft, June 2024

Cover Image: *A lone fisherman stands in the calm Geruwa branch of the Karnali River. Circular ripples around him disrupt the still water, hinting at the channel's nearly imperceptible flow. (taken in October 2023)*

Abstract

This study investigates the hydro-morphological processes driving the channel shift of the Karnali River in Western Nepal after the 2009 monsoon season. Exceptionally high discharge during this year caused significant morphological changes to the bifurcation system, leading to a drastic discharge reduction in the branch that flows into and provides habitat for the Bardiya National Park. The park is home to various endangered species, such as the Royal Bengal Tiger, and the change in flow distribution is impacting ecosystem dynamics and increasing human-wildlife conflict. An extensive field campaign, combined with satellite imagery analysis of planform evolution, provided the foundation for a conceptual model. Two hypotheses are tested: (1) bend sorting and flood-induced aggradation in the Geruwa branch, and (2) erosion-driven opening of the Kauriala branch. These hypotheses are tested using a schematized version of the bifurcation system in a depth-averaged 2D hydro-morphological numerical model (Delft3D).

Model results suggest a self-reinforcing feedback loop initiated by increased sediment load during peak flows in the Geruwa branch, leading to aggradation and reduced flow capacity. This process promoted further sedimentation and the eventual partial closure of the branch. The model highlights the critical role of mixed-sized sediment interactions, particularly the processes that influence the local sediment supply of finer grain sizes, such as hiding and exposure. Additionally, the processes that influence the direction of sediment particles, namely secondary flow and transverse bed slope gravity pull, significantly impact the discharge distribution. The size, magnitude, and direction of particles towards a particular branch can lead to exceeding its transport capacity and subsequent aggradation, resulting in the dominance of the other branch. Furthermore, the model reveals limited sensitivity to slope changes in the Kauriala branch. Although limited by the lack of calibration and validation data, the results from this schematized model offer valuable insights into the drivers behind the real-world system and may inform future studies and potential interventions.

Contents

1

Introduction

The Karnali River, the longest in Nepal, is an important tributary to the Ganges system. It originates on the Tibetan Plateau, flows through mountainous Nepali terrain, and reaches the town of Chisapani, where it has formed a fluvial (mega) fan and is an important lifeline for communities, agriculture, and protected areas, notably Bardiya National Park. The map in Fig. 1.1 shows the location of the Karnali basin and fluvial fan in its broader context in which the relevant places are indicated.

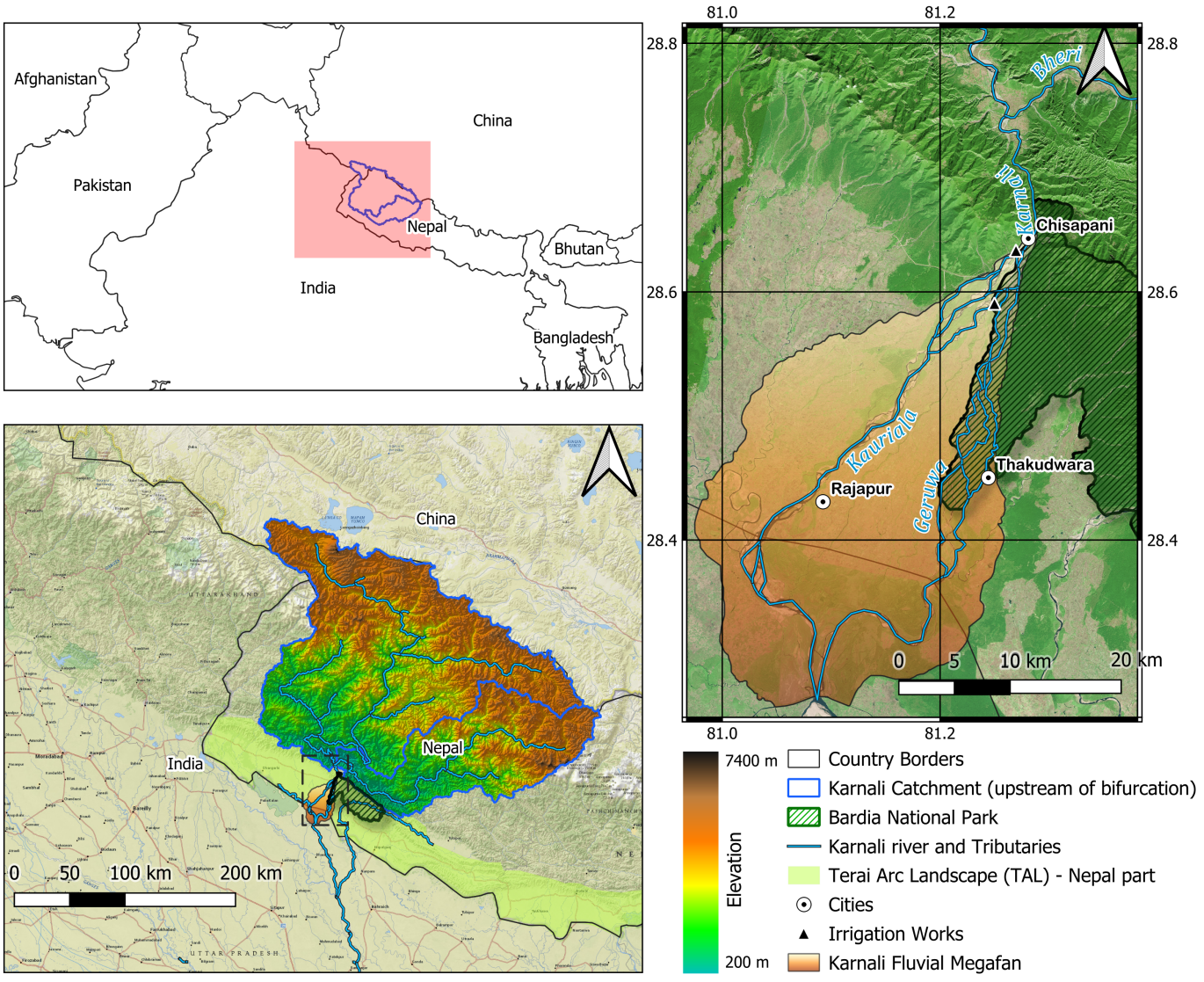

Figure 1.1: Map of Karnali river basin, fan area and relevant places.

The ecosystem of the Bardiya National Park, home to a growing population of endangered Royal Bengal Tigers, their prey and many other protected species, is critically dependent on the flow regime of the Geruwa branch of the Karnali. To the northwest of the park, the Karnali bifurcates into two branches, namely the Kauriala and the Geruwa. The Kauriala branch diverges from the Bardiya National Park, while the Geruwa branch follows along its border. Since 2009, the flow distribution at the bifurcation has strongly shifted towards the Kauriala branch. The drivers behind this phenomenon, known as channel-shifting, are the main focus of this study.

The Geruwa branch plays a crucial role in the renewal of tall alluvial grasslands that introduce heterogeneity in the habitat of the otherwise mixed forest of the Bardiya National Park. This heterogeneity is a key determinant of the abundance of tigers and prey (Bhattarai & Kindlmann, 2012; Moe & Wegge, 1994). Yearly overbank flows during monsoon seasons renew the grasslands and prevent forest encroachment. The image taken during the field campaign of this study in October 2023 shows the grasslands surrounding a Geruwa branch, see Fig. 1.2. Disruptions in the flow pattern, potentially caused by changes in Karnali bifurcation behaviour, could have cascading consequences for the grassland-dependent megafauna (Bijlmakers et al., 2022). Given the ecological significance of this system, it is critical to understand the mechanics of the Karnali River, particularly the bifurcation dynamics that directly influence the flow distribution over the two bifurcates. An altered flow distribution directly influences the water availability and habitat composition along the Western side of the Bardiya National Park. This study aims to investigate the Karnali River, focusing on the bifurcation dynamics and what drives channel-shifting behaviour.

Figure 1.2: Example of grassland around a Geruwa branch in Bardiya National Park, photo taken in October 2023.

Studies and History of Karnali's Channel shifting

Previous studies on the channel shifting of the Karnali River have been done using remote sensing techniques. Rakhal et al. (2021) used remote sensing data (1977-2013) and found a generally increasing trend in discharge distribution towards the Kauriala branch, showing that extreme rainfall and flooding are contributing factors to channel shifting in the Karnali Megafan. However, no decisive reason was given for the mechanisms of the shift. Roebroeck (2022) attempted to quantify the change in flow distribution based on a wet pixel area count of sections of the channels in both bifurcates. It is assumed that a relation exists between the discharge and the wet pixel area and that this is a proxy of the water discharge in both branches. Roebroeck's analysis showed an apparent change in wet pixel distribution and, thus, discharge after a heavy monsoon season (2009). The results of this study are shown in Fig. 1.3. Please refer to Section 2.2 to see how heavy the 2009 monsoon season was relative to other years.

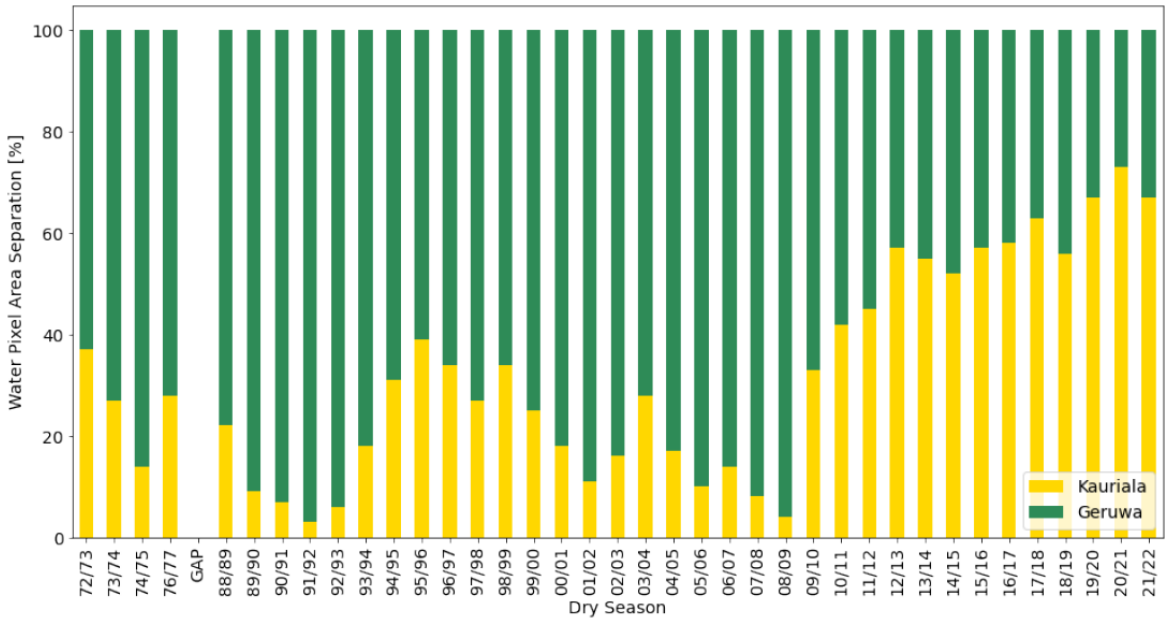

Figure 1.3: Wet area pixel distribution of a selected area in both bifurcates showing a shift after 2009, figure adopted from Roebroeck (2022).

Roebroeck (2022) also analyzed historical maps dating back to 1861, suggesting an avulsion frequency in the order of 100 years. These maps indicate Kauriala's dominance between 1861 and 1932, with the Geruwa becoming the primary channel from 1933 to 2009. Channel-shifting events are, therefore, not very common and the driving factor behind the changes in the Karnali rivers is poorly understood.

Dynamics of River Bifurcations and Time Development

Bifurcations are dynamic river features in which the distribution of water and sediment depends on morphology, upstream discharge, and backwater effects. The complex interplay of processes driving bifurcation evolution can lead to significant changes in flow and sediment distribution, sometimes resulting in full avulsions. These systems are often asymmetric and inherently unstable (Bertoldi, 2012; Kleinhans et al., 2013). This leads the system to form an avulsion, in which one channel gets abandoned. Bifurcations exhibit a wide variation in channel switching frequency (Kleinhans et al., 2013; Redolfi et al., 2016).

Bifurcations have been studied and successfully modelled in various ways, such as 1D, 2D and 3D models (Kleinhans et al., 2008; Redolfi et al., 2016; Schuurman et al., 2013; Sloff & Mosselman, 2012), these studies all use highly schematized models. One-dimensional models contain a node at the point where three branches join. Discharge distribution is determined by mass conservation. However, sediment division is a challenge in 1D models; therefore, these models are characterized by the nodal point relation. Various relations have been suggested, such as (Bolla Pittaluga et al., 2003; Wang et al., 1995); these relations do not take upstream morphology, such as bars and bends, into account, which is a considerable downside relative to the 2D and 3D models, especially for wider rivers (Kleinhans et al., 2008). This study concerns a bifurcation located within a river bend, therefore a model with more dimensions is preferred. A common approach is simplifying three-dimensional flow to two dimensions and adding parameterized secondary flow processes, resulting in a two-dimensional, depth-averaged (2DH) model. These models are significantly less computationally expensive and give results in good agreement with full 3D models (Kleinhans et al., 2008; Sloff & Mosselman, 2012). However, these models are limited by the large amount of calibration parameters, leading to equifinality. Additionally, until now, these models often still lack comprehensive mechanisms to account for bank erosion and use strongly simplified methods which do not reproduce bank erosion well (Parsapour-Moghaddam et al., 2023; Stecca et al., 2017).

Although highly schematized 1D and 2DH model studies have greatly improved the understanding of bifurcation developments, the closing mechanisms of a bifurcation branch are not well understood (Barile et al., 2024). Kleinhans et al. (2013) identifies several critical unanswered questions about river bifurcations despite advancements in the field. Research indicates that bifurcations tend to be unstable with highly variable avulsion durations, influenced by factors such as energy gradients, bends, and bars. This complexity results in low predictability of avulsion evolution. The reasons behind these uncertainties, including conceptual model limitations and empirical constants, are not fully understood. Additionally, local flow structures and turbulence significantly impact flow resistance and sediment transport at bifurcations, especially in rivers with cohesive banks and sharp bends. Factors influencing sediment sorting processes, such as hiding/exposure and gravity pull alongside transverse slope, play a crucial role in sediment transport. Still, their interactions and effects need more investigation (Baar et al., 2019). Furthermore, the dynamics of bed load material transport, influenced by spiral flow, and its spatial adaptation are poorly understood. Lastly, the interactions within river networks, affecting upstream and downstream dynamics, represent a complex area that requires further study. Processes of channel shifting in a bifurcation due to channel closure or avulsion occur with a timescale of 10^2-10^3 years (Kleinhans et al., 2013). Factors influencing the bifurcation morphology include approach conditions, secondary flow, transverse bed slope gravity pull, bar migration, sediment interaction and more. Chapter 3 outlines the various processes in more detail.

1.1. Problem Statement

The flow distribution of the Karnali River at the Chisapani bifurcation point has undergone a significant shift. Historically, the Geruwa branch received the majority of the discharge, but since the flood event during the 2009 monsoon season, the Kauriala branch has become dominant. The monsoon season was characterized by two intense flood peaks of short duration. The shift is clearly shown in Fig. 1.4, where the blue colour indicates new surface water and green represents a change from water to land between 2000 and 2023. This shift has paradoxically resulted in both challenges and benefits within Bardiya National Park. Although grasslands have historically experienced a decline, the flow change has allowed grasslands to expand in areas of bare substrates (Bijlmakers et al., 2022). This expansion, coupled with strong conservation efforts, may have contributed to a drastic increase in the tiger population.

While the discharge distribution change of the Karnali has initially benefited the tiger population by facilitating grassland expansion, this trend likely will not last (Bijlmakers et al., 2022). The WWF estimated a population of 18-27 individuals in 2009 (Karki et al., 2009). A 2013 estimate gave a number between 46 and 54 Bengal tigers in Bardiya National Park (Dhakal et al., 2014). The latest official estimate (2022) from the Nepalese Ministry of Forests and Environment records a population of 125 tigers in the park (Acharya et al., 2022).

Since the discharge distribution has changed after the 2009 monsoon season and the yearly overbank floods in the Geruwa branch decrease, these grasslands will likely transform into forests and reduce habitat heterogeneity (Bijlmakers et al., 2022). This is problematic for several reasons: first, tigers thrive in grasslands, and as their natural habitat shrinks, they may seek alternative living and hunting grounds. The buffer zone around the park is home to numerous communities, and lively farming villages exist outside its borders. Consequently, the potential for human-wildlife conflict, already a serious issue, is likely to escalate further. News reports highlight 38 human casualties from tiger and elephant encounters in 2023 alone (Ghimere, 2024).

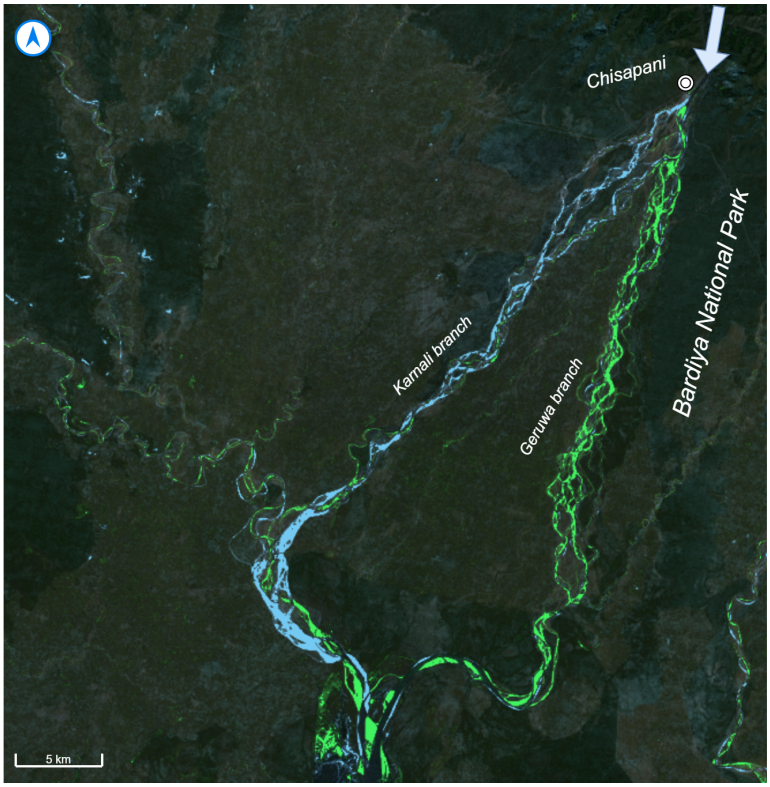

Figure 1.4: Map of the Karnali river changes downstream of Chisapani between 2000 and 2023. Green pixels show where surface water has been turned into land (accretion, land reclamation, droughts). Blue pixels show where land has been changed into surface water (erosion, reservoir construction). Picture created with the Aquamonitor tool (Donchyts et al., 2016).

1.2. Research Objective

To understand the drivers behind past and potential future shifts in the Karnali bifurcation, this study analyses the processes influencing its morphological development and their consequences on discharge distribution. Ultimately, the study intends to isolate the various processes and mechanisms that could explain why the Geruwa branch experiences strong sedimentation after the 2009 monsoon and how the Kauriala could have become the dominant channel after many decades of being less significant. The research questions to be answered are as follows:

1) How did the 2009 monsoon flood alter the morphology of the Karnali bifurcation and flow distribution between the Geruwa and Kauriala branches?

2) How can we model the impact of bend sorting and bifurcate steepening on the closure of the other bifurcate?

Climate change-induced shifts in precipitation and temperature patterns are expected to increase the frequency and magnitude of high-energy flood events in river systems globally (Trenberth, 2005). Such events have the potential to significantly alter channel morphology, particularly in dynamic settings like river bifurcations. More extreme extremes will lead to more peak sediment load in future monsoon seasons. The larger magnitude and coarser nature of future events will impact rivers and their bifurcations. This study aims to unravel the processes driving channel shifting in the Karnali River, offering insights into how bifurcations in gravel-bed rivers might respond to climate-driven hydrological changes.

1.3. Approach

This research employs an approach integrating field data collection, remote sensing analyses, and numerical modelling to investigate the dynamics and controlling factors of the river bifurcation. Firstly, initial theories are established using remote sensing data and previous studies. Combined with field data and observations, these form the basis for the conceptual model and will lead to hypotheses.

A 2D-hydro morphological model is then used, including parameterized 3D flow processes using DELFT3D-4 software (referred to as D3D). A reference model will be constructed using data collected during the field campaign and from satellite imagery, such as slope, bank full width, and sediment size classes. A parameter sensitivity analysis around the reference case will be performed using the processes involved in morphological development. Scenarios regarding slope advantages and forced initial sedimentation in the branches and different peak flow scenarios will give further insights into how the discharge and sediment are distributed in the branches.

Beyond local significance in understanding the Karnali bifurcation, this research aims to advance the general understanding of gravel-bed river bifurcation dynamics. Knowledge gained from modelling the Karnali system can potentially inform future studies and management strategies in similar river systems worldwide, where channel shifting significantly impacts water availability, flood risk, and communities.

1.4. Thesis Outline

This document will firstly present information about the Karnali river basin in Chapter 2. Afterwards, the physics of mixed-sized sediment river bifurcation systems are presented in Chapter 3 to serve as a theoretical background for the later model and parameter study. Field observations will be presented in Chapter 4. This chapter also includes results from the satellite imagery analysis. The thesis then presents a conceptual model, Chapter 5, and proposes hypotheses to explain the observed channel-shifting behaviour. These hypotheses serve as a framework for subsequent investigations. The next Chapter 6 details the setup of the numerical model. Relevant model results are then presented in Chapter 7, offering quantitative evidence to assess the validity of the proposed hypotheses.

The thesis concludes with a comprehensive discussion in Chapter 8, interpreting the results and connecting them to the conceptual model and hypotheses. Key findings are summarized, and their implications for river management and hazard mitigation are explored. Potential avenues for future research are also identified.

2

The Karnali Basin

2.1. Extent of Basin

The Karnali River stands as Nepal's longest, flowing through the western part of the country. The Karnali is a major transboundary tributary of the Ganges river system. Its source emerges from the Tibetan Plateau, nourished by numerous snow-fed tributaries (Khatiwada et al., 2016). The Karnali Basin is predominantly mountainous, spanning a large area of 45,269 square kilometres. As it flows through the mountain valleys, a significant transformation occurs at the city of Chisapani. Here, after leaving the mountainous terrain, the Karnali shifts from a confined, single-channel river to a braiding, anabranching waterway on the large alluvial fan in the Terai Arc Landscape (TAL), the lowlands of southern Nepal renowned for its fertile land and spectacular ecosystems. This transition initiates immediately after leaving the mountainous region, triggered by a change in slope that leads the Karnali to polyfurcate into braided channels just downstream of Chisapani, bifurcating into the Geruwa branch to the East and the Kauriala branch to the West (Dingle et al., 2020a; Rakhal et al., 2021). This alteration in terrain and gradient also induces a gravel-sand transition (GST) around 50 kilometres downstream of the bifurcation. The Geruwa and Kauriala branches join again upstream of the Kailashpuri Dam just over the border into India.

2.2. Climate and Hydrology

The basin experiences a monsoon-dominated climate, with the majority of its 1479mm average annual precipitation occurring between June and October (Dahal et al., 2020; Dingle et al., 2020b; Khatiwada et al., 2016). This seasonality results in a highly variable flow regime, as illustrated in Fig. 2.1.

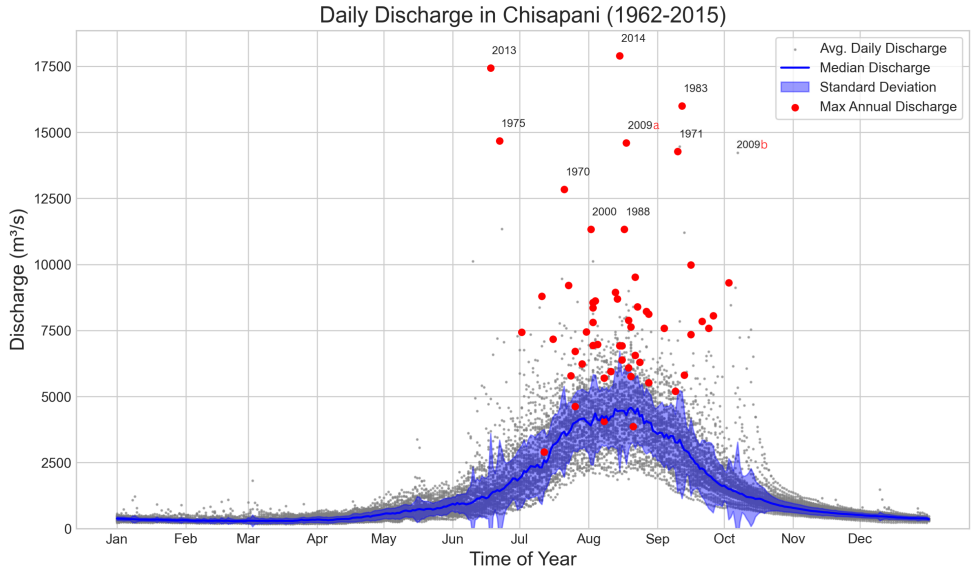

Figure 2.1: Hydrograph from the Chisapani gauging station

The figure highlights the extreme range of discharges recorded at the Chisapani gauging station. During the monsoon season, peak flows can exceed 10,000 m^3/s, marking the immense energy capable of reshaping the river channels. These events are annotated in the figure, see also the annotation of the year 2009, both flood peaks are indicated with 2009a and 2009b. This combination of high seasonal discharge variability and overall basin hydrology is crucial in driving morphological changes at the downstream bifurcation.

2.3. Geology

The Karnali River undergoes a geological transition at Chisapani, leaving behind its bedrock-confined channel as it enters the Terai Arc Landscape (TAL). As the river carves through the Himalayas upstream of Chisapani, it interacts with diverse rock types of varying erodibility (Dingle et al., 2017; Quick et al., 2019). This, coupled with the steep upstream terrain, results in a high sediment flux with the capacity to transport large boulders. Quick et al. (2019) estimate an average gravel flux of the Karnali basin of 0.7 Mt per year. While comprehensive bedload transport data is lacking, it is understood that peak flows during the monsoon season drive the majority of morphological change (Sah et al., 2022). The flow provides large quantities of nutrient-rich sediment, which has formed the large, fertile alluvial fan that supports the rich biodiversity and productive agriculture of the region.

2.4. Antropogenic Interventions

The Karnali river basin is the region in Nepal with the least amount of hydropower projects (Dahal et al., 2020). While the Karnali River currently maintains a largely natural flow and sediment regime, various human interventions, both existing and planned, have the potential to alter the bifurcation dynamics. Plans for the Karnali Chisapani Multipurpose Project (KCMP) envision a large hydropower dam that would disrupt the natural discharge and sediment transport regimes (Regmi, 2021). However, the timeline for this project remains uncertain.

Presently, human interventions along the Karnali include:

- Embankments & Groynes: The Kauriala branch, in particular, has seen significant embankment and groyne construction following a flood in 2014 (see Fig. 2.1). These structures constrict the channel, reducing sinuosity and increasing slope, potentially contributing to channel shifting. Fig. 2.2 shows part of the embankment and (failing) groynes.
- Irrigation: Water is diverted from the Karnali for irrigation projects, such as the Rajapur Irrigation Project (RIP) at the western bank at Chisapani and the Jamura Kulariya Irrigation Project (RJKIP) between the Kauriala and Geruwa branches. Locations are indicated in Fig. 1.1.
- Gravel Mining: Commercial gravel extraction likely influences river dynamics. USAID (2019) mention a permitted extraction of over 220 000 m^3 of gravel at the lower reaches of the bifurcates.

Figure 2.2: Embankment along the Kauriala branch, with failing groynes (Oct 2023).

3

Physics of Mixed-Sized Sediment River Bifurcation Systems

Bifurcations occur in a variety of riverine and deltaic environments, including alluvial fans, braided river systems, meandering lowland rivers, and anastomosing river networks (Kleinhans et al., 2013). The morphology or shape of the bifurcation area ultimately depicts the division of discharge and water. As outlined by Redolfi et al. (2019), bifurcation mechanisms can be classified into 'free' and 'forced'. Here free mechanisms lead to unbalanced configurations in geometrically symmetric bifurcations with a large width-to-depth ratio, while forced mechanisms result from factors like channel curvature and slope advantage. Both types of mechanisms usually coexist. When the main channel is relatively wide and shallow, the bifurcation consistently evolves towards unbalanced configurations, regardless of the combination of curvature and slope advantage values.

In alluvial fans, as is the case for the Karnali bifurcation, the river enters an unconfined area with a small gradient after it leaves its confined state from the mountain valley. Upstream of the fan, the river carries large quantities of erosional products and debris, this is then deposited in the fan area (Bull, 1977). The bulk of the coarse sediment is trapped in the fan as the lower gradient does not offer the capacity to transport that downstream (Harvey et al., 2005). A characteristic of alluvial fans is the highly variable sediment supply, and they experience pulse-like arrival of sediment during peak flow events (Kleinhans et al., 2013). Experiments from Bryant et al. (1995) have shown increasing avulsion or channel-shifting frequency with increasing sedimentation rates.

This chapter explains the generic processes that affect the development of channel and bifurcation geometry and links this to the Karnali river bifurcation. Therefore, we start with the theory of sediment mobility, as moving particles are the foundation for morphological development and determine the grain size distribution of the bed surface sediment.

3.1. Sediment Mobility

The mobility of a sediment particle is determined by the friction force or shear stress (τ) applied to the bed by the flowing water. In case this shear stress exceeds the critical threshold, referred to as critical bed shear stress (τ_{cr}) or critical shields parameter (θ_{cr}) in its dimensionless form, the particle will start moving. Bed shear stress under normal flow conditions, that is where the flow is steady, uniform, and fully developed, is given by:

$$\text{Bed shear stress (normal flow conditions):} \quad \tau_b = \rho_w g h I_w \qquad [\text{N/m}^2] \qquad (3.1)$$

$$\text{Dimensionless form (Shields, 1936 parameter):} \quad \tau^* = \theta = \frac{\tau_b}{(\rho_s - \rho_w) g D} \qquad [-] \qquad (3.2)$$

$$\text{Initiation of motion when:} \quad \theta > \theta_{cr} \qquad (3.3)$$

in which ρ_w is the density of water, g the gravitational constant, h the mean water depth, and I_w the slope of the water surface. The Shield parameter θ is related to the density of the sediment, ρ_s, and the grain diameter, D. The critical Shields parameter and with it its initiation of motion has first been determined by Shields (1936) as a function of the Reynolds number, Later on, with the development of new transport formulations, other relations have been determined. Buffington and Montgomery (1997) have shown that especially gravel bed rivers lack a universal critical shear stress value and that the value should be chosen carefully for each different application. Rather than seeking a universal critical shear stress value, emphasis should be placed on selecting methodologically defensible values customized to specific applications, while acknowledging the inherent uncertainties involved.

Regardless of how the critical shields parameter value is defined, either by a function or a constant, it is evident by Eq. (3.3) that smaller and/or lighter particles require less force exerted by the water to get in motion. Once this threshold is exceeded, particles slide, roll, or saltate over the bed. The earliest reliable formulation of bed load transport was developed by Meyer-Peter and Müller (1948). Their empirical formula is based on flume experiments with uniform particles and particle mixtures. The formula is still widely used due to its simplicity and, therefore, is also applied in the constructed numerical model, Meyer-Peter and Müller (1948) used a constant critical Shields parameter of 0.047. which was determined experimentally.

3.2. Sediment Sorting

Sorting of Bedload Sediment

River and floodplain surface bed grain size distributions are often not homogeneous. This is also the case for the bed composition of the Karnali bifurcation, see Section 4.3. Differences in grain size distribution are shaped by several sorting processes:

- **Transverse Sorting in River Bends**

  River bends exhibit intricate flow dynamics due to the influence of centrifugal forces, which generate asymmetric velocity profiles and induce secondary flow patterns, referred to as helical or spiral flow. These forces cause a lateral variation in shear stress across the river channel, which, in turn, affects sediment transport and deposition processes. The transverse bed slopes experience gravitational forces (Section 3.4) that contribute to the downslope movement of sediments, further enhancing the sorting patterns (Parker & Andrews, 1985).

  The interaction between these forces leads to differential sorting of sediments, with coarser particles typically being deposited on the outer banks of bends where shear stress applied by the faster-flowing water is higher and finer sediments accumulating on the inner banks where shear stress is reduced. This sorting mechanism is critical in shaping the morphological and grain size distribution characteristics of river beds and bifurcations.

  Upcoming cross-sectional profiles (Section 3.3) will provide detailed insights into the sediment transport direction deflection associated with river bends. This bend sorting effect is especially relevant for studying the Karnali bifurcation since it is located within a bend.

- **Streamwise sorting**

  Gravel rivers exhibit a characteristic downstream fining trend, culminating in a sometimes abrupt transition to a sand-dominated bed, known as the Gravel-Sand Transition (GST). This is attributed to the difference in entrainment (mobility) threshold for different grain sizes and the fact that slopes of rivers decrease over distance (Blom et al., 2016); finer grain sizes remain more mobile at lower flow velocities and slopes, therefore can travel further downstream, whilst the coarser material will not be able to entrain after a certain distance. Particle abrasion due to collision also plays a role in downstream fining, although not this effect is relatively small depending on the type of lithology of the sediment (Powell, 1998).

- **Vertical sorting**

  Gravel-bed rivers often exhibit surface armouring, a coarser surface layer compared to the underlying substrate (Powell, 1998). Studies like Andrews (1984) found surface median grain sizes 2-3

times larger than in subsurface layers. Vertical sorting of sediment fractions does not only arise from armouring effects but also develops at ripple and dune formations in the river bed forms. Vertical sorting also occurs in the formation of bedforms like ripples and dunes. However, the Karnali study area can be characterized as a plane-bed river according to the classification of Montgomery and Buffington (1997), lacking such features. Therefore, armouring likely plays the only role in vertical sorting within this specific context.

Hiding/Exposure

Sediment transport dynamics are significantly influenced by how different grain sizes interact, a phenomenon known as hiding and exposure effects. Fine-grained sediments preferentially locate themselves between coarser ones, thereby experiencing partial shielding from the dominant water flow. On the other hand, coarse-grained sediments are subjected to greater exposure compared to a scenario where they are surrounded by similar-sized particles, see Fig. 3.1. This phenomenon is incorporated into calculations by increasing the effective critical shear stress (θ_{cr}) for fine-grained sediments while decreasing it for the coarser sediment. A whole list of formulations has been proposed for this correction factor, ξ, by Einstein, Day, Proffitt & Sutherland, Parker, Egiazaroff, Ashida & Michiue, Hunziker, Wu et al. and Wilcock & Crow (Scheer et al., 2002).

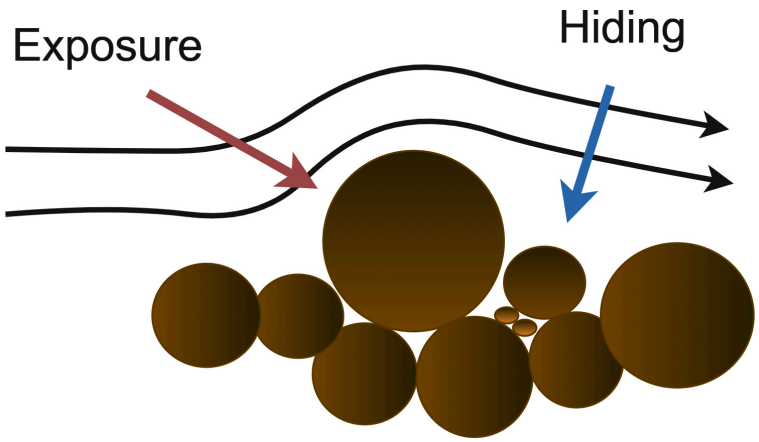

Figure 3.1: Hiding/Exposure effect, redrawn from Scheer et al. (2002).

This phenomenon significantly influences the local sediment supply. The supply of fine materials is reduced due to the hiding mechanisms and increased exposure of the coarser fraction results in a larger supply of those fractions. The large range of sediment and debris sizes coming from the mountainous upstream area of the Karnali River is subject to hiding and exposure effects.

All the above-mentioned sorting and hiding/exposure processes determine the grain size distribution of the river bed and floodplain. Looking at the patterns in the field can help conceptualize which processes influence the channel-shifting behaviour.

3.3. Secondary Flow

Water flow experiences a centrifugal force due to the curvature of the channel, leading to higher flow velocities near the outer bank. The result is an unbalance in the transverse (radial) pressure gradient (Bridge & Jarvis, 1982). The pressure gradient induces a flow component perpendicular to the river's main direction, moving water towards the inner bend near the riverbed and towards the outer bend near the surface. Fig. 3.2 displays the resulting transverse velocity profiles and the secondary flow patterns. The transverse flow component combined with the streamwise flow component, produces a spiral flow motion throughout the river bend, the so-called centre-region cell. In addition, a second secondary flow cell arises, the outer-bank cell, which is a weaker and counter-rotating circulation (Blanckaert & De Vriend, 2004).

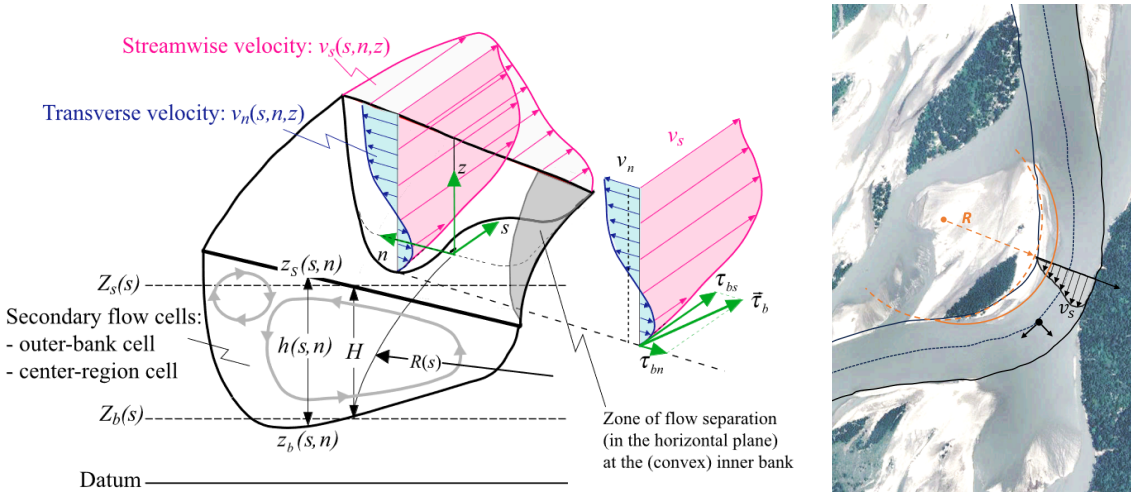

Figure 3.2: Drawing of the flow profiles that occur in a river bend. The flow directed to the inner bend near the river bed and the flow directed to the outer bend near the water surface cause the secondary flow, combined with the streamwise flow the river experiences a helical flow. Figure adopted from (Blanckaert, 2011). (right) Drawn streamwise velocity profile in the Karnali bifurcation (BIF3). The zone of flow separation at the inner bend is indicated with the orange line.

The spiral flow component has implications for sediment movement and morphological development:

- **Shear Stress:** The near-bed transverse component of the center-region cell adds a shear stress component(τ_{bn}) normal to the main flow component(τ_{bs}). This redirects sediment ($\vec{\tau}_b$), preferentially transporting finer material to the inner bend.
- **Channel Shape:** The resulting sediment redistribution shapes the classic channel geometry in river bends: deeper at the outer bend and shallower (with point bar formation) at the inner bend, as observed in the Karnali (see Fig. 4.6).
- **Sorting:** Transverse shear stresses are weaker then streamwise shear stress. This weaker component can only mobilize finer fractions on the slope towards the innerbend. Leading to size-dependent sorting. Smaller grains are transported to the inner bank, while larger grains may be influenced by gravity, rolling towards the outer bend (discussed in the next section).

The deflection angle towards the innerbend, referred to here as δ, at which the sediment transport vector is altered due to the spiral flow is shown in Fig. 3.3 and defined by Struiksma et al. (1985):

$$\delta = \arctan\left(\frac{v_s}{v_n}\right) - \arctan\left(A \cdot \frac{h}{R_*}\right) \tag{3.4}$$

$$\text{with} \quad A = \frac{2}{\kappa^2}\left(1 - \frac{\sqrt{g}}{\kappa C}\right) \tag{3.5}$$

with v_s and v_n the streamwise and transverse velocity vectors, R_* the streamline curvature (m), κ the Von Karman constant (0.4), and C the Chézy coefficient.

3.4. Transverse Bedslope Effect

The gravity pulls along transverse gradients in river bends and bifurcations significantly influence sediment transport and is a major contributing process to large-scale morphology (Baar et al., 2018). Like the spiral flow, the transverse gravity pull adds a force to the particles normal to the flow direction, causing a deflection of the particles path. Various mathematical formulations have been established to describe this influence on the particle trajectory such as (Engelund, 1974; Ikeda, 1982; Parker & Andrews, 1985; Talmon et al., 1995).

Large differences between the formulations exist, which could significantly reduce the reliability of physics-based morphodynamic models (Schuurman et al., 2013). Fig. 3.3 Shows the main components of the transverse bed slope effect; The normal path particles move in the direction ($\vec{u}$), the sum of the streamwise (u_s) and secondary flow vector (u_n), is deflected by downslope by factor ψ. Baar et al. (2018) shows how the stability of a bifurcation is highly sensitive to the bed slope effect and determines the further development of its morphology.

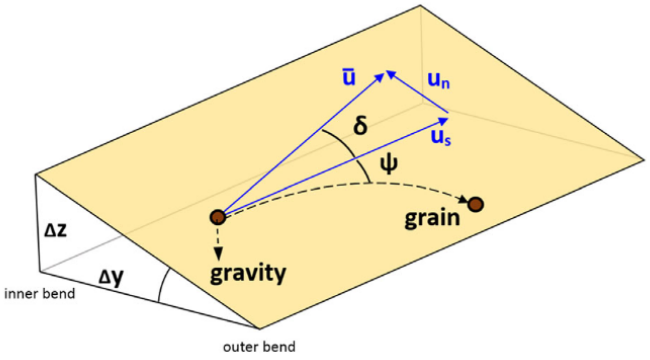

Figure 3.3: Drawing showing particle deflection due to transverse bed slope gravity pull and secondary flow. The trajectory of sediment particles travelling in the direction $\vec{u}$, are deflected downslope (ψ) due to gravity pull and upslope due to secondary flow (δ). Figure adopted from (Baar et al., 2018).

The Koch and Flokstra formulation is as follows (Koch & Flokstra, 1980; Struiksma et al., 1985) :

$$\tan(\psi) = \frac{\sin(\delta) + \frac{1}{f(\theta)}\frac{\partial z_b}{\partial y}}{\cos(\delta) + \frac{1}{f(\theta)}\frac{\partial z_b}{\partial x}} \tag{3.6}$$

$$\text{with} \quad f(\theta) = \alpha\theta^{\beta} \tag{3.7}$$

Where δ is given by Eq. (3.4). From Eq. (A.16) we can make out that increasing the α parameter (later referred to as Ashld) will result in a weaker effect of gravity pull on sediment particles as it is located in the denominator. With weaker deflection of particles, the river cross-section can develop steeper transverse slopes since the secondary flow deflection, δ, takes the upper hand.

3.5. Bifurcation Approach Conditions and Division of Sediment

Natural bifurcations exhibit significant asymmetry in terms of offtake angle, geometry, bed surface roughness, and channel width. These asymmetries influence and undergo various processes that shape the behaviour of discharge and sediment distribution. A factor influencing bifurcation dynamics is the Bulle effect. This effect refers to the flow separation and the generation of eddies that occurs at the intake of bifurcate take takes off under an angle. The flow separation leads to the formation of a recirculation zone, which can enhance sediment deposition at the entrance of one branch (Bulle, 1926; van Denderen et al., 2018). See this effect near the entrance of the offtaking channel in Fig. 3.4. This effect is similar to the flow separation that may occur near the innerbend of a river bend.

Additionally, the before-mentioned secondary flow and transverse bed slope gravity pull play an important role in sediment distribution over the bifurcates. Transverse bed slope directs bedload to the deeper channel (Kleinhans et al., 2008). When a bifurcation is located within a bend, such as the studied Karnali bifurcation, secondary flow components may direct slightly more sediment towards the innerbend near the bed (Kleinhans et al., 2008; van Dijk et al., 2014), this is also visible in the schematic Fig. 3.4. Sediment distribution is thus influenced by the balancing of the deflection due to transverse gravity pull and near-bed helical flow.

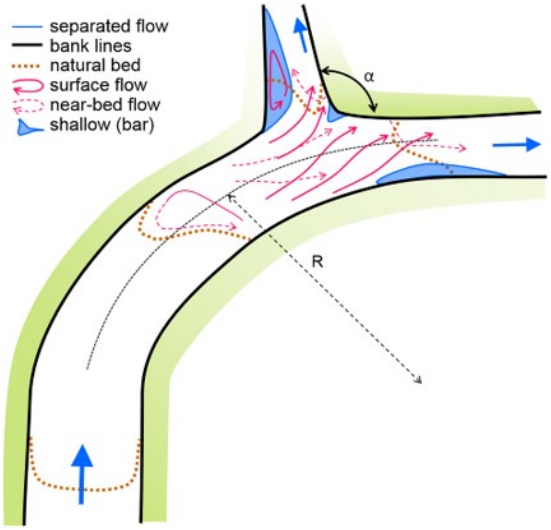

Figure 3.4: Schematic of processes at a bifurcation located near a river bend. Note the Bulle effect near the entrance of the offtaking channel. Arrows indicate the flow patterns influenced by the secondary flow. Figure adopted from (Kleinhans et al., 2013; van Denderen et al., 2018)

Research has shown that these processes, particularly in combination with a river bend and mixed-sized sediment composition, can significantly impact flow and sediment distribution. Sloff et al. (2006) have shown with 2D and 3D models that bifurcations with an upstream meander bend showcase highly asymmetrical division of flow and sediment. Kleinhans et al. (2008) have concluded that due to the influence of an upstream bend, one branch of the bifurcation receives a disproportionately large share of flow discharge, while the other branch experiences relatively more sediment load. They have confirmed with numerical computations that when the inner bend branch may start to be the dominant channel, it can lead to sediment overloading in the bifurcate starting in the outer bend. Exactly this seemed to have occurred in the Karnali system. Redolfi et al. (2019) consider the two main forcing factors, which are the curvature of the upstream channel and the slope advantage of one of the bifurcates and show that the free instability mechanism might lead to outcomes where most of the water and sediment flux is directed towards the inner bend bifurcate.

4

Observations from Satellite Imagery & Fieldwork

This chapter discusses the observations and measurements made during the field campaign at the Karnali river bifurcation area in October 2023. The observations are connected to their relevant theoretical underpinnings. Firstly, an analysis of satellite imagery regarding the bifurcation is shown. These observations and theories drive the formulation of the hypotheses in Chapter 5.

4.1. Planform Evolution Analysis

Fig. 4.1 shows short wave infrared (SWIR) composites of various years before, during and after the 2009 flood event. Here, the change in planform around the bifurcation is visible; red circles highlight areas with notable erosion and channel activation activities. Yellow rectangles indicate areas undergoing significant sedimentation and aggradation.

While the Geruwa channel remained dominant until 2009, it is noteworthy that during relatively high discharges in 1995 and 2000, some branches leading to the Kauriala were active earlier, indicating potential preconditions for the later channel shift. This suggests that these channels were likely not fully aggraded but merely dry and inactive, with peak discharges sufficient to restore flow in those channels leading to the Kauriala. In the composites up to the year 2020, it is visible that the Karnali follows the eastern side of the fan. Afterwards, the bifurcation points shift upstream, directing more water along the western side.

Recent observations suggest that the system is transitioning to a single-branch state as the discharge through the Geruwa branch decreases rapidly, particularly during low flow conditions. Dingle et al. (2020b) reported a more or less equal discharge distribution between the Kauriala and Geruwa branches after the 2017 monsoon season. However, during our post-monsoon 2023 field campaign, we performed simple surface velocity tests in both branches approximately 30 km downstream of the bifurcation. We determined the wet area and estimated the discharge from the measured cross-sections. This estimate indicates that the discharge distribution is now approximately 95% to the Kauriala and 5% to the Geruwa.

On the following page, Fig. 4.1 presents a compilation of SWIR satellite imagery from the LANDSAT 7 mission, with composites from the post-monsoon season (Oct-Dec).

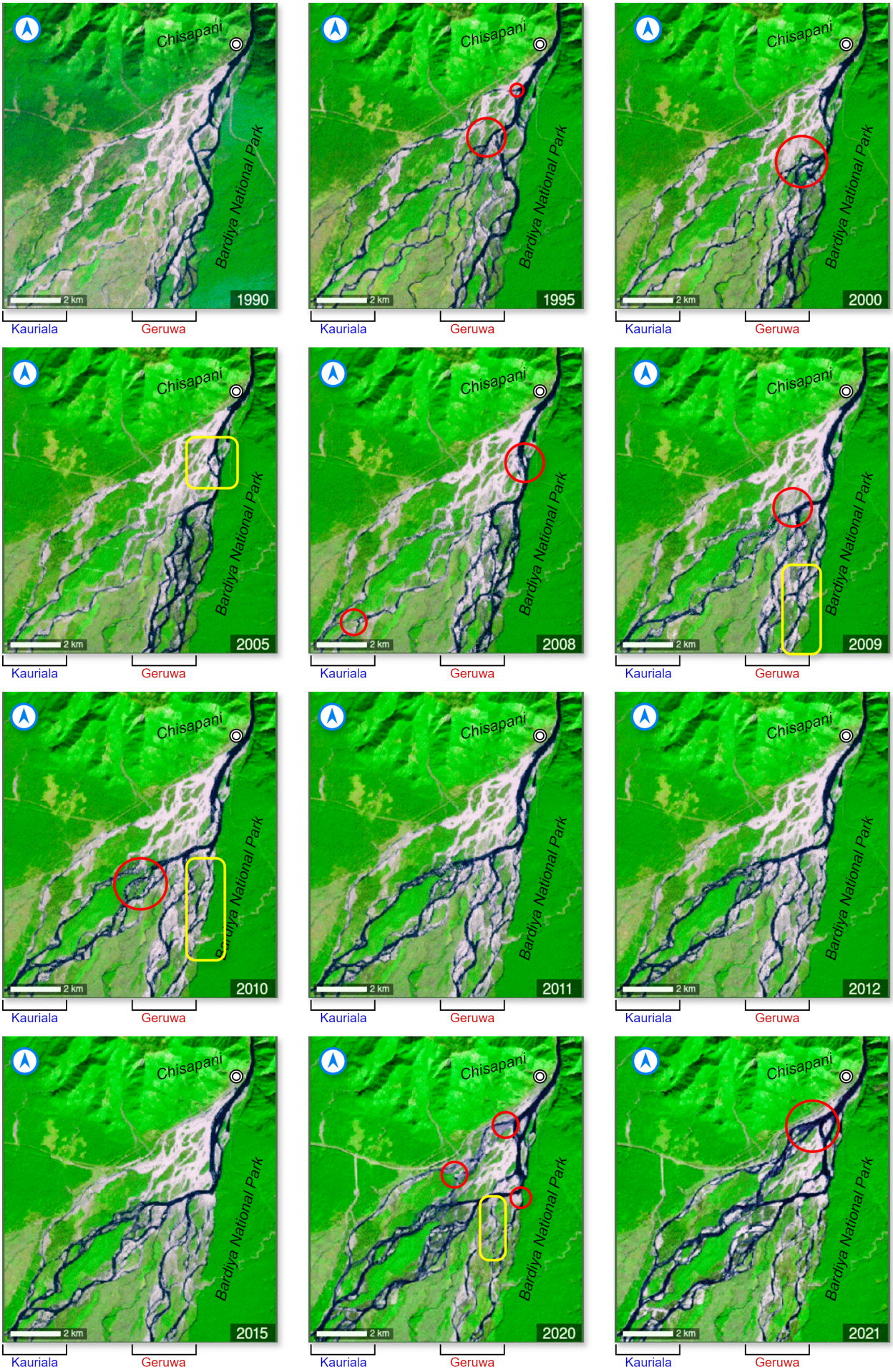

Figure 4.1: Recent history of the Karnali bifurcation (1990-2021) Landsat 7 SWIR composites after monsoon period (Oct-Dec), Notable erosion events or channel activations are highlighted with red circles and sedimentation with the yellow rectangle.

A field campaign was conducted to understand the behaviour of the Karnali bifurcation. Key data collected include:

- General topography and scale of the bifurcating area
- Cross-sectional profiles (including banks and floodplains) along different sections of the Karnali River and its distributaries
- Bed surface grain size distribution
- Waterlevel, high flood levels and channel slopes
- Installation of telemetric waterlevel gauges in both river branches for future monitoring

This data will be crucial for testing the hypotheses outlined further on in this thesis. Details on field methods and materials are in Chapter 9.

The 2022 fieldwork and initial survey with the supervisory team informed the strategic site selection for the 2023 campaign. It was aimed to collect cross-section data, sediment photographs, and high-precision coordinates approximately every 5km in each branch, prioritizing locations with single or well-defined channels. Using satellite imagery and insights from the survey, these locations were tracked. With necessary adjustments to the plan, a substantial amount of data and information was successfully gathered. Site selection was ultimately guided by accessibility, safety, and resource availability. Please refer to the overview map in Fig. 4.2 for location codes and to Table 4.1 for the used equipment.

Table 4.1: Equipment Used for River Survey and Data Collection

Name	**Abbreviation**	**Purpose**
ArduSimple RTK Base-Rover Kit	RTK GPS	High-precision mapping of shallow river areas (riverbeds, bars, floodplains). Provides longitude, latitude, and elevation data.
Deeper Sonar CHIRP+	CHIRP	Single beam sonar for bathymetry surveys of deeper river sections. Deployable from various watercraft and compatible with RTK GPS.
Obscape Level Gauge	Level Gauge	Real-time water level monitoring in multiple branches using radar, solar power, and GSM telemetry.
Measuring Tape	-	Provides a reference scale for sediment images.
Hawkeye Handheld Depth Finder	Hawkeye	Portable single beam sonar for quick depth checks and validation of CHIRP readings.
Nikon Forestry Pro	NFP	Laser rangefinder for measuring distance, angle, and height differences. Used in areas with limited RTK GPS connectivity.

Table 4.2: Overview of equipment used in the field.

The following subsections will detail the collected data, the methods employed for data collection, and the rationale behind their selection, highlighting their significance in studying the bifurcation area.

For more details on the equipment, methods, logistics and complete fieldwork data, see the full field rapport in the Appendix D.

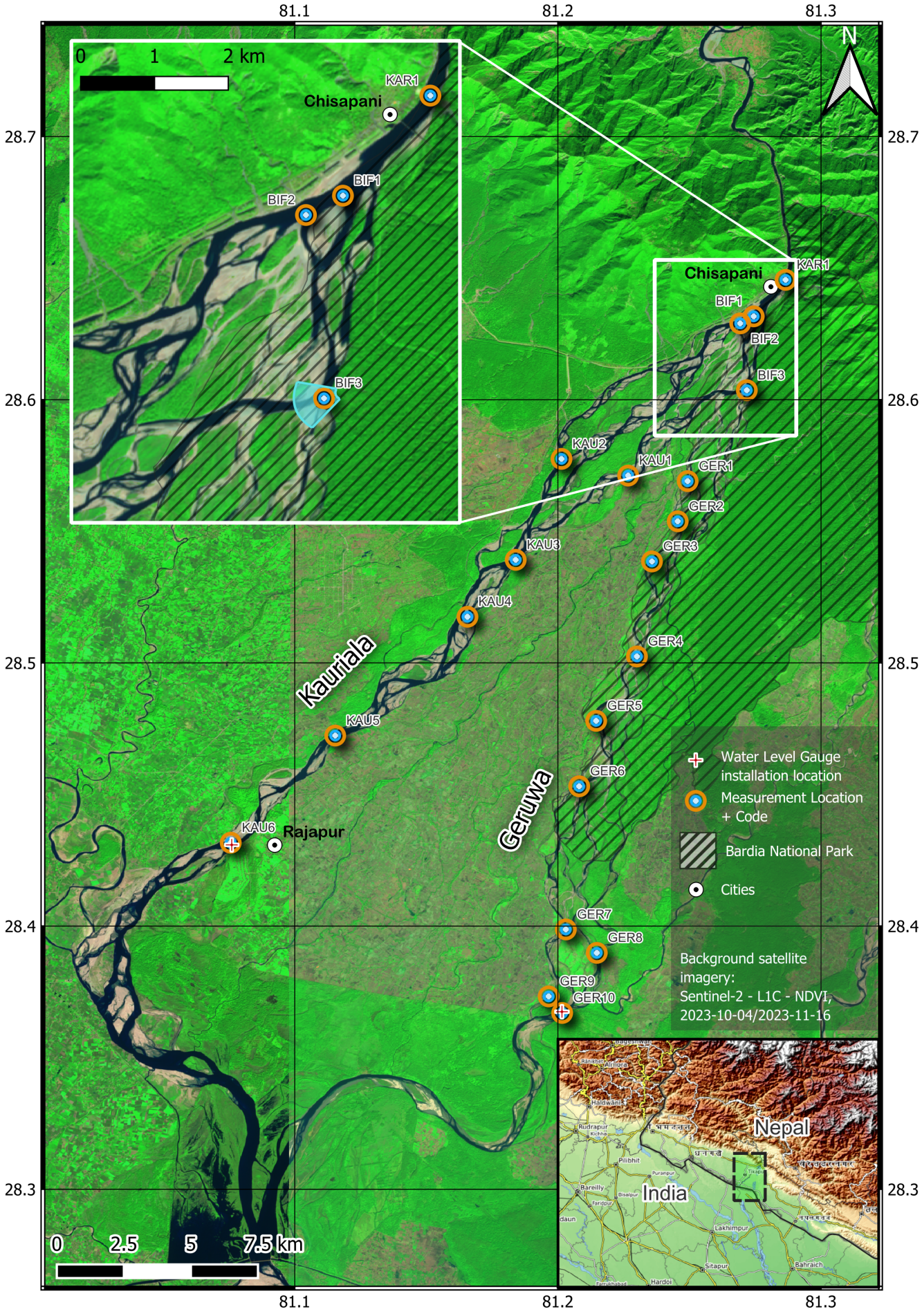

Figure 4.2: Field Campaign map of the Karnali river. All locations were data was collected are indicated, the background NDVI composite is from the time of fieldwork (October-December 2023).

4.2. Bifurcation and River Bend

The extensive deposition that likely contributed to, or resulted from, the abrupt channel switching after 2009 (as discussed in Section 2.1) was evident during the field campaign. The first Geruwa entry (BIF3) was found to be almost entirely blocked by cobbles and boulders. This sedimentation is notable in the left portion of Fig. 4.3. Local authorities have attempted to divert some flow back into the Geruwa branch by dredging two shallow channels (approximately 1.5 meters deep). However, these channels appear ineffective for diverting substantial flow. Compared to the depth of the main channel (4.5 meters), they likely dry up as water levels recede during the dry season, as confirmed by satellite imagery from March 2024.

Figure 4.3: Image taken during a field campaign at location BIF3 (Oct 2023), the field of view is marked in Fig. 4.2 and in the top right map. The image faces Westward and depicts the direction of the main flow with the dark blue arrow. Furthermore, the orange dotted line indicates the two small dredged channels. The dotted white line represents the path of the cross-section taken at BIF3, shown in Fig. 4.6.

While observing this area, it became evident that the larger sediment fractions are trapped near the entrance and beginning of the Geruwa bifurcation during peak flow. Sediment of this large size was not found in other parts of the study area, including the more upstream locations of BIF1 and BIF2 and in the Kauriala branches. Fig. 4.4 presents a conceptual schematic of the deposition at the Geruwa branch. Note that the orientation of the schematic aligns with the flow direction, with North and South reversed. During peak discharge, sediment originating from the steep, confined slopes of the Karnali tends to move towards the Geruwa in the outer bend, where it is deposited due to the lower conveyance capacity of the bifurcation. After peak discharge, there is insufficient transport capacity to move the deposited sediment downstream.

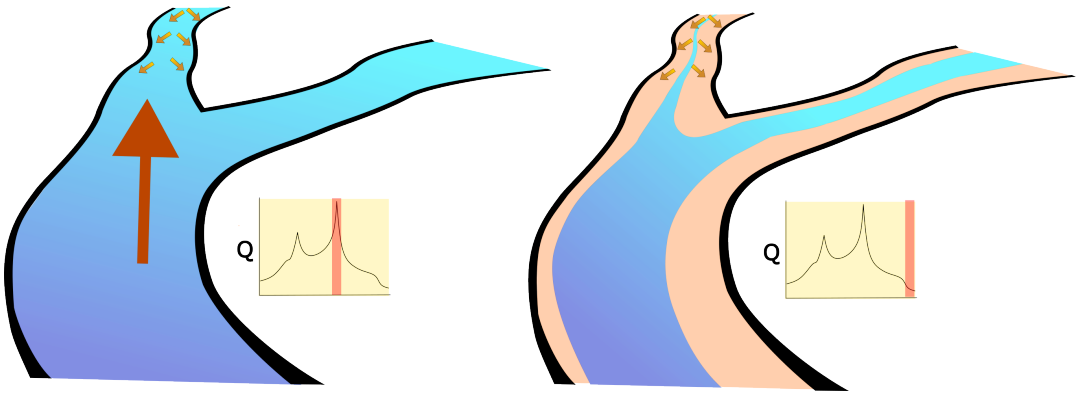

Figure 4.4: Conceptualized sediment flux and deposition during peak flood event (left) and during low flow conditions (right).

4.3. Bed Surface Grain Size Distribution and Bend Sorting

Field observations near bifurcation BIF3 (see Fig. 4.2) revealed an unequal distribution of grain sizes. Bend sorting was observed, with coarser sediment concentrated along the outer bend and finer gravel and sand dominating the inner bend. Numerous photographs of the dry bed were taken to quantify these patterns, oriented perpendicular to the surface systematically. The bend sorting is visible in the size difference of the sediment between the bed near the outer and inner banks, see Fig. 4.5.

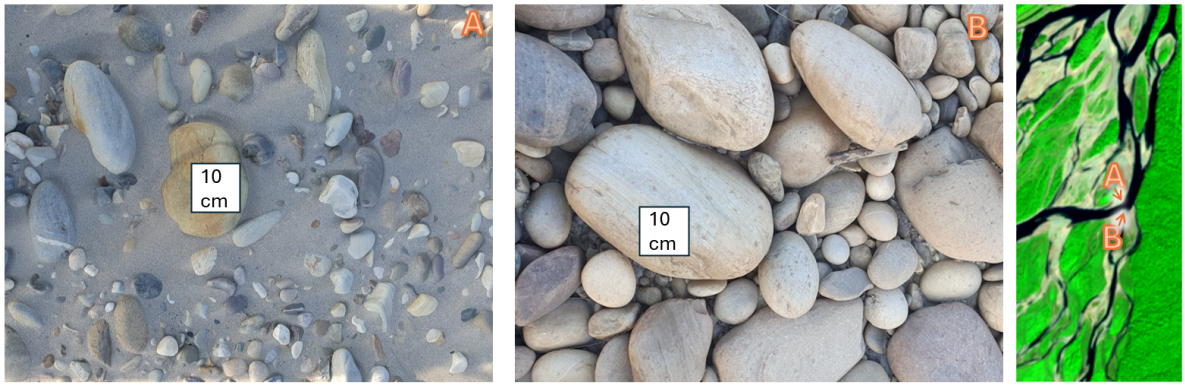

Figure 4.5: Example grain size images taken at location BIF3. Image A shows the grain size near the inner bend, while image B shows it near the outer bank. Both images use the same scale, indicated by the square representing 10 by 10 cm.

These images were then analyzed using PebbleCounts automatic grain image processing software (Purinton & Bookhagen, 2019) to assess streamwise and transverse changes in surface sediment distribution. The analysis mostly ignored the larger cobble and boulder particles. Since these sediment classes are a significant feature in the study area, this incomplete image analysis was not considered for later modelling efforts. Due to field constraints, subsurface investigation in our Karnali study was not feasible, preventing observation of the extent of armouring.

Gravel-Sand Transition: Dingle et al. (2020b) identified the gravel-sand transition GST in the Karnali River (Kauriala branch) approximately 40 km downstream of the mountain front (at Chisapani) during their 2016 field campaign. Our observations in October 2023 revealed a significant gravel presence at this location, suggesting a potential downstream shift of the GST in recent years, possibly due to increased discharge in the Kauriala branch. Unfortunately, due to border restrictions, we could not extend our fieldwork further downstream to confirm the current GST location.

4.4. Cross-sectional Profile

Cross-sectional profiles were taken at each location marked in Fig. 4.2 to investigate channel geometry. Cross-sections were obtained using both CHIRP sonar and the RTK system, achieving sub-10cm accuracy in all dimensions in most locations. On the floodplains and in wadable river sections, the RTK system was used to take point measurements at 50-cm intervals. For larger and faster-flowing sections of the river, including the Karnali (KAR), bifurcation (BIF), and Kauriala (KAU) locations, measurements were conducted from boats using the CHIRP sonar to capture the riverbed profile.

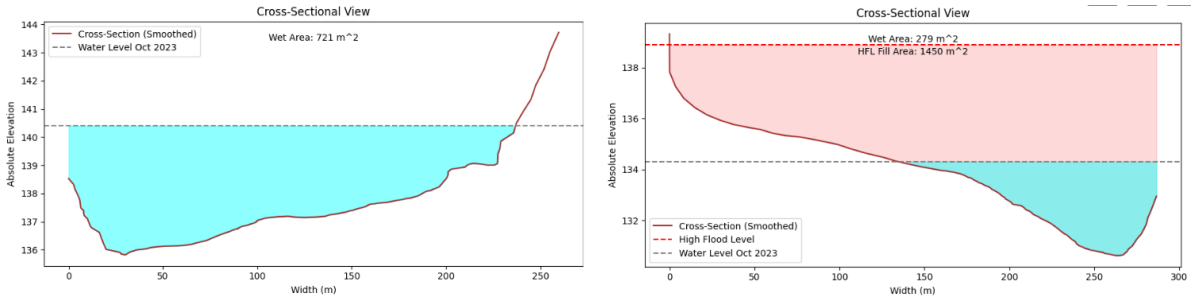

Figure 4.6: Cross sections; (left) KAR1, three kilometres upstream of the bifurcation. (right) Location BIF3, right before the bifurcation, located in the bend, see the white dotted line in Fig. 4.3.

The sonar data were then integrated with RTK data from the floodplain to create comprehensive cross-sectional profiles, as shown in Fig. 4.6. Data from these methods were combined and projected on a 2D plane using orthogonal translations as described by Parsons et al. (2013). Refer to the field report in Appendix D for a complete set of processed plots. Here, the focus is on two representative profiles within the study area of the bifurcation (Fig. 4.6). Note that in these plots, the Western bank is oriented on the left and the Eastern bank on the right. The cross-section at BIF3 (Fig. 4.6, right), located in the bend upstream of the bifurcation, exhibits a gentle transverse slope towards the inner bend and a steeper slope towards the outer bank. This geometry aligns with secondary flow patterns, typically resulting in deposition near the inner bend. Additionally, the transverse gravity pull deflects the particles towards the deepest part of the cross-section. As the bifurcation commences, this deflection will preferentially direct heavier sediment particles towards the Geruwa branch as its entrance is located in the outerbend.

4.5. Long Profile, Water Level & Slope

At each site shown in Fig. 4.2, the water level was measured with the RTK system. The accuracy of the station was for most locations within 0.1 meters, except for locations KAU2, KAU4, and KAU5 (<0.3 meters). Problems with GPS signal were experienced at location BIF3 where only DGPS signal was required (≈2 meters accuracy). The values at this location were later corrected by interpolating between the nearest upstream and downstream measurements. Additionally, high flood levels were noted in case markings by the local water authorities indicated them or if there were clear signs (e.g. wooden rubble/ vegetation breaks), and local inhabitants were asked if they could indicate the high flood levels. Therefore, these accounts are not always accurate, but they give a good indication of the magnitude of the flood level. The river bed level slope was determined by extracting the deepest points from the cross-sections and applying a linear fit through the data points. This data reveals key insights into the bifurcation and downstream divergence in the study area. Initially, the bed slopes in the branches are similar, but the water level of the Geruwa is significantly lower due to a blockage at its entry. A pronounced divergence in bed levels emerges approximately 7 km downstream of the bifurcation, with the Geruwa's bed being up to 10 meters lower than the Kauriala's. Around 29 km downstream, the slope of the Kauriala steepens, eventually falling below that of the Geruwa branch (see Fig. 4.7). To investigate the discharge distribution dynamics, two telemetric gauges have been installed downstream at locations (KAU6 and GER10) (see Fig. 4.2). These will provide continuous monitoring data, which is particularly useful during monsoon seasons. Preliminary cross-sectional surveys and velocity measurements at these locations in the dry season (November 2023) indicate a discharge distribution of approximately 5% through the Geruwa branch and 95% through the Kauriala branch.

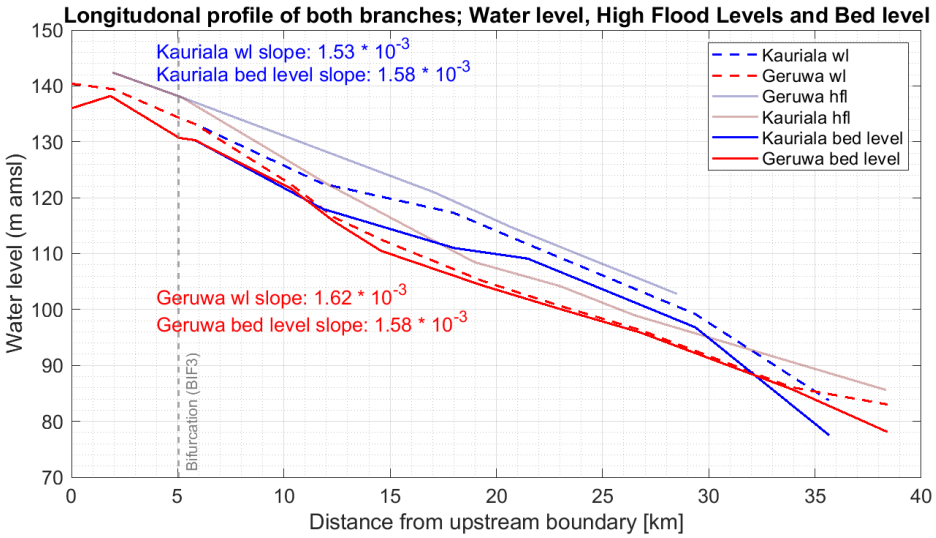

Figure 4.7: Measured water level and slope extraction in both bifurcates of the Karnali. The semitransparent lines indicate the high flood level in the locations where it could be identified by either markings from the waterboard or asking the local inhabitants. Bedlevel points were retrieved from the deepest point of the measured cross-sections.

5

The Conceptual Model of the Karnali Channel Shift

We have seen that the physics that govern river bifurcations and sediment transport are complex and multifaceted. Previous studies have highlighted several key mechanisms, such as sediment sorting, flow separation, and the influence of bed slopes, that significantly affect how water and sediment are distributed between river branches. These insights, combined with field observations and existing studies on the Karnali Bifurcation (Dingle et al., 2020a, 2020b; Iwasaki et al., 2013; Rakhal et al., 2021; Roebroeck, 2022), point towards specific patterns and processes that might have contributed to the significant morphological changes observed in the Karnali bifurcation post-2009. Here, two hypotheses are proposed to explain the observed discharge distribution shift. The provided schematics will help visualise the relevant processes. The hypotheses overlap rather than be mutually exclusive, and both proposed mechanisms could have coincided. Fig. 5.1 show the bifurcation in line with the direction of the flow and sediment fluxes. This perspective will serve as a basis for the schematics in this chapter.

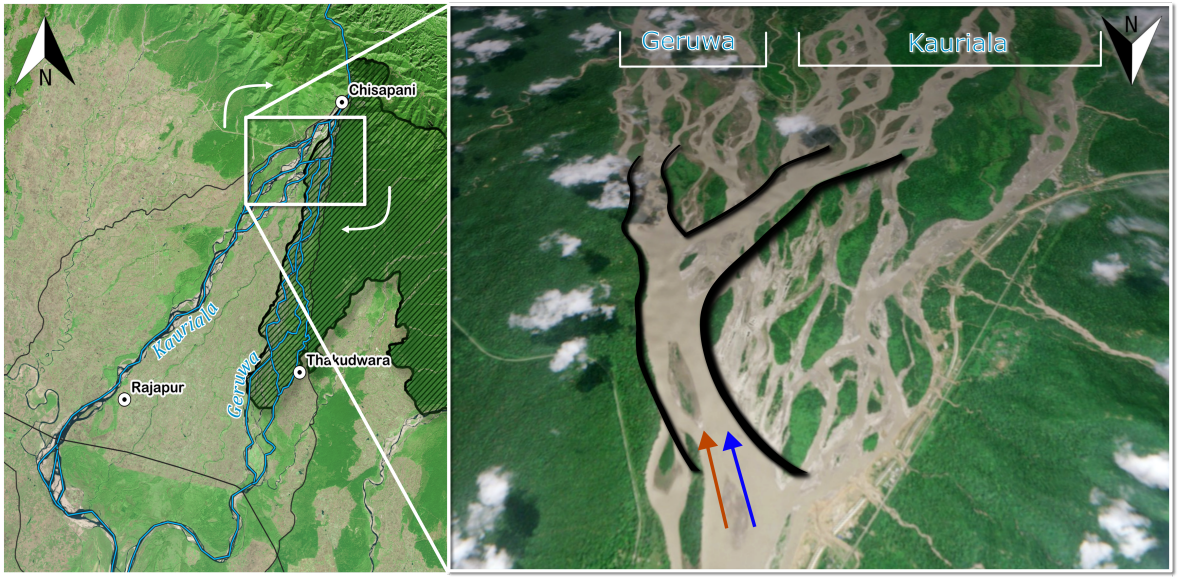

Figure 5.1: Left: Map of the Geruwa and Karnali branches. Right: detail of the bifurcation; note the change in orientation is reversed and shows the flow direction of water and sediment (blue and orange arrow). The Sentinel image is from 11-09-2019 during monsoon discharge. The black lines represent the study area.

Hypothesis 1: Bend sorting effects causing [Geruwa] channel entrance blockade

This hypothesis proposes that the processes of bend sorting, particularly during peak flow events, play a crucial role in sediment deposition at the Geruwa channel entrance, leading to blockages that alter the flow distribution between the river branches. The following points outline the key mechanisms involved:

1. Strong peak flow discharge, like during the heavy 2009 monsoon period, increases the flow's momentum, centrifugal forces and secondary flow, intensifying flow dynamics within the bifurcation. Additionally, sediment load is increased as the transport capacity increases with discharge.
2. This enhanced flow leads to stronger sediment sorting compared to average peak flows, particularly within the bend and along steep transverse slopes.
3. The transverse bed slope effect directs the larger cobbles and boulders (originating upstream) associated with the abnormal flood discharge toward the outer bend.
4. Accumulation of coarse sediment at the Geruwa inlet creates a plug or blockage.
5. Due to this blockage, high discharge seeks an alternative path, leading to the previously inactive Kauriala branches.

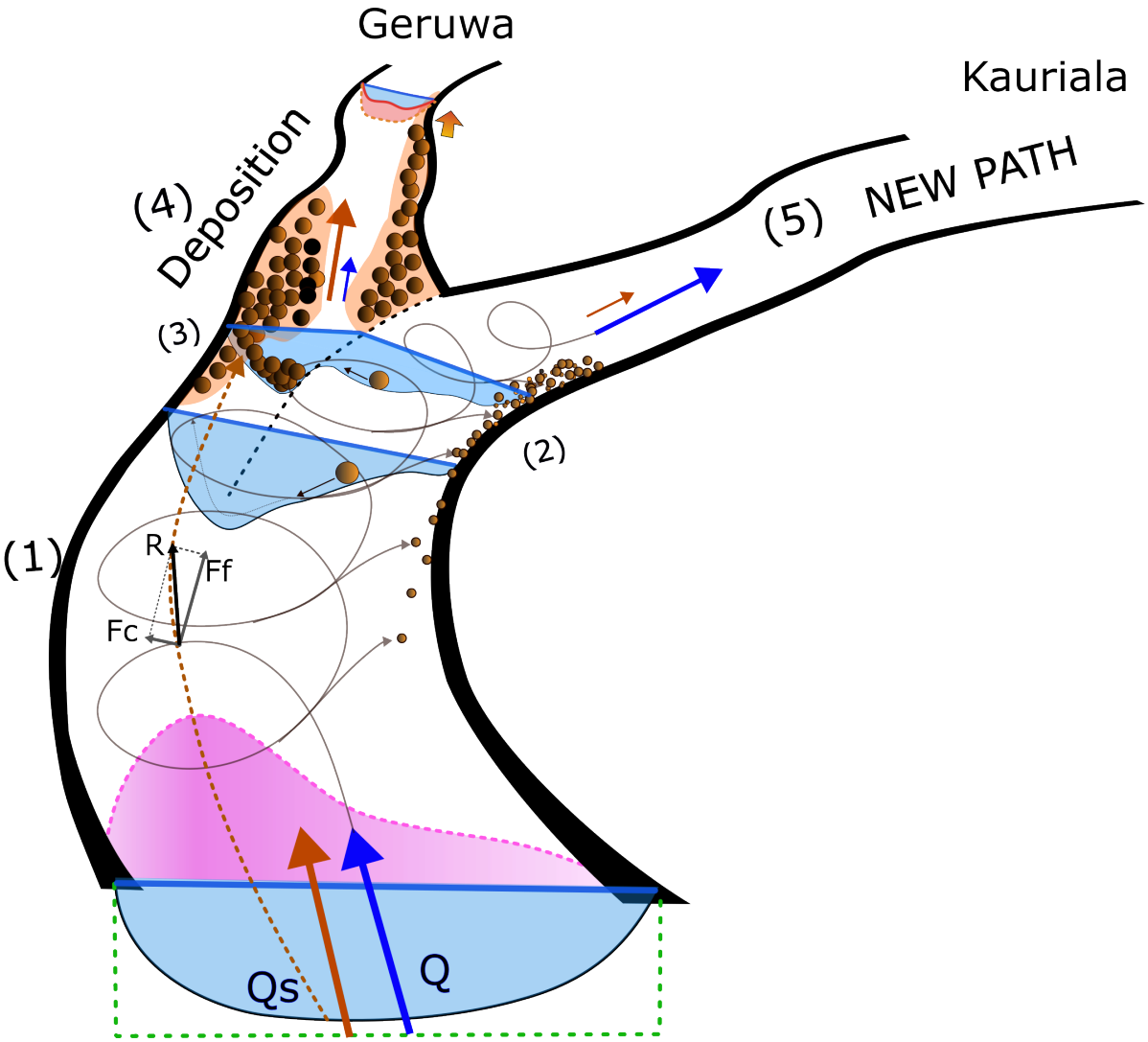

Figure 5.2: Processes involved in hypotheses two. The brown patches with sediment particles show deposition. Spiral flow is shown and the size of the arrows represents the magnitude of the discharge and sediment flux.

The provided schematics (Fig. 5.2 and Fig. 5.4) illustrate the processes. Note that the North-South orientation is reversed in these figures for a clearer flow-direction perspective. Multiple cross-sections (blue planes) and streamwise velocity profiles (pink planes) are included to showcase the dynamics at work. The figures depict the spiral flow pattern and its role in the preferential transport of finer sediment particles toward the inner bend. Additionally, Fig. 5.2 highlights the transverse bed slope effect (gravity pull) in the upper cross-sections, where sediment particles are shown moving towards the outer bend. The size of the blue (flow) and orange (sediment) arrows indicate the relative magnitude of their respective fluxes.

Connected to Hypothesis 1 but likely true for both hypotheses, the Geruwa channel aggradation is further facilitated by the fact that during discharge and sediment flux extremes, a larger proportion of the sediment continues straight into Geruwa due to increased grain sizes, water levels and the momentum of the fast-flowing water and rolling/sliding boulders. This excess sediment becomes immobile after peak flood events, contributing to a channel aggradation wave that migrates downstream. Furthermore, the rapid decrease in channel conveyance capacity during the falling limb of the hydrograph (flood discharge retreat) could explain the observed sedimentation further downstream of the bifurcation. A schematized view is shown in Fig. 5.3

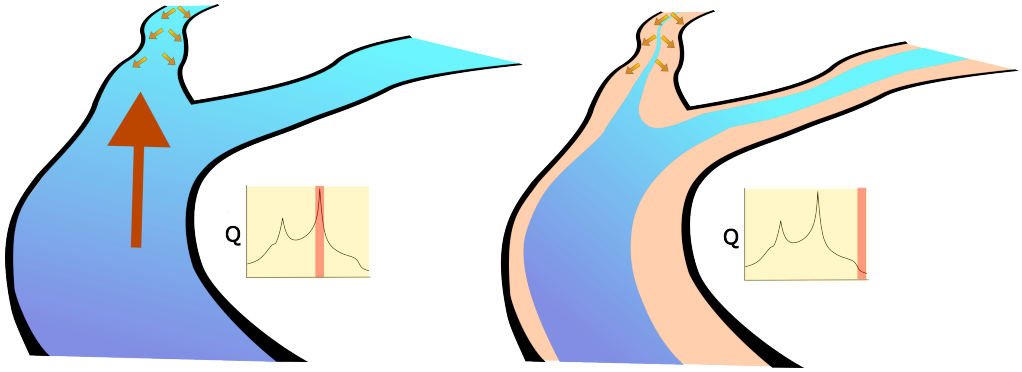

Figure 5.3: Conceptualised sediment flux and deposition during peak flood event (left) and during low flow conditions (right).

Hypothesis 2: Opening of Western [Kauriala] channel

The second hypothesis focuses on the role of erosion in forming and reactivating alternative channels leading to the Kauriala. This leads to a lowered transport capacity in the Geruwa, resulting in deposition. The schematics provided (Fig. 5.4) depict the processes associated with this hypothesis.

1. Unusually high erosion rates along the banks of the Karnali, especially on the inner bend made up of finer, more mobile sediment, resulted from the two flood peaks during the 2009 monsoon season. This erosion created an opening in the western branch that connects to the Kauriala.
2. This breach diverted a significant portion of the flow into the Kauriala branch.
3. Consequently, the Geruwa branch experienced a drastic reduction in discharge, leading to decreased transport capacity and flow separation at its inlet.
4. The resulting sedimentation at the Geruwa inlet further restricted its inflow, initiating a self-reinforcing decline in capacity.

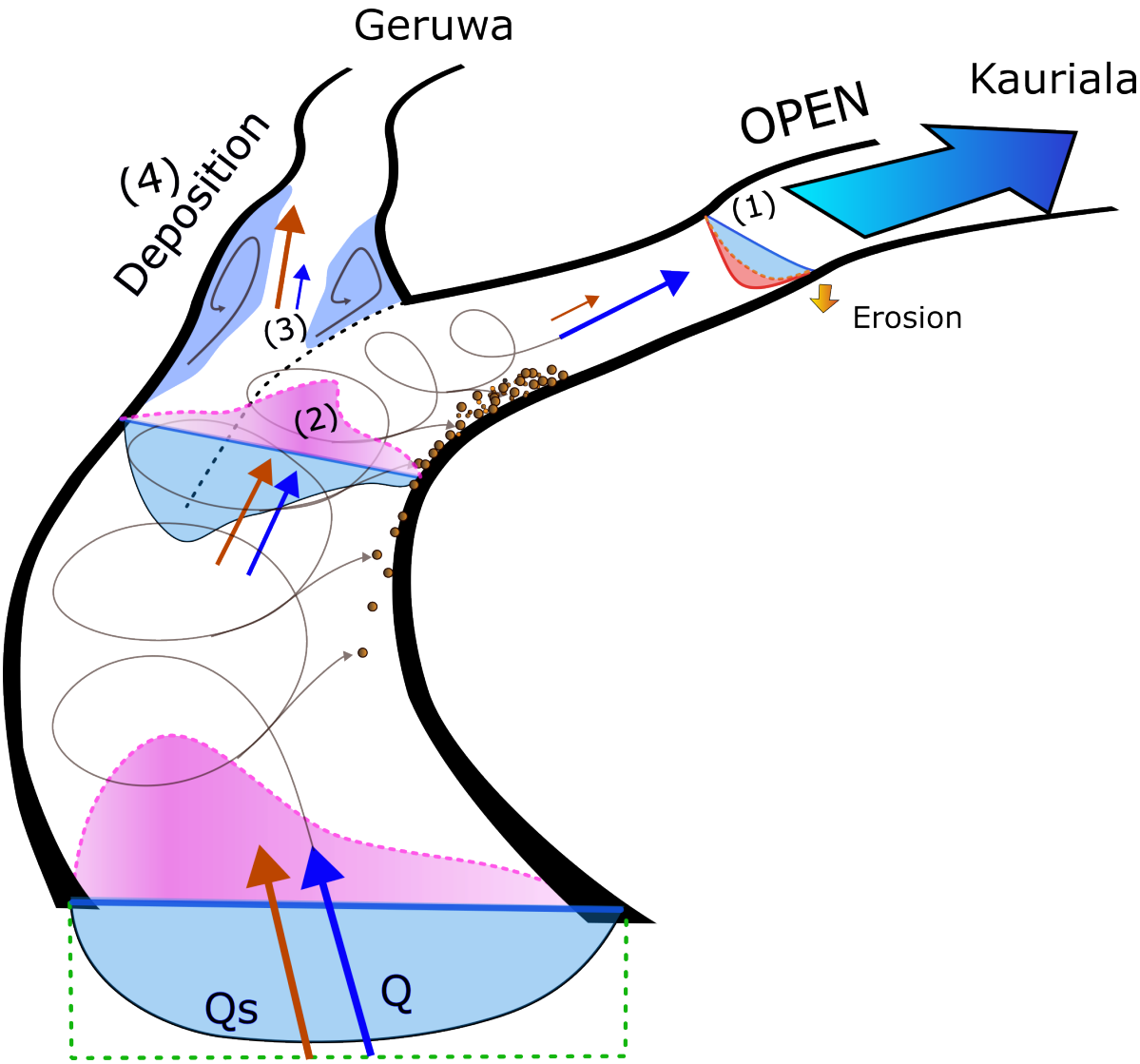

Figure 5.4: Processes involved in hypothesis two. The streamwise velocity profile is shown in pink, and the areas of flow separation are shown in dark blue. Spiral flow is shown and the size of the arrows represents the magnitude of the discharge and sediment flux.

Bifurcation Stability

We suggest a hypothesised potential feedback loop for the closure of the Geruwa that happened after the initial deposition from hypotheses: reduced flow towards Geruwa leads to decreased sediment transport capacity within that branch. This weaker transport capacity allows more sediment to deposit in Geruwa, further reducing its overall water depth. Shallower water in Geruwa likely discourages further flow into the branch, potentially creating a self-reinforcing cycle that promotes closure. This cycle could lead to a single-branch system in which the Kauriala is the only active branch. The bifurcation area could become a stable system until new extreme flood events significantly alter the morphology again.

6

Set Up of Numerical Model

It is important to create a model that incorporates all relevant physical processes to investigate the hypotheses related to the closure of the Geruwa branch (Chapter 5). Hydrodynamics to capture multi-dimensional flow processes and flood wave propagation. A morphological component is needed to model bedlevel changes, both erosion and deposition, and processes such as transverse downslope deflection due to gravity pull and hiding/exposure sediment interactions.

A two-dimensional, depth-averaged (2DH) model incorporating parameterized 3D flow effects and morphological updates was chosen to be suitable for testing the hypotheses. The parameterized approach allows for representing phenomena like spiral flow, which are crucial factors in the observed dynamics but are too complex and computationally expensive to model in full 3D. It is essential to emphasize the exploratory nature of this model. It is not intended to be a comprehensive replica of the whole reality of the Karnali bifurcation. Instead, it serves as a simplified tool for exploring possible processes that contribute to the partial closure of a river branch originating from the outer bend of the main channel. Our study will highlight the crucial role of external factors in this evolution. In essence, the investigated system is highly sensitive to its unique starting conditions, the influences at its boundaries, and its internal dynamics.

One might wonder why not fully schematize this bifurcation, perhaps by simplifying it as much as possible. The rationale for the chosen approach is that the initial conditions exert a profound influence on the morphological development. The processes that play a role in bifurcations have been extensively researched and are implemented in the modelling software. The focus is on how these processes affect the Karnali bifurcation. Therefore, it is essential to incorporate site-specific details to understand the factors contributing to the closure of the Geruwa branch. The current model aims to balance simplification and maintaining fidelity to real-world conditions. This is done by using field data such as slope, sediment composition and channel dimensions.

This chapter details the construction and model choices of the numerical model used to explore hypotheses regarding the Geruwa branch closure. The DELFT3D-4 software suite was chosen due to its robust sediment transport capabilities and validation studies. It can simulate sediment transport and morphological changes arising from erosion and deposition, in combination with the full suite of hydrodynamic processes (Lesser et al., 2004).

6.1. Model Equations

DELFT3D-4 (D3D) solves the unsteady shallow-water equations in depth-averaged two dimensions in the discrete spaces of a computational grid using a finite difference numerical method (Deltares, 2018; Lesser et al., 2004). The governing equations of Delft3D-FLOW comprise the continuity equation, the horizontal equations of motion and transport equations [mass-balance] for conservative constituents. An overview of the equations is given in Appendix A.

6.2. Closure Relations

The key closure relations used in the model are described here. These relations are essential for accurately capturing the physical processes governing sediment dynamics and river morphodynam-

ics. The primary closure relations include the sediment transport formula, bed slope formulation, and hiding/exposure effects.

D3D offers numerous sediment transport predictors for various sediment types (cohesive/non-cohesive) and transport modes (suspended/bedload). This study will focus solely on the bedload transport of non-cohesive sediments in this system. Based on field observation, it is assumed that bedload material has a far more significant impact on morphological development than suspended transport. The Meyer-Peter and Müller (1948) formula was selected to be the sediment predictor in the model. This formula was chosen for its relative simplicity and comprehensive development, derived from flume experiments with sand and gravel fractions. This stands in contrast to some alternative predictors that are solely calibrated for sand. Note that no perfect sediment transport predictors exist for such coarse gravel found in the study area. The general form is as follows:

$$S = \alpha D_{50}\sqrt{\Delta g D_{50}}\theta^{b}\left(\mu\theta - \xi\theta_{cr}\right)^{c} \tag{6.1}$$

with α as calibration coefficient and powers b, c and ripple factor μ and critical Shields parameter θ_{cr} as user-defined parameters. Meyer-Peter and Müller (1948) experimentally arrived on the following values: $\alpha = 8$ $b = 0$, $c = 1.5$ $\mu = 1$ $\theta_{cr} = 0.047$.

The Koch and Flokstra (1980) formulation for the transverse bed slope effect has been introduced in Section 3.4. This formulation is used in D3D and enables the downward deflection of particles due to gravity pull. Delft3D adds two more functionalities to the $f(\theta)$ function, namely the relation of particle size (D_i) with water depth (H) and mean sediment diameter (D_m), see Eq. (6.2).

$$f(\theta) = A_{shld}\theta_i^{B_{shld}}\left(\frac{D_i}{H}\right)^{C_{shld}}\left(\frac{D_i}{D_m}\right)^{D_{shld}} \tag{6.2}$$

As shown in Table 6.2, the Bshld parameter is determined to be 0.5. This leads to that the function of θ becomes a function of $\frac{1}{\sqrt{D_i}}$ (Eq. (3.2)). Each fraction, therefore, has its own $f(\theta)$ function.

If a Dshld parameter is chosen of 0.5, this will cancel out the $\sqrt{D_i}$. Therefore, the gravity pull deflection will become equal for all fractions and proportional to D_m. Since low values from the function lead to a more substantial gravity pull effect, more particles will roll down the transverse slope towards the outer bend. When Dshld is at 0 (default), this will be stronger for the larger D_i fractions, but when the Dshld is at 0.5, this effect will be cancelled out. When the Dshld is increased above 0.5, the opposite effect is true; finer particles will be preferentially transported towards the outer bend.

Multiple formulations for hiding and exposure effects on sediment transport are available in D3D. This study has chosen for the use of the Parker et al. (1982) formulation due to its simplicity and intention for gravel bed streams. The formula is as follows:

$$\xi = \left(\frac{D_m}{D_i}\right)^{\alpha} \tag{6.3}$$

where ξ is used in Eq. (6.1) to alter the critical Shields' number depending on the particle size in question, D_i, relative to the mean diameter D_m.

6.3. Description of the Reference Model

6.3.1. Reference Model Criteria

Selecting a reference model in a system with countless parameter combinations can be challenging. When developing the reference model of the Karnali river bifurcation, several criteria were considered to be desired to ensure the model captures the relevant processes and has the potential to test various parameter studies and scenarios. These criteria are meant to keep the features of the river system that

were observed while recognizing that it is a highly simplified and schematized model. The following key criteria were incorporated into the model design:

- **Bend Radius**: The model includes the bend radius observed in the real river to capture the flow dynamics around bends accurately.
- **Slopes**: The longitudinal slopes in the model reflect the actual slopes found in the Karnali River, ensuring that the gravitational forces driving flow and sediment transport are realistic.
- **Geometry of Bifurcates**: The initial geometry of the bifurcate channels is desired to be equal, with widths and shapes inspired by satellite images and cross-sectional data collected from the field. This ensures that we can observe how the channel morphology changes with various without the effect of initial geometry differences.
- **Discharge distribution**: The model was designed to have a balanced discharge distribution over the branches, so the effects of parameter changes and scenarios can be compared to a relatively equal division (at least at the start of the simulation)
- **Hydrograph**: The input hydrograph should include both base monsoon flows and peak flows that reflect actual discharge in order of magnitude and duration of peak flow events as observed in the river (data from official Chisapani gauging station).
- **Sediment Classes**: All sediment classes observed in the field were included in the model to capture the full range of sediment dynamics, this includes sand, fine gravel, coarse gravel, cobbles and boulders.
- **Bend Sorting Effects**: The model should represent bend sorting effects, with coarser sediment in the outer bend and finer near the inner bank.
- **Hiding/Exposure**: The model incorporates hiding and exposure effects to simulate the interaction between different sediment sizes.
- **Transverse Bed Slope Gravity Pull**: The influence of gravity on sediment particles moving across the transverse bed slope should be included.

The model contains a large number of calibration parameters, which, as noted by Sloff and Mosselman (2012), could lead to issues of equifinality. This means that multiple combinations of parameter values may produce similar results. Throughout the construction process, attention was given to ensuring that the parameter values remained within a physically logical and realistic range. Additionally, no calibration or validation data is available for the Karnali system except for a single temporal snapshot collected during the field campaign. Therefore, we consider the model a schematized version of reality, allowing us to test the influences of specific processes under controlled conditions. Calibration with data from the system was thereby minimized.

6.3.2. Model Domain and Numerical Settings

Model Domain

To effectively test hypotheses regarding its partial closure, the bifurcation model must include upstream and downstream sections of the river. The selected model domain spans approximately 3 km upstream and downstream of the bifurcation. Fig. 6.1 show the grid on top of land boundaries. The domain starts at the point where the river enters its alluvial fan. While water partitioning occurs further North at locations BIF1 and BIF2, we focus on BIF3 as it was the dominant bifurcation point during the 2009 monsoon event and has been before that. The recent upstream and eastward flow increase at BIF1 and BIF2 is not directly relevant to testing the hypotheses regarding the Geruwa inlet closure.

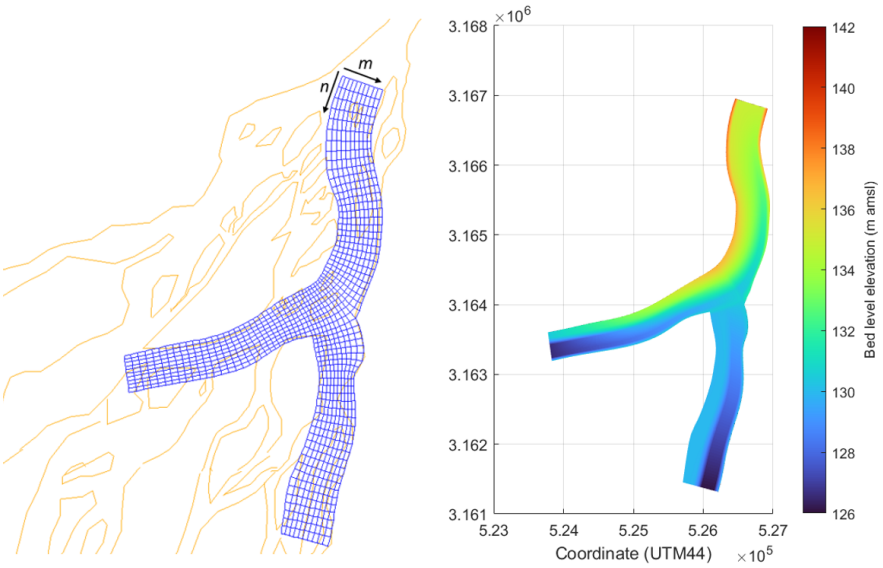

Figure 6.1: Left image shows the computational grid overlayed on the Karnali land boundaries (October 2023), m and n directions are shown. On the right, the initial bathymetry of the reference model is shown.

Computational Grid

The computational grid of the model features 10 grid cells across its width in all three sections and a maximum of 70 cells in the streamwise direction. It aims to balance accurate hydro-morphological calculations with computational efficiency. See the figure on the left in Fig. 6.1: the total grid consists of exactly 1000 cells, with grid sides varying between 40 and 110 meters. The cells are purposefully elongated in the streamwise direction for better stability (Deltares, 2005). The grid resolution is slightly finer at the bifurcation area to better capture dynamics relevant to hypothesis testing. Finally, cells were orthogonalized to minimize errors in computing the pressure term in D3D.

Morphological acceleration factor

Since morphological changes occur much slower than typical flow variations, simulation can take up significant computation times. To address this, D3D includes the option to apply a morphological acceleration factor (MorFac) to the hydro-morphological simulations. By multiplying bed-flow exchanges by MorFac at each step, the model simulates morphological evolution at an accelerated rate, effectively compressing the timescale and allowing faster capture of morphological changes. This essentially simulates morphology at a larger timescale than the hydrodynamics, for instance, 10x faster with MorFac 10. MorFacs over 1000 have remained computationally stable (Deltares, 2018). When using the MorFac, all other time-varying processes/boundaries (e.g., hydrograph) must be adjusted accordingly. Large MorFac could change the nature of hydrodynamic events, for example it compresses a flood periods to very short flood peaks, therefore results should always be compared to runs with no or low factors.

We employ morphological acceleration factors of 10 and 100 to reduce computational time while ensuring model stability. This allows us to efficiently simulate 60 monsoon seasons using a MorFac of 100. MorFac 100 has been tested and compared to results from MorFac 10, and similar results came from the model. Therefore, it was chosen to be suitable.

Time Frame and Time step

We aim to observe how the bifurcation develops and responds to setup changes over time. The assumption is that most morphological changes occur during the monsoon season. Therefore, only the monsoon period is modelled. An average monsoon period spans from June to September, lasting 3-4 months. The model duration of each season was set to 100 days as this is easily scalable with the morphological acceleration factor. With a MorFac of 10, six monsoon seasons of 100 days can be simulated with a 'real' simulation time of 60 days, corresponding to a computer runtime in the order of

3 hours. To investigate the longer-term stability of the bifurcation, the majority of presented runs were conducted with a MorFac of 100, extending the simulated period to approximately 60 years.

The timestep should be small enough to capture the relevant changes in the modelled processes. Within a single timestep, numerical information (like a wave, bed disturbance, etc.) should not propagate further than the grid cell length. A minimum time step of 26 seconds was determined for the model; however, a time step of 12 seconds (0.2 min) provides superior stability. More information is available in the appendix Appendix A.

Sediment Layer Thickness

To effectively calculate sediment interaction, a layered sediment approach, similar to Hirano (1972), can be used in D3D (Sloff & Mosselman, 2012). By defining an active layer in which the model will calculate sediment interaction and transport, instead of having one very thick layer of mixed sediment where the model would stir up the entirety, it now calculates with the first meter. The model can only interact with sediment located in the active layer, where sediment is initially perfectly mixed. Bed level changes result in vertical sediment mixing between the layers underneath the active layer per cell (Buis, 2023). The reference model employs a total of five layers with a 1-meter thickness.

6.3.3. Initial Conditions and Closure Relation Settings

Bathymetry and slope

Cross-sectional data from the field campaign informed the initial bathymetry construction. Satellite imagery from monsoon periods is rare due to the constant cloud coverage. However, at one instance in September 2019, it was possible to extract river widths at a total discharge of 2790 m^3/s (Chisapani gauging station data), see also Fig. 6.4. These widths were then used to calculate the equilibrium depths at the downstream boundaries. The initial morphological state was constructed within the D3D suite. While simplified due to the absence of extensive bathymetric surveys, the actual river bed was loosely represented whilst preserving the significant features. Field data was crucial for determining channel depth, slope and shape within the bifurcation zone, including upstream and downstream boundaries. The initial bathymetry is found on the right in Fig. 6.1. The longitudinal profile of the system is shown in Fig. 6.2.

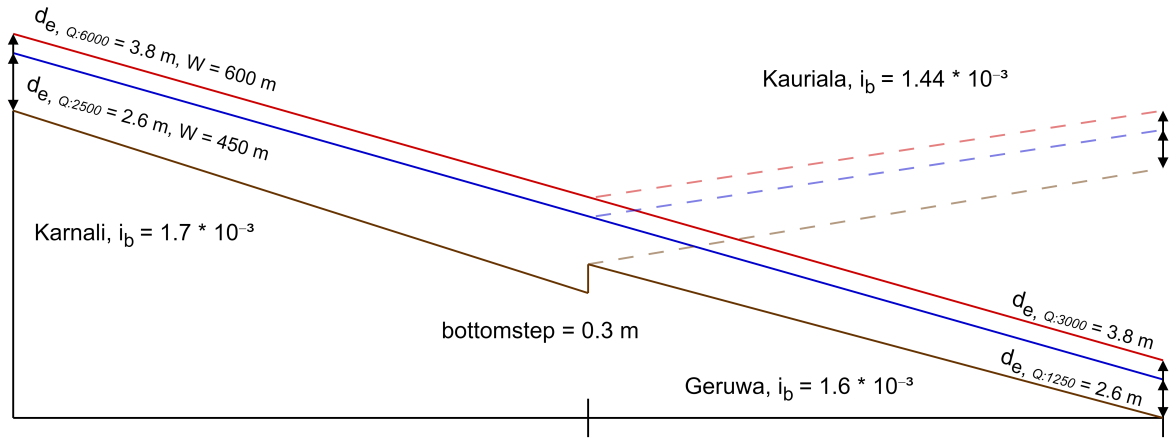

Figure 6.2: Initial longitudinal profile of the system. Section slope, width and corresponding equilibrium depth are added.

Using RTK GPS data, the river slope before the bifurcation is set to $1.7 * 10^{-3}$, and the slopes of the Kauriala and Geruwa were initially set to $1.6 * 10^{-3}$. The slope of the Kauriala branch in the reference model was given a slope disadvantage of 10% compared to the Geruwa. The resulting difference between the upstream and downstream bed levels is 9.6 meters for the Geruwa and 9.1 meters for the Kauriala. The reason for the slope disadvantage is the fact that from field measurement, the Kauriala seems to have a gentler slope than the Geruwa branch, especially seen between 12 and 30 km in Fig. 3.3. Even though the part of both branches showcased a similar slope right after the bifurcation

during the 2023 measurements, the slope of the Kauriala likely underwent erosion and steepening while the discharge distribution shifted after 2009. Runs with equal slopes and slope advantage of the Kauriala will also be presented later.

Bed Surface Grain Size Composition

The model employs five grain size fractions to represent the sediment: 1 mm (sand), 2 cm, 5 cm (gravel), 10 cm (cobbles), and 40 cm (boulders). This discretization aims to capture the full range of observed sediment sizes. The volume fraction in the active and underlayers is shown in Table 6.1. The bed composition of the floodplain is assumed to be similar to that of channels.

Sediment size	1 mm	2 cm	5 cm	10 cm	40 cm
Volume fraction in sediment layers	0.22	0.22	0.22	0.22	0.11

Table 6.1: Sediment size and volume fraction.

Roughness

Bed roughness can be defined using either Manning or Chézy coefficients. The Manning system was chosen for this study due to the broader availability of reference studies reporting Manning roughness coefficients in gravel-bed rivers (e.g., Chow (1959), Barnes (1967)). The USGS guide (Arcement and Schneider (1989)) was used to determine an approximate Manning coefficient of 0.035 [s/$m^{1/3}$]. While maximum velocities during peak discharge remain under 4.5 m/s, which seems appropriate for the system, the lack of flow velocity data during monsoon periods limits the ability to validate this choice fully.

Sediment Transport Predictor Setting

During initial runs with MPM coefficients in Eq. (A.13), minimal to no mobility of the coarsest sediment class was observed. Consequently, the critical Shields' parameter (θ_{cr}) was adjusted to 0.040, effectively reducing the threshold for mobility for all sediment fractions. Subsequent simulations (not presented here) involved a further reduction of the threshold θ_{cr} until reaching 0.025, a value previously used by Sloff and Mosselman (2012) following calibration of the Rhine model in conjunction with $\alpha = 5$. However, it was determined that the value of 0.040 proved adequate in facilitating the mobility of the coarse material. The complete set of parameters utilized in the general formula is as follows: $\alpha = 8$ $b = 0$, $c = 1.5$ $\mu = 1$ $\theta_{cr} = 0.040$.

Transverse Downslope Transport Settings

The transverse bed slope effect plays a critical role in morphodynamic models. However, it is often not explicitly stated in the literature. For this study, we draw inspiration from the settings used in relevant studies (see Table 6.2). Baar et al. (2019) reveals that 60% of the literature concerning morphodynamic models fails to mention the bed slope effect setting despite its significance. In line with most studies, the parameter (B_{shld}) is commonly set to 0.5 and will, therefore, remain constant in this study, effectively reducing one degree of freedom.

Tranverse bed slope setting in literature	A_{shld}	B_{shld}	C_{shld}	D_{shld}
Struiksma et al. (1985)	0.4, 1.5, 4	1	–	–
Talmon et al. (1995) (fair agreement with flume experiments)	1.7	0.5	–	–
Talmon et al. (1995) (reasonable for natural rivers with bed load transport)	9	0.5	0.3	–
Sloff and Mosselman (2012)	1.5	0.5	–	–
Schuurman et al. (2013)	0.35–1.5	0.5	–	–
Schuurman and Kleinhans (2015)	0.7	0.5	–	–

Table 6.2: Transverse bed slope settings in the relevant literature.

A complete list of the parameters used in the reference model can be found in Appendix B.

6.3.4. Boundary conditions

Upstream Boundary conditions

The upstream boundary is defined as total discharge. The input hydrograph substantially simplifies the natural patterns but maintains the order of magnitude of the discharge regime. See Fig. 6.3 for the actual hydrograph from the Chisapani Gauging station and the model input.

- Base Monsoon Discharge: 2500 m^3/s
- Peak Discharge: 6000 m^3/s (lasting 10 days per season, scaled accordingly with MorFac)

The base monsoon discharge was chosen based on observations from satellite imagery (see Fig. 6.4). The model domain covers approximately $\frac{2}{3}$ of the width of the incoming channels. A discharge of 2500 m^3/s appears to be of the same order of magnitude as $\frac{2}{3}$ of the discharge at the Chisapani Gauging Station. This peak discharge estimation is also based on observed data from the gauging station (excluding the 2009 season) and aims to represent a typical yearly flow extreme within the model domain. In Fig. 6.3, we can observe a peak discharge between 7000 and 9000 m^3/s in the years before and after 2009 (excluding the 2009 season). The figure includes the simplified model input hydrograph in red and the double peak scenario in purple. Fig. 6.4 shows the flow distribution during monsoon discharge. Fig. 6.5 show the input hydrographs in the constructed model. The peak discharge will increase the amount and coarseness of the incoming sediment in the D3D model.

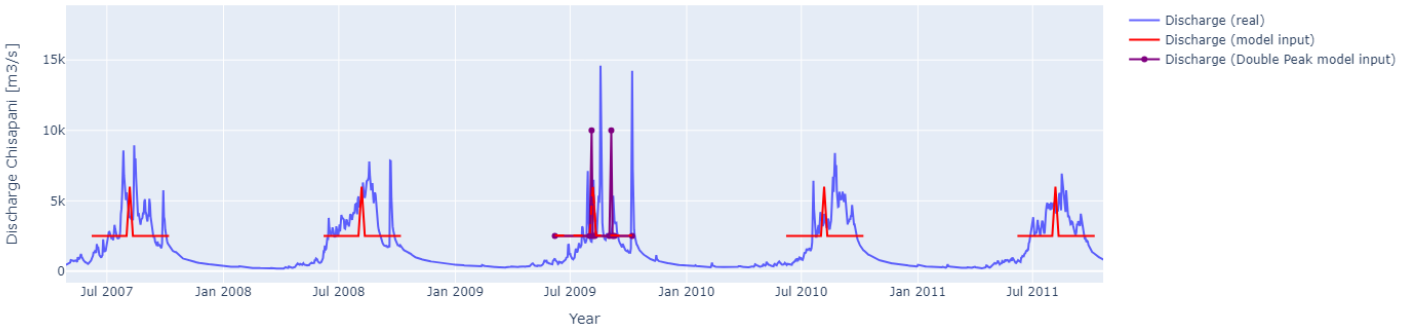

Figure 6.3: Discharge, Chisapani gauging station data and model input simplification, from 2009 and surrounding years. Note the two distinct peaks of high intensity.

Figure 6.4: Model Domain on top of Sentinel image from 11-09-2019 when 2790 m^3/s was measured at the Chisapani gauging station.

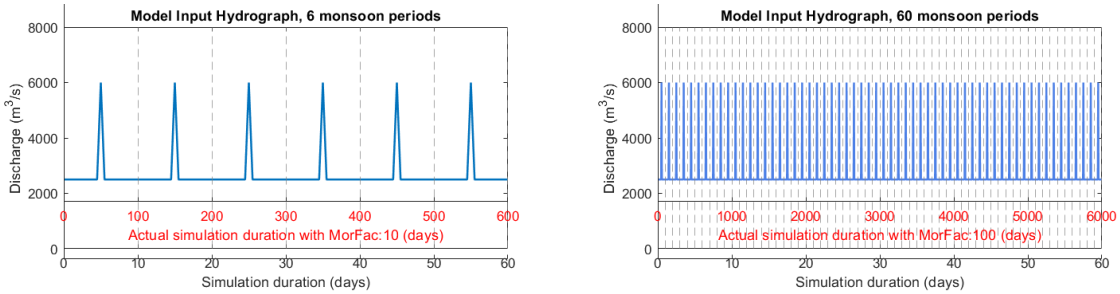

Figure 6.5: Model Input hydrographs for (left) 6-year simulation period and (right) 60-year simulation period. The dashed vertical lines indicate the different years.

The reference model will be tested with a discharge input similar to the 2009 flood. During that monsoon season, there were two large flood peaks with discharges of over 14000 m^3/s registered at the Chisapani gauging station, see Fig. 6.3. The duration of both peaks was similar at around 5 days. During these runs, the 10th monsoon season will be replaced to accommodate two 10000 m^3/s (since part of the discharge will bypass the model domain) of 5 days.

Downstream Boundary Conditions

Downstream boundaries were set as fixed water levels. Ideally, we let the model calculate the downstream water levels, but a downstream boundary is required. D3D has options for defining a Q/H relationship. However, this only works with the discharge of the upstream boundary. Implementing a Q/H relationship based on the discharge of each separate channel is impossible. The downstream cross-sections were made equal in shape, with the width inspired by the satellite imagery and field observations. The imposed water levels were the equilibrium depths based on a width of 225 meters for upstream discharge of 2500 m^3/s and 300 meters width for 6000 m^3/s, see Fig. 6.2.

The backwater adaptation length estimation ($L \approx \frac{d_e}{3 \cdot i_b}$) is, in this case, in the order of 500 meters. Therefore, the effect of the imposed water levels on the water levels at the bifurcation (located 2800 meters from downstream boundaries) is minor.

The downstream boundary conditions are crucial for imposing changes at the bifurcation. They allow us to test different downstream scenarios and observe their effect on the bifurcation. Equally important is observing how the area downstream of the bifurcation develops in response to these changes.

6.4. Model Testing

The reference model is tested with both MorFac 10 (6 monsoon seasons) and 100 (60 monsoon seasons. All other model runs are done for 60 monsoon seasons to see the longer-term morphological developments. The reference model is also run with a double peak flow discharge scenario, as shown in the hydrograph in Fig. 6.3.

Parameter study

A parameter study or sensitive analysis is performed based on the reference model with the hydrograph varying from 2500 to 6000 m^3/s. See Table 6.3 for the selected parameters and their respective ranges.

Parameter	Value Range	Reference Value
Spiral Flow Intensity ($Espir$)	0 - 2	1
A_{shld}	0.4 - 1.3	0.7
D_{shld}	0 - 1.0	0
Active Layer Thickness	0.5 - 2.0 meters	1 meter
Hiding/Exposure Coefficient (α)	0 - 0.982	0.8

Table 6.3: Parameters used in parameter study, their value ranges for the model run, and reference values.

It is hypothesized that the spiral flow intensity influences bend sorting effects by allowing preferential

transport of the finer fraction to the inner bend. The bedslope formula parameter runs (A_{shld} and D_{shld}) will affect the downslope deflection of sediment particles travelling in a streamwise direction, allowing for the formation of steeper or gentler transverse slopes. Varying the active layer thickness will allow us to see the role of sediment interaction on morphological development. Furthermore, varying the hiding exposure power parameter (Eq. (6.3)) will allow us to check the effect of hiding exposure on the mobility of the 40cm fraction and the consequences on discharge distribution.

Scenario runs

Various scenarios were implemented in the model, see Table 6.4. Firstly, we will look at the effect of an abnormal monsoon peak flow with double discharge peaks. Comparing mixed-size sediment runs to those with uniform sediment (identical D50), sand-excluded runs, and coarse fraction-excluded runs will reveal the role of sediment sorting in bifurcation evolution and the role of sediment supply per fraction on morphological development. Increasing the slope of the Kauriala and forcing initial sedimentation in the Geruwa will allow for the testing of hypothesis 2.

Scenario	**Variations**
Discharge	2500-6000 m^3/s (reference) 2500-6000 m^3/s, with double flood peak of 10000 m^3/s
Changes in Sediment Composition	Uniform (D_{50}) Sand-excluded Coarse fractions-excluded
Steepening of Kauriala Branch	Equal slopes 10% slope advantage 20% slope advantage
Initial Sedimentation in Geruwa Branch	25 cm 50 cm 100 cm

Table 6.4: Scenario runs and their variations for the model.

7

Results of Numerical Model Runs

This chapter presents the results of the numerical model, investigating the morphological evolution of the Karnali bifurcation. Results directly addressing the hypotheses about the partial closure of the Geruwa branch have been selected. The analysis will focus on:

- Discharge and Sediment Partitioning: How the distribution of water and sediment between the Geruwa and Kauriala branches changed over the 60-year simulation.
- Morphological Change: The identification of erosion and deposition areas and the evolution of these patterns over time.
- Sediment Sorting: How the grain size distribution evolved within the bifurcation, providing insights into bend sorting processes.

The chapter will begin with the reference model run analysis to establish the baseline results. Sensitivity analyses will then reveal how changes in key parameters affect the discharge distribution between the Geruwa and the Kauriala branches. A comprehensive overview of bed level changes for each run can be found in Appendix C.

7.1. Reference Model Analysis

The metrics mentioned above are plotted for the reference model in Fig. 7.1. The plot in the top-left corner displays the ratio of sediment and discharge for the entire system entering the Geruwa branch, which will also be used in subsequent graphs within this chapter. The y-axis label, 'Ratio Geruwa', represents the proportion obtained by dividing the sediment and discharge entering the Geruwa branch by the sum of the entering sediment and discharge in both bifurcates. In plot (a), a steady decline in the discharge fraction entering the Geruwa branch over the 60-year model run is observed. This suggests a progressive decrease in flow towards Geruwa relative to Kauriala, while the Kauriala receives a disproportional amount of sediment. However, it can also be observed that directly after the morphological spin-up time, when the sediment starts to become mobile, all sediment enters the Geruwa (initial peak of the blue line in top left Fig. 7.1). The top-right D50 distribution plot indicates that sand dominates the top layer of sediment depositions in the Geruwa branch and less presence of the coarse fractions.

The bed level change compared to the initial situation shows a large sedimentation hump at the bifurcation of around 4.5 meters in height, the development of this hump can also be seen in the longitudinal cross-section of the Geruwa branch. After 30 simulation years, the discharge is divided relatively equally and passes along the Eastern flank of the Geruwa branch, where it has eroded that side. Deposition dominates in the Geruwa branch, particularly in the upstream section. The Kauriala channel has undergone minimal erosion and seems to be more or less stable. The upstream bend before the bifurcation has experienced much erosion in the outer bend and some sedimentation in the inner bend, mainly consisting of the sand fraction. After 60 years, sediment deposition partly counteracted the previous erosion in the Geruwa branch, and more erosion occurred in the Kauriala. Please refer to Fig. C.1 for the bed level change plots for each decade.

The bottom two plots show the evolution of the bed level (longitudinal profiles) in all branches. The black line represents the initial bed level, whereas the blue line represents the initial water level.

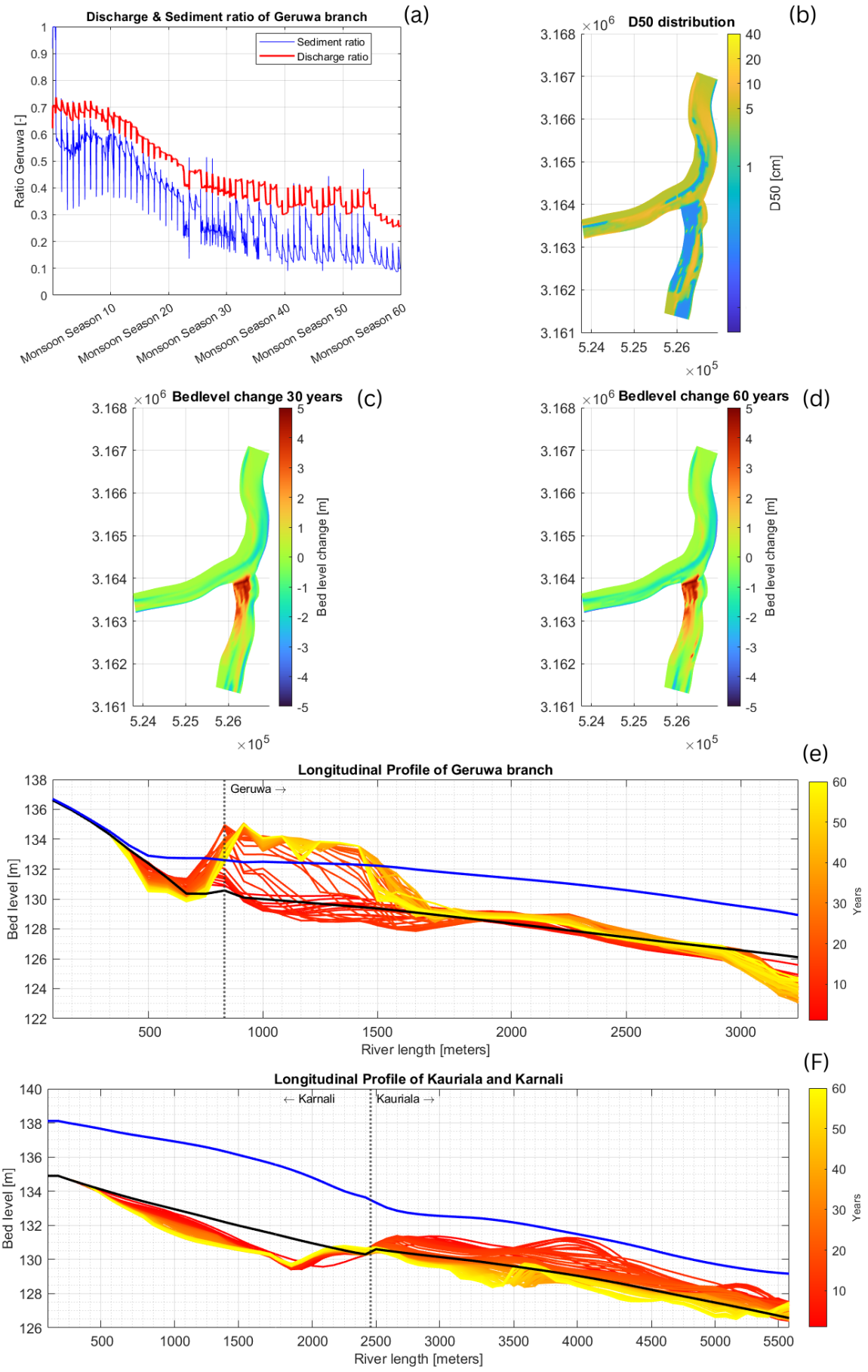

Figure 7.1: Results of the reference model. (a) The ratio of total discharge and sediment flux entering the Geruwa branch. (b) Sediment grain size distribution of the bed surface after the simulation period. (c) and (d) Cumulative erosion and deposition after 30 and 60 years. (e) and (f) the longitudinal profiles of all three branches and their development during the simulation period.

Fig. 7.1 subfigures (e) and (f) show the evolution of the longitudinal profiles. The location of these profiles is shown in Fig. 7.2.

In the longitudinal plot of the Geruwa (Fig. 7.1 (e)), we see initial erosion downstream of the bifurcation. This area then quickly starts aggrading, and the differently coloured lines in the longitudinal profiles represent the bed level per year. This profile also shows the deep erosion at the downstream end of the Geruwa branch, which later reduces in depth. In the bottom profile (f), the Kauriala branch initially aggregated significantly and then started eroding, coming close to the initial bed level at the end of the 60-year simulation. A significant erosion hole emerged quickly just before the bifurcation and slowly moved upstream over the years.

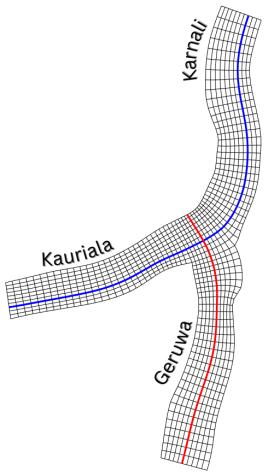

Figure 7.2: Coloured lines in the grid indicate the location of the longitudinal profiles presented in Fig. 7.1 and Fig. 7.3. Blue: Karnali and Kauriala, Red: Geruwa.

The criteria used when constructing the model, presented in Section 6.3.1, are mostly met. The bend radius, slope, input hydrograph and sediment classes incorporated in the model match well with the field data and satellite imagery observations. The initial geometry of the channels has been simplified so that the model can develop its geometry during the computations. The depth of the thalweg and transverse slopes (channel and part of floodplains) are in correspondence with reality. The reference model bend sorting criteria are partially met (Fig. 7.1 (b)), fine sediment deposition in the inner bed is found and coarser near the outer bank before the bifurcation. However, the deposition at the Geruwa branch's entrance primarily consists of finer fractions. This is an undesirable model result as it does not align well with the field observations or hypothesis.

These results provide a foundation for further analysis. The following sections will explore how sensitive the model is to changes in specific parameters and how these changes affect the closure process.

Morphological Evolution with Double Flood:

A more drastic discharge and sediment distribution change is observed when a double extreme flood event is introduced in the 10th monsoon season, with a similar duration and magnitude as the 2009 flood peaks. Results are shown in Fig. 7.3. The double flood event accelerates the closure of the Geruwa branch, compared to the reference run with constant peak flows. In this scenario, the Geruwa closes in order of 30 years after the double peak flood event(Fig. 7.3 (a)). See Fig. C.2 for decadal bed level changes. In the D50 plot (b), an accumulation of coarse material can be seen downstream of the start of the Kauriala branch.

In the 30-year bedlevel change plot (c), we can observe an increase of erosion near the upstream boundary, in the middle of the Karnali branch before the bifurcation, near the downstream boundary of the Geruwa and along the Eastern flank. After 60 years (d), the Geruwa is nearly completely aggraded and does not convey any discharge except during peak flows. Again, the sand fraction is dominant in the top layer of the aggradation, which does not match field observations.

The Kauriala has eroded to increase its capacity to transport all the incoming water and sediment. This is well visualized in the longitudinal plots (Fig. 7.3 (e) and (f)), where the Kauriala is initially aggregated just like in the reference run, but then erodes quickly, significantly below the initial bed level. The Geruwa seems to develop a large hump at its downstream end.

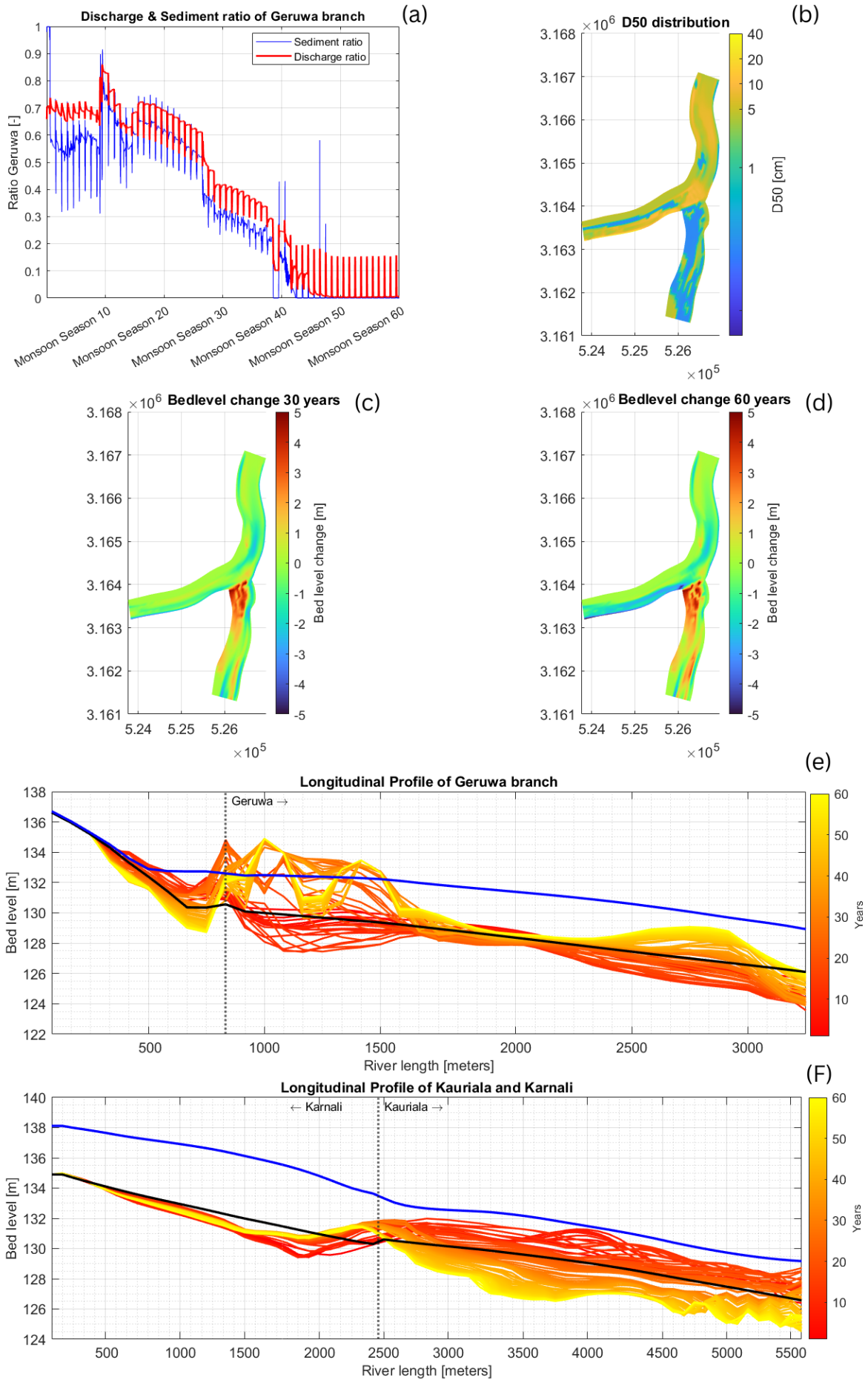

Figure 7.3: Results of reference model with double flood peak on the tenth year. (a) The ratio of total discharge and sediment flux entering the Geruwa branch. (b) Sediment grain size distribution of the bed surface after the simulation period. (c) and (d) Cumulative erosion and deposition after 30 and 60 years. (e) and (f) the longitudinal profiles of all three branches and their development during the simulation period.

When the sediment transport per fraction of the 10th monsoon season is plotted, we can compare the difference between the branches and the effect of the double flood peak, see Fig. 7.4. The bottom row shows the increased sediment discharge at 10000 m^3/s. The figure illustrates that during the double peak flow event, the bedload transport of coarser fractions is significantly higher in the Geruwa branch than in the Kauriala. For instance, the transport of the 10 cm fraction in the Geruwa is four times greater during peak discharge. It is also apparent from these graphs that during normal monsoon discharge, only the sand fraction is mobile in the model. In the reference case, no movement of the boulder fraction was detected, although there is some mobility of this fraction in different monsoon peak flows (not shown here). In the double flood peak run, the boulders are mobile in both branches yet almost double the amount in the Geruwa branch. An important takeaway is that virtually all sediment transport of the gravel, cobble and boulder fractions occurs during the peak flow conditions. The duration and magnitude of the peak are, therefore, very impactful on morphological development.

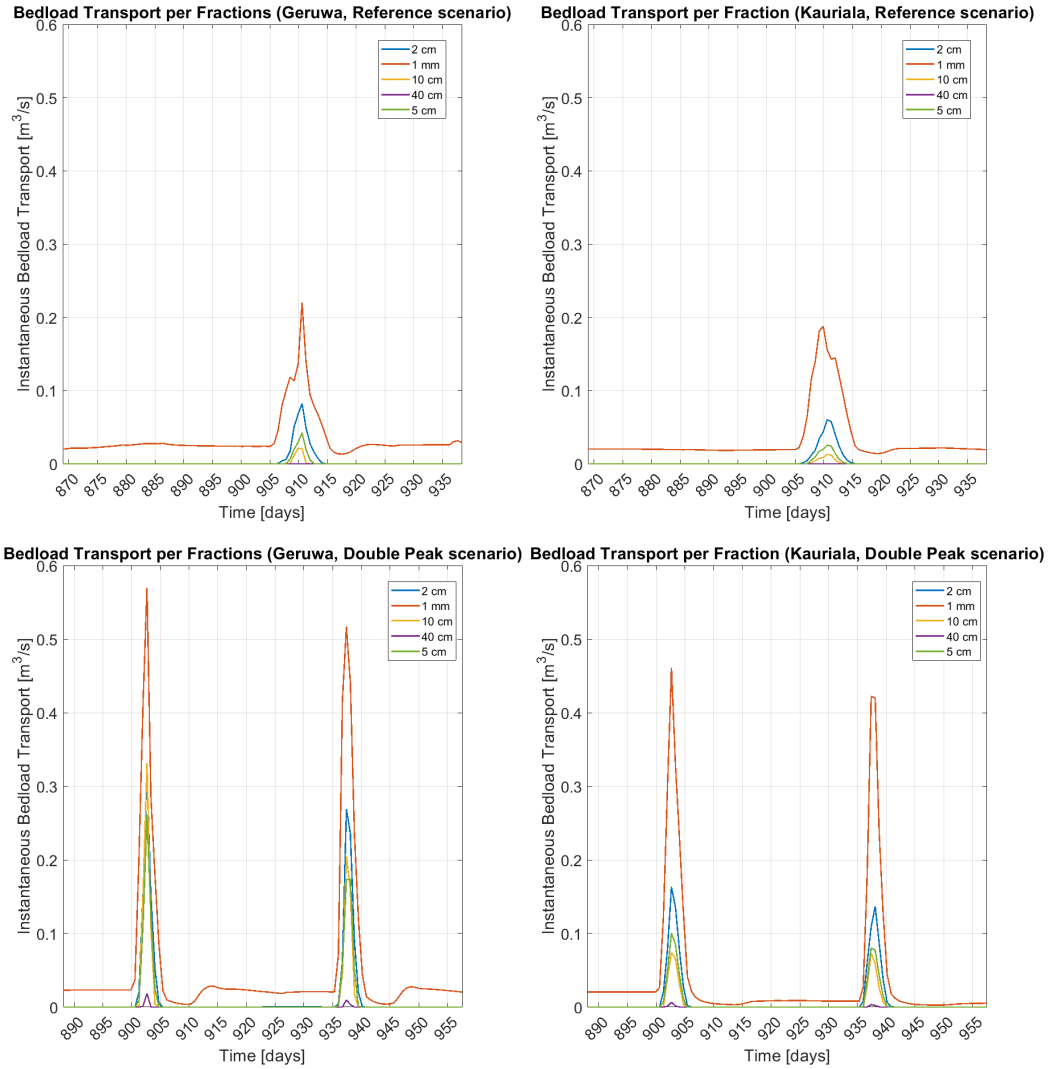

Figure 7.4: Bed load transport of each fraction. Top row, 10th monsoon season of reference model. Bottom row; 10th monsoon season during the double peak scenario

7.2. Results of Sensitivity Analysis

This section explores how varying key model parameters affect the discharge distribution between the Geruwa and Kauriala branches.

Spiral Flow Intensity

The effect of varying the spiral flow parameter on the resulting discharge distribution is shown in Fig. 7.5. Increasing the spiral flow component results in a substantial shift of the discharge distribution towards the Geruwa due to the near-bed transverse component of the spiral flow directing sediment towards the innerbend (Kauriala branch). The sediment exceeds Kauriala's transport capacity, leading to deposition and eventual closure of the branch. This results in strong erosion and flow preference in the Geruwa. The opposite is true when spiral flow is deactivated in the calculation. Sediment enters the Geruwa in the outerbend and exceeds its transport capacity, causing its closure and erosion of the Kauriala. The decadal bed level change can be found in Appendix C Fig. C.4 and Fig. C.3.

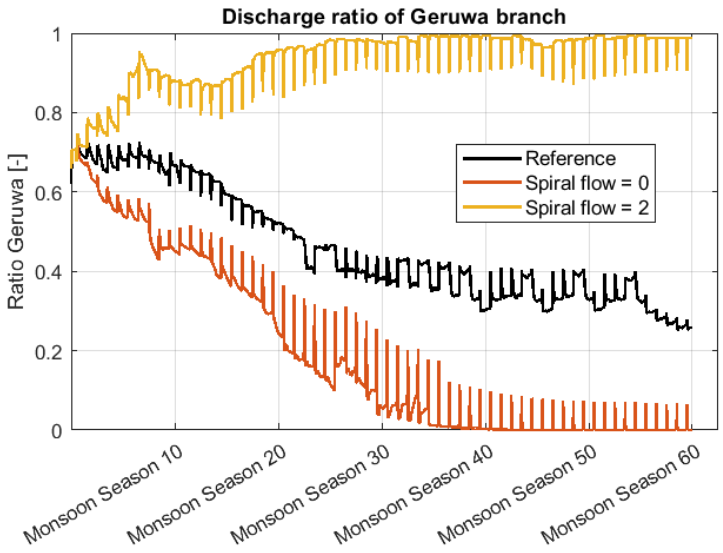

Figure 7.5: Discharge distribution with varying spiral flow intensities.

The difference in sediment composition at the end of the simulation can be seen in Fig. 7.6. It is visible that the increased magnitude of the spiral flow leads to finer material entering the Kauriala branch. Patches of very coarse composition can be found in the Geruwa channel. The opposite is true when the spiral flow is not considered; fine particles will travel straight and, together with the other fractions, clog up the Geruwa branch.

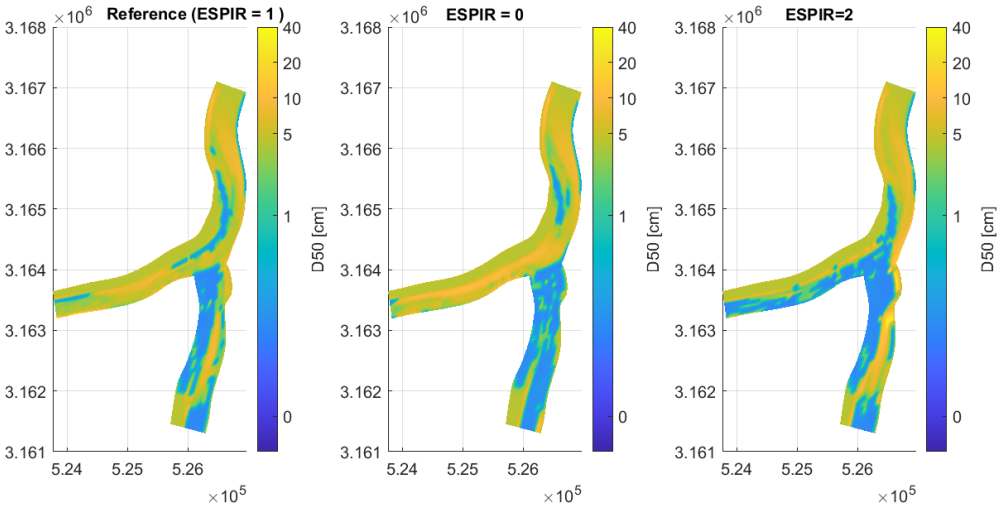

Figure 7.6: D50 distribution of the model runs with different spiral flow (ESPIR) magnitudes.

Bedslope Parameters

The effect on discharge distribution of varying Ashld parameter values is shown in Fig. 7.7. Interestingly, an increase in discharge distribution towards the Geruwa for each Ashld parameter value is observed. With a value of 0.4, the ratio in the first ten years is very similar to the reference model, and after that, it remains relatively stable. With higher Ashld values than the reference model, 1.0 and 1.3, the flow partitioning more strongly favours the Geruwa. In Fig. C.6 and Fig. C.7, it is shown that the sedimentation hump, starting from the bifurcation, travels upstream and the Kauriala aggrades completely. The increase and decrease in bed level are more significant than with smaller Ashld parameter values. Higher Ashld values correspond to the ability to form steeper slopes since the effect of secondary flow on (upslope) sediment deflection becomes relatively more dominant (see Eq. (3.6)). This leads to more sediment transport into the Kauriala, similar to the runs with increased spiral flow intensity, aggrading the branch. Surprisingly, the lowered Ashld run also led to less water entering the Kauriala.

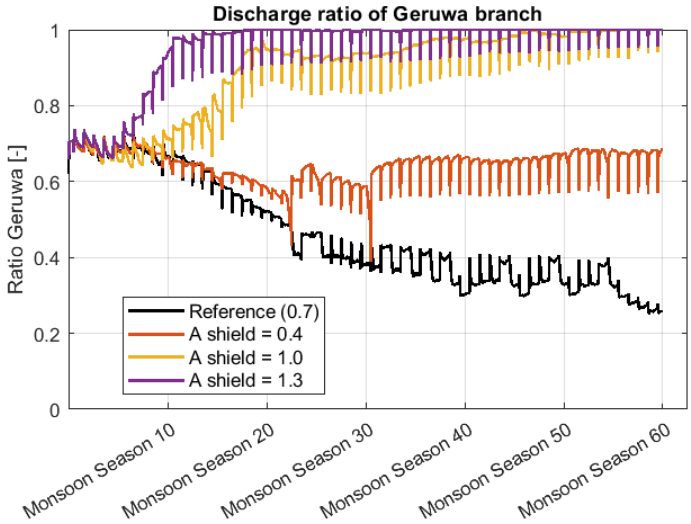

Figure 7.7: Discharge distribution with Ashld parameter values.

Modifying the Dshld parameter, which affects the gravity pull component according to sediment fraction size in relation to the mean sediment size within the bed slope formulation, significantly influences the distribution patterns (Fig. 7.8). In the case of 0.5 value, in which the gravity pull function is equal for each fraction (see Section 6.2), strong erosion in the Geruwa branch occurs. With a value of 1.0, abnormally high erosion is witnessed which does not seem realistic. See Fig. 7.9 for how this parameter influences the grain sizes in the branches.

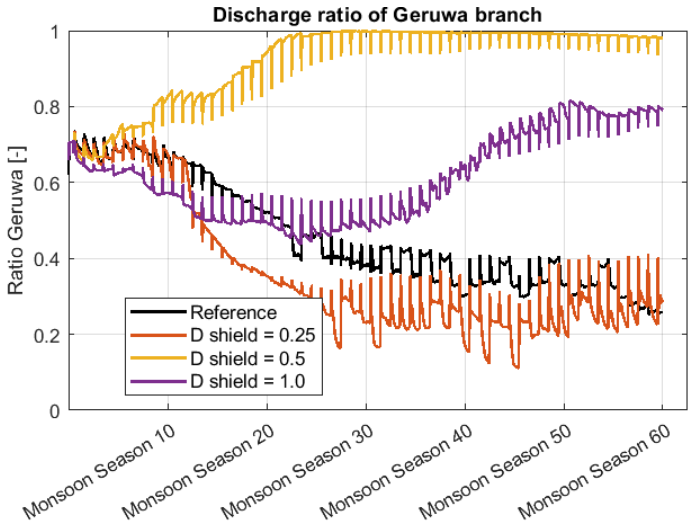

Figure 7.8: Discharge distribution with various Dshld parameter values

Increasing the parameter value significantly coarsens the bed-level composition of the Geruwa branch. Patches of boulders arise when the parameter is set to 1.0. The innerbend, which contains fine material in the reference model, is coarsened with each increase of the Dshld parameter.

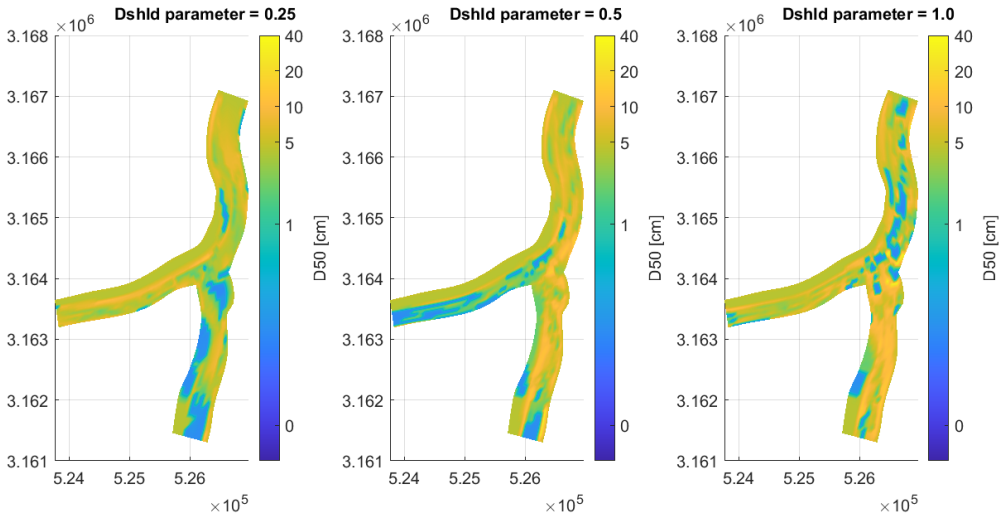

Figure 7.9: D50 distribution of the model runs with Dshld coefficient values

Effect of Active Layer Thickness

The active layer thickness, where sediment interaction and transport calculations occur, significantly influences morphological development in the model. This sensitivity is particularly evident for sorting processes affected by the hiding/exposure formulation. For example, the active layer composition affects sorting processes due to the hiding and exposure formulation. If this layer is thin, these processes can occur more rapidly. In the reference model, the active layer is set to be 1.0 meters in thickness, the model is also run with a layer thickness of 0.5 and 2.0 meters, see Fig. 7.10. There it can be seen that a change in thickness significantly influences discharge distribution and morphological development, see also Fig. C.15 and Fig. C.16. The thickness reduction results in smaller erosion and deposition numbers and develops a reasonably stable bedform. The 2.0-meter model run intensifies aggradation within the Geruwa branch, ultimately leading to its complete closure.

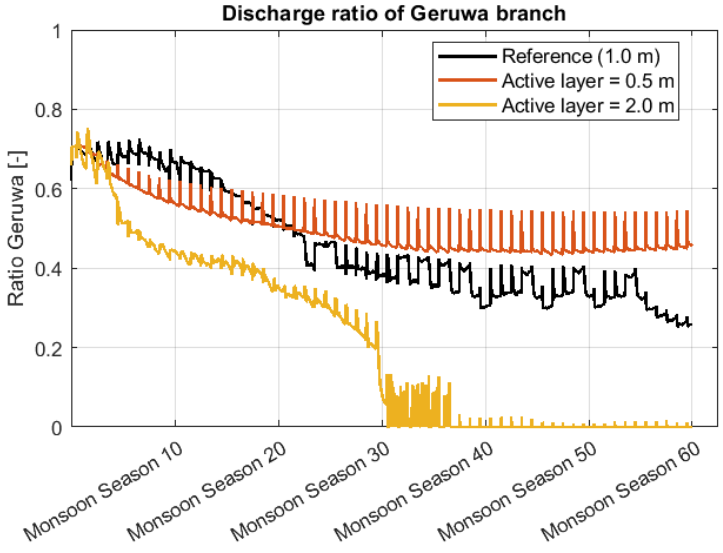

Figure 7.10: Discharge distribution with different active layer thickness.

The D50 distribution in the 0.5-meter active layer model reveals a key finding (Fig. 7.11): coarser material accumulates at the outer bend. This aligns better with field observations than the reference model or the 2-meter thickness scenario. The faster interaction between sediment fractions in a thinner active layer influences the sediment supply. Fine particles are quicker to hide, and coarse particles are exposed more rapidly. The effect of changing the active layer thickness has, therefore, similarities with altering the hiding/exposure magnitude. The interaction is slowed down when the model has a thicker active layer. This results in more fine sediment being mobile and coarse fractions being immobile. The decadal bedlevel change can be found in Fig. C.15 and Fig. C.16.

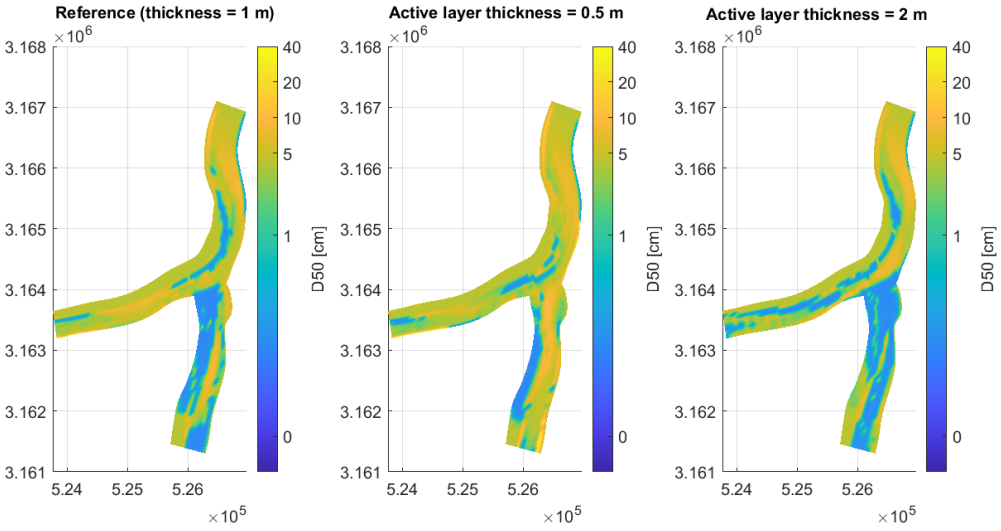

Figure 7.11: D50 distribution of the model runs with various active layer thicknesses.

Hiding/Exposure Magnitude

Fig. 7.12 demonstrates an apparent sensitivity to the hiding/exposure coefficient within the model. The rate of channel closure varies significantly based on this parameter.

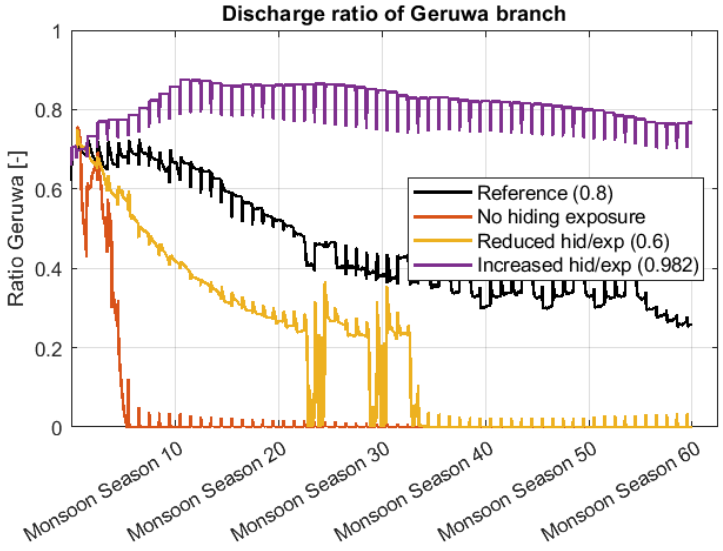

Figure 7.12: Discharge distribution with different Hiding/Exposure coefficient, see Eq. (A.14).

A lower magnitude leads to channel abandonment after 33 seasons, whilst without any hiding exposure, the Geruwa gets abandoned after only seven seasons. Increasing the component to 0.982, as determined by Parker and Andrews (1985), leads to a discharge preference for the Geruwa branch. The decadal bed level evolution can be found in Fig. C.24, Fig. C.25 and Fig. C.26. With reduced hiding/exposure, the finer sediment supply is increased significantly and consequently, the final sediment distribution is significantly finer, as can be seen in Fig. 7.13.

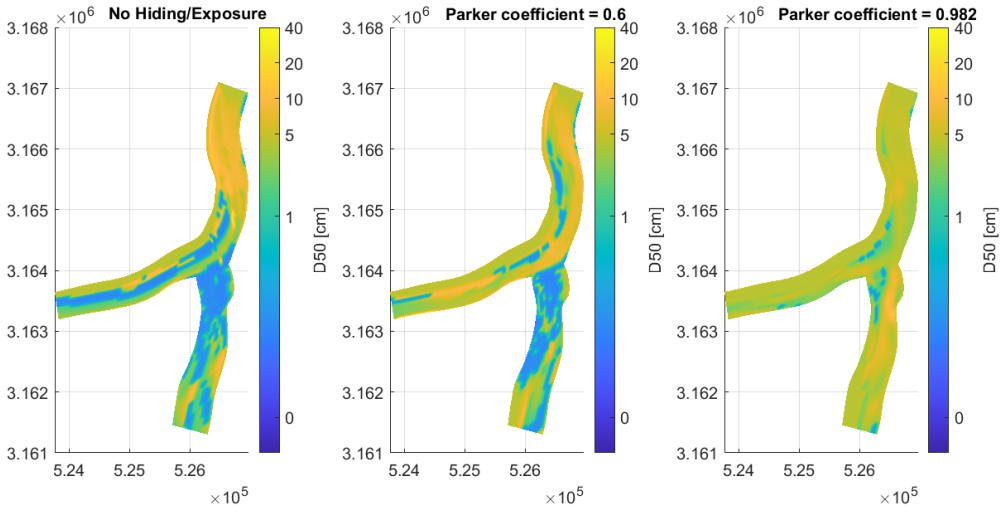

Figure 7.13: D50 distribution of the model runs with hiding/exposure coefficients.

7.3. Results of Model Scenarios

Results of runs excluding certain sediment fraction

The model was run without the coarse material (cobbles [10 cm] and boulders [40cm]) and once without the finest sand [1 mm] fraction. The resulting effect on the discharge distribution is shown in Fig. 7.14

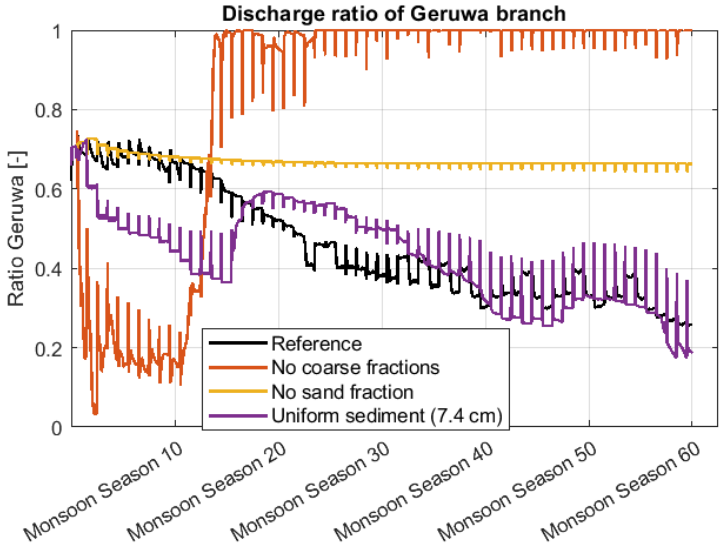

Figure 7.14: Discharge distribution with different sediment compositions.

Significant differences in discharge distribution result from the change in sediment composition. Without cobbles and boulders, an initial Kauriala preference quickly shifts to complete Geruwa domination. Morphological evolution (Fig. C.14) shows upstream-migrating deposition in the Kauriala and enhanced meandering with deep scour holes in the Geruwa. Spiral flow towards the innerbend transports the larger supply of the finer fractions, compared to the reference model, towards the Kauriala in the innerbend, leading to aggradation. The innerbank deposition grows so wide that it completely blocks the Kauriala entrance, resulting in the abrupt flow distribution change towards the Geruwa after 11 monsoon seasons.

When sand is removed from the model input, the distribution is remarkably stable at $\frac{2}{3}$ of flow going into the Geruwa. The morphological evolution can be found in Fig. C.13, where the bed level change remains virtually the same for each decade. Without sand, virtually no bedload material is transported in the model during base monsoon flow (see Fig. 7.4), and therefore, bed level changes are much reduced.

Slope change Kauriala

The model's response to Kauriala slope adjustments (bed and water levels) are shown in Fig. 7.15. Surprisingly, in the case that the Kauriala's slope is steepened to be equal to the Geruwa's slope (from $1.44 * 10^{-3}$ to $1.6 * 10^{-3}$ the eventual discharge fraction into the Geruwa is increased. Increasing the slope to $1.76 * 10^{-3}$ only leads to a slight favour of the Kauriala compared to the reference run. A further slope increase to $1.92 * 10^{-3}$ leads to a significant change in distribution, but no complete channel abandonment is observed. The model's sensitivity to slope change seems to be limited. In these runs, during peak flow, the Geruwa receives a higher fraction of discharge than during base monsoon flows, in line with Fig. 5.3.

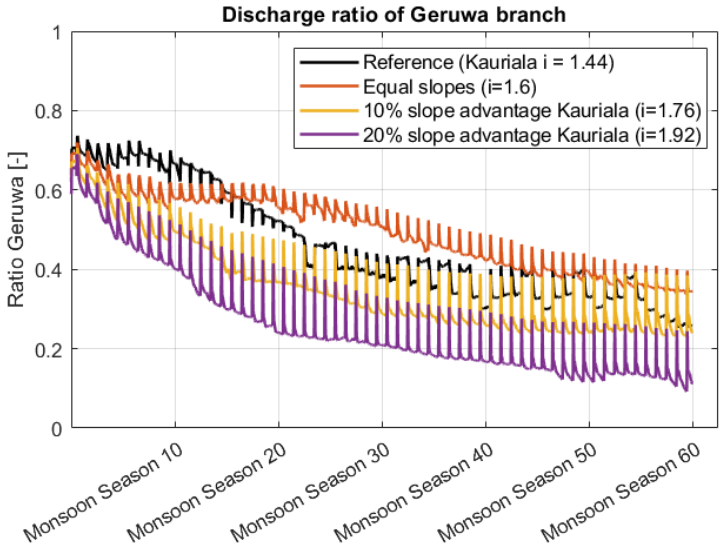

Figure 7.15: Discharge distribution with different slope of Kauriala branch.

Initial Heightening Geruwa

Fig. 7.16 Reveals the discharge distribution under varying degrees of initial Geruwa sedimentation (25 cm, 50 cm, 100 cm). While the slope remains unchanged, the bed elevation simulates aggraded conditions.What is striking is the fact that this graph of Fig. 7.16 closely resembles Fig. 7.15. An initial 25 cm sedimentation of the Geruwa results in very similar discharge distribution as in the scenario where both branches have an equal slope (where thus the Kauriala is steepened by 10% compared to the reference model). The 50 cm initial sedimentation corresponds closely to a 10% slope advantage of the Kauriala channel. Only at 100 cm of bed level heightening do we observe less than 10% of the flow going into the Geruwa during base monsoon discharge. Note that even in the case of a 100 cm forced sedimentation in the Geruwa, it still receives around 30 % of the discharge during peak flows at the end of the simulation.

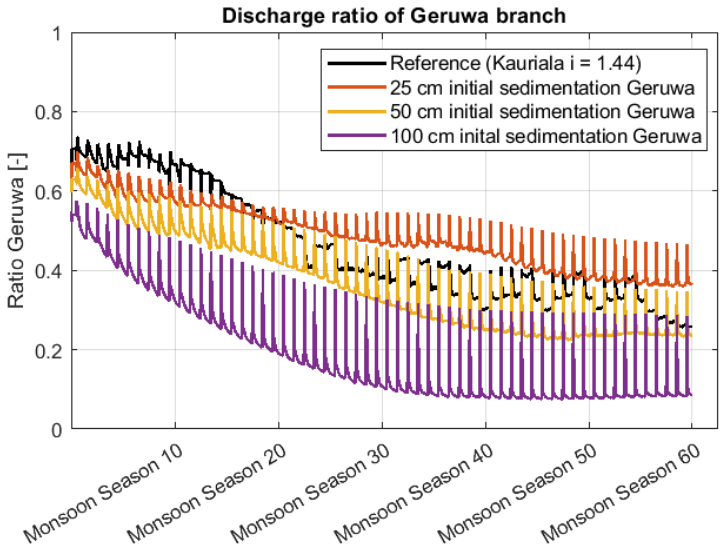

Figure 7.16: Discharge distribution with different amounts of bed level increase of the Geruwa branch.

See Fig. 7.17 for the slightly increasing erosion of the Kauriala branch resulting from the Geruwa sedimentation. In each case, firstly the Kauriala bed level is increased, however after some years the bed level returns to around the initial level or below. The scour hole upstream of the bifurcation is nearly equal for each scenario.

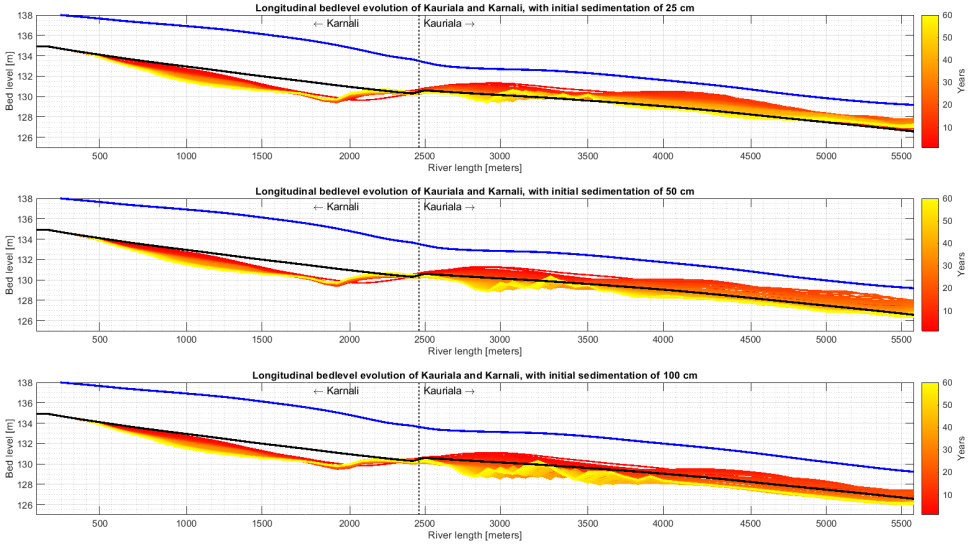

Figure 7.17: Bed level evolution of the Kauriala branch at different initial sedimentation of the Geruwa branch.

An overview of discharge distribution classification of all runs can be found in the Appendix C.

8

Discussion & Synthesis

In this chapter, we revisit the hypotheses and explore how the model results provide insights into the origin of the Karnali channel shift. The objective is to identify the factors driving the partial closure of the Geruwa branch and evaluate the applicability of the model results to the real-world scenario.

The first hypothesis theorised that the flood peak increased the sediment load in the Geruwa branch and the intensity of bend sorting processes, and the subsequent aggradation forced the river to (re)open Kauriala channels. The second hypothesis considered the possibility that increased forces first eroded a new path in the Kauriala, after which the flow component and sediment transport capacity drastically reduced in the Geruwa, leading to sedimentation. Both hypotheses thus lead to the same outcome of a (partial) closure of the Geruwa branch, a significant problem for the region and ecosystems after 2009.

8.1. Interpretation of Model Results

The parameter study, which involves bed slope gravity pull, spiral flow intensity, and hiding/exposure settings, primarily tests the effects of bend sorting processes theorised in hypothesis 1, as well as scenarios with varying sediment compositions. Additionally, the scenario runs that increase the slope of the Kauriala and impose initial sedimentation layers of various heights on the Geruwa branch are designed to test hypothesis 2.

Reference Model Behaviour

The reference model demonstrates a relatively stable discharge distribution under average monsoon conditions over the 60-year simulation period. Deposition patterns and magnitudes align well with field observations, particularly concerning the location of the deposition. However, a notable discrepancy exists: the predicted aggradation of the model consists of only finer sediment, contrary to field observation.

This inconsistency raises questions about the accuracy of the model's sediment input parameters. A possible explanation is that the model's input fine sediment fraction is much larger than the actual sand fraction within the Karnali system. Alternatively, the model may not fully capture the complex sorting mechanisms that govern sediment transport and deposition at the bifurcation.

Impact of Flood Event

The introduction of a double flood event significantly affected the bifurcation evolution. Significantly more and coarser bed load transport led to cascading effects (sedimentation) in the Geruwa branch. Model results suggest the heavy peak flood, while not as rapid as observed in reality, initiated a self-reinforcing mechanism that ultimately led to the closure of the Geruwa branch and enhanced erosion in the Kauriala. Compared to the reference case, the ratio of sediment coming into the Geruwa was higher. This, in turn, likely led to a decrease in Geruwa flow capacity, further increasing sedimentation and reinforcing the closure process.

This model run gives a morphological development that aligns well with hypothesis 1 and the observations made in the field. However, changes in the real world have developed in a shorter period than the model predicts.

Role of Sediment Fractions and Interaction

The model results highlight the critical role of sediment sorting and local sediment supply in the evolution of the modelled bifurcation. Both the reference model and scenario runs with modified sediment compositions underscored the dominance of sand transport in shaping the morphology of the modelled Geruwa branch. Runs that excluded the sand fraction led to remarkably stable morphologies and discharge distribution, whereas the absence of coarser fractions led to highly unstable configurations strongly favouring the Geruwa branch. This can be attributed to the fact that the transverse flow component, resulting from spiral flow in the river bend, only has the ability to transport the finest fractions towards the innerbend, the location of the Kauriala.

These model results do not align well with field observations, where sand deposition was not a prominent feature in the upstream section of the Geruwa. Compared to field observations, most model runs underestimate grain sizes, most notably in the Geruwa.

The sensitivity of the model to the active layer thickness further highlights the significance of sediment sorting. A thinner active layer led to more realistic sediment sorting patterns, with coarser material accumulating at the outer bend of the Kauriala, consistent with field observations. This raises the question of whether the layer thickness alters the sediment supply or the composition in the bifurcates itself. From the decadal bed level (Fig. C.15 and Fig. C.16) and the D50 plot (Fig. 7.11), it seems that the increased supply of the sand fraction (due to slower sorting processes in the thick active layer run) led to the strong sedimentation. This is also in line with the results from the various hiding/exposure coefficient runs, suggesting that sedimentation in the Geruwa occurs rapidly if the supply of the finer fraction increases due to the reduced hiding effect of the sand fraction. The impacted sediment supply, higher for the finer fractions and lower for the coarse fraction, leads to sedimentation in the Geruwa, reducing its transport capabilities.

Spiral Flow Intensity

Varying the spiral flow intensity in the model led to surprising outcomes: The absence of spiral flow caused a complete closure of the Geruwa, and the doubling of the secondary flow magnitude made the Geruwa receive the near complete flow in the system.

This partially contradicts hypothesis 1, which theorised that spiral flow influences the bend sorting effects and would cause a coarser fraction to enter the Geruwa, causing sedimentation. However, the model results have shown that the spiral flow component only mobilises the sand fraction in the transverse direction (towards the innerbend). Leaving the coarser fractions relatively untouched. Since the branches in the model are sensitive to clogging due to an increased sand fraction supply, the spiral flow strongly affects channel dominance. In this way, the dominance of the Geruwa with increased spiral flow is explained: the increased supply of finer sediment towards the Kauriala exceeds the branch's capacity, leading to long-term aggradation. The dominance of the Kauriala in the model run without spiral flow is explained by decreased sediment transport towards the inner bend. Consequently, the Geruwa in the outer bend lacks the capacity to convey the additional fine sediment.

Impact of Slope Changes and Initial Sedimentation

Model runs exploring the effects of Kauriala slope steepening and initial Geruwa sedimentation revealed a surprisingly low sensitivity to these factors. It was found that even with a 20% slope advantage for the Kauriala branch, the Geruwa branch did not completely close. The relationship between slope, forced sedimentation, and discharge was not always linear. For example, increasing the Kauriala's slope to match the Geruwa's or forcing a 25 cm initial sedimentation in the Geruwa both unexpectedly favoured the Geruwa compared to the reference run.

The 100 cm forced sedimentation of the Geruwa gives slight clues in favour of hypothesis 1 since this led to erosion (although subtle) of the Kauriala branch and reduced the flow in the Geruwa significantly. However, it does not support any information on how this sedimentation came to be as it is forced upon as an initial condition. It raises the question: could an abnormally strong monsoon flood peak(s), like in 2009, cause a 100 cm sedimentation in the Geruwa? The double flood peak scenario run results indicate that the order of magnitude is possible.

The steepened Kauriala slope runs do not favour hypothesis 2, as even relatively significant advantages for the Kauriala that simulate an opening in the channel do not drastically influence discharge distribution.

8.2. Synthesis: Connecting Model Results to Karnali Channel Shift Hypotheses

The model results show that the discharge distribution is most significantly affected by the supply and transport of the finer fractions and their tendency to exceed the branch's transport capabilities. We discuss whether the model results support or refute each hypothesis regarding the real-world closing of the Geruwa branch.

Model results and Hypothesis 1: Flood-induced aggradation

Model simulations support the notion that a flood event, particularly one of extreme magnitude, can significantly increase sediment load in the Geruwa branch. This heightened sediment input triggers aggradation, reducing flow capacity and contributing to the branch's closure. However, specific model runs gave results that might suggest hypothesis 1 is not the complete picture. The model scenario with a double flood peak supports the hypothesis since the results show that more and coarser sediment enters the Geruwa during peak flows.

The hypothesis further theorised that extreme peak flow would enhance sediment sorting due to steeper transverse slopes. Model runs with increased spiral flow and increased Ashld parameter, both leading to steeper transverse slopes, have refuted this part. Steeper slopes in the model are associated with a more dominant role of the fine fraction transport towards the innerbend and discharge dominance of the Geruwa. Surprisingly, increasing the downslope deflection of particles, by decreasing the Ashld in the model, also led to more discharge in the Geruwa. Therefore, this part of the hypothesis is not supported.

Lastly, it was hypothesised that the resulting plug would lead to an opening towards the Kauriala branch. This is supported since model runs, for example, the ones with forced sedimentation in the Geruwa, lead to erosion and steepening of the Kauriala.

Overall, hypothesis 1 is partially supported by model results and gives a plausible explanation of the origin of the Karnali channel shift that occurred after the 2009 monsoon season. Increased peak flow does lead to a more substantial bend sorting effect, although these are not attributed to the steepness of transverse slopes.

Model results and Hypothesis 2: Erosion driven channel opening

While the model supports the general idea that erosion and slope advantages can alter flow distribution, the results challenge the linear relationship initially proposed in Hypothesis 2. Increasing the slope of the Kauriala in the model, which simulates the channels opening, has not led to a complete channel shift. Only in extreme cases do we see a partial closure of the Geruwa branch in the model. Therefore, this hypothesis is not supported, although it may have played a minor coincidental role alongside hypothesis 1.

8.3. Limitations

Modelling hydro-morphological processes in a dynamic river bifurcation poses inherent challenges. The selection of appropriate formulations, parameters, calibration, and validation data is highly case-specific and requires careful consideration. Furthermore, the sensitivity of such systems to initial and boundary conditions makes model development and calibration a complex task, particularly in data-sparse environments. This study faced limitations due to the limited data availability for the Karnali River. Upstream discharge was known, but detailed information on sediment composition, branch discharges, and long-term trends was lacking. This lack of data constrained the model's calibration and validation potential, introducing uncertainties in the results. Consequently, drawing definitive conclusions about the real-world event based on the model results proved challenging.

A problem with having the discharge distribution as the most important metric is that previous studies

(e.g. (Roebroeck, 2022)) and our fieldwork observations are based on dry season periods. The model only simulates the wet seasons, therefore it cannot be directly compared to the wet pixel distribution and the discharge distribution measured in October 2023. Thus, the installed telemetric radar water level gauges will be able to provide calibration and verification data for the future. As it will continuously measure the water level and, combined with the cross-section taken during fieldwork and simple velocity estimates, discharge can be reasonably estimated.

The model employs fixed downstream boundaries, simplifying the representation of complex downstream dynamics. While the backwater effect on the bifurcation is likely minimal, a more realistic model would allow for variable downstream conditions to better capture the system's response to changing flows.

The results from the reference model and most other scenarios indicate a dominant role of the sand fraction. The top layer of sediment deposition is almost always primarily composed of the finest fraction. This finding does not align well with our field observations, which showed that the deposition at the entrance of the Geruwa consisted of cobbles and boulders. Additionally, only the sand fraction is mobile in the model during base monsoon discharge. To improve the accuracy of future modelling efforts, it is recommended that the critical Shields parameter for the larger sediment fractions be lowered.

Other issues with the model's numerous parameters can lead to equifinality issues, where different parameter combinations produce similar outcomes. This complicates the identification of the most influential factors and increases the uncertainty associated with model predictions. As presented in this study, sensitivity analyses are crucial for exploring this parameter space and understanding the potential range of model behaviours.

8.4. Recommendations

Understanding the mechanisms behind channel shifts in the Karnali bifurcation is crucial for effective river management and ecological conservation. The insights gained from this study could inform interventions aimed at restoring a balanced discharge and sediment distribution between the channels, potentially mitigating adverse impacts on the Bardiya National Park and its protected species.

Future Research

The installation of telemetric water level gauges will offer promising data for future research. These gauges will provide continuous data, enabling model calibration and validation across both wet and dry seasons. Future studies could leverage this data to refine the model, explore the role of seasonal variations in channel dynamics, and assess the effectiveness of potential interventions.

For future modelling efforts, increasing the model domain to include the bifurcations at locations BIF1 and BIF2 is recommended. These upstream bifurcation points have since become the more dominant discharge divider, see the years 2020 and 2021 in Fig. 4.1. In case authorities want to increase discharge into the Geruwa branch, these upstream bifurcating points should be included in the modelling of potential interventions. This research focused on finding an explanation for the channel shifting that occurred after 2009 and, therefore, solely focused on the bifurcation of location BIF3.

The results indicate the need to accurately represent the full range of sediment sizes and their interactions within the model. Refining the hiding/exposure formulation and calibrating the active layer thickness are potential avenues for improvement. Another aspect to consider is the extent and effect of the gravel mining that occurs in the lower reaches. This study did not quantify how these antropogenic alterations affect the systems.

Increasing the Dshld parameter led to the coarsening of the Geruwa sedimentation, suggesting that the influence of fraction-specific bed slope processes should be further investigated and implemented in future models. This study does not include a robust method of comparing D50 with model results and field data.

Practical Interventions

Although this study aimed to identify the causes of the Karnali River's channel shifting rather than recommend restoration strategies for its discharge distribution, some potential recommendations can

be speculated. Firstly, the bifurcation area is highly dynamic and experiences significant variability in sediment load, making it unsuitable for construction. Secondly, much of the bifurcation zone lies within the boundaries of Bardiya National Park, where construction work is restricted. Thus, interventions should focus on leveraging natural processes to sustainably alter the morphology, promoting more discharge toward the Geruwa.

During peak monsoon flows, the enormous forces and sediment loads are challenging to prevent from entering the first Geruwa inlet located in the outer bend. The momentum of the particles prevents them from following the bend, causing sediment to block the inlet even if the current deposition is removed. Therefore, it is recommended that the current blockage be left as is. Instead, the focus should shift to the second Geruwa inlet, which was not modelled in this study, to ensure it remains open for water entry. During peak discharge, sediment may continue to deposit in the already blocked western Geruwa channel, while the discharge is free to enter the second inlet. This channel may require frequent dredging, but it is hoped that the natural erosive forces of the discharge will help keep it open.

Additionally, attention should be given to the upstream bifurcation points, BIF1 and BIF2, which have become significant discharge dividers since 2020. Addressing these points is now crucial for managing the overall discharge distribution in the system.

9

Conclusion

This study aims to investigate the factors driving the partial closure of the Geruwa branch of the Karnali River after the 2009 monsoon season and to assess the applicability of schematized model results to real-world scenarios. The research questions posed in the introduction chapter guide this investigation, and the key findings are summarized below:

1) How did the 2009 monsoon flood alter the morphology of the Karnali bifurcation and flow distribution between the Geruwa and Kauriala branches?

The 2009 monsoon flood had a significant impact on the morphology of the Karnali bifurcation. First, satellite imagery showed that the extreme flood event led to substantial changes in the planform of the bifurcation, leading to a channel shift favouring the Kauriala branch in subsequent years. Observations from the field lead to two overlapping hypotheses, which are tested using a depth-averaged 2D hydromorphological model with a simulation period of 60 years. The results from the model give good indications of the drivers behind a channel-shifting event in a schematized domain that reflects the real-world Geruwa bifurcation system. In essence, sediment supply exceeding the transport capacity of either branch causes aggregation. We show that the sediment supply in the branches depends on flood magnitude and duration, sediment fraction interaction (hiding/exposure, active layer thickness and bed composition) and transverse direction (secondary flow and bed slope deflection).

Field observations and model results indicate that a flood, which occurred in 2009, is associated with a large increase in bedload material grain size and amount, favouring the outerbend bifurcate, the Geruwa. This led to a coarse deposition at the Geruwa's entrance that became immobile in subsequent years and started a self-reinforcing feedback loop. The deposition reduces flow towards Geruwa and decreases sediment transport capacity within that branch. This smaller transport capacity allows more sediment to deposit in Geruwa, further reducing its overall water depth and promoting its closure. Understanding the peak flow bedload transport preference for (the first entrance of) the Geruwa branch should influence potential interventions.

2) How can we model the impact of bend sorting and bifurcate steepening on the closure of the other bifurcate?

The study shows that a schematized 2DH-hydromorphological model can replicate bend sorting effects to a certain extent with the right closure relations and parameter ranges. The parameter study reveals that the balance between transverse downslope gravity pull (bed load material directed towards outerbend) and the spiral flow component (directed towards innerbend) strongly determines the discharge distribution in the system. Increased spiral flow intensity mobilizes finer sediments towards the inner bend (Kauriala), causing excessive sedimentation and reducing its flow capacity. On the other hand, when gravity pull is relatively dominant, it results in sediment accumulation in the outer bend bifurcate (Geruwa) and its eventual closure.

Scenario model runs with an increasing gradient of a bifurcate show its impact on the flow distribution and sediment transport dynamics of the other. Our model demonstrates that steepening the innerbend branch has a moderate effect on discharge distribution in the long-term model run.

However, limitations of the models set up are identified, such as the limited bed load transport during

base monsoon flow, overrepresentation of sand, lack of calibration data, and fixed water levels at the downstream boundaries. The results show the value of such a model even in data-scarce studies where the model could not be validated. Future modelling efforts should increase the domain to incorporate the more recent and upstream bifurcation points and use the data from the installed water level gauges in the bifurcates.

Bibliography

Acharya, H. R., Thapa, A., Lamichhane, B. R., Subba, S. A., Thapa, G. J., Kadariya, R., Joshi, L. R., Acharya, H., Shah, M. K., Shah, S. K., Shrestha, B. P., Mehta, K. K., Pant, G., Pathak, S., Subedi, N., Pokheral, C. P., Thapa, K., Dahal, B. R., Representative, D.-C., & Kandel, R. C. (2022). STATUS OF TIGERS AND PREY IN NEPAL 2022, department of national parks and wildlife conservation and department of forests and soil conservation. ministry of forests and environment, kathmandu, nepal.

Andrews, E. D. (1984). Bed-material entrainment and hydraulic geometry of gravel-bed rivers in colorado [Publisher: Geological Society of America]. *Geological Society of America Bulletin*, *95*(3), 371–378.

Arcement, G. J., & Schneider, V. R. (1989). *Guide for selecting manning's roughness coefficients for natural channels and flood plains*. USGPO; For sale by the Books and Open-File Reports Section, US Geological …

Baar, A. W., Boechat Albernaz, M., van Dijk, W. M., & Kleinhans, M. G. (2019). Critical dependence of morphodynamic models of fluvial and tidal systems on empirical downslope sediment transport [Number: 1 Publisher: Nature Publishing Group]. *Nature Communications*, *10*(1), 4903. https://doi.org/10.1038/s41467-019-12753-x

Baar, A. W., de Smit, J., Uijttewaal, W. S. J., & Kleinhans, M. G. (2018). Sediment transport of fine sand to fine gravel on transverse bed slopes in rotating annular flume experiments [_eprint: https://onlinelibrary.wiley.com/doi/pdf/10.1002/2017WR020604]. *Water Resources Research*, *54*(1), 19–45. https://doi.org/10.1002/2017WR020604

Barile, G., Redolfi, M., & Tubino, M. (2024). Analysis of autogenic bifurcation processes resulting in river avulsion [Publisher: Copernicus GmbH]. *Earth Surface Dynamics*, *12*(1), 87–103. https://doi.org/10.5194/esurf-12-87-2024

Barnes, H. H. (1967). *Roughness characteristics of natural channels*. US Government Printing Office.

Bertoldi, W. (2012). Life of a bifurcation in a gravel-bed braided river. *Earth Surface Processes and Landforms*, *37*(12), 1327–1336. https://doi.org/10.1002/esp.3279

Bhattarai, B. P., & Kindlmann, P. (2012). Habitat heterogeneity as the key determinant of the abundance and habitat preference of prey species of tiger in the chitwan national park, nepal. *Acta Theriologica*, *57*(1), 89–97. https://doi.org/10.1007/s13364-011-0047-8

Bijlmakers, J., Griffioen, J., & Karssenberg, D. (2022, June 27). *Environmental drivers of space-time dynamics in floodplain vegetation: Grasslands as habitat for megafauna in bardia national park (nepal)* (preprint). Biodiversity and Ecosystem Function: Freshwater. https://doi.org/10.5194/bg-2022-129

Blanckaert, K. (2011). Hydrodynamic processes in sharp meander bends and their morphological implications [_eprint: https://onlinelibrary.wiley.com/doi/pdf/10.1029/2010JF001806]. *Journal of Geophysical Research: Earth Surface*, *116*. https://doi.org/10.1029/2010JF001806

Blanckaert, K., & De Vriend, H. J. (2004). Secondary flow in sharp open-channel bends [Publisher: Cambridge University Press]. *Journal of Fluid Mechanics*, *498*, 353–380.

Blom, A., Viparelli, E., & Chavarrías, V. (2016). The graded alluvial river: Profile concavity and downstream fining [_eprint: https://onlinelibrary.wiley.com/doi/pdf/10.1002/2016GL068898]. *Geophysical Research Letters*, *43*(12), 6285–6293. https://doi.org/10.1002/2016GL068898

Bolla Pittaluga, M., Repetto, R., & Tubino, M. (2003). Channel bifurcation in braided rivers: Equilibrium configurations and stability [_eprint: https://onlinelibrary.wiley.com/doi/pdf/10.1029/2001WR001112]. *Water Resources Research*, *39*(3). https://doi.org/10.1029/2001WR001112

Bridge, J., & Jarvis, J. (1982). The dynamics of a river bend: A study in flow and sedimentary processes [Publisher: Wiley Online Library]. *Sedimentology*, *29*(4), 499–541.

Bryant, M., Falk, P., & Paola, C. (1995). Experimental study of avulsion frequency and rate of deposition. *Geology*, *23*(4), 365–368. https://doi.org/10.1130/0091-7613(1995)023<0365:ESOAFA>2.3.CO;2

Buffington, J. M., & Montgomery, D. R. (1997). A systematic analysis of eight decades of incipient motion studies, with special reference to gravel-bedded rivers [Publisher: Wiley Online Library]. *Water resources research*, *33*(8), 1993–2029.

Buis, A. (2023). Morphological model for the river rhine.

Bull, W. B. (1977). The alluvial-fan environment [Publisher: SAGE Publications Ltd]. *Progress in Physical Geography: Earth and Environment*, *1*(2), 222–270. https://doi.org/10.1177/030913337700100202

Bulle, H. (1926). Investigations into bedload drainage when watercourses split: Model experiments from the river engineering laboratory of the technical university of karlsruhe. *(No Title)*.

Chow, V. T. (1959). Open-channel hydraulics: New york. *US Army Corps of Engineers, Hydrologic Engineering*.

Dahal, P., Shrestha, M. L., Panthi, J., & Pradhananga, D. (2020). Modeling the future impacts of climate change on water availability in the karnali river basin of nepal himalaya. *Environmental Research*, *185*, 109430. https://doi.org/10.1016/j.envres.2020.109430

Deltares. (2005). Delft3d-RGFGRID. generation and manipulation of curvilinear grids for FLOW and WAVE. *User Manual; WL Delft Hydraulics,(Deltares): Delft, The Netherlands*.

Deltares. (2018). Delft3d-FLOW user manual. *Deltares Delft, The Netherlands*, *330*.

Dhakal, M., Karki, M., Jnawali, S. R., Subedi, N., Pradhan, N., Malla, S., Lamichhane, B. R., Pokheral, C., Thapa, G., Oglethorpe, J., et al. (2014). Status of tigers and prey in nepal. *Department of National Park and Wildlife Conservation, Kathmandu, Nepal*, *74*.

Dingle, E., Attal, M., & Sinclair, H. D. (2017). Abrasion-set limits on himalayan gravel flux [Publisher: Nature Publishing Group]. *Nature*, *544*(7651), 471–474. https://doi.org/10.1038/nature22039

Dingle, E., Creed, M., Sinclair, H., Gautam, D., Gourmelen, N., Borthwick, A., & Attal, M. (2020a). Dynamic flood topographies in the terai region of nepal. *Earth Surface Processes and Landforms*, *45*(13), 3092–3102. https://doi.org/10.1002/esp.4953

Dingle, E., Sinclair, H. D., Venditti, J. G., Attal, M., Kinnaird, T. C., Creed, M., Quick, L., Nittrouer, J. A., & Gautam, D. (2020b). Sediment dynamics across gravel-sand transitions: Implications for river stability and floodplain recycling. *Geology*, *48*(5), 468–472. https://doi.org/10.1130/G46909.1

Donchyts, G., Baart, F., Winsemius, H., Gorelick, N., Kwadijk, J., & van de Giesen, N. (2016). Earth's surface water change over the past 30 years [Publisher: Nature Publishing Group]. *Nature Climate Change*, *6*(9), 810–813. https://doi.org/10.1038/nclimate3111

Engelund, F. (1974). Flow and bed topography in channel bends [Publisher: American Society of Civil Engineers]. *Journal of the Hydraulics Division*, *100*(11), 1631–1648.

Ghimere, B. (2024, April 1). *58 people died in last fiscal year as human-animal conflict gets deadlier*. Retrieved May 22, 2024, from https://kathmandupost.com/national/2024/03/01/58-people-died-in-last-fiscal-year-as-human-animal-conflict-gets-deadlier

Harvey, A. M., Mather, A. E., & Stokes, M. (2005). Alluvial fans: Geomorphology, sedimentology, dynamics — introduction. a review of alluvial-fan research [Publisher: The Geological Society of London]. *Geological Society, London, Special Publications*, *251*(1), 1–7. https://doi.org/10.1144/GSL.SP.2005.251.01.01

Hirano, M. (1972). Studies on variation and equilibrium state of a river bed composed of nonuniform material [Issue: 207]. *Proceedings of the Japan Society of Civil Engineers*, *1972*, 51–60.

Ikeda, S. (1982). Lateral bed load transport on side slopes [Publisher: American Society of Civil Engineers]. *Journal of the Hydraulics Division*, *108*(11), 1369–1373.

Iwasaki, T., Akahori, R., Giri, S., & Shmizu, Y. (2013, September 2). *Numerical study on the flow and the sedimentation during 2008 flood in the koshi river in nepal*.

Karki, J., Jnawali, S., Shrestha, R., Pandey, M., Gurung, G., & Thapa Karki, M. (2009). Tigers and their prey base abundance in terai arc landscape, nepal. *Kathmandu: Government of Nepal, Ministry of Forests and Soil Conservation, Department of National Parks and Wildlife Conservation, and Department of Forests*.

Khatiwada, K. R., Panthi, J., Shrestha, M. L., & Nepal, S. (2016). Hydro-climatic variability in the karnali river basin of nepal himalaya [Number: 2 Publisher: Multidisciplinary Digital Publishing Institute]. *Climate*, *4*(2), 17. https://doi.org/10.3390/cli4020017

Kleinhans, M. G., Jagers, H. R. A., Mosselman, E., & Sloff, C. J. (2008). Bifurcation dynamics and avulsion duration in meandering rivers by one-dimensional and three-dimensional models [_eprint: https://onlinelibrary.wiley.com/doi/pdf/10.1029/2007WR005912]. *Water Resources Research*, *44*(8). https://doi.org/10.1029/2007WR005912

Kleinhans, M. G., Ferguson, R. I., Lane, S. N., & Hardy, R. J. (2013). Splitting rivers at their seams: Bifurcations and avulsion [_eprint: https://onlinelibrary.wiley.com/doi/pdf/10.1002/esp.3268]. *Earth Surface Processes and Landforms*, *38*(1), 47–61. https://doi.org/10.1002/esp.3268

Koch, F., & Flokstra, C. (1980). *Bed level computations for curved alluvial channels: Prepared for the 19th IAHR congress, new delhi, india, february 1981*. Waterloopkundig Laboratorium.

Lesser, G. R., Roelvink, J. A., van Kester, J. A. T. M., & Stelling, G. S. (2004). Development and validation of a three-dimensional morphological model. *Coastal Engineering*, *51*(8), 883–915. https://doi.org/10.1016/j.coastaleng.2004.07.014

Mellor, G. L., & Blumberg, A. F. (1985). Modeling vertical and horizontal diffusivities with the sigma coordinate system [Publisher: American Meteorological Society Section: Monthly Weather Review]. *Monthly Weather Review*, *113*(8), 1379–1383. https://doi.org/10.1175/1520-0493(1985)113<1379:MVAHDW>2.0.CO;2

Meyer-Peter, E., & Müller, R. (1948). Formulas for bed-load transport. *IAHSR 2nd meeting, Stockholm, appendix 2*.

Moe, S. R., & Wegge, P. (1994). Spacing behaviour and habitat use of axis deer (axis axis) in lowland nepal [Publisher: NRC Research Press]. *Canadian Journal of Zoology*, *72*(10), 1735–1744. https://doi.org/10.1139/z94-234

Montgomery, D. R., & Buffington, J. M. (1997). Channel-reach morphology in mountain drainage basins [Publisher: Geological Society of America]. *Geological Society of America Bulletin*, *109*(5), 596–611.

Parker, G., & Andrews, E. D. (1985). Sorting of bed load sediment by flow in meander bends [_eprint: https://onlinelibrary.wiley.com/doi/pdf/10.1029/WR021i009p01361]. *Water Resources Research*, *21*(9), 1361–1373. https://doi.org/10.1029/WR021i009p01361

Parker, G., Klingeman, P. C., & McLean, D. G. (1982). Bedload and size distribution in paved gravel-bed streams [Publisher: American Society of Civil Engineers]. *Journal of the Hydraulics Division*, *108*(4), 544–571.

Parsapour-Moghaddam, P., Rennie, C. D., Slaney, J., Platzek, F., Shirkhani, H., Jamieson, E., Mosselman, E., & Measures, R. (2023). Implementation of a new bank erosion model in delft3d [Publisher: American Society of Civil Engineers]. *Journal of Hydraulic Engineering*, *149*(10), 04023038.

Parsons, D. R., Jackson, P. R., Czuba, J. A., Engel, F. L., Rhoads, B. L., Oberg, K. A., Best, J. L., Mueller, D. S., Johnson, K. K., & Riley, J. D. (2013). Velocity mapping toolbox (VMT): A processing and visualization suite for moving-vessel ADCP measurements. *Earth Surface Processes and Landforms*, *38*(11), 1244–1260. https://doi.org/10.1002/esp.3367

Powell, D. M. (1998). Patterns and processes of sediment sorting in gravel-bed rivers.

Purinton, B., & Bookhagen, B. (2019). Introducing *PebbleCounts*: A grain-sizing tool for photo surveys of dynamic gravel-bed rivers. *Earth Surface Dynamics*, *7*(3), 859–877. https://doi.org/10.5194/esurf-7-859-2019

Quick, L., Sinclair, H., Attal, M., & Singh, V. (2019). Conglomerate recycling in the himalayan foreland basin: Implications for grain size and provenance. *GSA Bulletin*, *132*(7), 1639–1656. https://doi.org/10.1130/B35334.1

Rakhal, B., Sharma, S., Ghimire, G., & Adhikari, T. (2021, January 15). *Assessment of channel shifting of karnali megafan in nepal using remote sensing and GIS*.

Redolfi, M., Zolezzi, G., & Tubino, M. (2016). Free instability of channel bifurcations and morphodynamic influence. *Journal of Fluid Mechanics*, *799*, 476–504. https://doi.org/10.1017/jfm.2016.389

Redolfi, M., Zolezzi, G., & Tubino, M. (2019). Free and forced morphodynamics of river bifurcations [_eprint: https://onlinelibrary.wiley.com/doi/pdf/10.1002/esp.4561]. *Earth Surface Processes and Landforms*, *44*(4), 973–987. https://doi.org/10.1002/esp.4561

Regmi, R. K. (2021). Sedimentation modeling of karnali chisapani multipurpose project reservoir, nepal. *Journal of The Institution of Engineers (India): Series A*, *102*(3), 815–827. https://doi.org/10.1007/s40030-021-00550-z

Roebroeck, M. E. (2022). Morphodynamics of the karnali fluvial fan.

Sah, R. K., Nagesh Kumar, D., & Das, A. K. (2022). Avulsion distribution on rivers in the himalayan foreland region [Publisher: Taylor & Francis _eprint: https://doi.org/10.1080/02626667.2022.2136000]. *Hydrological Sciences Journal*, *67*(14), 2175–2190. https://doi.org/10.1080/02626667.2022.2136000

Scheer, P. v. d., Ribberink, J. S., & Blom, A. (2002). Transport formulas for graded sediment. behaviour of transport formulas and verification with data [Publisher: University of Twente]. Retrieved February 23, 2024, from https://research.utwente.nl/en/publications/transport-formulas-for-graded-sediment-behaviour-of-transport-for

Schuurman, F., & Kleinhans, M. G. (2015). Bar dynamics and bifurcation evolution in a modelled braided sand-bed river. *Earth Surface Processes and Landforms*, *40*(10), 1318–1333. https://doi.org/10.1002/esp.3722

Schuurman, F., Marra, W. A., & Kleinhans, M. G. (2013). Physics-based modeling of large braided sand-bed rivers: Bar pattern formation, dynamics, and sensitivity. *Journal of Geophysical Research: Earth Surface*, *118*(4), 2509–2527. https://doi.org/10.1002/2013JF002896

Shields, A. (1936). *Application of similarity principles and turbulence research to bed-load movement*. Soil Conservation Service.

Sloff, K., Jagers, B., Mosselman, E., & Kleinhans, M. (2006, August 28). Effect of upstream meanders on bifurcation stability and sediment division in 1d, 2d and 3d models. In *River flow 2006*. Taylor & Francis. https://doi.org/10.1201/9781439833865.ch144

Sloff, K., & Mosselman, E. (2012). Bifurcation modelling in a meandering gravel–sand bed river [_eprint: https://onlinelibrary.wiley.com/doi/pdf/10.1002/esp.3305]. *Earth Surface Processes and Landforms*, *37*(14), 1556–1566. https://doi.org/10.1002/esp.3305

Stecca, G., Measures, R., & Hicks, D. (2017). A framework for the analysis of noncohesive bank erosion algorithms in morphodynamic modeling [Publisher: Wiley Online Library]. *Water Resources Research*, *53*(8), 6663–6686.

Struiksma, N., Olesen, K. W., Flokstra, C., & De Vriend, H. J. (1985). Bed deformation in curved alluvial channels. *Journal of Hydraulic Research*, *23*(1), 57–79. https://doi.org/10.1080/00221688509499377

Talmon, A., Struiksma, N., & Van Mierlo, M. (1995). Laboratory measurements of the direction of sediment transport on transverse alluvial-bed slopes. *Journal of Hydraulic Research*, *33*(4), 495–517. https://doi.org/10.1080/00221689509498657

Trenberth, K. E. (2005, October 21). The impact of climate change and variability on heavy precipitation, floods, and droughts. In M. G. Anderson & J. J. McDonnell (Eds.), *Encyclopedia of hydrological sciences* (1st ed.). Wiley. https://doi.org/10.1002/0470848944.hsa211

USAID. (2019). Lower karnali watershed profile: Status, challenges and opportunities for improved water resource management.

van Denderen, R. P., Schielen, R. M. J., Blom, A., Hulscher, S. J. M. H., & Kleinhans, M. G. (2018). Morphodynamic assessment of side channel systems using a simple one-dimensional bifurcation model and a comparison with aerial images [_eprint: https://onlinelibrary.wiley.com/doi/pdf/10.1002/esp.4267]. *Earth Surface Processes and Landforms*, *43*(6), 1169–1182. https://doi.org/10.1002/esp.4267

van Dijk, W. M., Schuurman, F., van de Lageweg, W. I., & Kleinhans, M. G. (2014). Bifurcation instability and chute cutoff development in meandering gravel-bed rivers. *Geomorphology*, *213*, 277–291. https://doi.org/10.1016/j.geomorph.2014.01.018

Wang, Z., De Vries, M., Fokkink, R., & Langerak, A. (1995). Stability of river bifurcations in ID morphodynamic models [Publisher: Taylor & Francis _eprint: https://doi.org/10.1080/00221689509498549]. *Journal of Hydraulic Research*, *33*(6), 739–750. https://doi.org/10.1080/00221689509498549

Appendices

List of Appendices

A

Model Equations of Delft3D

Computational Grid

DELFT3D-FLOW 4 (hereafter referred to as D3D) solves the following equations within the discrete spaces of a computational grid using a finite difference numerical method. The model employs a staggered grid system in the vertical dimension, offering a choice between σ-coordinates or Z-coordinates. Unlike the Z-grid's equidistant vertical levels, the σ-grid allows flexible vertical grid sizes . The σ-grid maintains a constant number of layers across the entire horizontal computation area, regardless of water depth. This coordinate system is used in 2DH (depth-averaged) models, where σ varies between 0 (water level) and -1 (bed level). The system is defined as follows (Deltares, 2018; Lesser et al., 2004; Mellor & Blumberg, 1985):

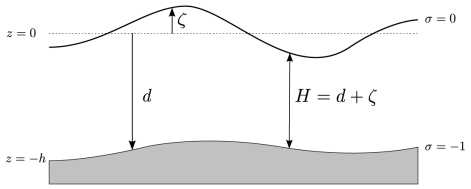

Figure A.1: Definition of water level ζ, depth h and total depth H, figure adopted from Deltares (2018)

$$\sigma = \frac{z - \zeta}{d + \zeta} = \frac{z - \zeta}{H} \tag{A.1}$$

Where;
z: the vertical coordinate in physical space
ζ: the free surface elevation above the reference plane (at $z = 0$)
d: the depth below the reference plane
H: the total water depth, given by $d + \zeta$

The model's computational grid defines water levels (or depths) at the center of each cell, while velocity components are calculated at cell edges. This staggered arrangement ensures accurate representation of water flow between cells, as it naturally accounts for the fluxes across cell boundaries. RGFGRID software is used to generate this grid, which underpins all subsequent calculations. Fig. A.2 illustrates a schematic of the staggered computational grid used by D3D.

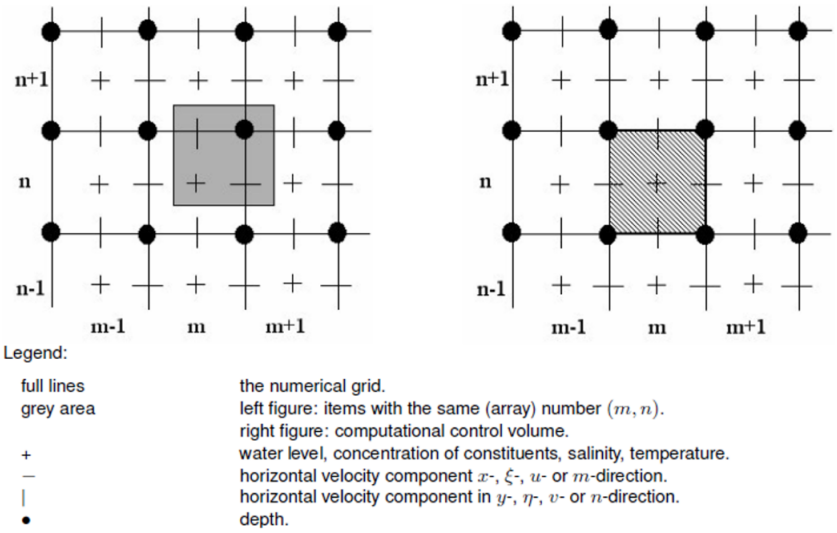

Figure A.2: Computational grid and components. Image retrieved from Deltares (2018)

Computational grids are constructed with D3D RGFGRID software tool. The process involves defining the model domain, generating a basic grid structure, and then refining it to capture important features such as channels, banks, and floodplains. Users can control grid resolution, ensuring finer grids in areas of interest while maintaining coarser grids elsewhere to optimize computational efficiency. Using the D3D QUICKIN program, a .dep files are generated to construct the initial morphological state.

Timestep The timestep should be small enough to capture the relevant changes in the modelled processes. Within a single timestep, numerical information (like a wave, bed disturbance etc) should not propagate further than the grid cell length, $\frac{\Delta t}{\Delta x} c \leq 1$, with c representing celerity; propagation speed. A fundamental principle for ensuring numerical stability in explicit numerical schemes is the Courant Friedrichs Lewis (CFL) condition:

$$CFL = \frac{\Delta t \sqrt{gH}}{\{\Delta x, \Delta y\}} < 1 \tag{A.2}$$

where $\Delta x, \Delta y$ are the dimensions of the gridcells. It is important to note that D3D adopts a semi-implicit numerical scheme as a fully implicit scheme can be time and storage-intensive; therefore, the Crank-Nicholson implicit finite difference approximation is used in D3D to solve the shallow water equations (Deltares, 2018). While Delft3D-FLOW uses a semi-implicit scheme, the CFL condition remains a useful guideline.

Hydrodynamics

D3D-FLOW solves the unsteady shallow-water equations in three dimensions or in depth-averaged two dimensions. The governing equations of Delft3D-FLOW are comprised of the continuity equation, the horizontal equations of motion and transport equations [mass-balance] for conservative constituents. These equations can be expressed in either orthogonal curvilinear coordinates in which the free surface level and bathymetry are defined relative to a flat horizontal reference plane or in spherical coordinates for large-scale global applications (Deltares, 2018; Lesser et al., 2004). The streamwise direction is referred to as the ξ direction and the transverse direction as η direction. The shallow water equations are derived from integrating the three-dimensional Navier-stokes equations over the depth. The depth-averaged continuity equation is derived from the integration of the continuity equation for incompressible fluids over the total depth and given by;

$$\frac{\partial \zeta}{\partial t} + \frac{1}{\sqrt{G_{\xi\xi}}\sqrt{G_{\eta\eta}}} \frac{\partial \left((d+\zeta)U\sqrt{G_{\eta\eta}}\right)}{\partial \xi} + \frac{1}{\sqrt{G_{\xi\xi}}\sqrt{G_{\eta\eta}}} \frac{\partial \left((d+\zeta)V\sqrt{G_{\xi\xi}}\right)}{\partial \eta} = (d+\zeta)Q \tag{A.3}$$

Where U and V are the depth-averaged velocities (ξ and η direction) and Q represents the global source or sink per unit area [m/s].
$\sqrt{G_{\xi\xi}}$ and $\sqrt{G_{\eta\eta}}$): coefficients used to transform curvilinear to rectangular coordinates, e.g. Δx and Δy (grid cell length) [m]

The momentum equations in the horizontal (ξ and η direction) directions are given by;

$$\begin{aligned} &\frac{\partial U}{\partial t} + \frac{U}{\sqrt{G_{\xi\xi}}}\frac{\partial U}{\partial \xi} + \frac{V}{\sqrt{G_{\eta\eta}}}\frac{\partial U}{\partial \eta} + \frac{UV}{\sqrt{G_{\xi\xi}}\sqrt{G_{\eta\eta}}}\frac{\partial \sqrt{G_{\xi\xi}}}{\partial \eta} - \frac{V^2}{\sqrt{G_{\xi\xi}}\sqrt{G_{\eta\eta}}}\frac{\partial \sqrt{G_{\eta\eta}}}{\partial \xi} + \\ &-fV = -\frac{1}{\rho_0\sqrt{G_{\xi\xi}}}P_\xi - \frac{gU\sqrt{U^2+V^2}}{C_{2D}^2(d+\zeta)} + F_\xi + F_{s\xi} + M_\xi \end{aligned} \tag{A.4}$$

and,

$$\begin{aligned} &\frac{\partial V}{\partial t} + \frac{U}{\sqrt{G_{\xi\xi}}}\frac{\partial V}{\partial \xi} + \frac{V}{\sqrt{G_{\eta\eta}}}\frac{\partial V}{\partial \eta} + \frac{UV}{\sqrt{G_{\xi\xi}}\sqrt{G_{\eta\eta}}}\frac{\partial \sqrt{G_{\eta\eta}}}{\partial \xi} - \frac{U^2}{\sqrt{G_{\xi\xi}}\sqrt{G_{\eta\eta}}}\frac{\partial \sqrt{G_{\xi\xi}}}{\partial \eta} + \\ &+fU = -\frac{1}{\rho_0\sqrt{G_{\eta\eta}}}P_\eta - \frac{gV\sqrt{U^2+V^2}}{C_{2D}^2(d+\zeta)} + F_\eta + F_{s\eta} + M_\eta \end{aligned} \tag{A.5}$$

f_v and f_u: Coriolis parameter in ξ, η-directions, respectively [1/s].
ν_V: Vertical eddy viscosity [m^2/s].
P_ξ and P_η: Gradients of hydrostatic pressure in ξ, η-directions [kg/(m^{2}s^2)].
F_ξ and F_η: Turbulent momentum fluxes in ξ, η-directions [m/s^2].
$F_{s\xi}$ and $F_{s\eta}$: The effect of the secondary flow on the depth-averaged velocities (shear stresses by depth-averaging the non-linear acceleration terms)
M_ξ and M_η: Source or sink of momentum in ξ, η-directions [m/s^2].

Parameterized Secondary Flow
The spiral motion intensity of the secondary flow is defined as the a velocity component normal to the depth-averaged main flow. The magnitude of this intensity I, is calculated as follows;

$$I = \int_{-1}^{0} |v(\sigma)|\, d\sigma \tag{A.6}$$

To incorporate the secondary flow effects in the model, an additional advection-diffusion equation is added as well as additional terms in the momentum equation to account for the additional shear stresses ($F_{s\xi}$ and $F_{s\eta}$ term in Eq. (A.4) and Eq. (A.5).

$$\begin{aligned} F_{s\xi} = &\frac{1}{d+\zeta}\left\{\frac{1}{\sqrt{G_{\xi\xi}}}\frac{\partial\left[(d+\zeta)T_{\xi\xi}\right]}{\partial \xi} + \frac{1}{\sqrt{G_{\eta\eta}}}\frac{\partial\left[(d+\zeta)T_{\xi\eta}\right]}{\partial \eta}\right\} \\ &+\left\{\frac{2T_{\xi\eta}}{\sqrt{G_{\xi\xi}}\sqrt{G_{\eta\eta}}}\frac{\partial\sqrt{G_{\xi\xi}}}{\partial \eta} + \frac{2T_{\xi\xi}}{\sqrt{G_{\xi\xi}}\sqrt{G_{\eta\eta}}}\frac{\partial\sqrt{G_{\eta\eta}}}{\partial \xi}\right\} \end{aligned} \tag{A.7}$$

and,

$$F_{s\eta} = \frac{1}{d+\zeta}\left\{\frac{1}{\sqrt{G_{\xi\xi}}}\frac{\partial\left[(d+\zeta)T_{\eta\xi}\right]}{\partial\xi} + \frac{1}{\sqrt{G_{\eta\eta}}}\frac{\partial\left[(d+\zeta)T_{\eta\eta}\right]}{\partial\eta}\right\} + \left\{\frac{2T_{\eta\eta}}{\sqrt{G_{\xi\xi}}\sqrt{G_{\eta\eta}}}\frac{\partial\sqrt{G_{\xi\xi}}}{\partial\eta} + \frac{2T_{\eta\xi}}{\sqrt{G_{\xi\xi}}\sqrt{G_{\eta\eta}}}\frac{\partial\sqrt{G_{\eta\eta}}}{\partial\xi}\right\} \tag{A.8}$$

The intensity is taken into account in the morphological calculations, leading to the change in bed shear stress direction and therefore the sediment transport direction. The bed shear stress component normal to the flow directions is given by;

$$\tau_{br} = -2\rho\alpha^2(1-\alpha)\left|\vec{U}\right| I, \quad \text{with} \quad \alpha = \frac{\sqrt{g}}{\kappa C_{2D}} < \frac{1}{2} \tag{A.9}$$

Where $|\vec{U}|$ is the magnitude of the depth-averaged velocity and C_{2D} the 2D Chézy coefficient. in which T represent the shear stresses in the various directions.

The updated direction for bedload transport , refered to as φ_τ in D3D, which is comparable to δ given in Eq. (3.4), is given by,

$$\tan(\varphi_\tau) = \frac{v - \alpha_I \frac{u}{U} I_s}{u + \alpha_I \frac{v}{U} I_s}, \quad \text{where} \quad \alpha_I = \frac{2}{\kappa^2} E_s \left(1 - \frac{\sqrt{g}}{\kappa C}\right) \tag{A.10}$$

α_I Is equal to Eq. (3.5) except for the addition of E_s, this coefficient is user-definable in the D3D input files.

Roughness and Bed Shear Stress

The roughness of the bed determines the friction coefficient, which is essential in calculating the equilibrium depth, velocity, bed shear stress and bedforms. Higher roughness mean the riverbed exerts greater shear stresses on the flowing water. These shear stresses have a cascading effect: they slow down the overall flow velocity, influence how sediment is transported, and shape the river channel's depth and form. Over the last centuries, various empirical relations have been developed. Most widely adopted are Chézy and Manning. D3D allows the following methods for computing the bottom roughness; Manning, White-Colebrook and Chézy. The roughness values are specified for both streamwise and transverse directions within the main input file. In the depth-averaged 2DH model the shear stresses are calculated a quadration friction law;

$$\vec{\tau}_b = \frac{\rho g \vec{U}|\vec{U}|}{C^2} \tag{A.11}$$

, where C is the Chézy coefficient [m1/2/s] and $\vec{U}$ the magnitude of the depth-averaged horizontal velocity. Manning's coefficient (n) and the Chézy coefficient (C) are related by the equation;

$$C = \frac{H^{\frac{1}{6}}}{n} \tag{A.12}$$

where n is Manning coefficient [s/m1/3]. The Manning roughness value is thus dependent on the water depth.

Sediment Transport Predictor

DELFT3D offers numerous sediment transport predictors for various sediment types (cohesive/non-cohesive) and transport modes (suspended/bedload). This study will only focus on bedload transport of non-cohesive sediment and therefore avoid solving the suspended load advection-diffusion equation,

Among DELFT3D's 12 transport predictors, this study focuses on the Meyer-Peter and Müller (1948) formula and potential variations of it. Its general form is as follows:

$$S = \alpha D_{50}\sqrt{\Delta g D_{50}}\theta^{b}\left(\mu\theta - \xi\theta_{cr}\right)^{c} \tag{A.13}$$

with α as calibration coefficient and powers b, c and ripple factor μ and critical Shields parameter θ_{cr} as user-defined parameters. Meyer-Peter and Müller (1948) experimentally arrived on the following values: $\alpha = 8\ b = 0$, $c = 1.5\ \mu = 1\ \theta_{cr} = 0.047$. This formula was chosen for its relative simplicity and comprehensive development, having been derived upon with both sand and gravel fractions in flume experiments. This stands in contrast to some alternative predictors that are solely calibrated for sand. Note that there are no perfect sediment transport predictors for such coarse gravel found in the study area. The MPM formula was developed for unisized sediment but underwent subsequent adaptations to accommodate mixed-sized sediment dynamics (Scheer et al., 2002). Notably, adaptations such as the Ashida-Michiue method have been introduced, which incorporate factors related to hiding and exposure. Although compatible with D3D modeling, it was decided against using the Ashida-Michiue transport predictor due to the intention of implementing hiding/exposure effects separately within D3D. This approach offers advantages in terms of enhanced transport predictions with reduced complexity, along with increased flexibility for tuning the hiding/exposure factors.

Interaction of sediment fractions

Again, here multiple formulations can be used in the software. This study has chosen for the use of the Parker et al. (1982) due to its simplicity and intention for gravel bed streams;

$$\xi = \left(\frac{D_m}{D_i}\right)^{\alpha} \tag{A.14}$$

, where ξ is used in Eq. (A.13) to alter the critical Shields' number depending on the size of the particle in question, D_i, relative to the mean diameter D_m (or D_{50}).

Transverse bed slope

The previously described Koch and Flokstra (1980) adjustment (Eq. (3.6)) for bed slope effects on bedload transport is implemented using the Talmon et al. (1995) extension (Eq. (3.7)).

$$\tan\left(\varphi_s\right) = \frac{\sin\left(\varphi_\tau\right) + \frac{1}{f(\theta)}\frac{\partial z_b}{\partial y}}{\cos\left(\varphi_\tau\right) + \frac{1}{f(\theta)}\frac{\partial z_b}{\partial x}} \tag{A.15}$$

with,

$$f(\theta) = A_{shld}\theta_i^{B_{shld}}\left(\frac{D_i}{H}\right)^{C_{shld}}\left(\frac{D_i}{D_m}\right)^{D_{shld}} \tag{A.16}$$

Therefore updating the direction of sediment transport with angle φ_τ.

Morphology, bed level update

Bedlevel is updated using the expression (Deltares, 2018);

$$\Delta_{SED}^{(m,n)} = \frac{\Delta t f_{\text{MORFAC}}}{A^{(m,n)}}\left(\begin{array}{c} S_{b,uu}^{(m-1,n)}\Delta y^{(m-1,n)} - S_{b,uu}^{(m,n)}\Delta y^{(m,n)} + \\ S_{b,vv}^{(m,n-1)}\Delta x^{(m,n-1)} - S_{b,vv}^{(m,n)}\Delta x^{(m,n)} \end{array}\right) \tag{A.17}$$

B

Reference Model Parameters

Parameter	Symbol	Unit	Value
Total Length		[km]	5.5
Slope Upstream of bifurcation		[-]	1.7×10^{-3}
Slope Kauriala branch		[-]	1.44×10^{-3}
Slope Geruwa branch		[-]	1.6×10^{-3}
Bankfull width upstream boundary		[m]	500
Bankfull width downstream branches		[m]	300
Number of sediment classes			5
Sediment class sizes		[cm]	0.1, 2, 5, 10, 40
Median sediment grain size	D_{50}	mm	74.2
Morphological acceleration factor	MorFac		100
Runtime		days	60
Simulated time		monsoon years	60
Base monsoon discharge		$[m^3/s]$	2500
Peak discharge		$[m^3/s]$	6000
Peak duration (total)		days	10
Morphological spin-up time (simulation time)	MorFac	days	55.6
Longitudinal bed gradient factor	AlfaBs	[-]	1.0
Hiding/exposure parameter (Eq. (A.14))	ASKLHE		0.8
Spiral flow coefficient (Eq. (A.10)	Espir		1.0
Multiplicative factor for bedslope formulation (Eq. (A.16))	Ashld		0.7
Powerfactor for bedslope formulation (Eq. (A.16))	Bshld		0.5
Powerfactor for bedslope formulation (Eq. (A.16))	Cshld		0.0
Powerfactor for bedslope formulation (Eq. (A.16))	Dshld		0.0
Sediment layer schematisation model	IUnderLyr	[-]	2
Transport layer thickness formulation	TTLForm	[-]	1
Transport layer thickness	ThTrLyr	[m]	1.0
Max number of underlayers	MxNULyr	[-]	5
Underlayer thickness	ThUnLyr	[m]	1
Calibration coefficient transport formula (Eq. (A.13))	α	[-]	8
Calibration powerfactor (Eq. (A.13))	b	[-]	0.0
Calibration powerfactor (Eq. (A.13))	c	[-]	1.5
Ripple factor (Eq. (A.13))	μ	[-]	1
Critical Shields' mobility parameter(Eq. (A.13))	θ_{cr}	[-]	0.040
Manning coefficient		$[s/m^{1/3}]$	0.035

Table B.1: List of relevant settings used in the reference model.

C

Model Data - Decadal Bed Level Change

Discharge distribution classification of all runs

In Table C.1 an overview of the resulting discharge distribution of all run is given. What stands out is that increasing the Ashld and Dshld parameters compared to the reference settings leads to strong favouring of the Geruwa branch. Kauriala is dominant in the run shown in the column on the right.

Geruwa Domination (>75 % Discharge)	Balanced (Between 25%-75% Discharge)	Kauriala Domination (>75 % Discharge)
	REFERENCE	
Excluding Coarse Fractions	Excluding Sand Fraction	Uniform Sediment (7.4 cm)
Increased Hiding/Exposure (0.982)	Active Layer Thickness: 0.5 m	Active Layer Thickness: 2 m
Spiral Flow : 2	Equal slopes branches (i : 1.6)	No Hiding/Exposure
Ashld : 1.0	10% slope advantage Kauriala	Reduced Hiding/Exposure (0.6)
Ashld : 1.3	Sedimentation Geruwa 25 cm	Spiral Flow : 0
Dshld : 0.5	Sedimentation Geruwa 50 cm	20% slope advantage Kauriala
Dshld: 1.0	Ashld: 0.4	Sedimentation Geruwa 100 cm
	Dshld : 0.25	Double Peak flood discharge

Table C.1: Table summarizing all the runs and their effect on discharge distribution.

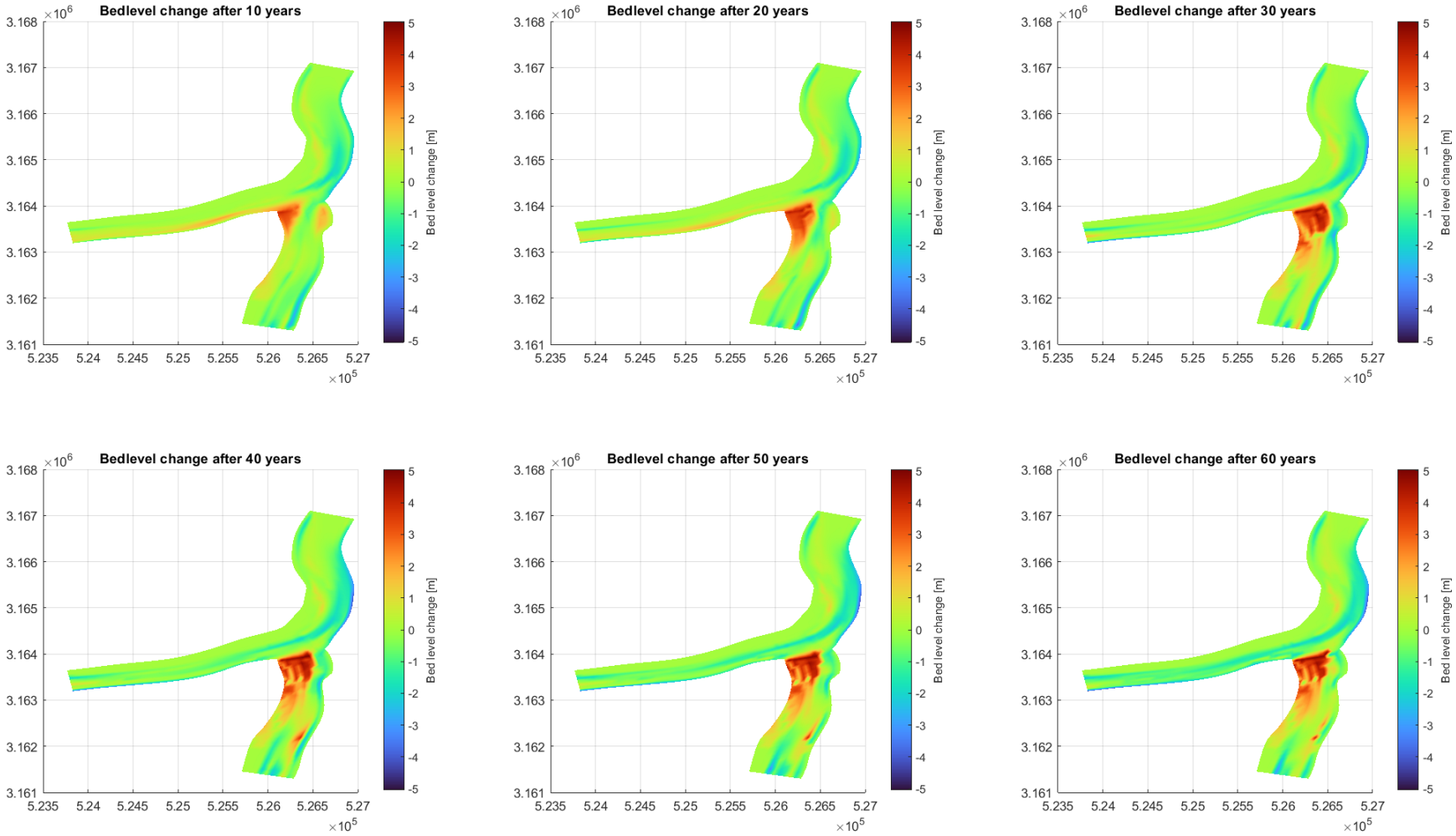

Figure C.1: Model evolution; **reference model**

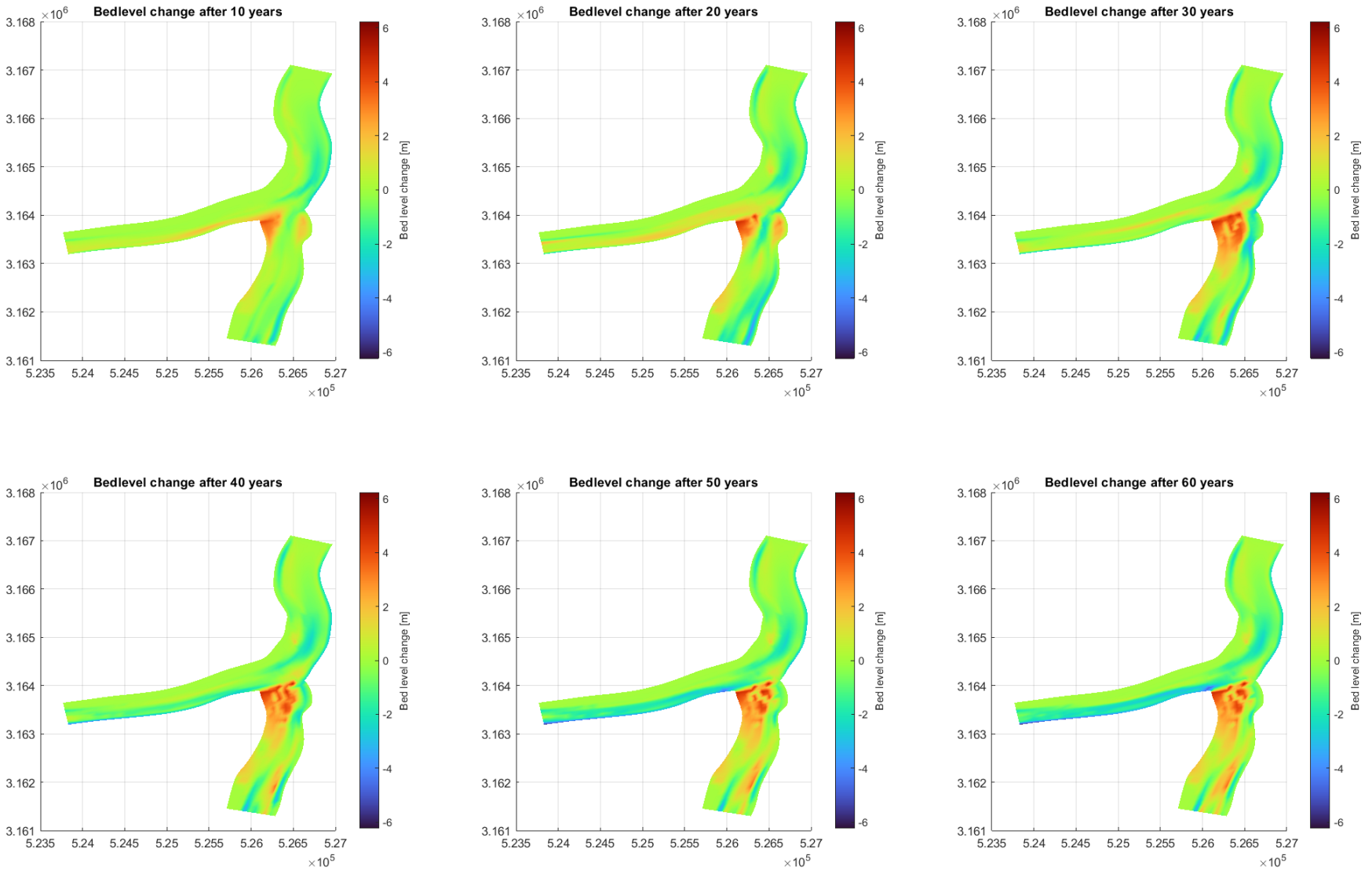

Figure C.2: Model evolution; **Double Peak of 10000 m^3/s in 10th monsoon season**

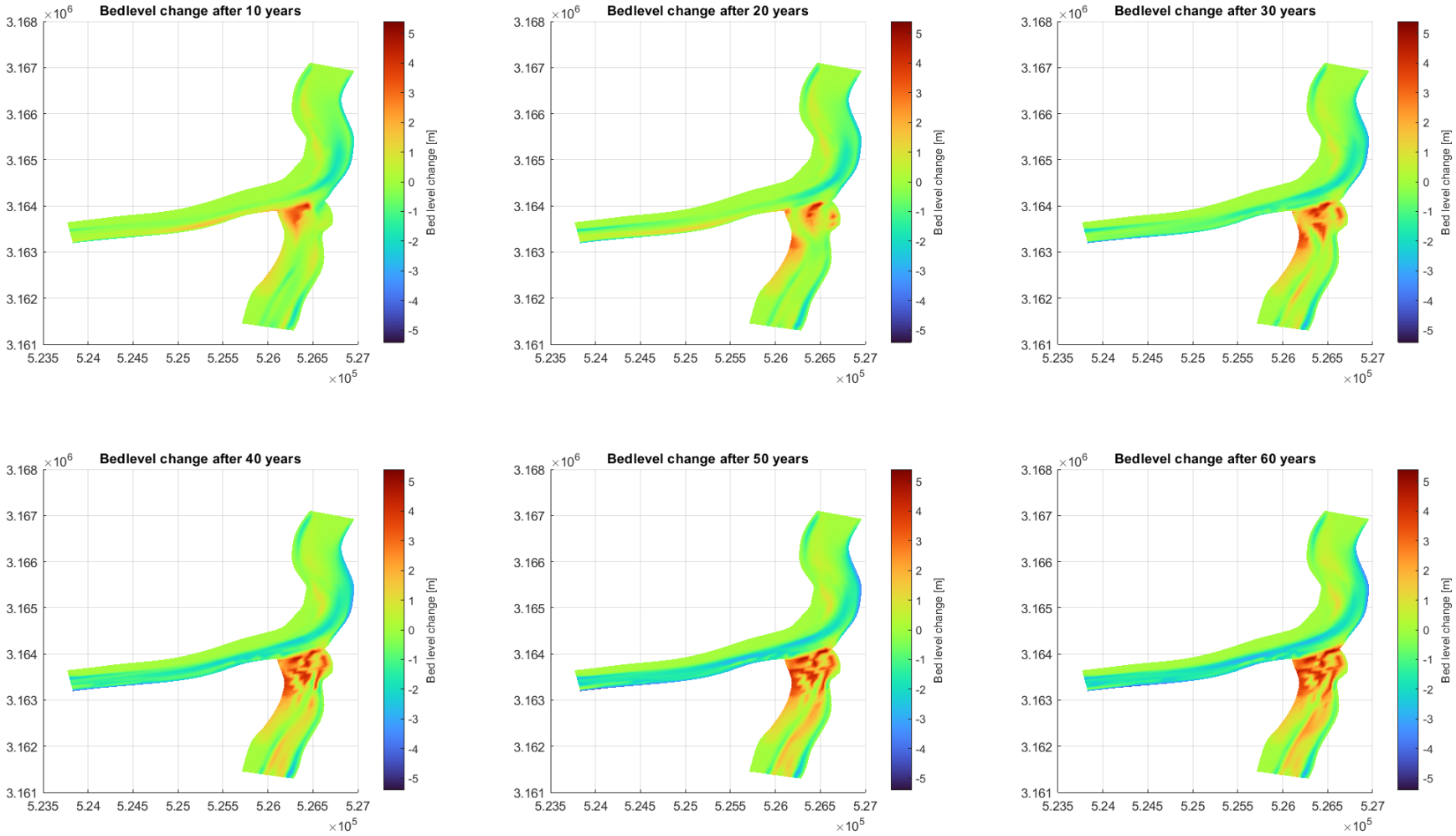

Figure C.3: Model evolution; **Spiral flow at 0**

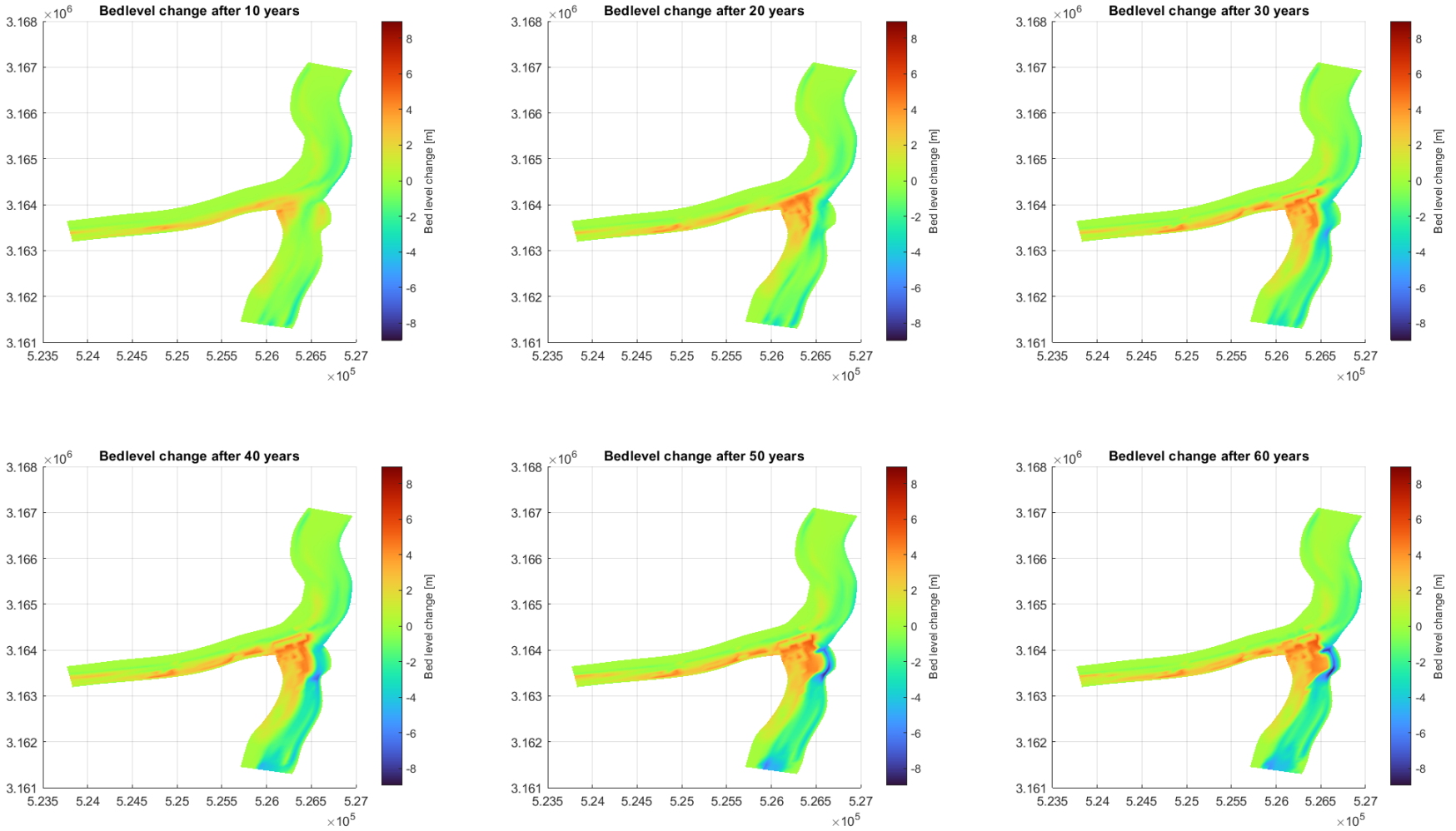

Figure C.4: Model evolution; **Spiral flow at 2**

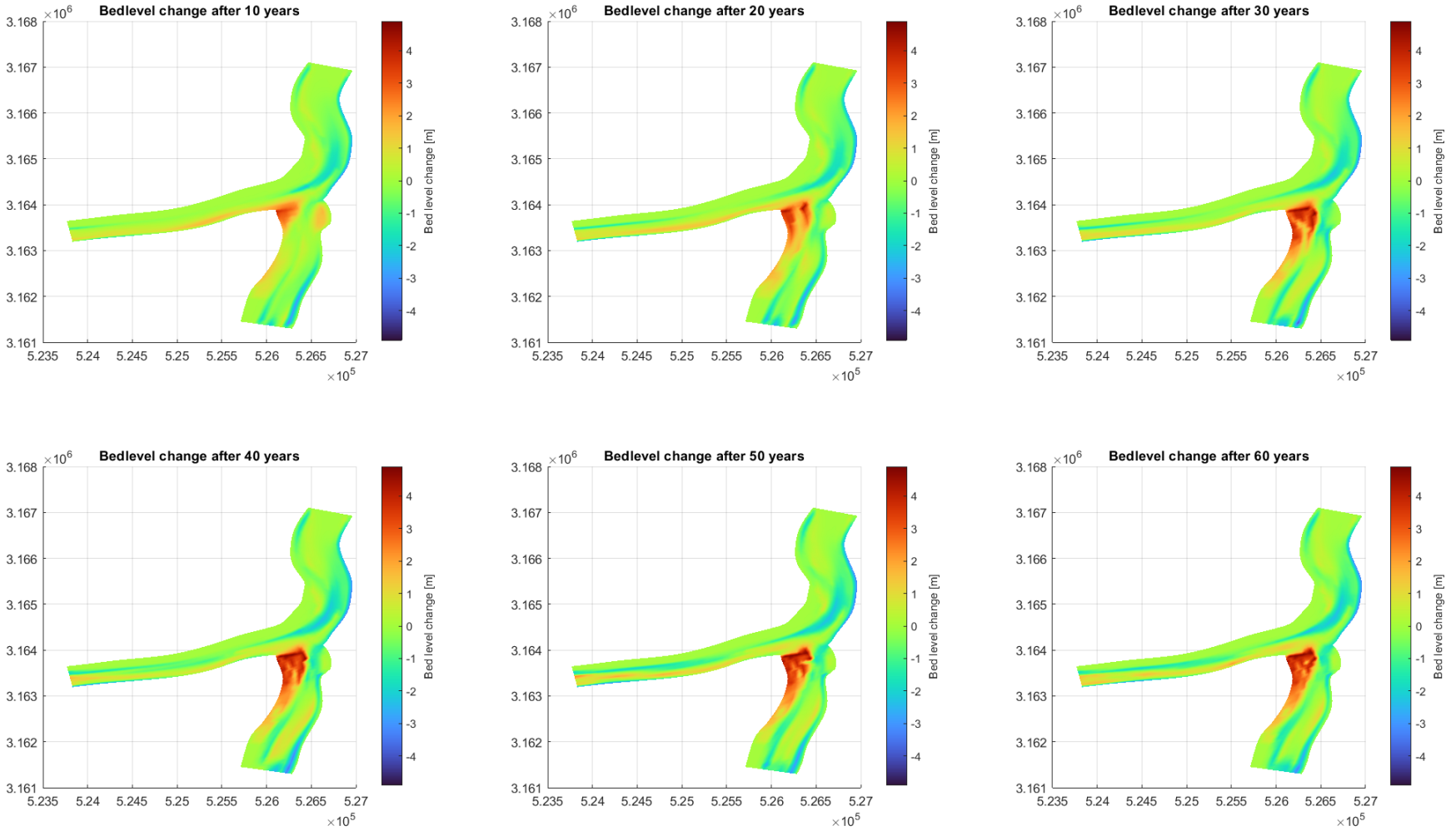

Figure C.5: Model evolution; **A shield = 0.4**

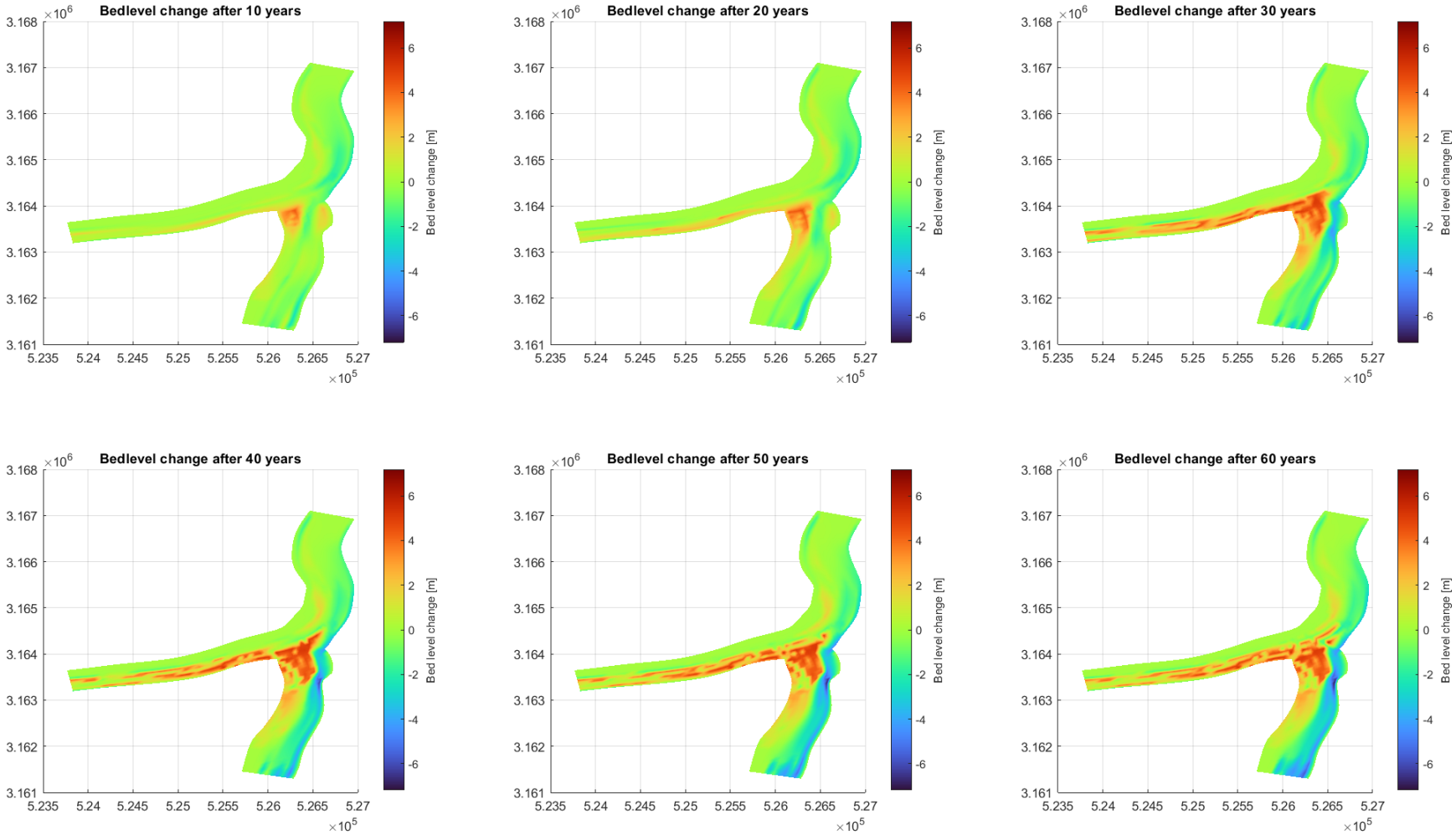

Figure C.6: Model evolution; **A shield = 1.0**

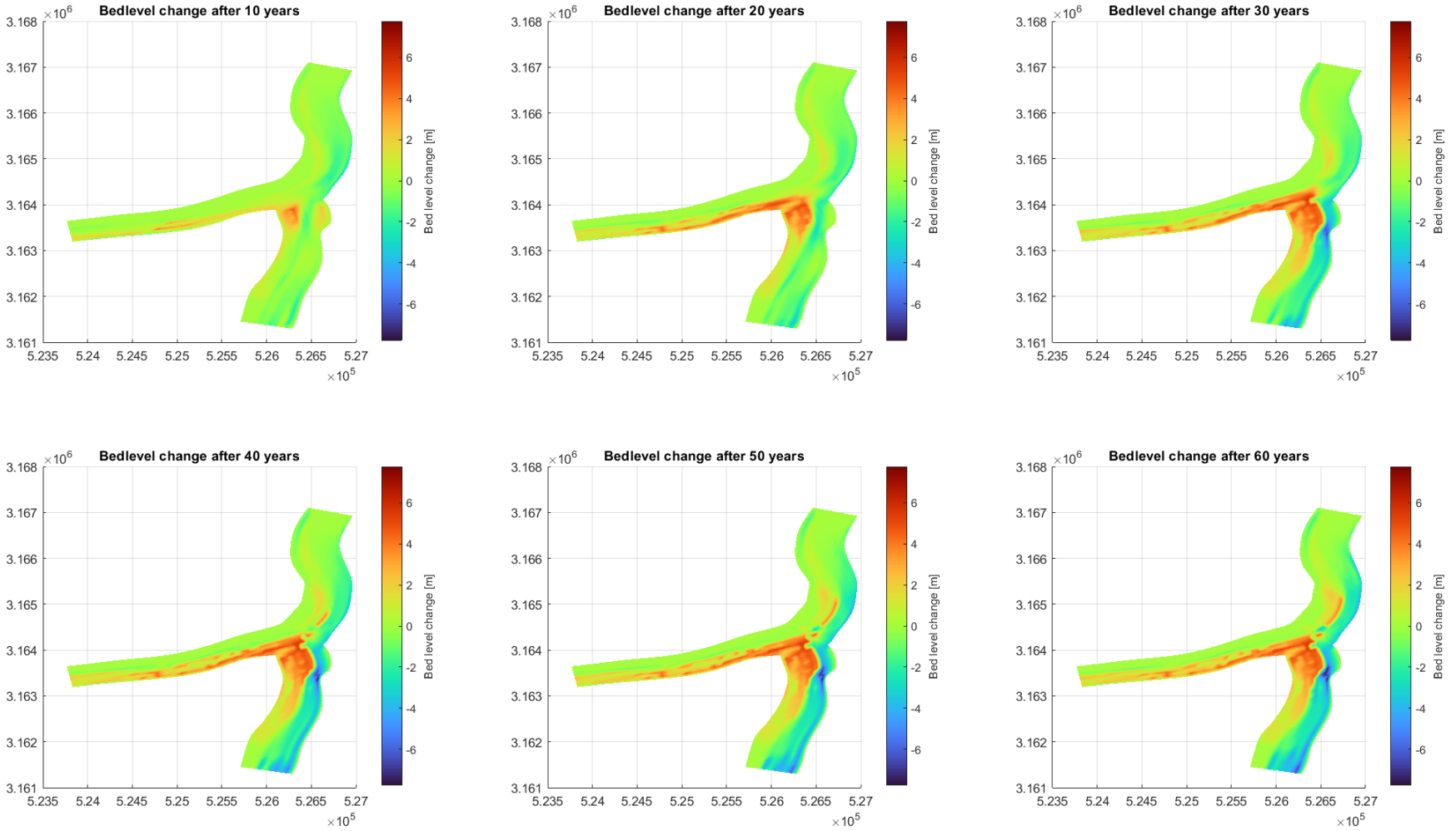

Figure C.7: Model evolution; **A shield = 1.3**

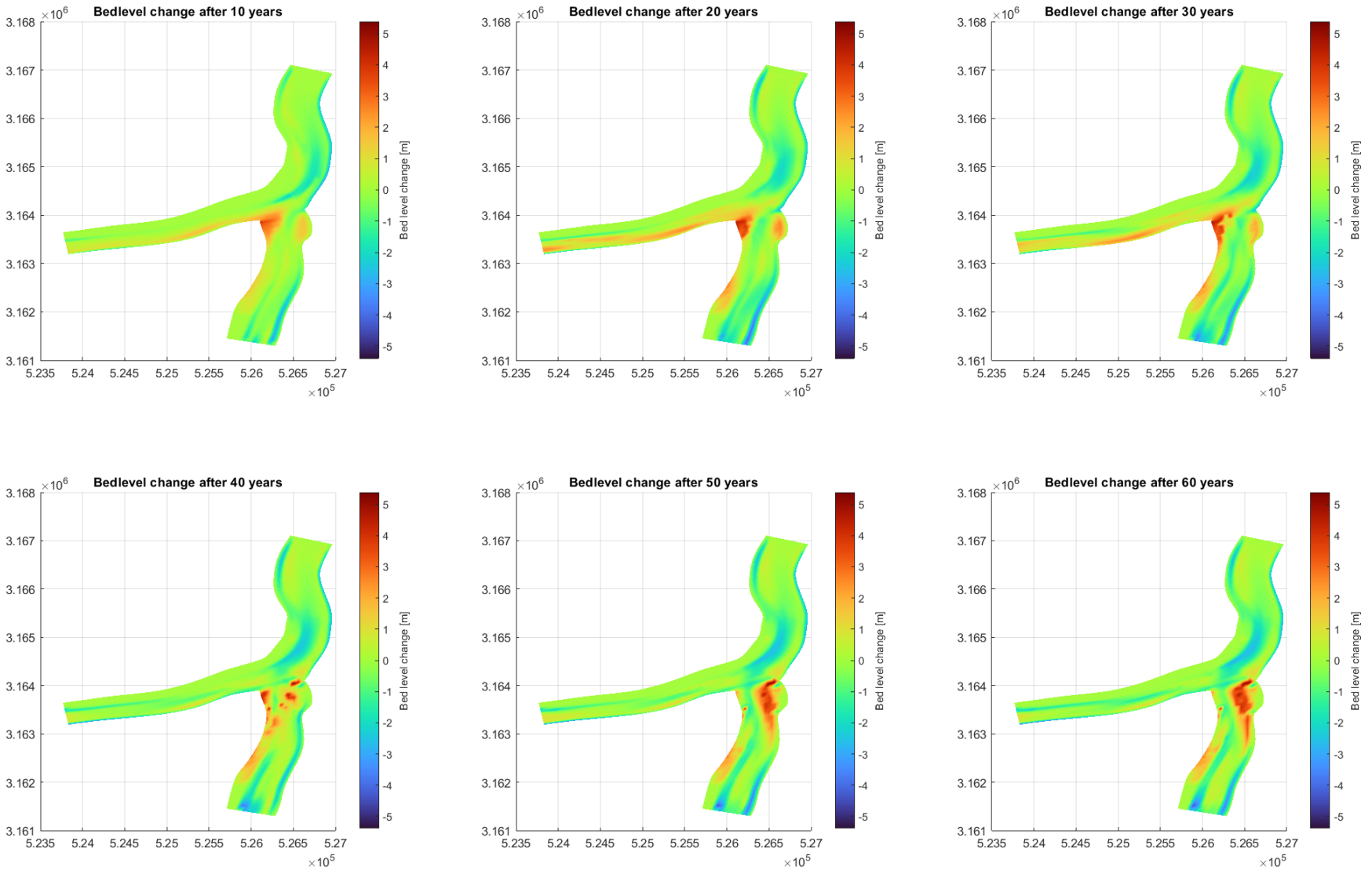

Figure C.8: Model evolution; Double peak run with **A shield = 0.4**

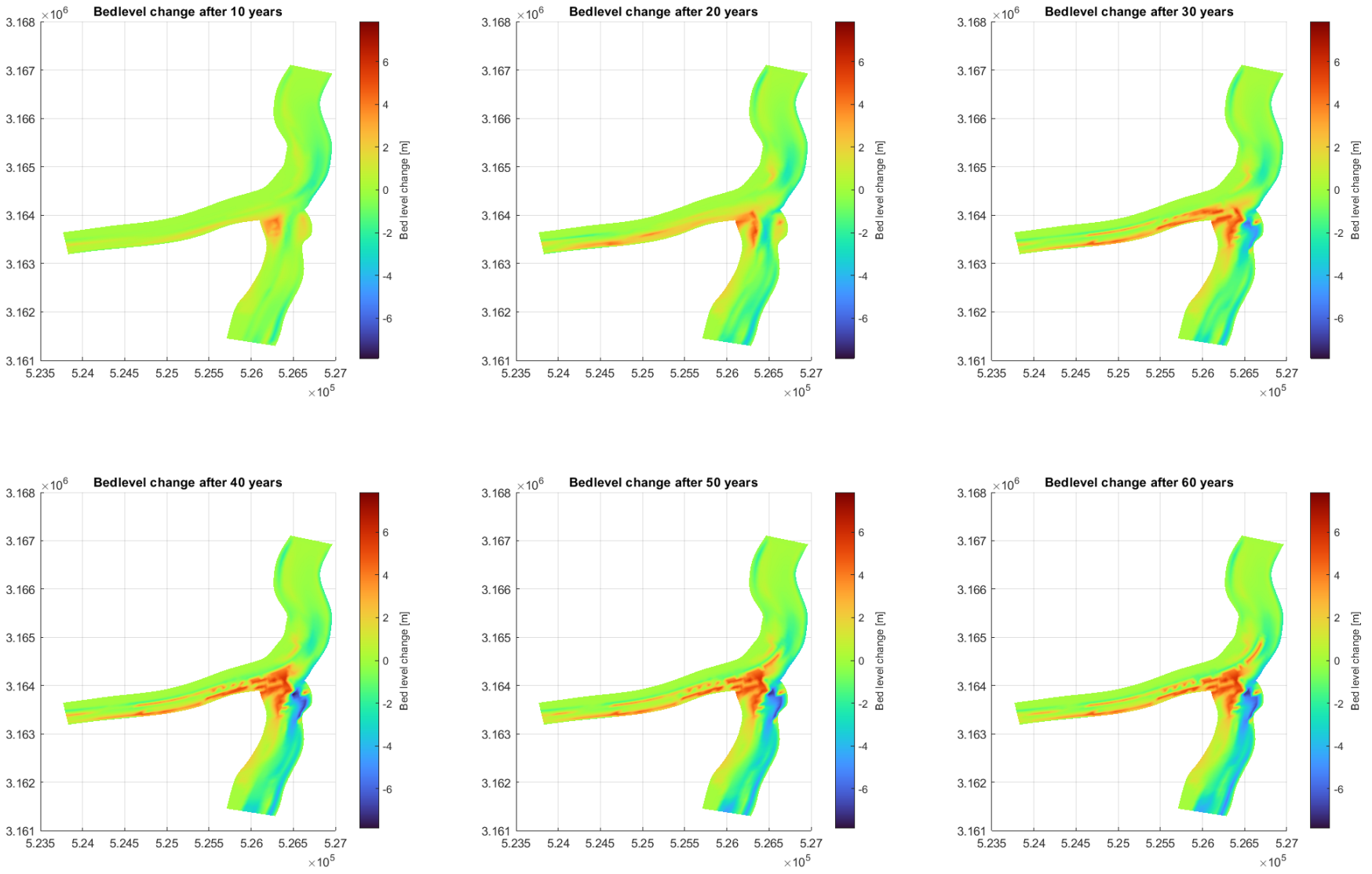

Figure C.9: Model evolution; Double peak run with **A shield = 1.0**

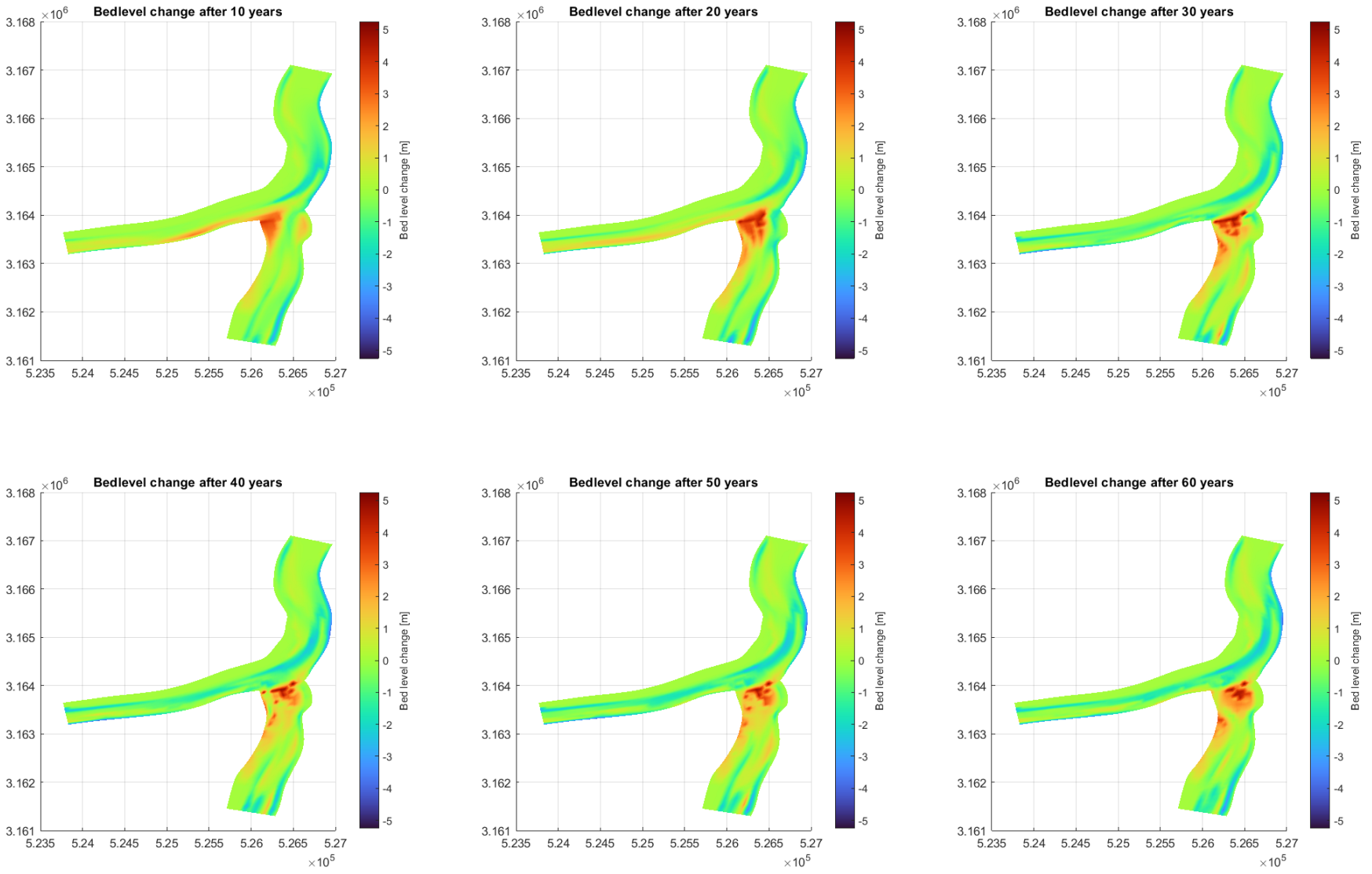

Figure C.10: Model evolution; **D shield = 0.25**

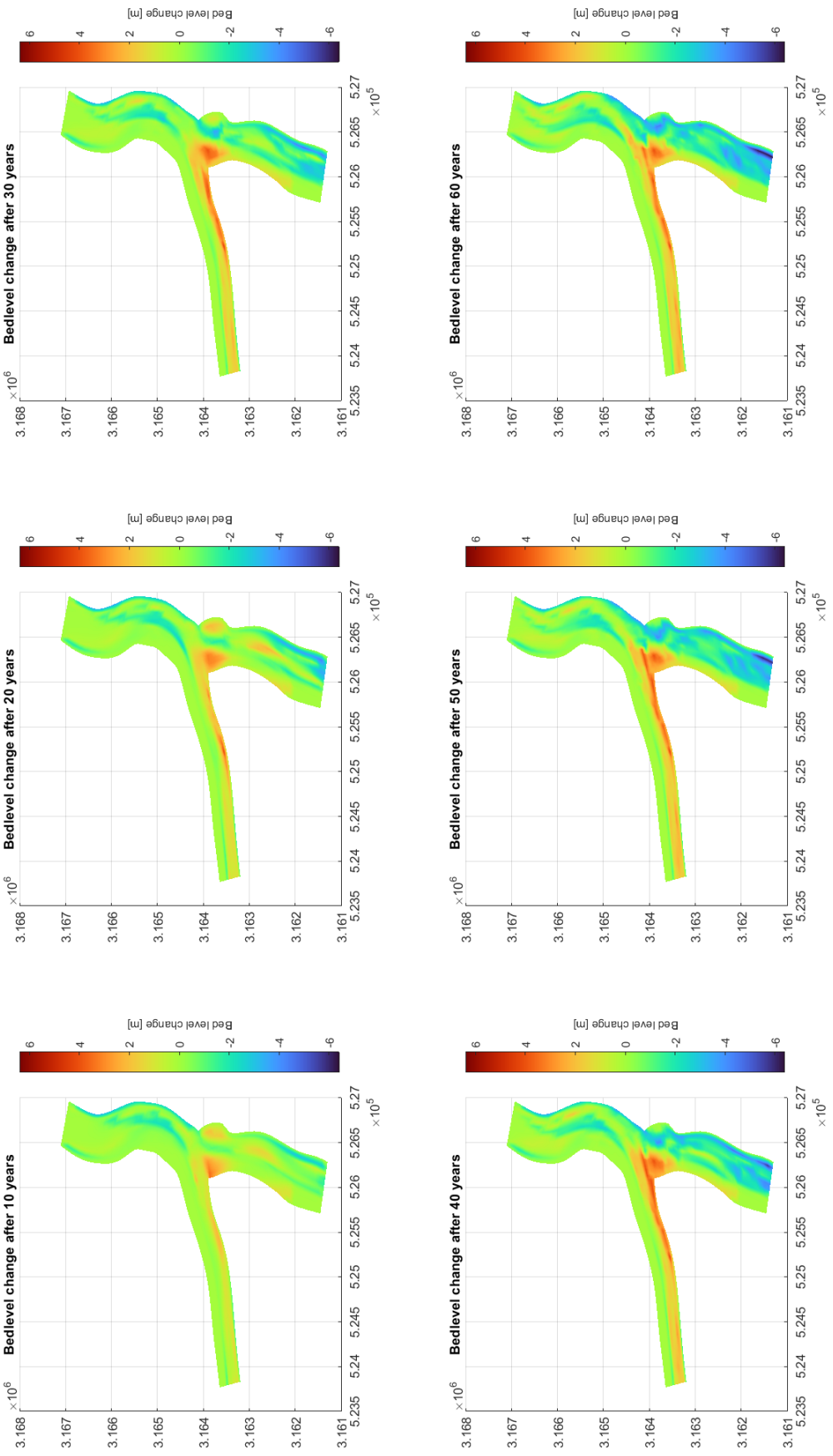

Figure C.11: Model evolution; **D shield = 0.5**

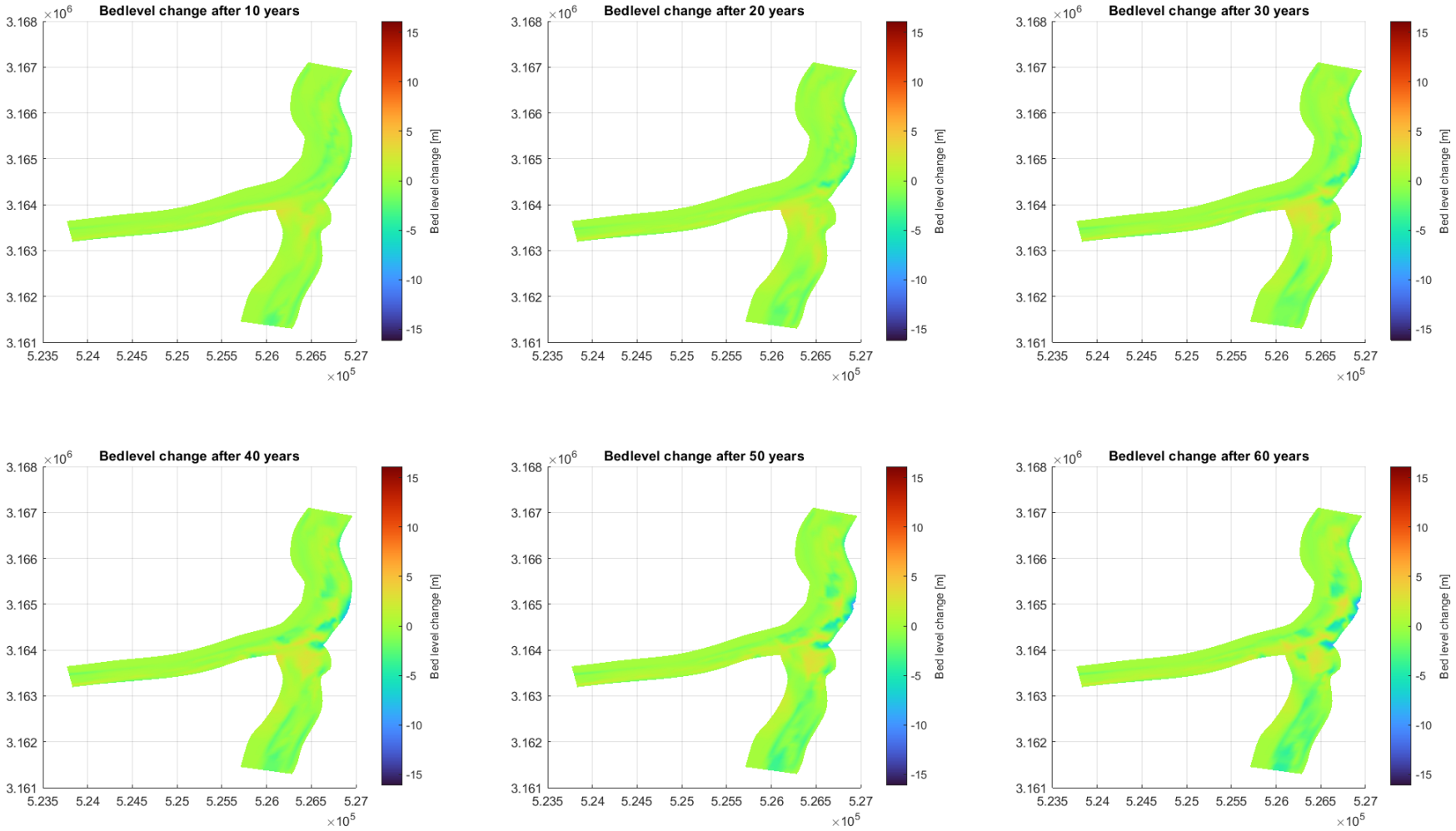

Figure C.12: Model evolution; **D shield = 1.0**

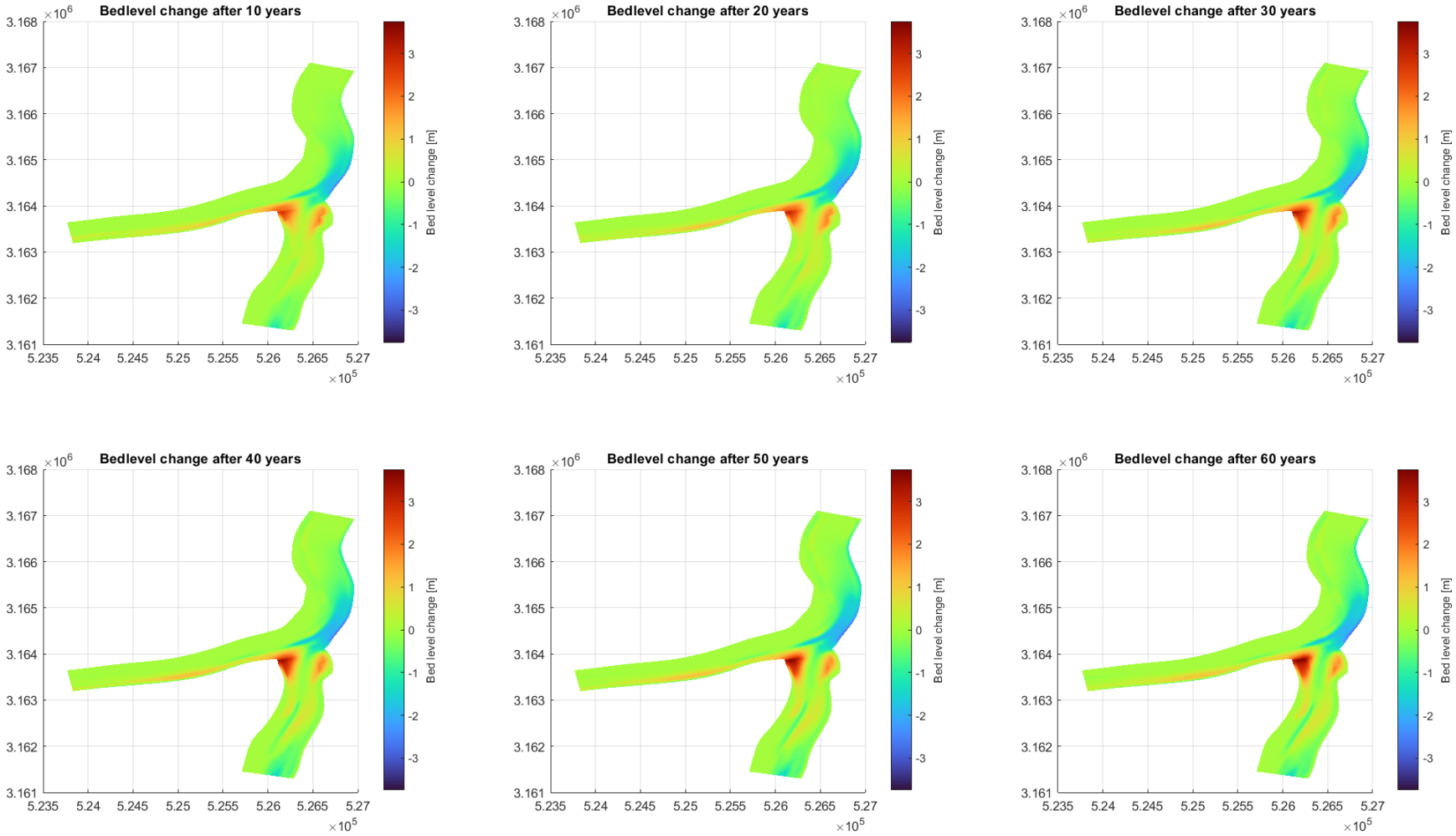

Figure C.13: Model evolution; **without sand** [1 mm] fraction

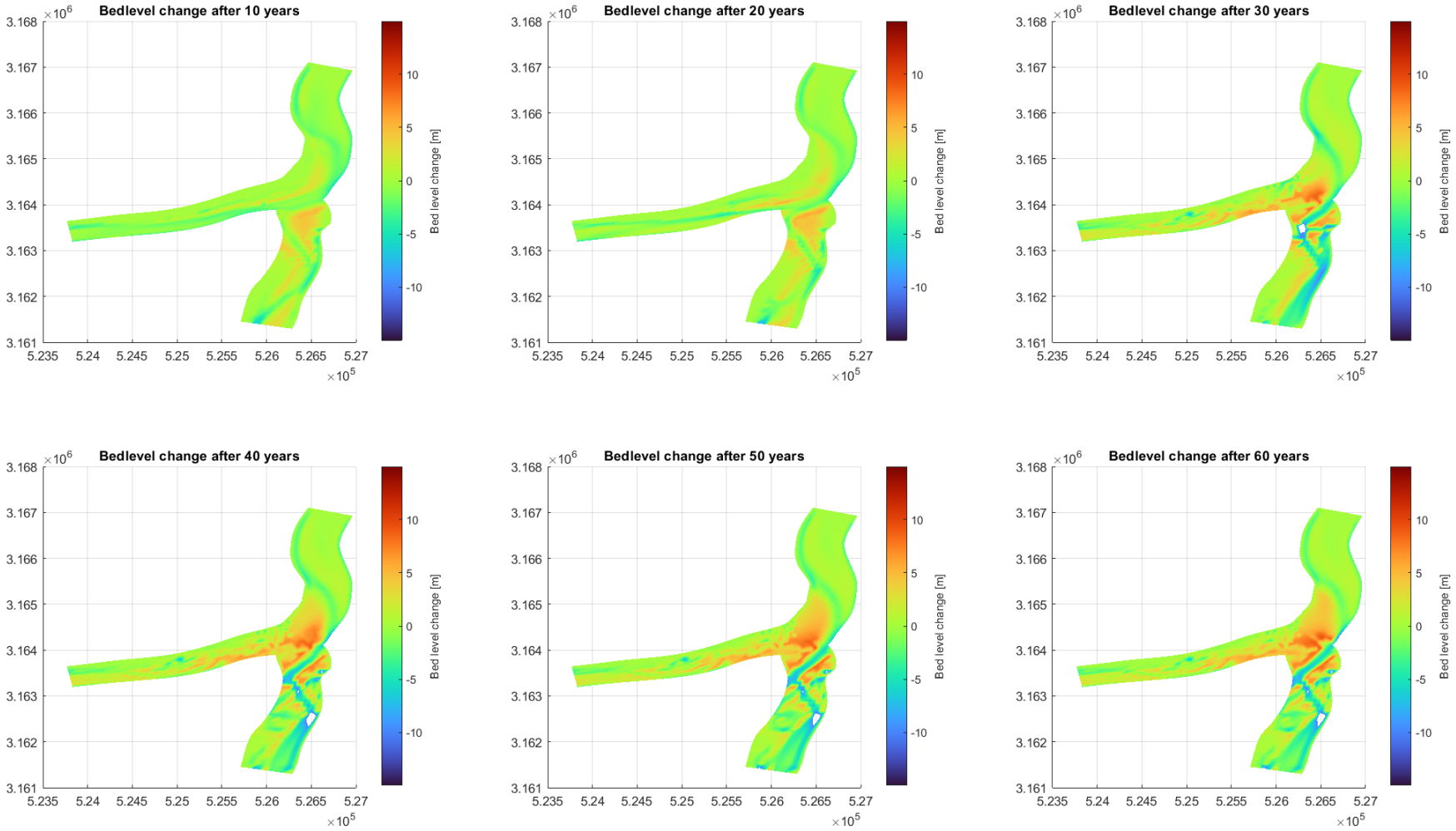

Figure C.14: Model evolution; **without coarse fractions** [10 cm and 40 cm]

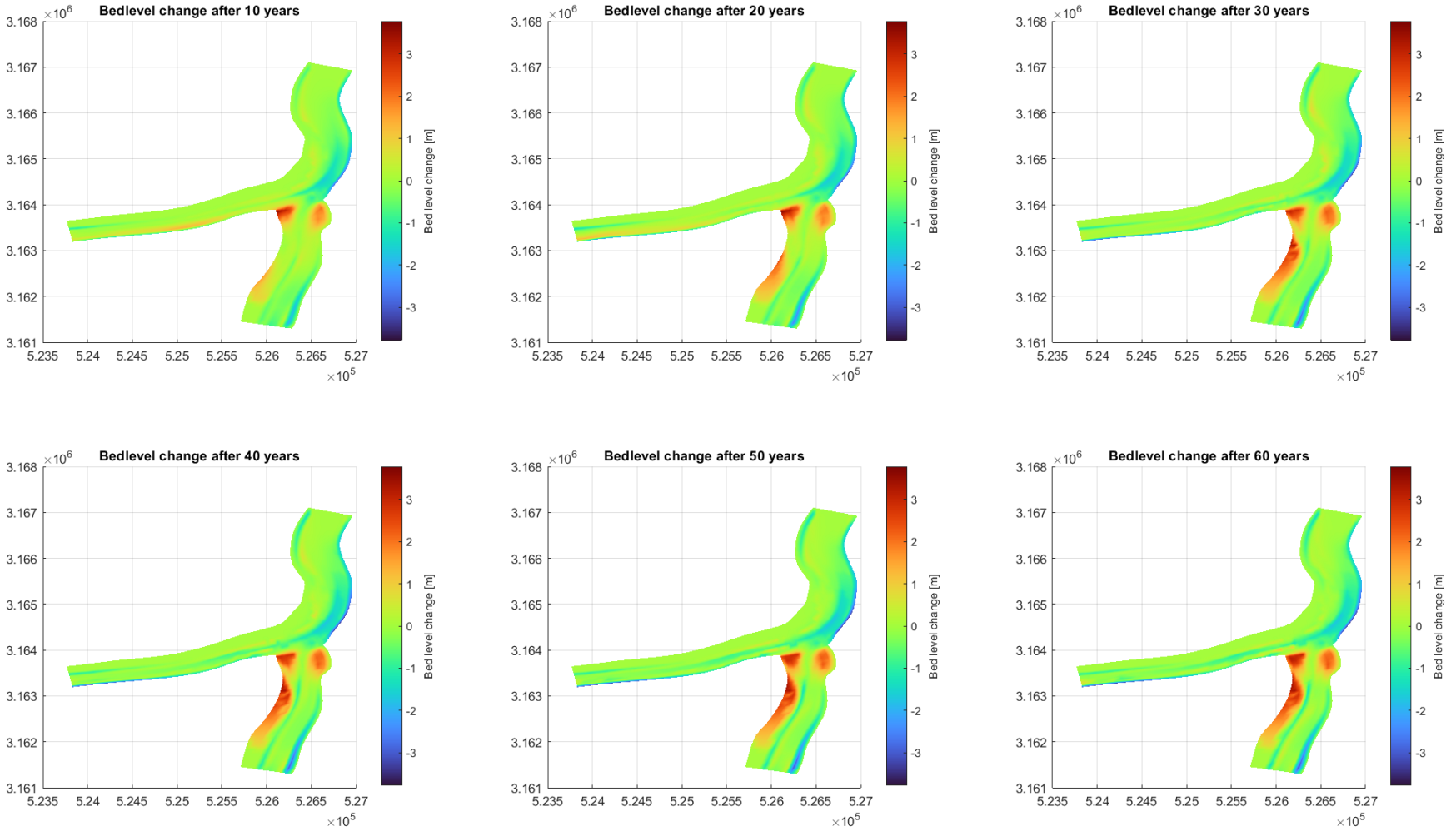

Figure C.15: Model evolution; **active layer of 0.5 meter**

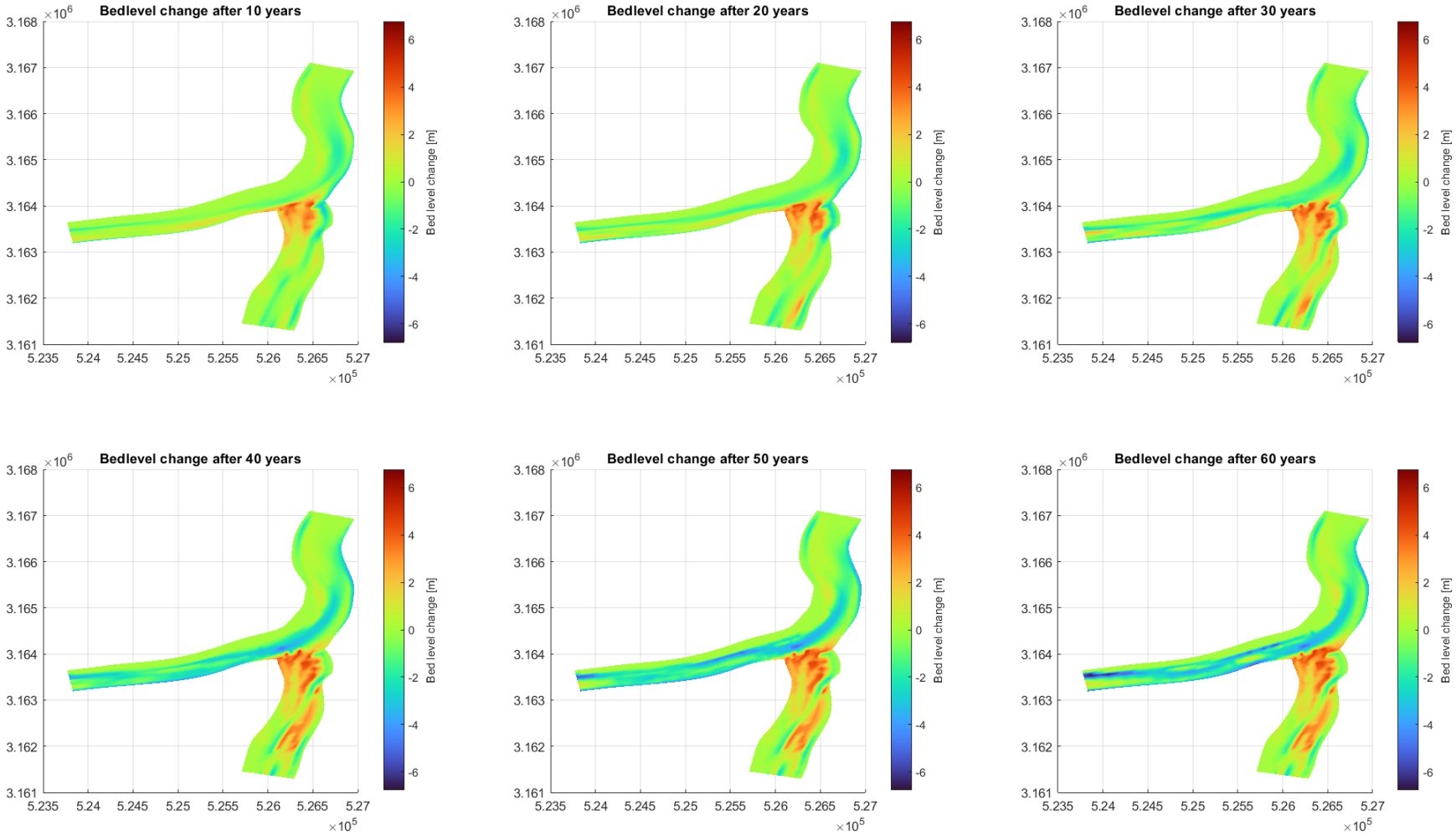

Figure C.16: Model evolution; **active layer of 2.0 meter**

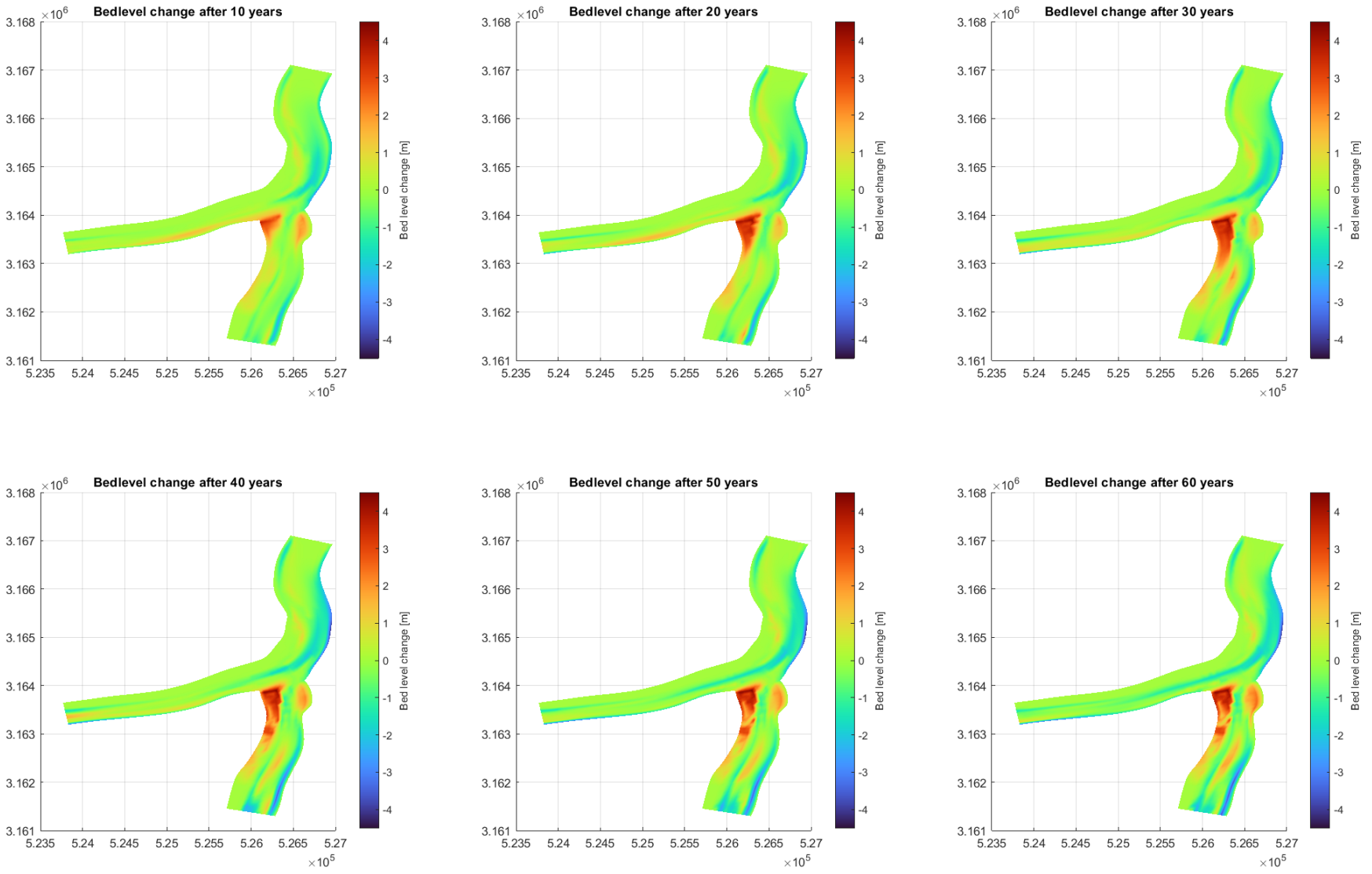

Figure C.17: Model evolution; **Imposed 25 cm initial sedimentation of Geruwa branch** (bed level height increased whilst slope remains the same)

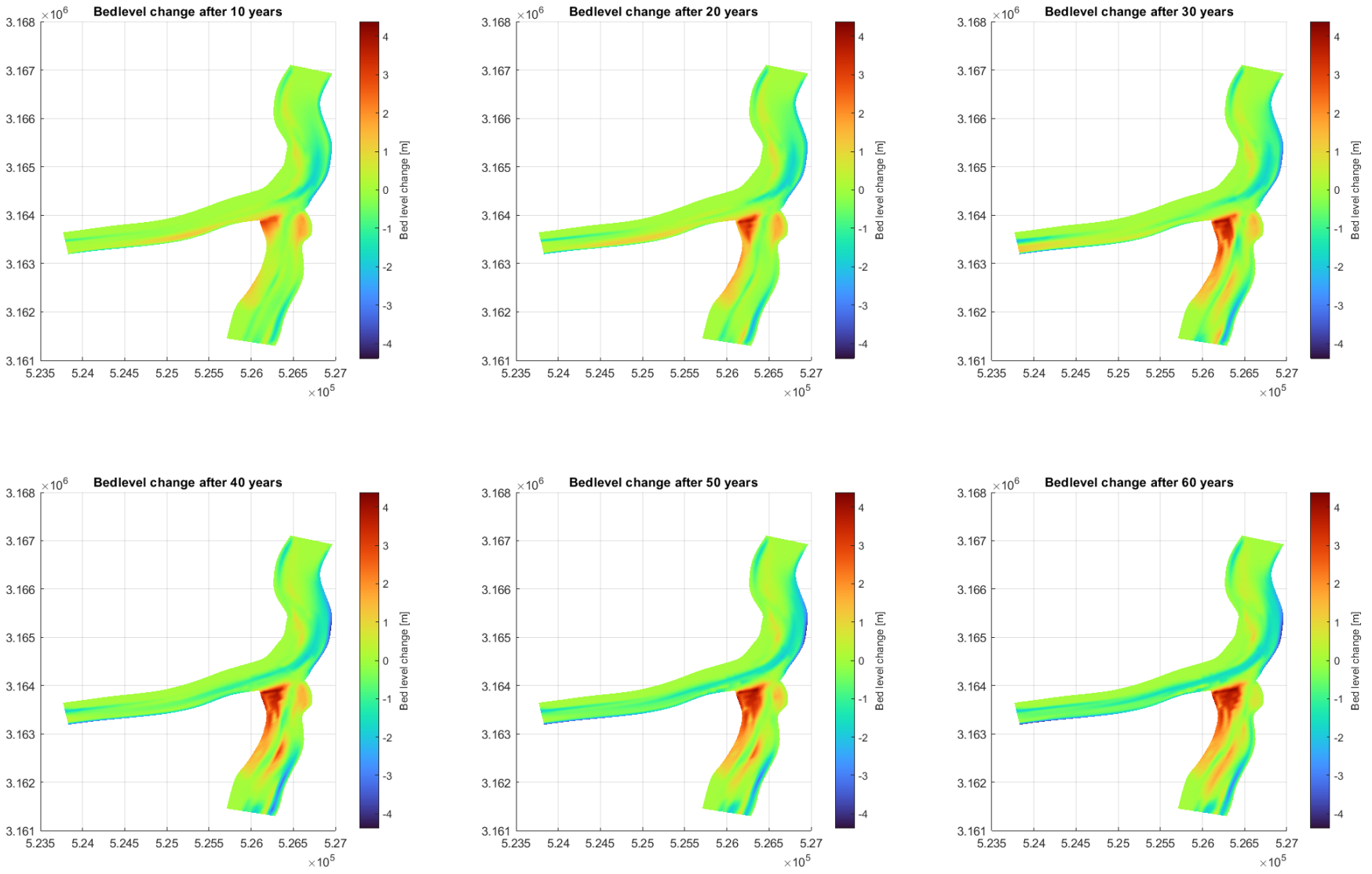

Figure C.18: Model evolution; **Imposed 50 cm initial sedimentation of Geruwa branch** (bed level hight increased whilst slope remains the same)

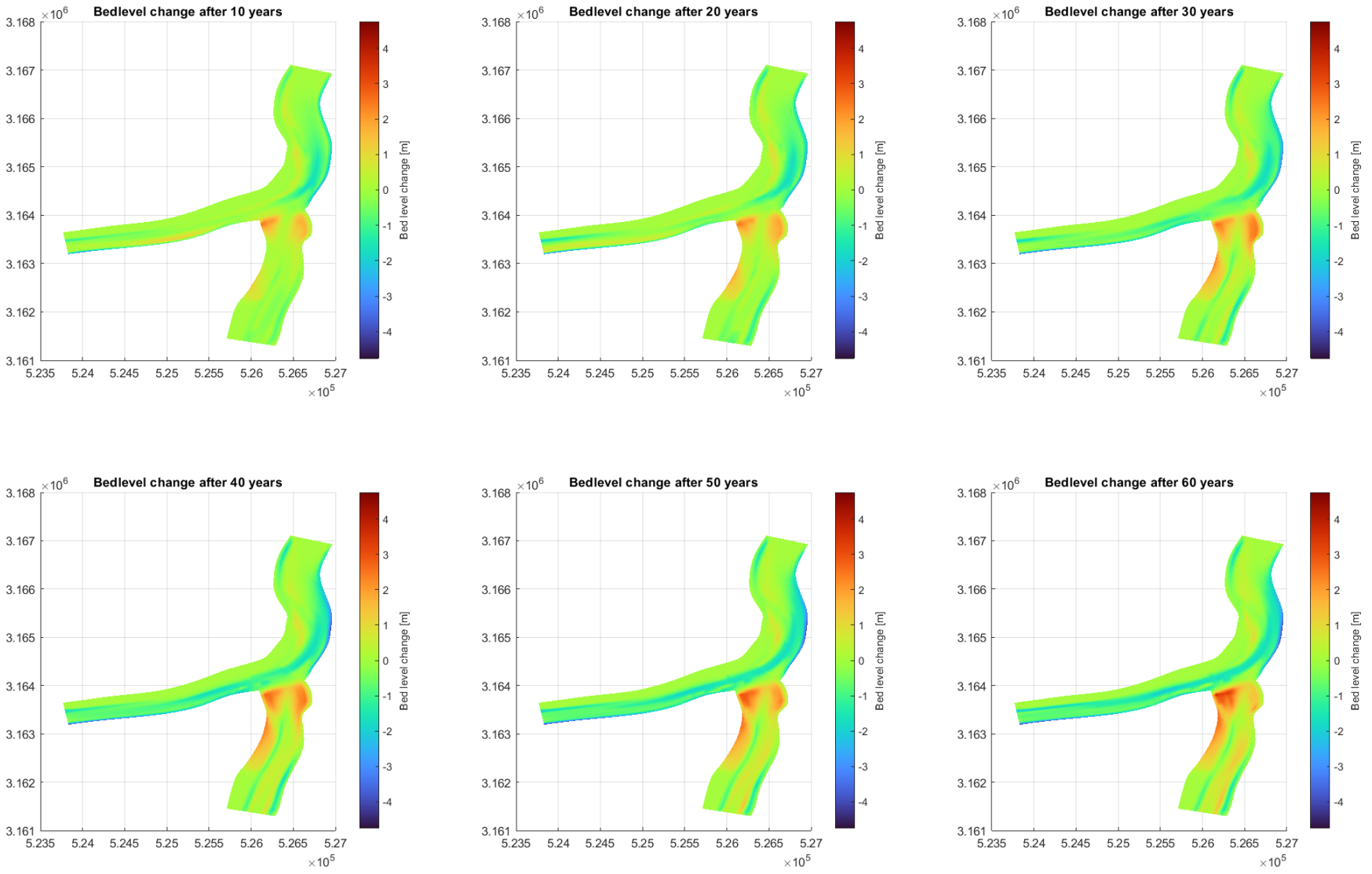

Figure C.19: Model evolution; **Imposed 100 cm initial sedimentation of Geruwa branch** (bed level hight increased whilst slope remains the same)

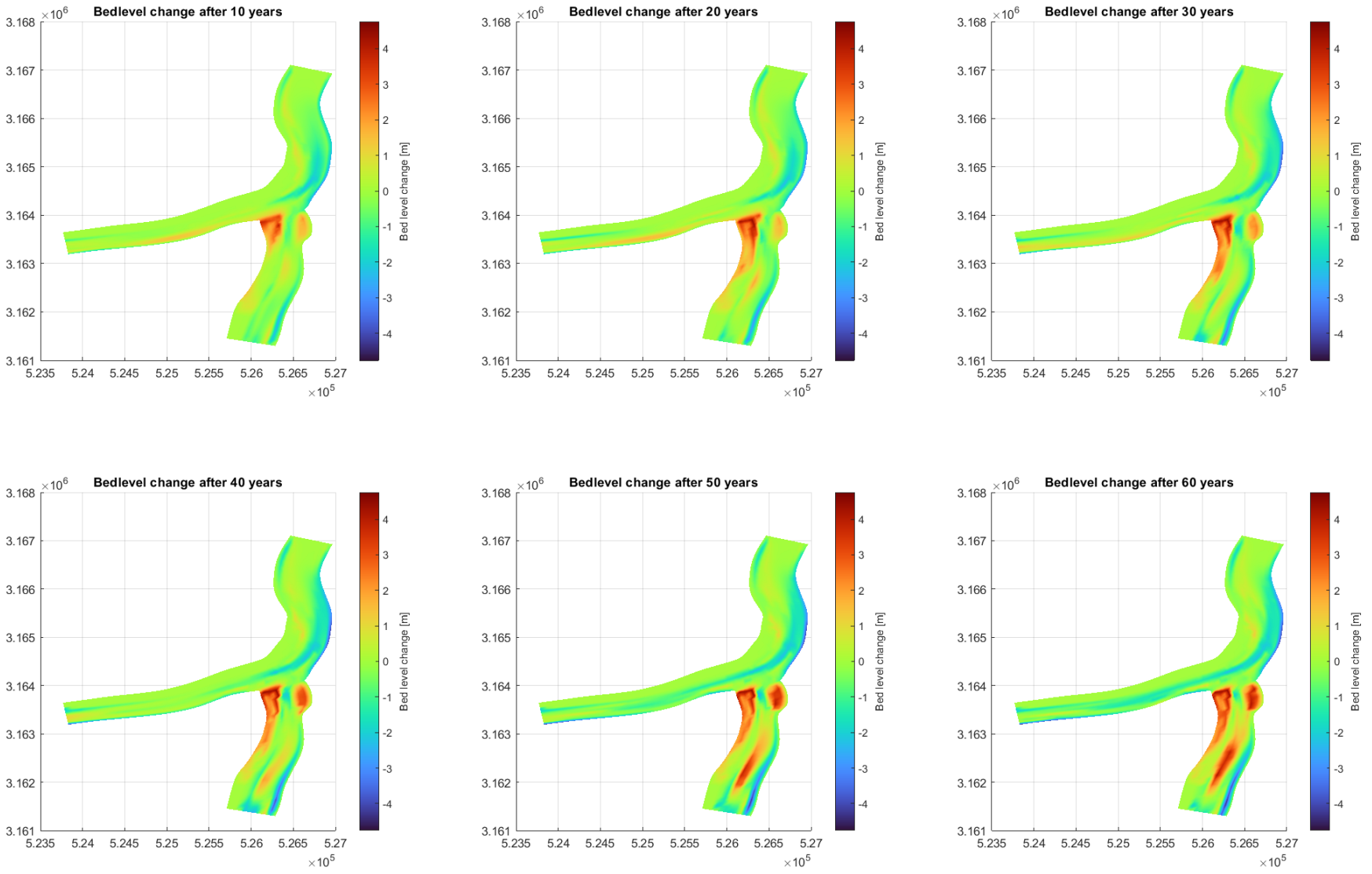

Figure C.20: Model evolution; **Kauriala slope lowered to be equal to Geruwa (1.6)**

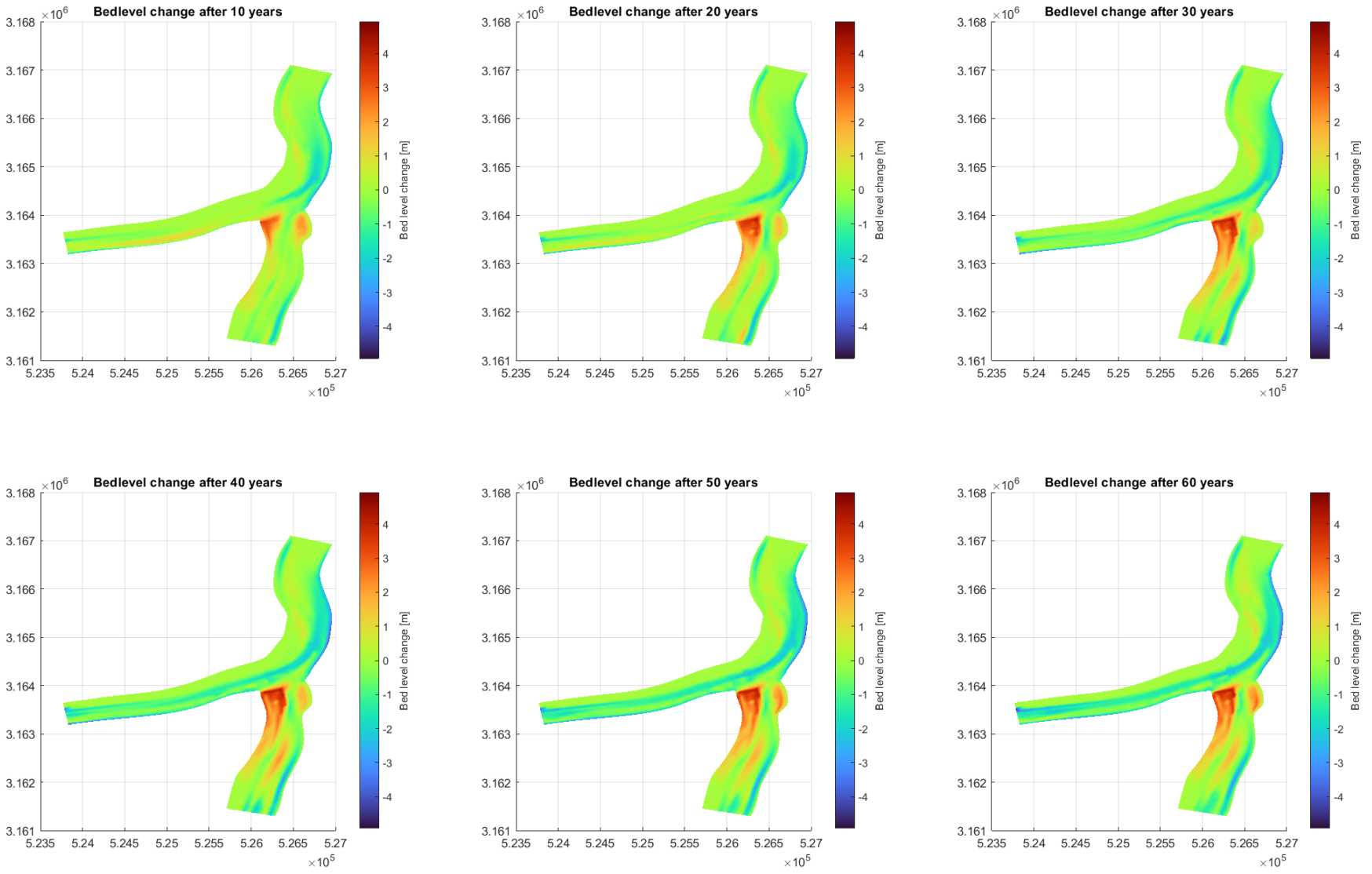

Figure C.21: Model evolution; **Kauriala slope advantage of 10%**

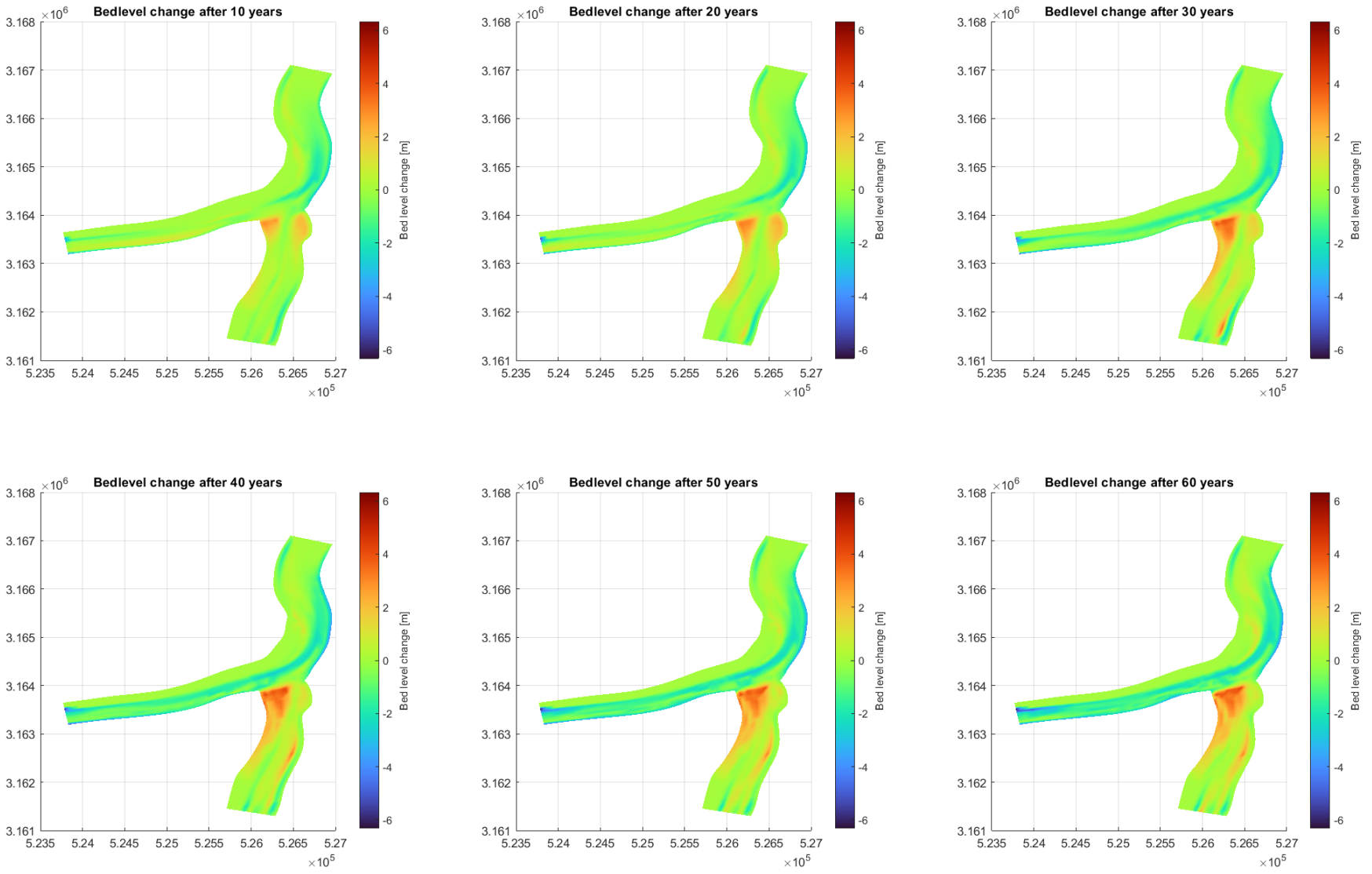

Figure C.22: Model evolution; **Kauriala slope advantage of 20%**

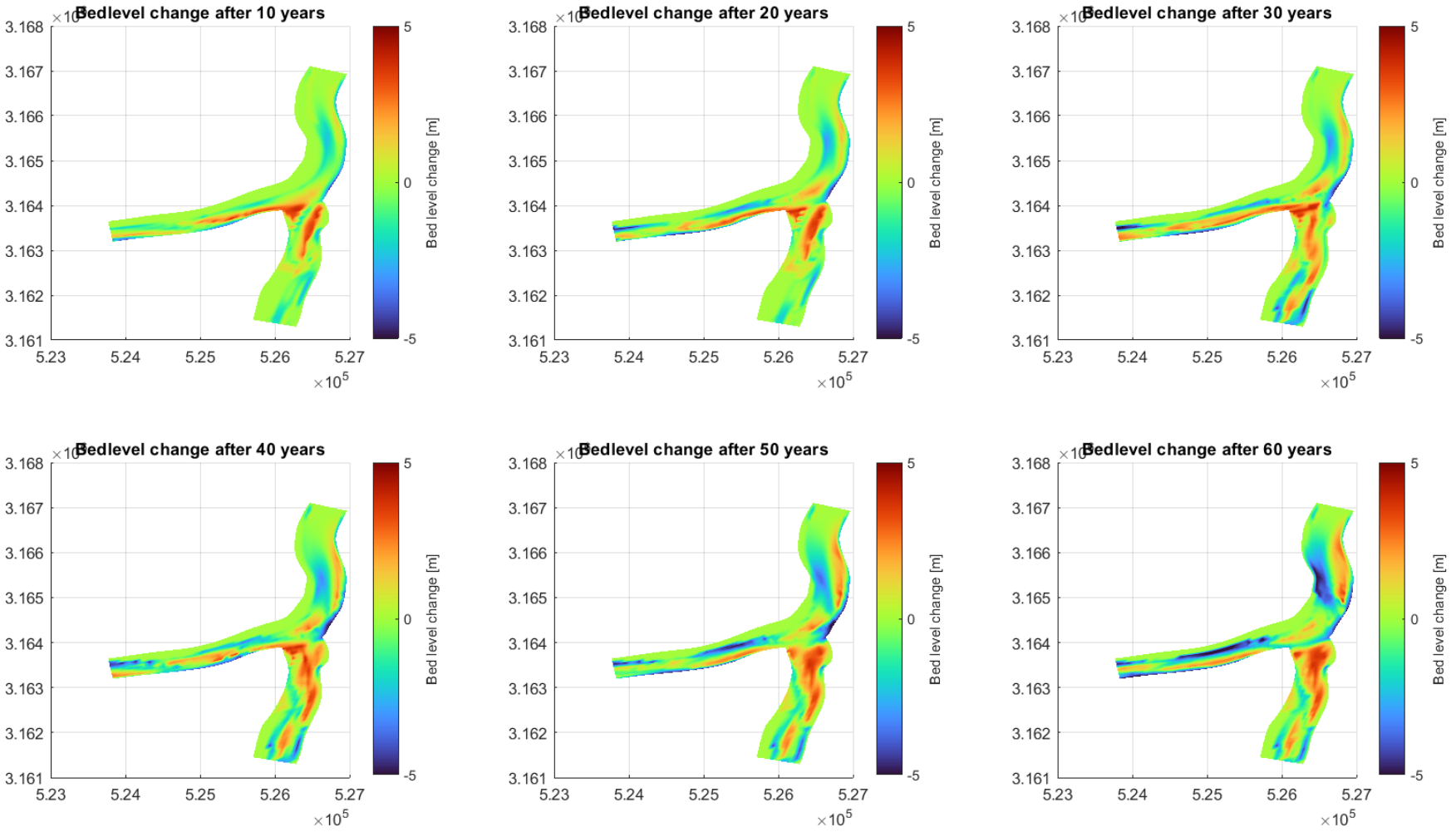

Figure C.23: Model evolution; **Uniform sediment** with a diameter equal to D50 of sediment mixture of reference run; 7.4 cm

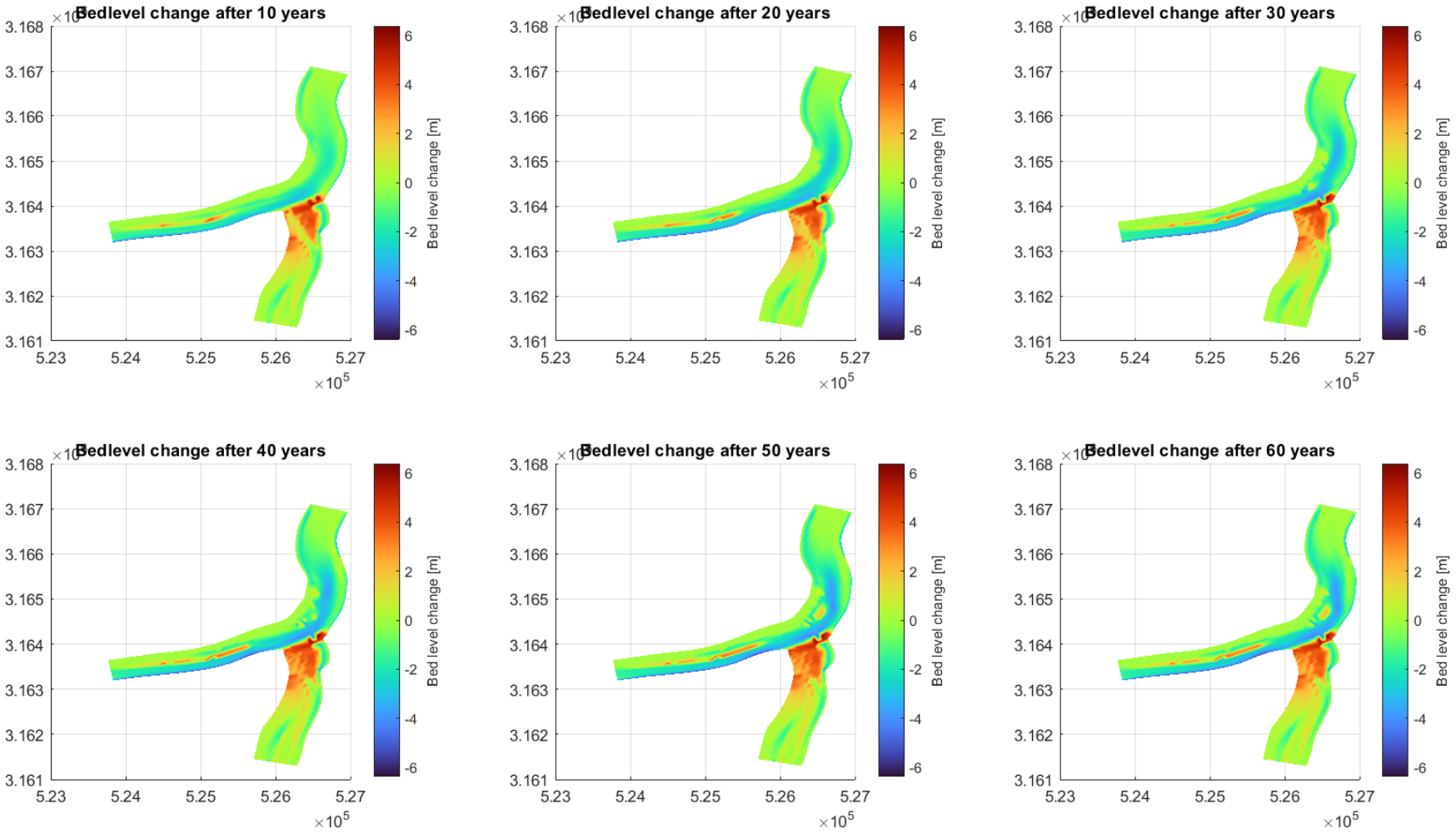

Figure C.24: Model evolution; **Hiding exposure turned off**

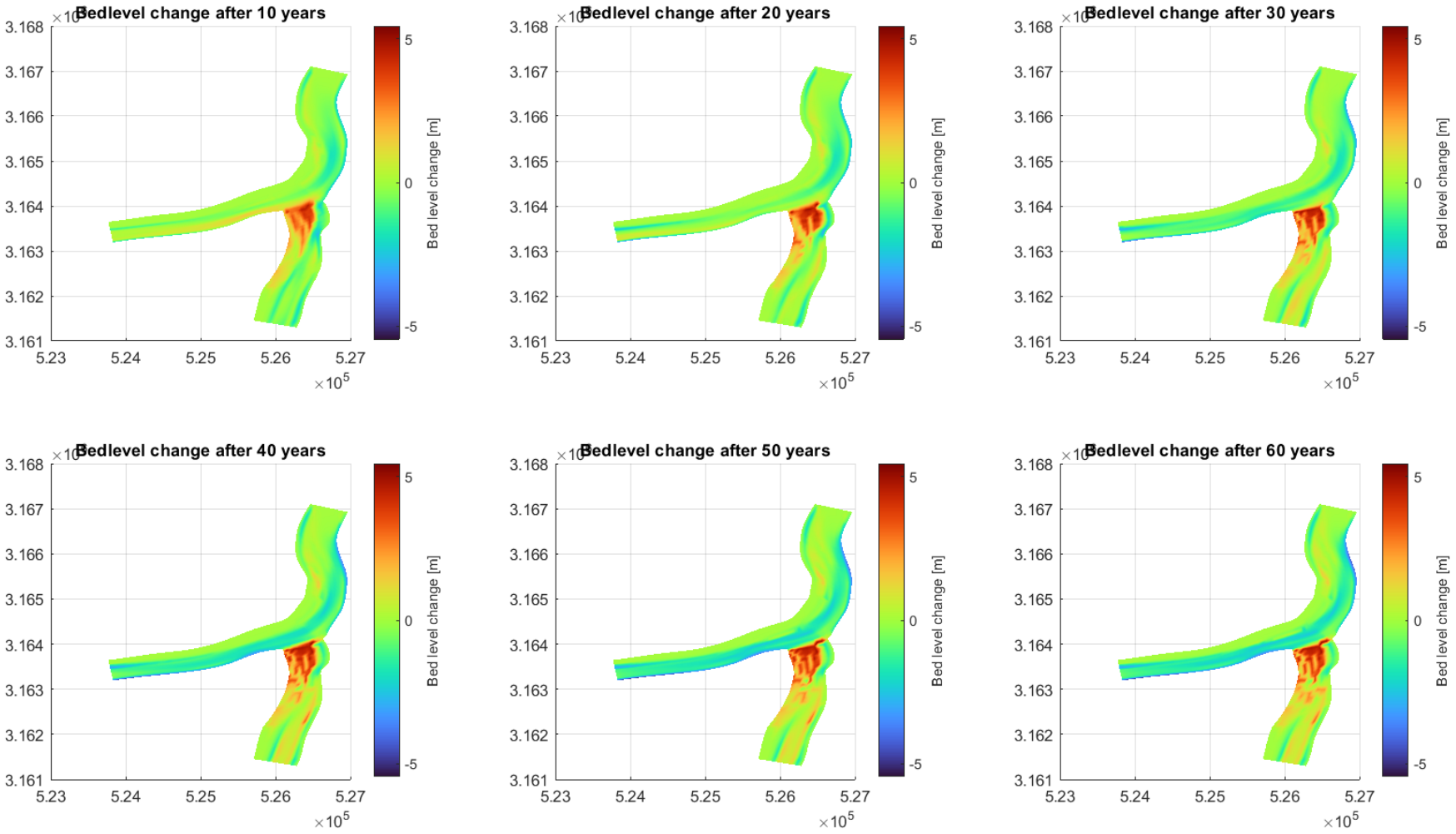

Figure C.25: Model evolution; **Hiding exposure parameter at 0.6** (reference;0.8)

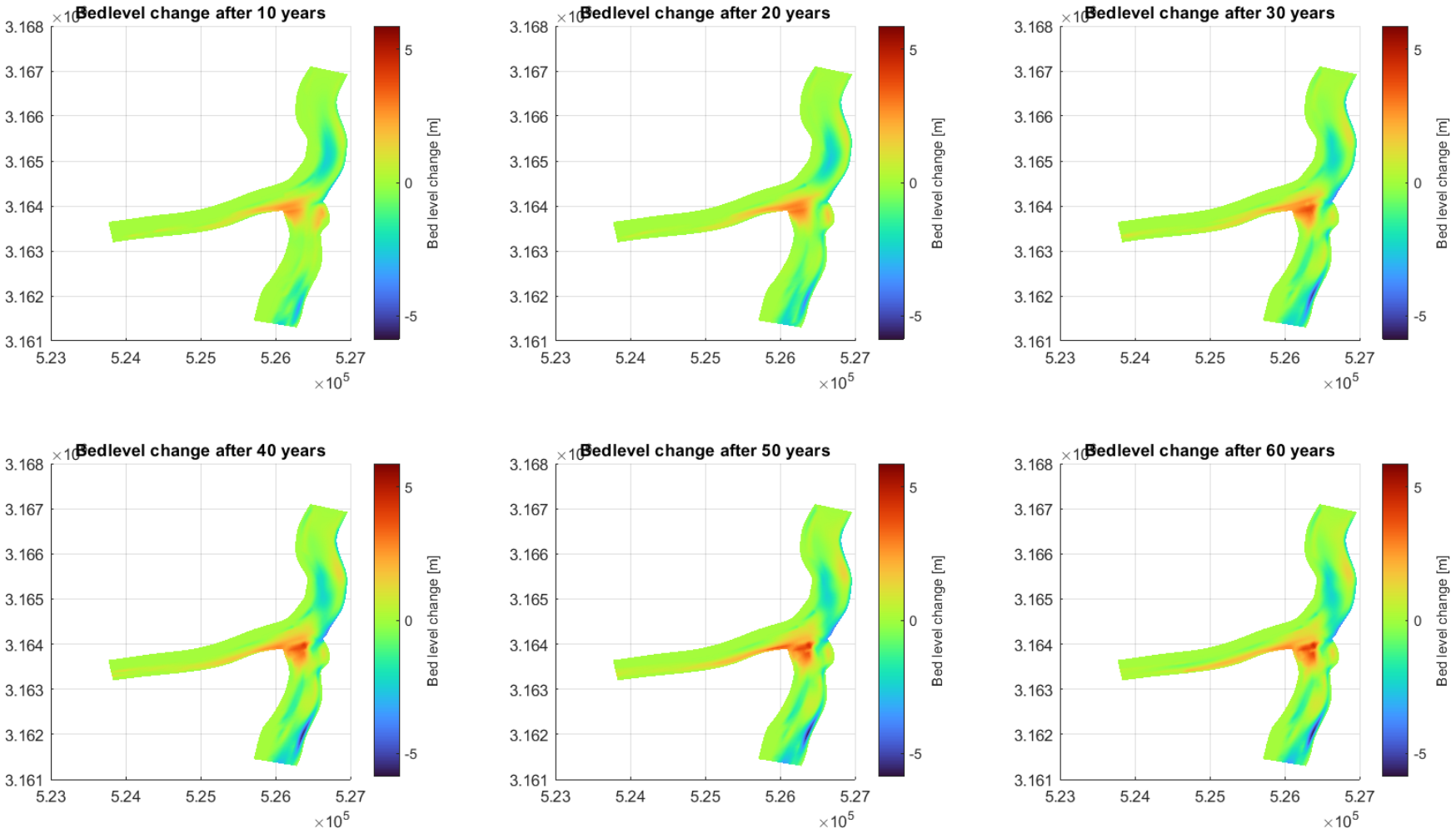

Figure C.26: Model evolution; **Hiding exposure parameter at 0.982** (reference;0.8)

D

Field Rapport

KARNALI RIVER FIELD CAMPAIGN

2023

FIELD REPORT

Sediment and Hydro-Morphological Study as part of PhD and MSc Thesis Water Management: *Morphological Study of the Closure of the Geruwa Branch*

Authors

PhD Candidate: Kshitiz Gautam

MSc Student: Marijn Wolf

Supervisors:

Dr. Thom Bogaard

Dr.ir. Astrid Blom

Dr.ir. Kees Sloff

Date: 17/01/2024

Contents

1. Introduction

1.1 Background Information

Karnali is a representative river system in the TAL landscape. The river drains the western Himalayas in Nepal to the flat lands of Terai and bifurcates. The Geruwa branch passing through the national park serves as the lifeline for the habitat of species such as the Royal Bengal Tiger. The Geruwa branch used to carry a major portion of the flow for at least 25 years until 2009 when a major flood event changed the flow partitioning at bifurcation and made Kauriala the dominant channel with the reduced flow in the Geruwa channel. This changed flow partitioning has been of growing concern, as decreasing river discharge is often associated with decreasing grassland (Bijlmakers et al., 2023), a major habitat for tigers and prey. Moreover, morphodynamic behaviour and floodplain vegetation in the rivers are closely connected affecting the development of each other (Church & Ferguson, 2015; Steiger et al., 2005; Tal & Paola, 2010; Vargas-Luna et al., 2019). Studies have been conducted to understand the lateral movement and sediment dynamics of the Kauriala branch (e.g. Dingle et al., 2020) but knowledge of flow and sediment partitioning between the Geruwa and Kauriala branches is still lacking. Understanding the causes of channel switching is of prime importance for understanding the natural morphodynamic development in Karnali. In the near future with increased anthropogenic interventions and changing climatic conditions, the Geruwa branch faces the threat of complete closure. Hence, understanding the morphodynamic behaviour of the Karnali, its branches and the dynamics of the bifurcation is of utmost importance for the sustainability of the wildlife habitat in the region. Furthermore, this pilot study can be taken as an example of sustainable water management for the wildlife habitat not only in TAL but also in similar mountain river systems around the world.

The change in flow distribution since 2009 over the branches has made a significant impact on the vegetation state in Bardia National Park. Wildlife populations require time to adapt to new environments, and rapid changes in discharge distribution do not allow sufficient time for adaptation ecosystem. An increase in human-wildlife conflict linked to changing forests caused by the Geruwa closure is observed and is alarming. Therefore it is vital not only for the populations of the critically endangered Royal Bengal Tiger and other species but also for the surrounding human populations, to investigate the bifurcation dynamics and possible interventions to restore it to a more balanced distribution.

1.2 Objectives of the Fieldwork Campaign

The aim of this field campaign

- Retrieving the pressure sensor data and sensors installed in 2022 at Geruwa and Kauriala
- Installation of Telemetric water level gauges at Geruwa and Kauriala
- Collect the field data on sediment distribution in the river channel of Karnali, its branches (Kauriala and Geruwa) and associated flood plains.
- Measure cross-section and bed level elevation at different sections of the Karnali, Geruwa and Kauriala.
- Outreach program at Mid-Western University, Surkhet

The main objectives of the fieldwork campaign are to survey the bifurcation area and sediment distribution in order to study its dynamic morphology and test hypotheses of the origin of the partial Geruwa branch closure. This includes investigating the streamwise change in surface sediment distribution and obtaining a sense of the channel geometry at the various bifurcating areas for input into models, and to collect representative cross-section data of the downstream branches to create a cumulative distribution function (CDF). Additionally, the campaign aims to identify and document the differences in bed level elevation between the Geruwa and Kauriala branches. Another important objective is to identify the high flood levels in both branches, as this information is crucial to understanding the water surface elevation during peak flow for estimating discharge distribution. Lastly, the fieldwork campaign intends to determine the discharge division over the branches, providing valuable insights into the spatial distribution and flow characteristics of the river system.

1.3 Relevance of Sediment Analysis, Water Level, and Topographic Measurements

This research aims to develop hydro-morphodynamic models for understanding natural dynamics and the effects of anthropogenic interventions on the discharge distribution and channel switching of the bifurcating Karnali system. For the development of the model, we need the ground truth. For the model setup, we need the bed and water slope, cross-sections at various locations and streamwise sediment distribution. For the model input, we require the upstream discharge and downstream water level as boundary conditions. However, the only data available for the Karnali system within our area of interest is only the upstream boundary condition of discharge at Chisapani. Hence, this fieldwork was extremely necessary to collect data for the continuation of our research. Moreover, the on-site examination of the field also motivated us to experiment with some phenomena such as bend sorting, reverse fining, and bimodality of streamwise sediment distribution which may help to explain the channel switching and bifurcation dynamics of the Karnali system.

1.4 Scope and Limitations

The area of interest for this project lies from Chisapani in the upstream, where the river emerges out of mountains, to about 35km downstream of Chisapani where the two branches of Karnali have permanent bridge structures, the Kothiyaghat bridge (Gerua) and the Sattighat Bridge (Kauriala). The research interest is limited to hydrodynamics and the system's morphology. For the same, we limit our field campaign to the collection of the water level, discharge, bed sediment, and cross-sectional data. Since the bed sediment is mostly coarse in the system and the resources are limited, we limit our data collection to photographs of the bed sediment (and not physical sampling). The cross-sectional data are also limited to the areas where there are no safety risks due to wildlife, river flow and availability of resources such as raft/boat. The accuracy of the data is limited due to methodological limitations, however, the accuracy is adequate for the purpose of our study.

The MSc Thesis scope is concentrated on the bifurcation behaviour, see the locations marked BIF in Figure 2. This was done by surveying the channels, bars and banks with single-beam sonar and point surveying with RTK GPS. This limits the data to areas where we could safely physically visit, which was not the case for the large, vegetated bars/islands as large wildlife were present there. Access to for example LiDAR equipped drones for topography measurements was not available. In addition, due to the lack of motorized boats and shallow waters, we could not take all the different cross-sections in the bifurcation area, however we were able to cover the major channels.

2. Practicalities and Logistics

We were based in Rajapur for the majority of the fieldwork campaign, the small city is marked in Figure 2. A motorcycle was used to reach the sites as the roads in the area between the river branches were of varying quality and width, see Figure 1. Logistics assistance and local contacts were given by two employees from the Karnali River Management Project Office. For the data collection at the bifurcation, we stayed in Chisapani. There, a commercial raft company could provide us with a raft and personnel. We also made use of the accommodation from the NTNC office in Thakurdwara inside the National Park, NTNC kindly provided transport in the National Park by all-terrain vehicles.

Figure 1: Example of modes of transport during the field campaign. (left) Commercial rafts are used for the bifurcation in Chisapani to take various cross-sections and visit gravel bars. (raft) Favoured mode of transport on roads of varying quality between the selected sites.

- Problems with equipment:

Despite having an advanced RTK system for measurement of the elevations, the device did not perform to its full capacity as expected. The RTK system range was limited to 2 km from the base station. However, after interaction with the manufacturing company and reconfiguring the system, we were able to get the range up to 5km. Since the field area was remote and not very populated, another issue encountered was the availability of tall buildings or towers to install the base station, which may have limited the range. The RTK device was rather fragile to be used in such a rugged environment. Especially the communication antenna attached to the main board was too heavy and damaged the board connections which had to be repaired locally very often. The RTK did not communicate at Lalmati (bend and Geruwa inlet point, BIF3) inside the national park even after 16 hours of installation. The reason behind this was unknown. There may be a RF jamming in the area but that could not be verified.

The single beam sonar, at a high velocity of flow, would not stay perpendicular to the water surface which gave erroneous measurements and the experiments had to be repeated several times.

- Problems with logistics:

The availability of sophisticated boats or rafts for measurement of the cross-sections and crossing of the river was a big challenge. Some local wooden boats were arranged through individual personal contacts and used for measuring cross-sections. However, they could not be used for transporting the dry equipment and hence the sediment data and the elevation data at certain cross sections are limited to one bank of the river.

- Problems with permits:

Most of the locations were accessed via the Rajapur Triangle which was a perfect place for accessing both the branches of the Karnali. However, some instances required entry through the Bardiya National Park, especially the bend from where the Geruwa separates. Unfortunately, the requests for our research permits were not processed until the end of our field campaign due to some internal issues within the permit-issuing organization. Since this was a follow-up fieldwork for Kshitiz, he could obtain a temporary permit, however, Marijn could not obtain the new permit to work from the BNP. This issue has been well reported to the concerned authorities and supervisors.

3. Methodology

3.1 Site Selection and Rationale

The fieldwork of 2022 and preliminary reconnaissance with the supervisory team provided a basis for the strategic site selection in the fieldwork of 2023. The initial plan was to obtain the data on cross-section, sediment photographs and RTK mapping every 5km in each branch. The approximate locations were tracked via satellite images and insight from the reconnaissance. Mostly sites where the river was flowing in a single channel or least number of channels were prioritized for data collection. With slight improvisation to the initial target, we did manage to obtain a large amount of data and information. The site selection was mostly based on 3 factors:

1. Accessibility:

Primarily, accessibility to the selected site was considered. Data were collected at locations which could be accessed by motorbike, boats/rafts, and authorized vehicles (especially within the National Park).

While placing the base station of the RTK, the highest possible building in the highest landscape within the range of the RTK system was searched for and corresponding landlords were approached for the installation.

For water level gauges, installation accessibility was considered, including easy access to the instrument for maintenance.

2. Safety:

Considering the accessible area, their corresponding safety was assessed. Safety was assessed with respect to proximity to wildlife, estimated depth and flow of the river, safety from theft and robberies. All the measurements and installation of instruments were performed in co-operation with the local people who had detailed knowledge of the surrounding area. These personnels were hired or were compensated for their contribution. The sites where there were incidents with wildlife and where there were frequent sightings of the wildlife were avoided and the areas in proximity to the grassland and forest were approached with special caution. Similarly, the sites with remarkably high flow velocity and depth were accessed with special caution.

Regarding instrument safety, the instruments were placed in a house inhabited by people. For the installation of the water level gauges, the police personnel were requested to keep an eye on the instruments.

3. Availability of resources

Resources such as boats, rafts and local human power were also considered during the site selection. Sites which had availability of at least local wooden boats were identified and where there was no availability as such, concerned fishermen were contacted and requested for their support with the boats. At such locations, all the measurements were not possible as it was quite a risk to carry all the instruments in such boats.

The permanent bridge structures in the two branches were assessed as the ideal site for installing our water level gauges, with easy accessibility, safety, and stability of the substrate.

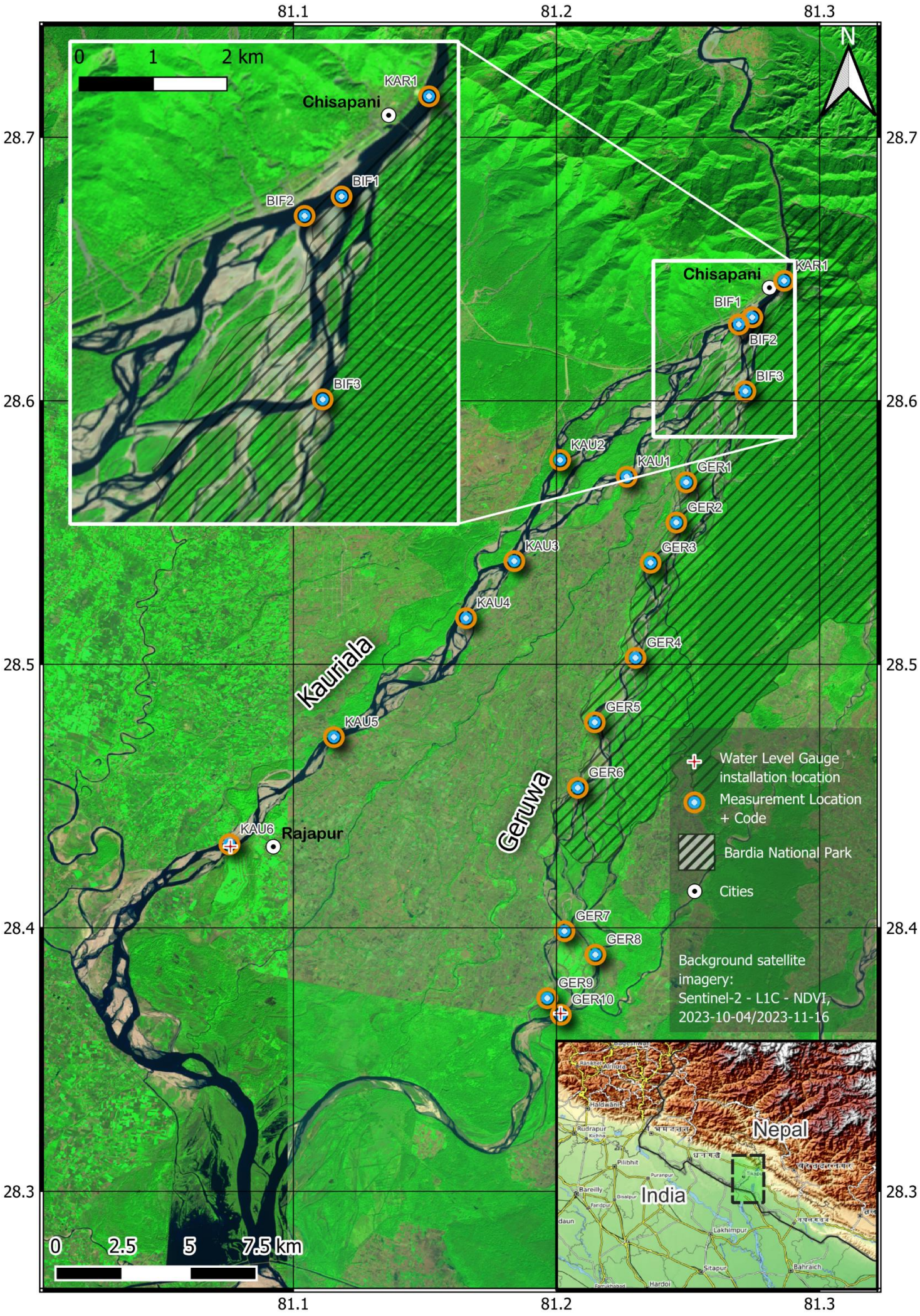

Figure 2: Overview map of the research area with codes for the locations. Measurement and water level gauge locations are marked. The background map represent the situation when fieldwork was performed

3.2 Description of Instruments and Equipment Used

The necessary equipment was collected before the fieldwork campaign. All devices that were used in the field can be found in Table 1. The devices, except for the Level Gauge, were configured and installed before departure. The most important devices for the success of the fieldwork were the RTK GPS and the CHIRP single-beam sonar. The RTK GPS was ordered with the extra long-range antenna module that would allow us to have a communication range of 50-60 km between the base and rover GPS. The set from ArduSimple was ordered preconfigured with the extra long-range antennas. The set was tested with different accuracies numerous times and worked as desired, however, the maximum range test was not tested before departure.

	Name	***Abbreviation***	***Purpose***
	*ArduSimple RTK Base-Rover Calibrated Surveyor Kit*	*RTK GPS*	*Mapping of shallow riverbeds, bars and floodplains with great accuracy (<10 cm). Longitude, latitude and elevation.*
	*Deeper Sonar CHIRP+*	*CHIRP*	*Single beam sonar used for bathymetry surveying of the deeper river sections. Attached to homemade raft, motorized boat or raft and dragged across river sections. Can be combined with RTK GPS through Android phone.*
	*Obscape Level Gauge*	*Level Gauge*	*Real-time water level measurements in both the Kauriala and Geruwa branches. Works with a highly accurate radar sensor, solar panels and GSM telemetry.*
	*Measuring tape*	*-*	*Simple measuring tape for reference in sediment images.*
	*Hawkeye Handheld Depth Finder*	*Hawkeye*	*Handheld single beam sonar, able to get single depth readings. Mainly used to check CHIRP's readings.*
	*Nikon Foresty Pro*	*NFP*	*Laser rangefinder for measuring distance, angle and height differences. Used in situations where the RTK GPS connection was limited.*

Table 1: Overview of equipment used for field measurements.

3.3 Methods: Cross sections

The fieldwork was conducted in the dry months after the monsoon season. The water depth at this time of year is several meters lower than at peak discharge, for this reason, we not only take the 'wet' cross-section but also continue the sections along the 'dry' banks, bars and floodplains.

Wet

For river sections in which it was not possible to wade through, a single beam sonar device was used, the Deeper CHIRP+. That includes the entirety of the Karnali (KAR), bifurcation (BIF) Kauriala (KAU) locations. The device is intended to be used by fishermen to locate fish but also maps the depth of a river with a user-defined beam angle of 7°, 16° or 47°. With more accurate reading when using a narrower beam angle, during the fieldwork, we opted for the 'autoselect beam angle' mode as it would choose the optimal angle based on water depth. The depth range of the sonar is 0.25 – 100 meters. The small sonar device is coupled to a convenient smartphone and web app (Fish Deeper™). Communication between the device and smartphone is via Bluetooth and has a stable connection up to 100 meters. The sonar has a built-in positioning sensor (supports GPS, GLONASS, Galileo, BeiDou and QZSS) and operates for up to 4.5 hours with the GPS enabled.

Using the 'boat' mode, the CHIRP can use the GPS data from the smartphone. The smartphone can in turn be set up to work with the RTK GPS through the USB port and by enabling mock location in Android developer settings. With these settings, the latitude and longitude of the cross sections can be determined with centimetre precision. However, in most of our measurements, we used the CHIRP's 'bait boat' mode, in which it uses its own GPS readings. This was done from a practical perspective as it was cumbersome to hold the phone + RTK GPS exactly above the CHIRP during boat rides. In addition, the absolute position of the cross sections is not required to be centimetre precise.

The Karnali River lacks the availability of motorized boats with two exceptions, namely the ferry boats at locations KAU4 and KAU5. Here the ferries were used to cross the river while the sonar user laid down on the deck and attempted to hold the sonar at the water surface pointing downwards to prevent tilting of the beam. This was quite challenging as waves from the ship's bow and the flow velocity in general were quite high. During excess tilting, the device cannot record the depth accurately and the connection to the phone is easily lost when the device is completely submerged, e.g. by a bow wave. At the other locations on the Kauriala branch, the assistance of local fishermen was required. They would peddle us across the river in the local hollowed-out tree trunk canoes. Due to the strong flow in the Kauriala branch, perfect perpendicular crossings were not possible.

The data from the sonar device can be viewed in the application and exported in CSV format. The data was then processed and linked to the precise elevation of the water level and projected onto a defined plane to create the cross-sections, see section 5.1. For the shallower river sections of the Geruwa branch, the RTK GPS was used, see the following section for more details on the configuration. More or less every meter or less, the stick was put on the river bed and recorded. The water levels were recorded with a special note so that could be identified later.

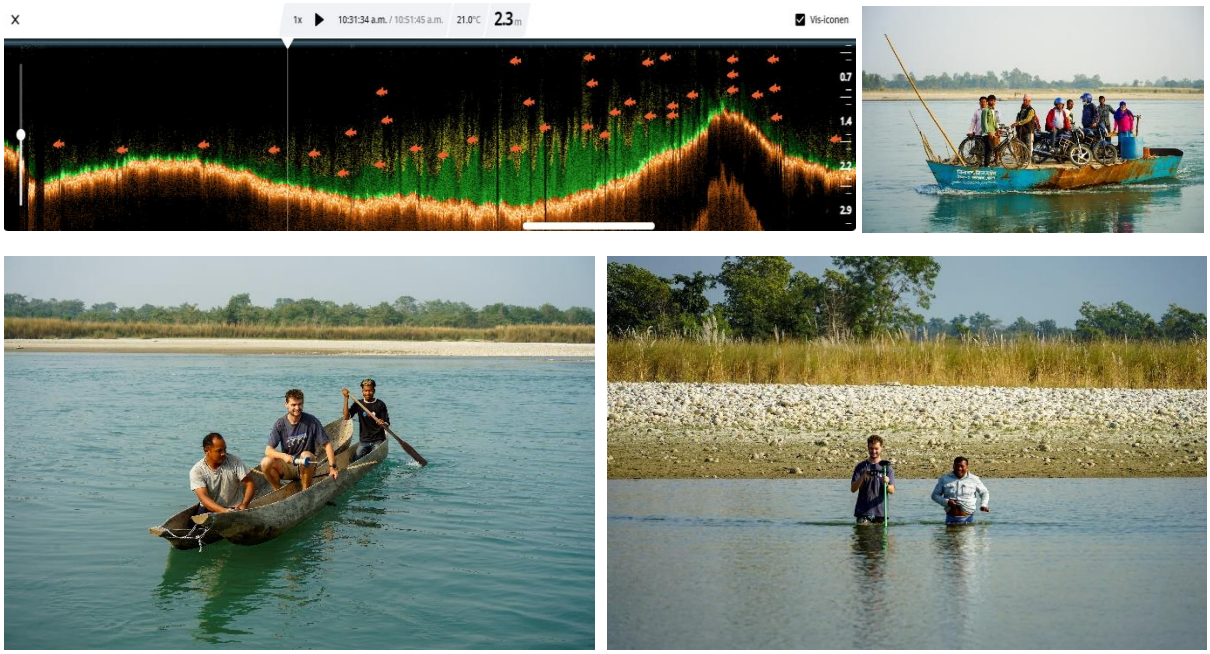

Figure 3: (top left) Screenshot of the (web) application of the Deeper CHIRP+ sonar. (top right) A motorized ferry about to cross a section of the Kauriala branch (KAU1). (bottom left) Assistance from local fishermen who could canoe us across the river at location KAU1. Marijn holds the sonar at the water's surface. (bottom right) In shallower river sections, e.g. all Geruwa (GER) sections, the RTK GPS was used to take elevation data of the bed and water level.

Dry

A calibrated RTK GPS from Ardusimple was used for the surveying of the banks, bars and floodplain. The system comprises a base and rover module which consists of a weatherproof GNSS multiband antenna, XBeeRadio module + dipole antenna and the simpleRTK2B Pro processing unit. The simpleRTK2B Pro board is based on the u-blox ZEF-F9 module, and has a high-power XBee socket, up to 1 Watt. Due to the large area of interest, this configuration was chosen as it facilitated the use of the extra long-range radio module, which has a range of up to 100 km in ideal conditions and if configured in a 1-Watt way. The rover is connected to an Android phone through its USB C cable, and when mock location is activated in the developer settings, the phone will use the RTK GPS data for surveying. In the field, the GNSS Master app was used to connect the phone to the rover and the application SW maps was used for recording the points. From SW maps, the data can be exported in CSV files. The rover was mounted locally on a 1.5-metre-long PVC pipe, and the smartphone and processing board could be mounted on the same pipe with a clamp for easy control.

The desired accuracy and other characteristics of the base station are configured with the U-center software from Ublox. The configuration of the XBee radio module can be changed with the XCTU software of Digi XBee. From our experience, the time for the base station to get a fixed signal with 0.1 meters of accuracy is around 10 hours and 2.5 hours for 0.3 meters of accuracy. Numerous issues were experienced with the range of the radio modules during the field campaign. During the start of the field campaign, only 1 km of range was possible. This would significantly slow the workflow as the area we conducted measurements in was around 40x40 km and the 10-hour GPS fix time of the base station. When the wrong factory configuration of the XBee socket (100 mW instead 1 Watt) was resolved, a range of max 7 km was obtained. The promised 50+ km range was never reached likely due to the violation of the radio frequency policy by others in Nepal, as has been explained by ArduSimple. This fact slowed down our progress since we were only able to do 2-3 locations per day. Eventually, we were able to use the equipment on most of the desired locations with the sub 10 cm

precision. Only at 3 locations is the accuracy lower at 30 cm in the x, y and z. At one location, BIF3, radio communication was not working at all, possibly due to the vicinity of a military camp and its radio usage. See table 2 for an overview of the base station accuracy per location and date. Relative accuracy between the base and rover station is <2 cm.

At every location, attempts were made to identify the high flood levels (hfl) by looking at the deposition of woody materials, signs on vegetation and discussions with local people. If we found sufficient clues about the hfl, the location would be marked with the RTK GPS. This method is of arguable accuracy and will only be used to serve as an indication of the high water levels during monsoon seasons.

Figure 4: (left) Documenting the height of the embankment at KAU3. (right) Measuring the dry part (large bar) for the cross-section at KAU4.

ACCURACY BASE STATION RTK GPS	***LOCATIONS***	***DATES***
0.1 METER	*KAR1, BIF1, BIF2, KAU1, KAU3, KAU6, GER1, GER2, GER3, GER4, GER5, GER6, GER7, GER8, GER9, GER10,*	*4-11, 6-11, 7-11, 10-11, 22-11, 23-11*
0.3 METER	*KAU2, KAU4, KAU5*	*8-11, 9-11*
0.5 METER	*KAU6**	*2-11*
DGPS (>2M)	*BIF3*	*25-11, 26-11*

*Table 2: Accuracy of the base station for the different locations and dates of use. *Measurements have been repeated with better accuracy.*

3.4 Methods: Water level monitoring

The telemetric radar water level gauges from Obscape were installed on the only bridges over the Kauriala (KAU6) and Geruwa (GER10) branches, about 30 km south of the bifurcation. The bridges allowed good mounting options and security due to the always present army employees. Custom mounting constructions were made locally for both devices to ensure a sturdy installation, see Figure 5. The gauges are charged by solar panels and are supplied by Obscape with a SIM card for GSM communication and an SD card for backup storage of the data. The device is very easy to set up and after installing them at the bridge, the exact location and elevation were measured with the RTK GPS. This point was then used to set the reference levels for the water level measurement in Obscape's

data portal. The depth data from the CHIRP sonar was used to monitor the water depth changes. The gauges are installed to last many years and monitor the water level and depth throughout all the seasons.

The sensors have a 2 mm accuracy and a range of 40 meters. The sampling interval was put at 30 minutes for our long-term monitoring purposes and the communication interval to 6 hours. During measuring the sensor averages the reading for a duration of five seconds, small waves/objects will not influence the data. Preliminary data from the gauges can be found in section 5.3.

Figure 5: (left) RTK GPS is being used to get the exact elevation and coordinates of the radar gauge at GER10. (top right) Local engineer attaches the custom mount to the bridge. (bottom right) Installation of the second gauge at KAU6.

Velocity & Discharge

Simple series of surface velocity measurements were performed at the location of the water level gauges by timing floating objects that travel a measured distance. This information is used in combination with the cross-sectional area to estimate the discharge distribution at these locations ca. 30 km downstream of the bifurcation.

3.5 Methods: Sediment analysis

Throughout the fieldwork campaign, numerous images were taken consistently to prepare them for automatic grain detection software. Images were taken according to the manual of the software (Detert & Weitbrecht, 2013); perpendicular to the bed surface and an umbrella or sheet was used to create shade to avoid harsh shades that could hinder the detection process. A scale or a known-length object was included in each frame.

The MATLAB-based automatic object detection software BASEGRAIN will be used for the analysis of the sediment images. The software calculates a quasi-grain size distribution based on a sophisticated five-step object detection algorithm which has proven itself to agree well with results from more traditional, non-image-based techniques, like in-situ line sampling and square hole sieving. (Detert & Weitbrecht, 2012, 2013; Stähly et al., 2017). Figure 6 shows an example analysis of coarse bed material with the GUI of BASEGRAIN.

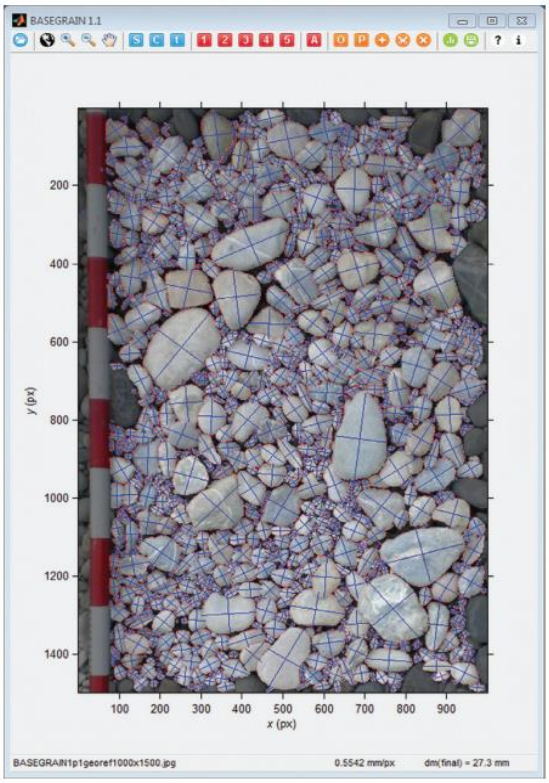

Figure 6: (top) example sentiment image taken during fieldwork. All pictures can be found in Appendix 9.2. (bottom). Snapshot of BASEGRAIN's interface of the MATLAB software package.

3.6 Data Collection Timeline

	FIELDWORK CAMPAIGN							
	October			November				December
	Week 41	Week 42	Week 43	Week 44	Week 45	Week 46	Week 47	Week 48
National Holidays			Daishan			Tihar		
Meet officials, logistics, materials								
Preliminary reconnaissance with the supervisory team								
Site selection								
Installation Obscape gauges								
Cross-sections								
Sediment sampling								
RTK topography measurements								

Table 3: Fieldwork timeline

3.7 Quality Control Measures

Following quality control measures were taken during data collection:

Cross sections were tried to measure as perpendicular as possible to the flow. However, the boat used was manual and could not be crossed directly at right angles, we tried to take multiple cross-sections which were then projected to a plane perpendicular to flow while processing. The RTK measurements were taken after providing ample time for the base station to reach the desired accuracy (see table below for the accuracy (See Table 2). The water level points were taken at multiple points and where possible, on both sides of the channel being measured which are then averaged.

The instruction for the gauging station installation from the manufacturing company was followed. The vertical angle of the gauges are within the permissible limit of 1o-3o. The elevation of the stations are measured using the RTK to an accuracy of 10 cm.

Sediment samples are taken throughout the cross- section and wherever possible on the both sides of the channel being measured. The distance between two samples are as equal as possible (pacing technique was used) to avoid the bias that may induced while visualizing the sediments. Same object is used in almost all pictures to provide it a uniform perspective of scale.

4. Preliminary data

This chapter gives a short overview of the collected data. An overview of collected data per location, field map illustrations and sediment pictures can be found in Appendix 9.1

4.1 Cross-sections

The datapoints are orthogonally projected onto a user-defined plane, using the same method as described in (Parsons et al., 2013). Furthermore is the wet area calculated and displayed in the figures

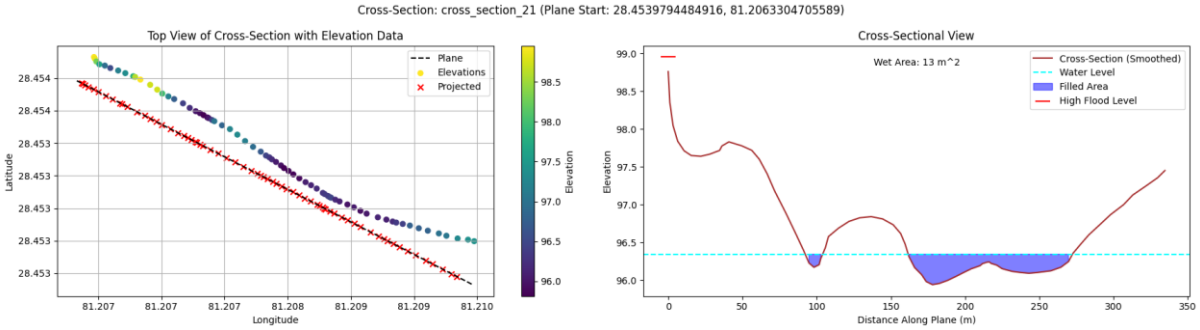

Figure 7:(left) cross-section at location GER6. Water level and high flood level are marked and wet parts are coloured blue. Two channels are present in this cross-section separated by a narrow bar. On the left, we have a small third non-flowing stream of water. (right) Top view of the RTK GPS data points and the defined plane on which the points are projected (orthogonal translation).

4.2 Slope

Based on the water level measurements obtained using RTK GPS, it has been observed that the slope of the Kauriala branch is 1.63×10^{-3}, while for the Geruwa branch, it is 1.49×10^{-3}. Figure 8 provides a graphical representation of the absolute elevation of the water level, measured from the northernmost point at the upper bifurcation. The data suggests that the Kauriala branch has a slightly

steeper slope compared to the Geruwa branch. Additionally, it is evident that the water level in the Geruwa branch is considerably lower than that in the Kauriala branch.

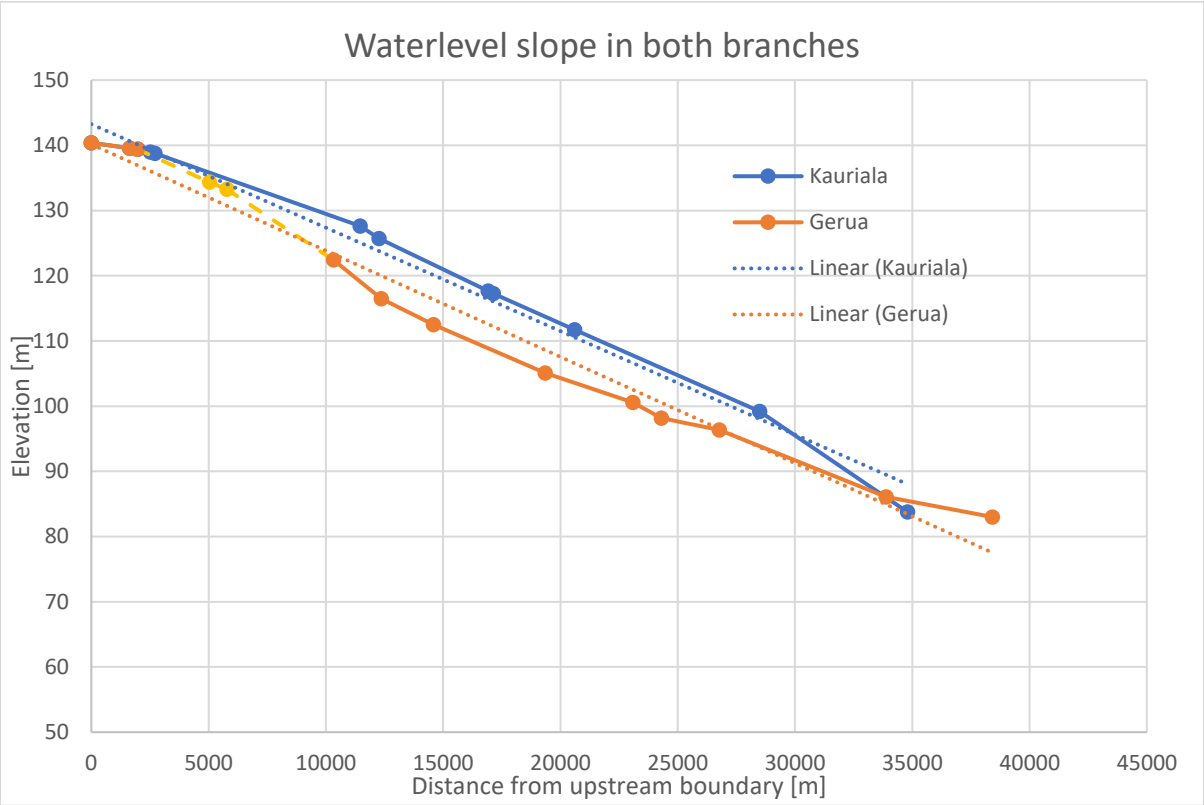

Figure 8: The slope of the measured water levels along the Kauriala and Geruwa branches. The upstream boundary is the most upstream data point. Note the yellow, dashed line represents the measured point at location BIF3, the only location where the RTK GPS did not have a fixed signal and where we had to rely on a DGPS signal with poor accuracy of a couple of meters.

4.3 Water level

The water level gauges were installed in the first week of November 2023, therefore, the data from the last 2 months can be observed. An example of the water level change can be seen in Figure 9. A steady decrease in the water level is observed. The data from the monsoon seasons, which occur from June to August, will be of particular interest.

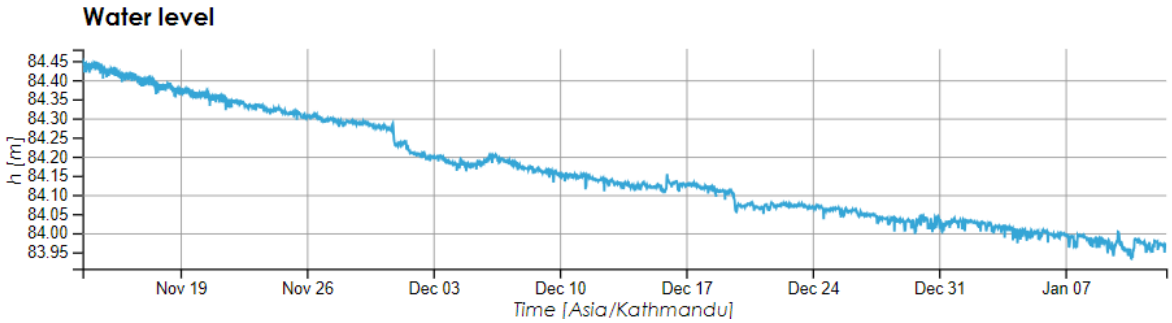

Figure 9: Example water level data of the Kauriala gauge on Obscape's data portal.

4.4 Surface velocities

Taking the average of numerous float velocity tests at the exact locations of the water level gauges reveals a surface velocity test at the location GER10 of only **0.11 m/**s and **1.09 m/s** at KAU6, a

significant difference. The surface velocity will be used to get an estimate of the depth-average velocity by multiplying it by a factor. This can then be multiplied by the wet cross-sectional area to get an estimate of the discharge in the branches.

5. Discussion

5.1 Implications of the Data Collected

The data on cross-section and water level are crucial for identifying the bed level, slope and geometry of the Karnali system and its branches. This will help us to understand the effects of different slopes in the water distribution in the branches. Furthermore, data on the sediment distribution will be helpful in understanding the status of the sediment partitioning, deposition, erosion and mining in the system. These all data will be essential to understand the system well and develop hydro-morphodynamic model representing the Karnali system. The water level being monitored will be useful in understanding the discharge partitioning and will also provide boundary conditions for the models to be developed. Additionally, the observation and data is expected to be useful in explaining the phenomena like bend sorting in rivers.

MSc Thesis: Data from BIF locations very valuable for constructing a 2D morphological model of the bifurcation for understanding its dynamics. The general shape of the channel opening and heights of bars and floodplains will be used as a input for a 2D hydromorphological model. Whilst the aim is not to replicate the current morphology in detail, the collected data will have a large influence on the general model construction.

5.2 Comparison with Last Years Fieldwork

The fieldwork of 2022 mostly comprised of reconnaissance, measurement of cross sections, estimation of discharge, fine sediment sampling and analysis, and installation of pressure sensors in the downstream of the two branches. The field work in 2023 provides additional data on cross section, the elevation at different locations, coarse sediment analysis in streamwise direction, the data from the pressure sensors on water level. Furthermore, the installation of telemetric water level gauging stations on the two branches provide us with real-time water level data. Moreover, the 2023 fieldwork provided a chance to observe the differences in morphology of the Kanali system over a year. The key difference in field campaign of 2023 from that of 2022 is the area and accuracy of the data. The 2022 field campaign also included the Babai River system east to Karnali whereas in 2023 we only focused on Karnali system. Since it was a reconnaissance study in 2022, the water level and elevation were taken using a hand held GPS with low accuracy (3-5m) whereas in 2023 we used RTK with accuracy ranging from 10-50 cm. Another difference is in the location of the measurements which are shown in Figure 10.

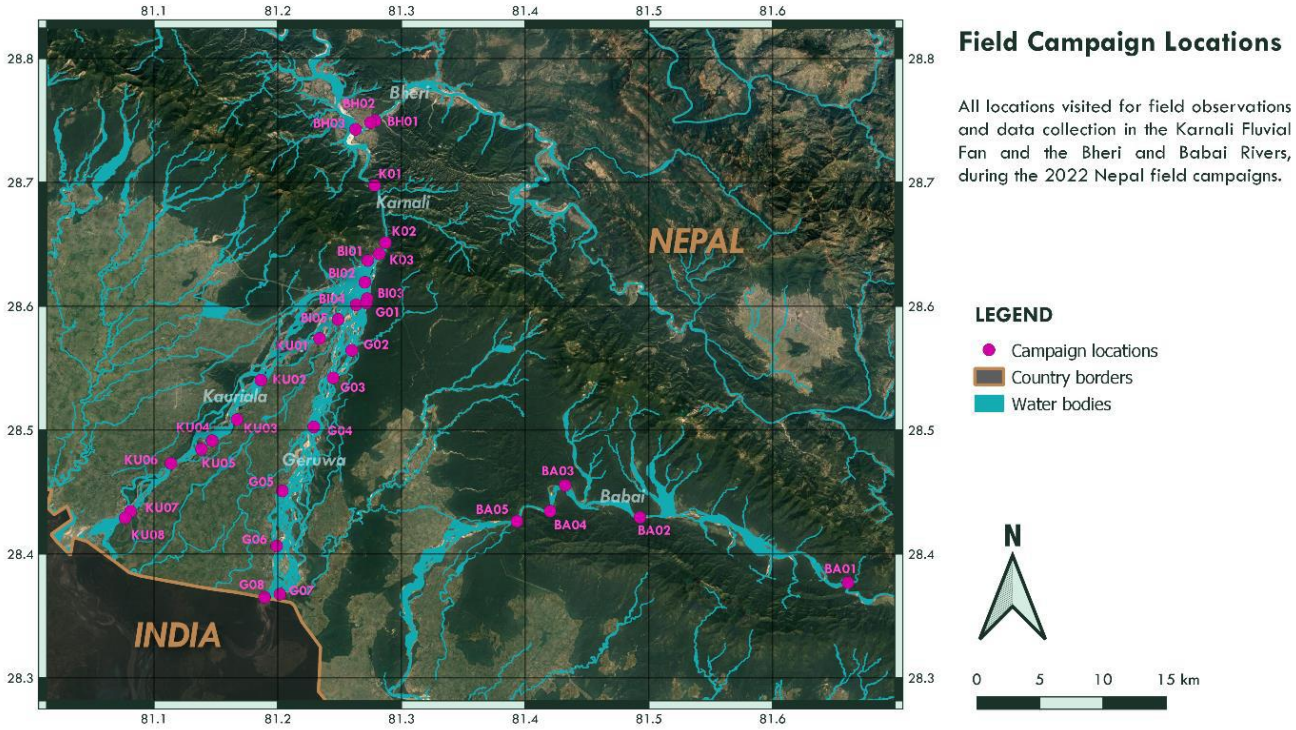

Figure 10: Map of measurements locations during the 2022 field campaign.

6. Conclusion

6.1 Summary of Key Findings

The fieldwork campaign successfully achieved its predefined objectives. Valuable data pertaining to channel geometry, sediment size distribution, and bar and floodplain topography has been collected. The installation of telemetric water level gauges allows for the collection of highly useful future data for analyses throughout the different seasons. When combined with the cross-sections, the data enables a more reliable assessment of discharge distribution compared to the previously used remote sensing methods. This fieldwork significantly expanded our understanding of the bifurcation area, providing a comprehensive perspective. Notably, it marked the first successful application of single-beam sonar mapping for the various channels at BIF 1-3. The incorporation of elevation measurements for banks and bars further enhances the quality of input data for future modeling efforts. The extensive collection of photographs in this area offers a good amount of material for testing hypotheses related to the closure of the Geruwa branch.

6.2 Recommendations for Future Research

Looking towards the future, it is recommended to conduct a systematic comparison of channel geometry and bar locations at identical sites in subsequent years. These observations will give insights into the speed of morphological changes. If more topographic measurements are required, employing a more robust RTK system is advisable. Furthermore, fostering collaboration with fellow researchers, particularly those affiliated with the University of Edinburgh, holds promise for advancing our research. Specifically, it could focus on refining bed load estimates during monsoon periods, as this is now an unknown factor.

References

Detert, M., & Weitbrecht, V. (2012). *Automatic object detection to analyze the geometry of gravel grains – a free stand-alone tool*.

Detert, M., & Weitbrecht, V. (2013). *User guide to gravelometric image analysis by BASEGRAIN*.

Parsons, D. R., Jackson, P. R., Czuba, J. A., Engel, F. L., Rhoads, B. L., Oberg, K. A., Best, J. L., Mueller, D. S., Johnson, K. K., & Riley, J. D. (2013). Velocity Mapping Toolbox (VMT): A processing and visualization suite for moving-vessel ADCP measurements. *Earth Surface Processes and Landforms*, *38*(11), 1244–1260. https://doi.org/10.1002/esp.3367

Stähly, S., Friedrich, H., & Detert, M. (2017). Size Ratio of Fluvial Grains' Intermediate Axes Assessed by Image Processing and Square-Hole Sieving. *Journal of Hydraulic Engineering*, *143*(6), 06017005. https://doi.org/10.1061/(ASCE)HY.1943-7900.0001286

7. Appendices

7.1 Observations per location

KAR1

Overview

Sediment images	Waterlevel	Highflood level	Cross-section	Width
0	140.4	-	CHIRP+RTK GPS	250 m

Observations

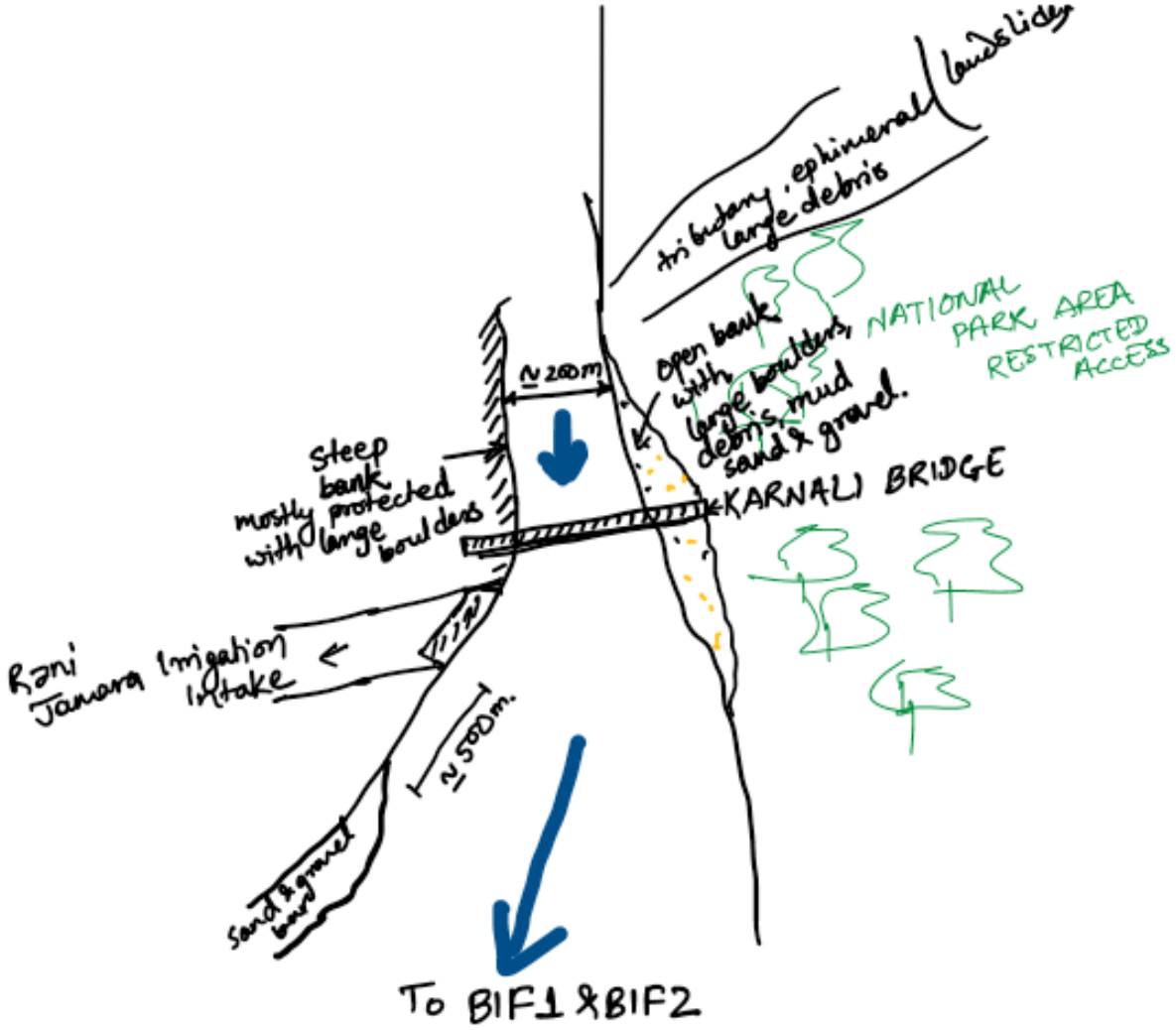

Cross-section

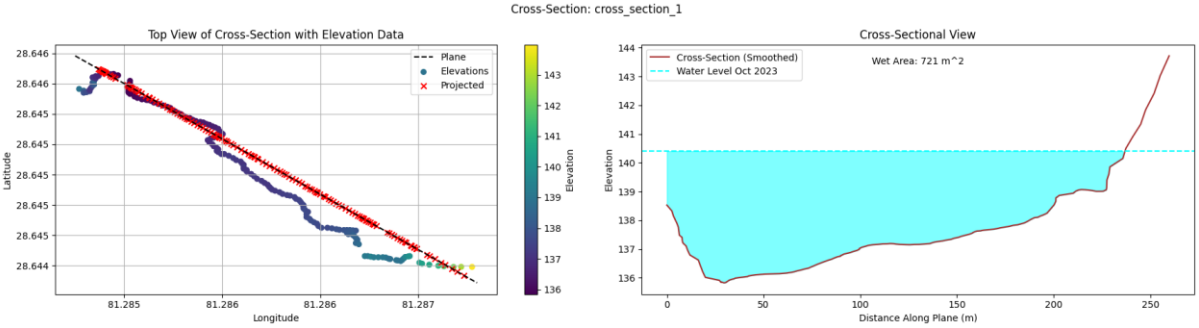

BIF1

Overview

Sediment images	Waterlevel	Highflood level	Cross-section	Width
15	139.5	-	#2 CHIRP+RTK GPS	700 m

Observations

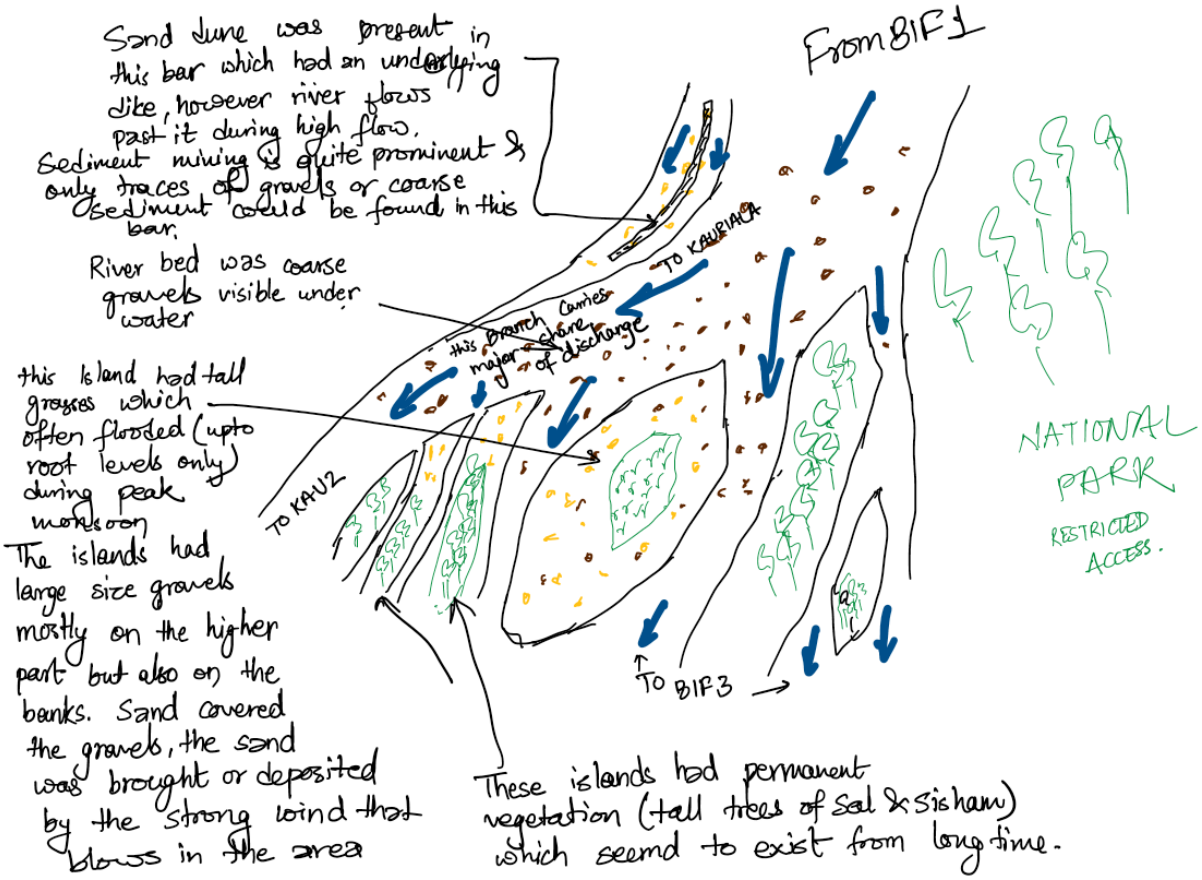

First bifurcation point of the river. The western bank consist mainly of sand due to intake structure of the irrigation channel just upstream of the point. Some gravel and boulders are present on top of the sand. The first large bar (0.260 km²) that starts to split the Karnali channel consists of coarse gravel and boulders and has little grasses in the middle. The other large, more stretched out bar to the west is covered in multi year vegetation.

Cross-section

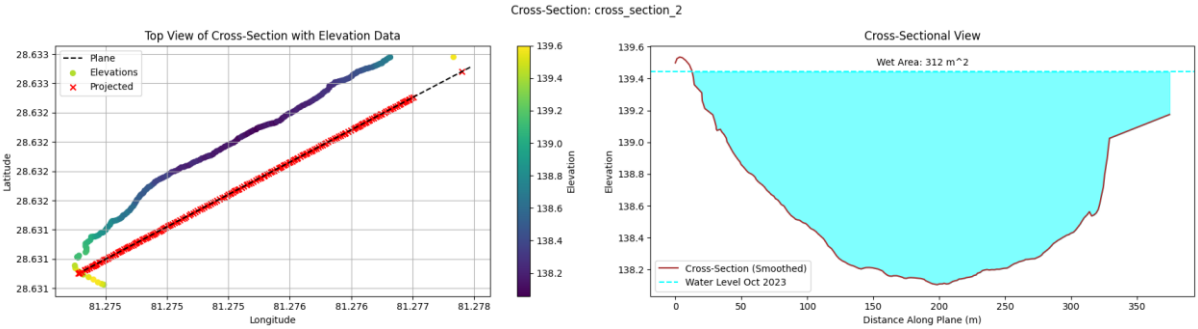

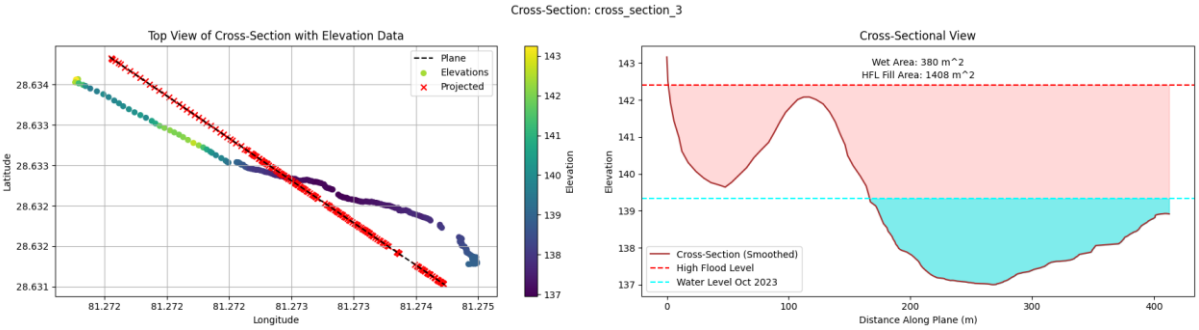

BIF2

Overview

Sediment images	Waterlevel	Highflood level	Cross-section	Width
20	139.0	140.8	#2 CHIRP+RTK GPS	550 m

Observations

Second bifurcation point. Majority of flow goes West to the Kauriala branch. The bar/island that start at this bifurcation is very large (4 km^2) and most of the island seems to be permanently vegetated.

Cross-section

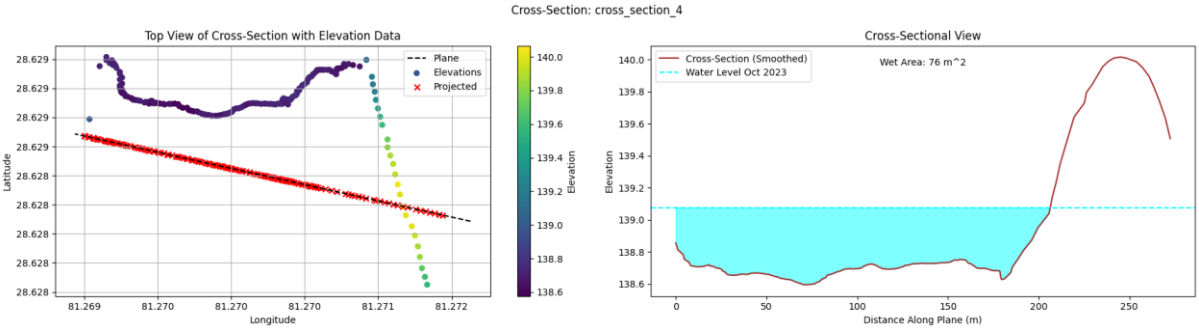

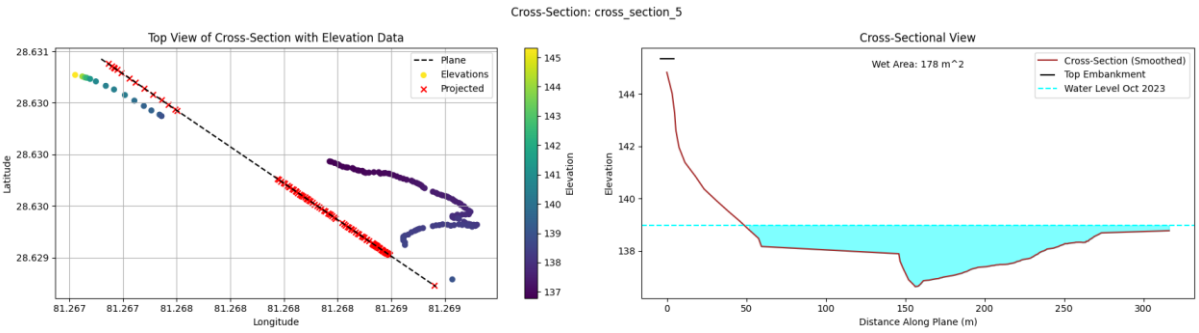

BIF3

DGPS

Overview

Sediment images	Waterlevel	Highflood level	Cross-section	Width
55	133-134	138.9	CHIRP+RTK DGPS	350 m

Observations

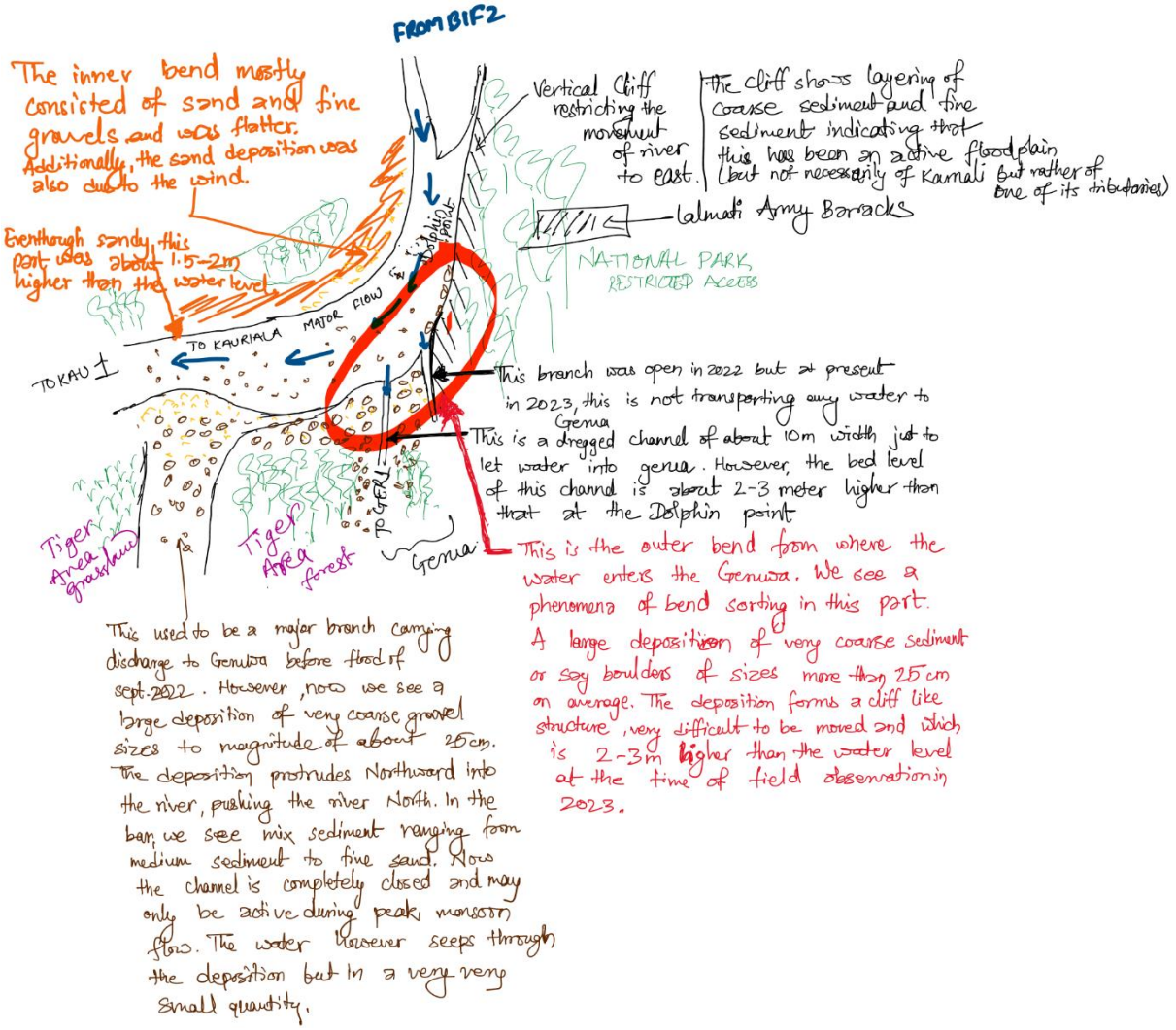

The third major bifurcation point and most crucial for the supply of the Geruwa branch. Entry to the Geruwa branch is completely blocked by a deposition of large boulders. Efforts by the national park authorities to dredge a channel through the blocked entrance seem insufficient to reestablish the at around 1 – 1.5 meters deep, far less than the depth of the main channel at 4 m. Sediment size on the inner bend is significantly smaller than in the outer bend.

Cross-section

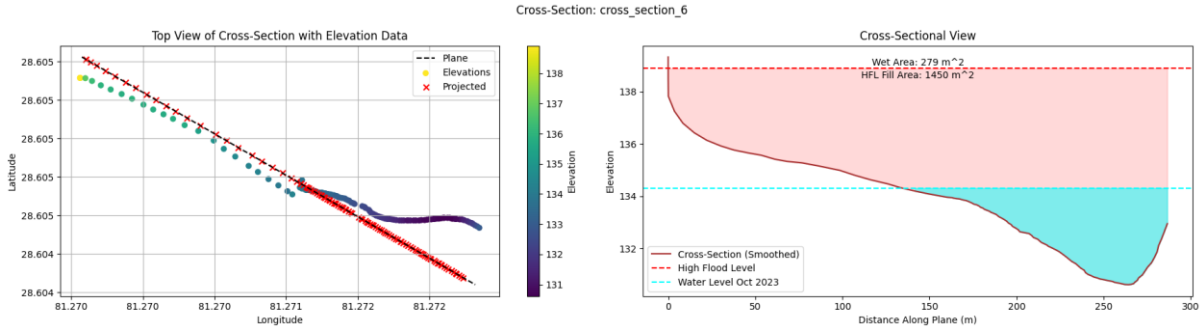

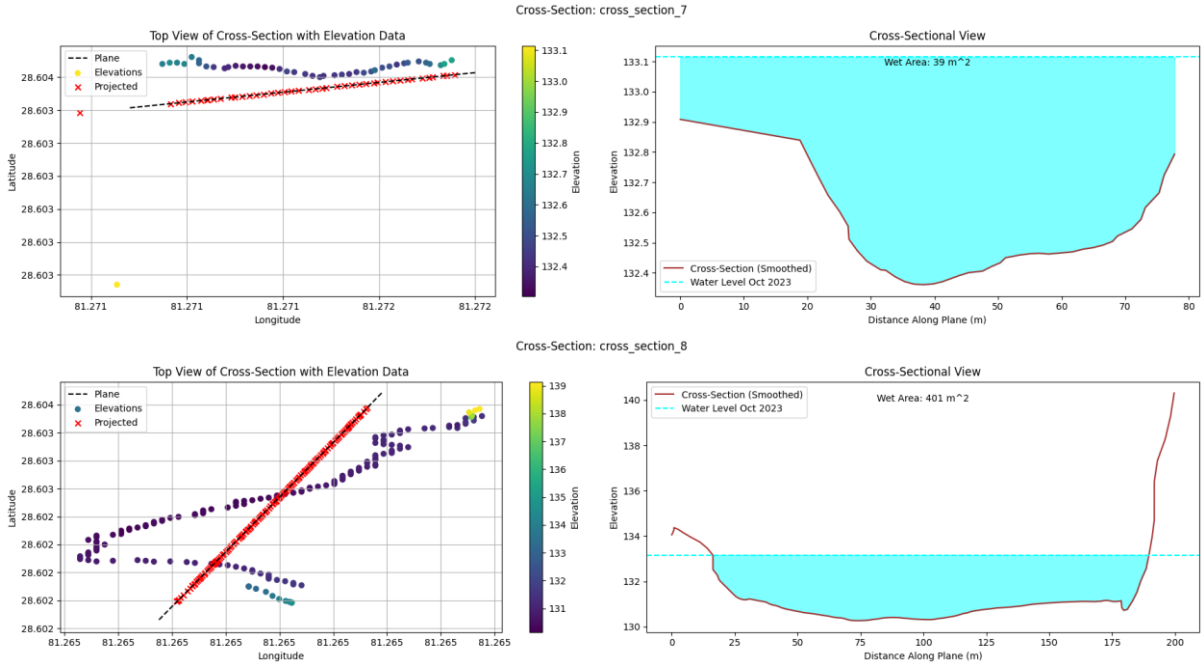

KAU1

Overview

Sediment images	Waterlevel	Highflood level	Cross-section	Width
9	121.5	-	CHIRP+RTK GPS	140 m

Observations

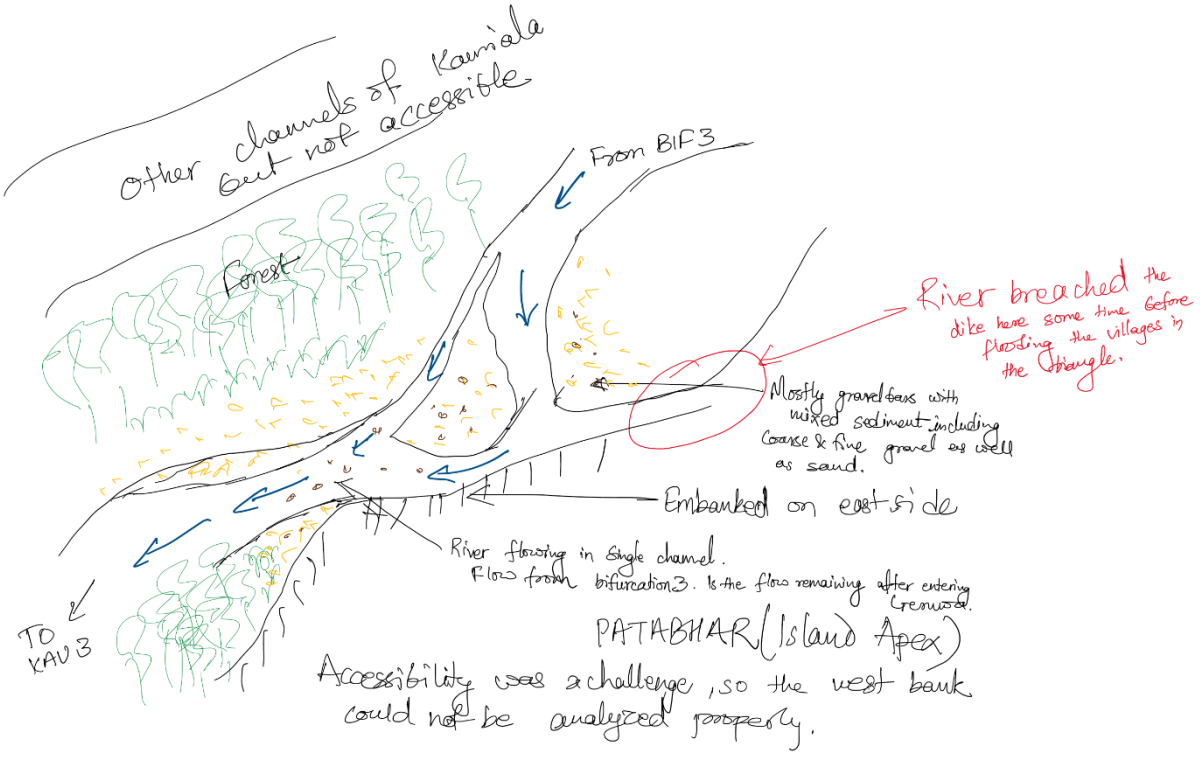

Cross-section

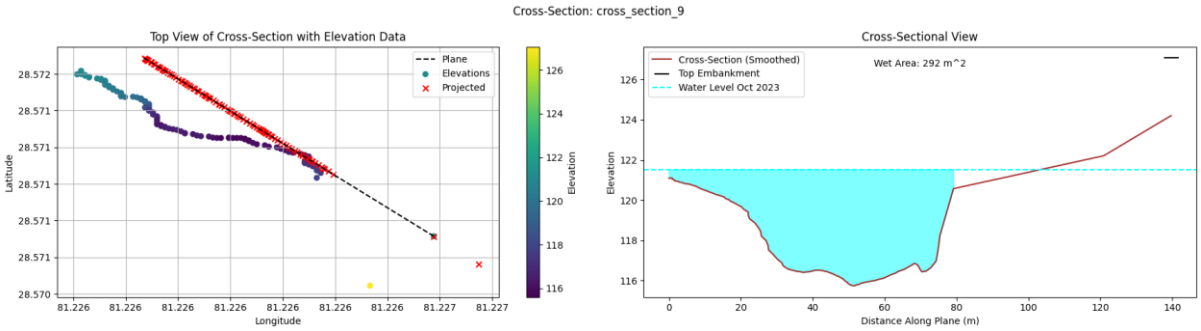

KAU2

Overview

Sediment images	Waterlevel	Highflood level	Cross-section	Width
12	125.6	129.3	#2 CHIRP+RTK GPS	240 m

Observations

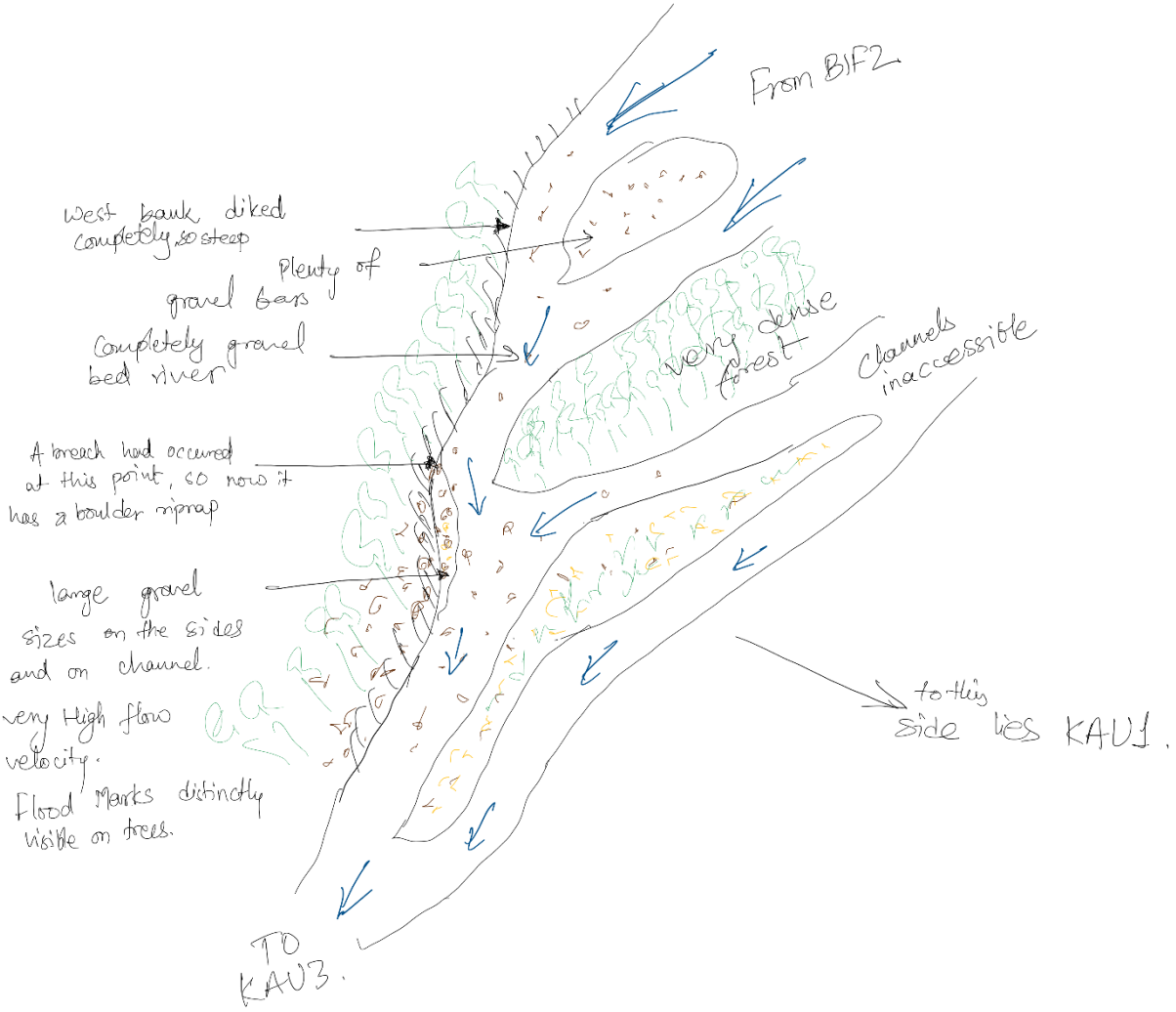

Cross-section

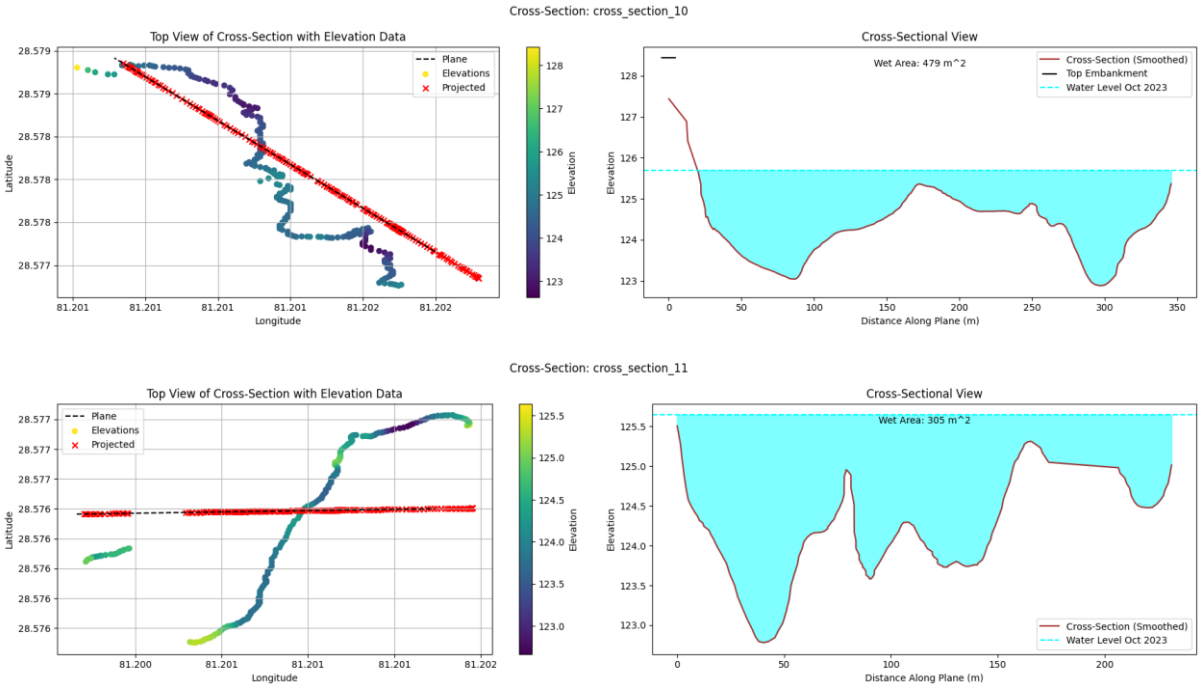

KAU3

Overview

Sediment images	Waterlevel	Highflood level	Cross-section	Width
0	117.2	120.8	CHIRP+RTK GPS	130 m

Observations

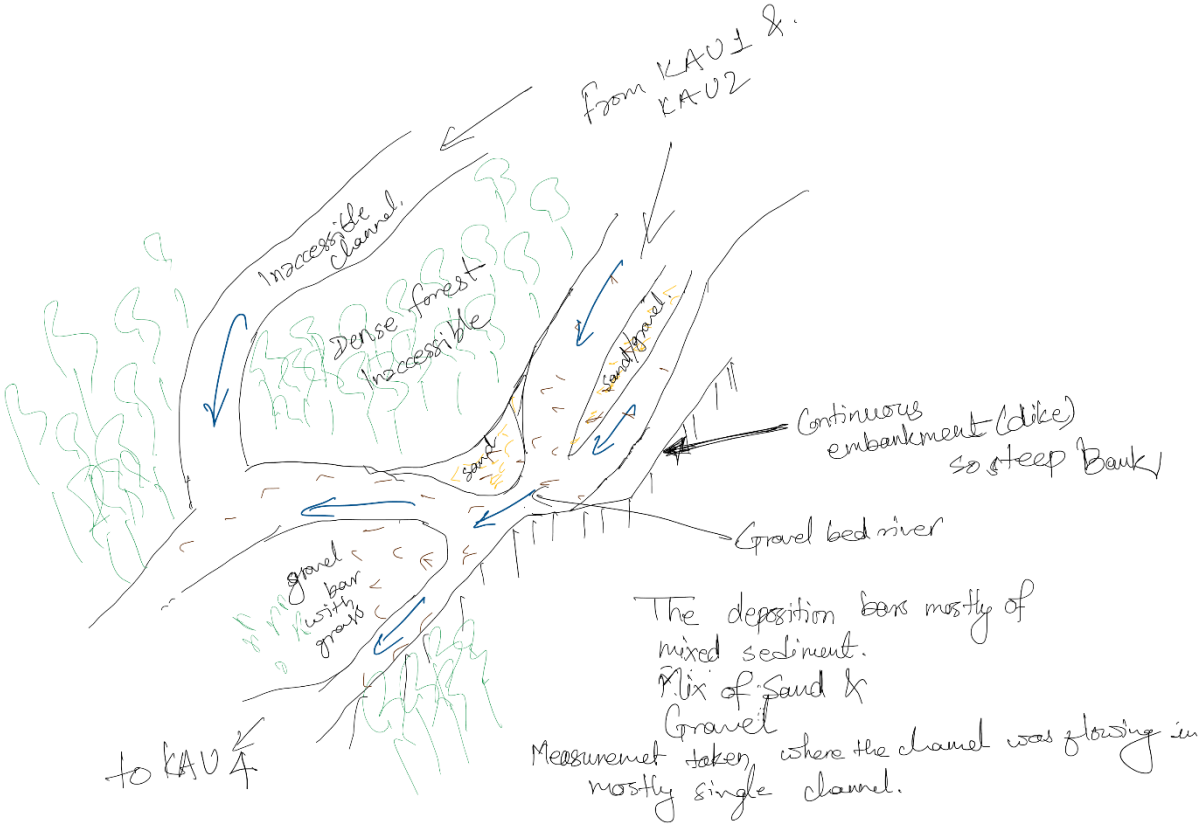

Cross-section

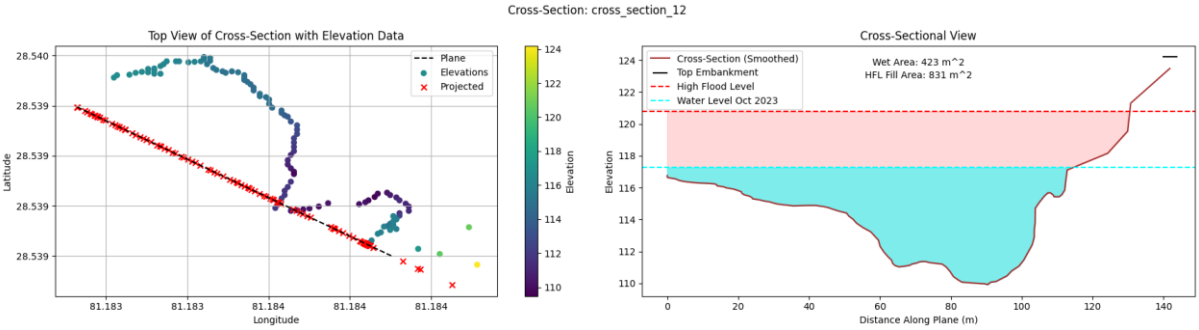

KAU4

Overview

Sediment images	Waterlevel	Highflood level	Cross-section	Width
20	111.7	114.7	CHIRP+RTK GPS	720 m

Observations

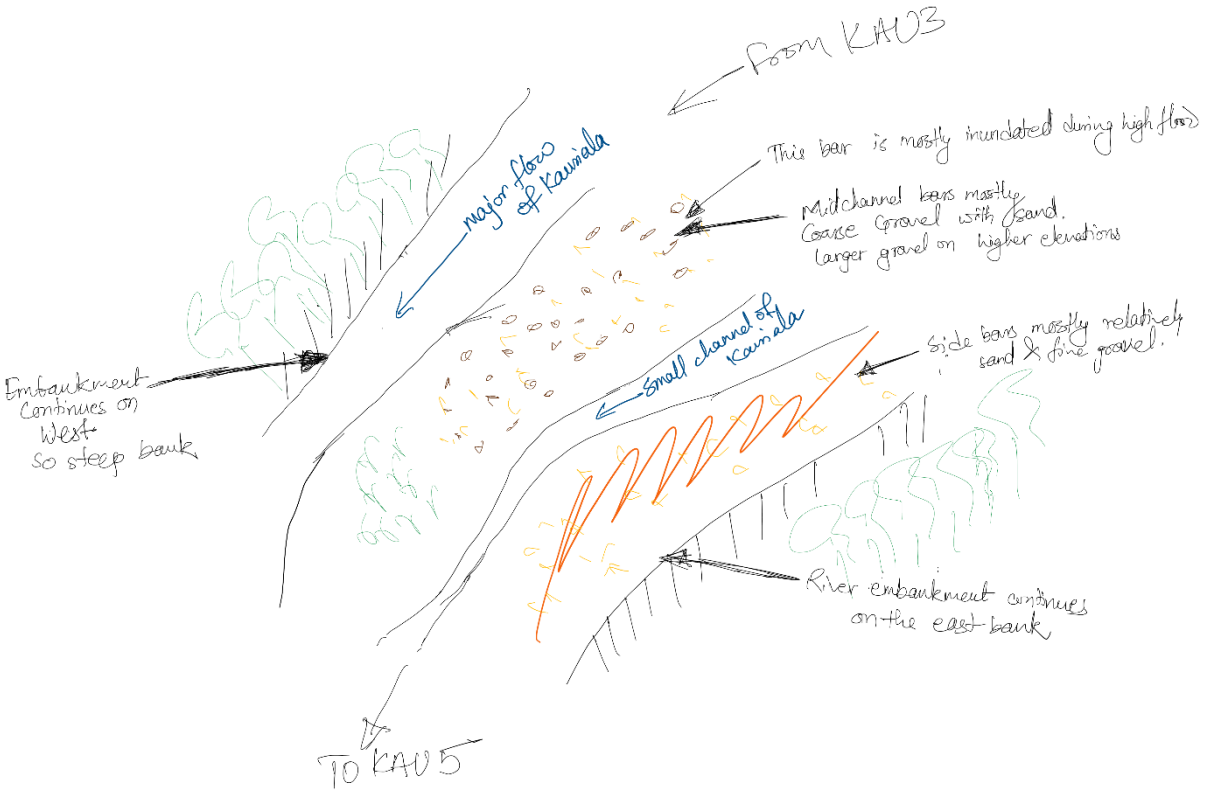

Cross-section

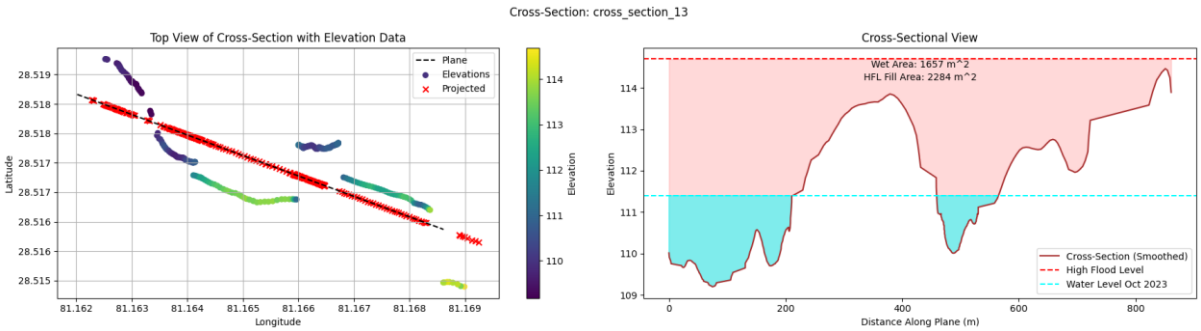

KAU5

Overview

Sediment images	Waterlevel	Highflood level	Cross-section	Width
5	99.2	102-104.5	CHIRP+RTK GPS	400 m

Observations

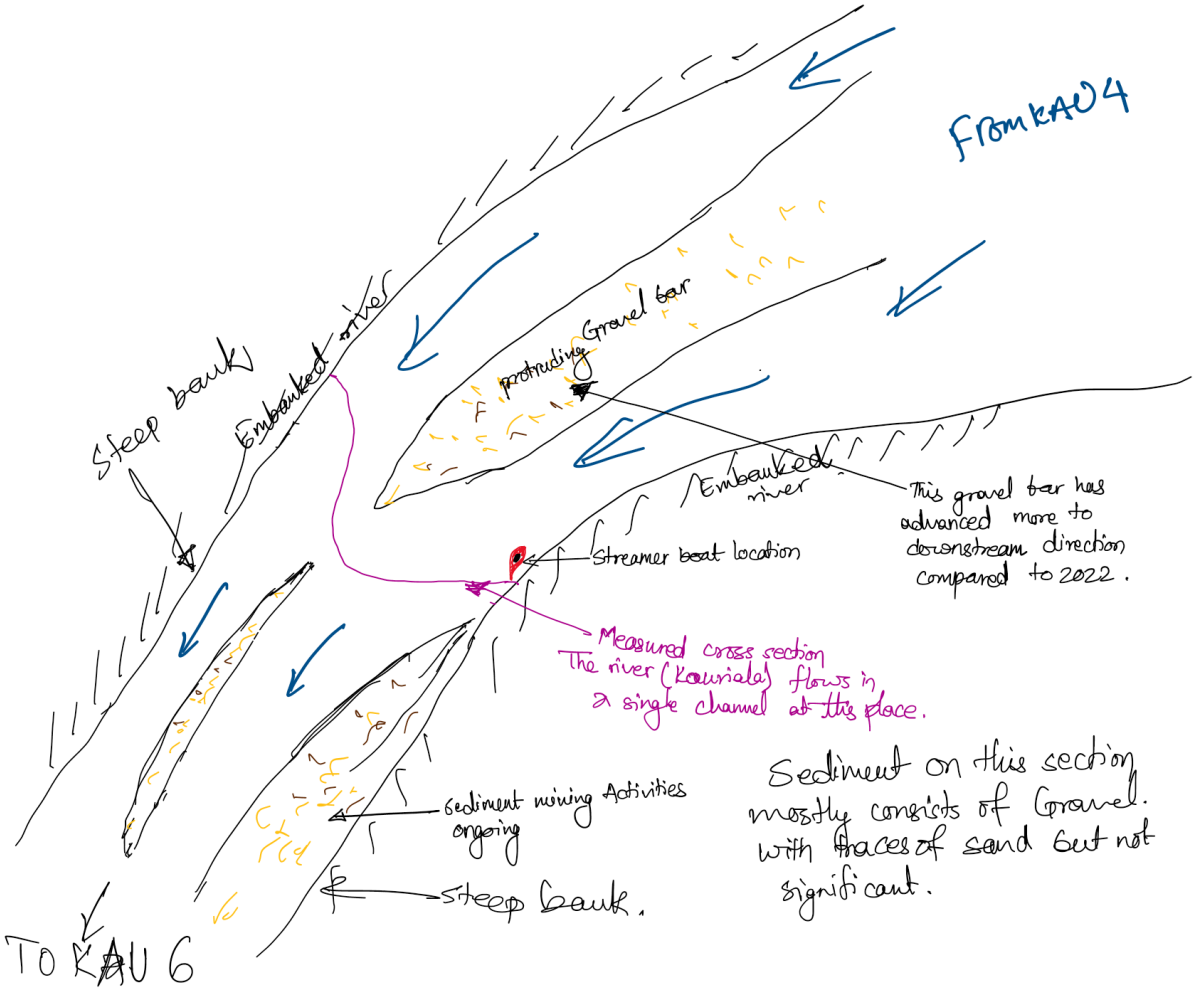

Cross-section

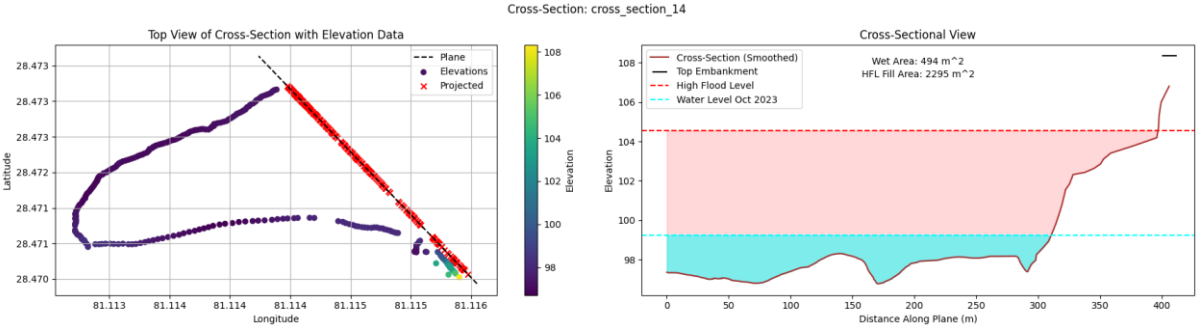

KAU6

Overview

Sediment images	Waterlevel	Highflood level	Cross-section	Width
19	83.8	-	CHIRP+RTK GPS	580 m

Observations

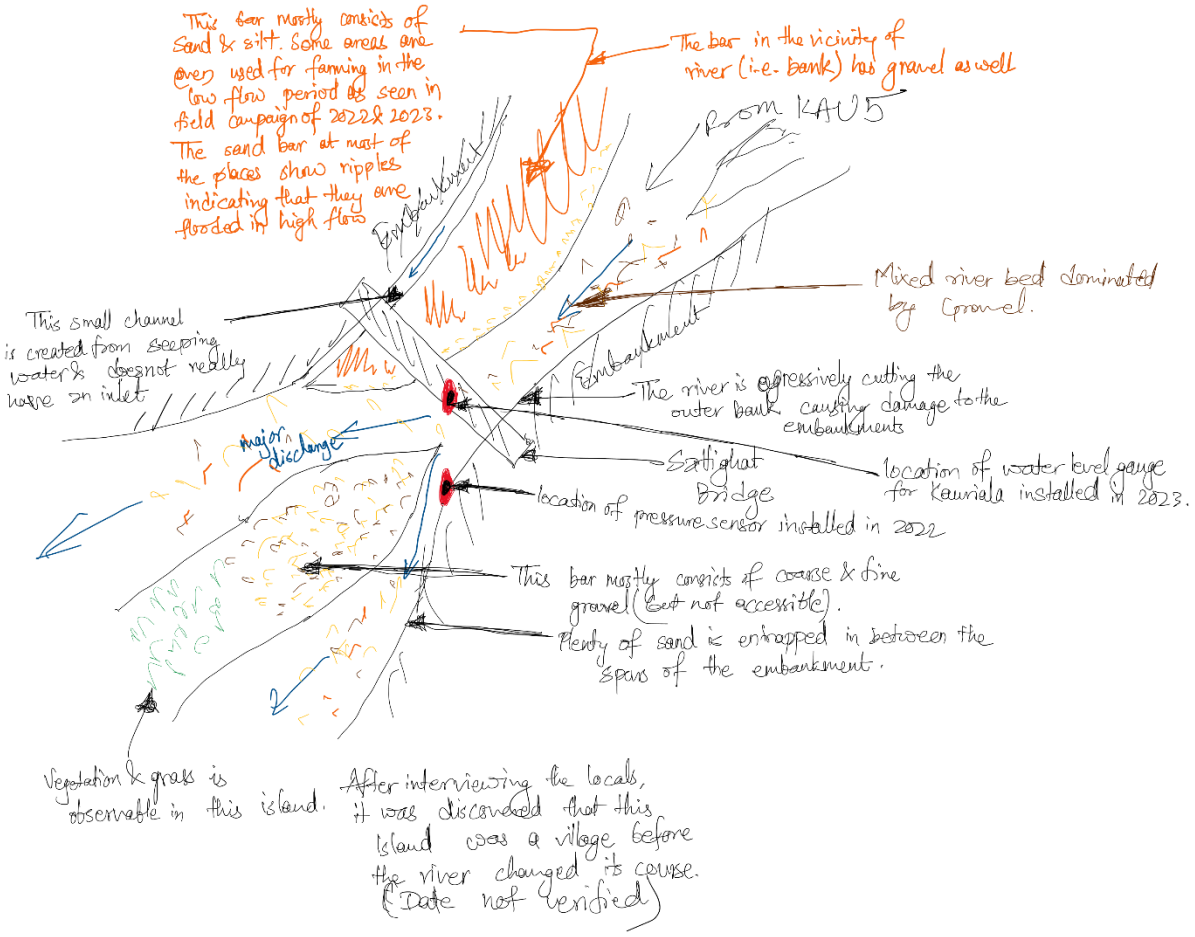

Cross-section

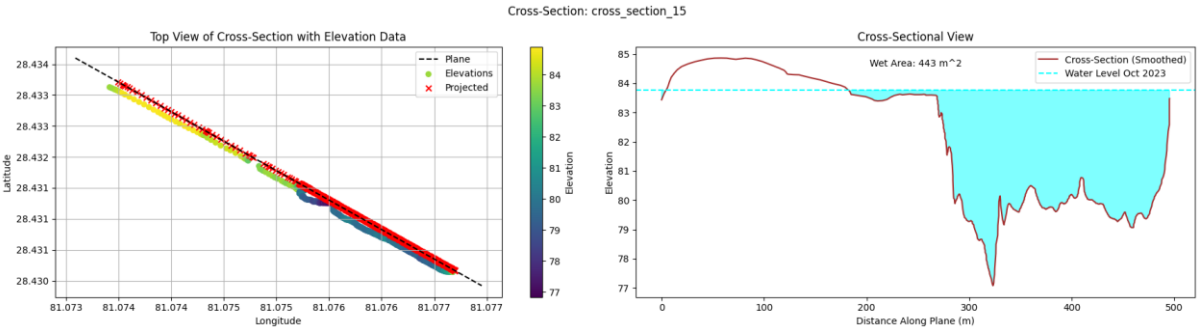

GER1

Overview

Sediment images	Waterlevel	Highflood level	Cross-section	Width
14	122.4	-	RTK GPS	380 m

Observations

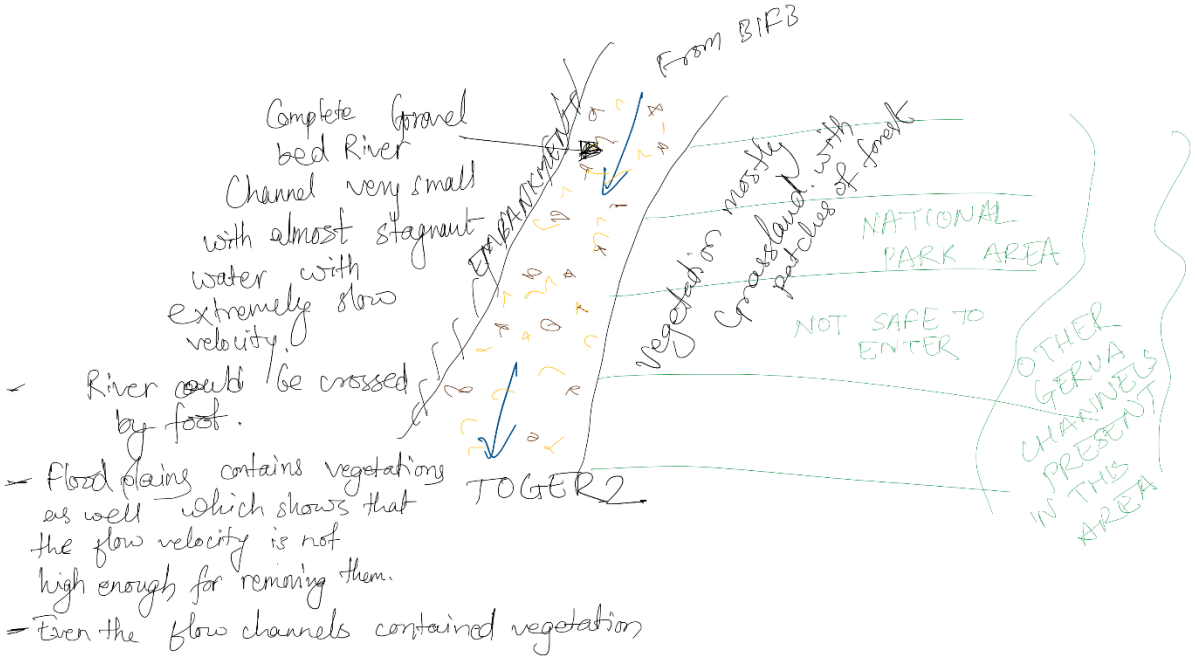

Cross-section

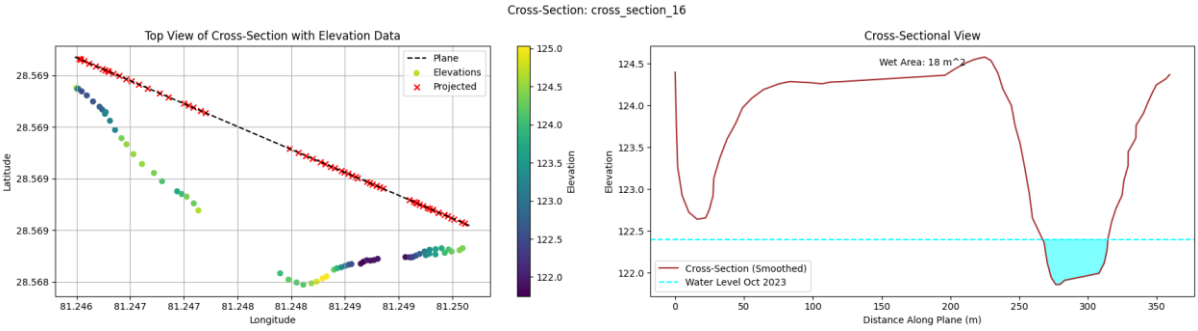

GER2

Overview

Sediment images	Waterlevel	Highflood level	Cross-section	Width
8	116.5	122.4	RTK GPS	150 m

Observations

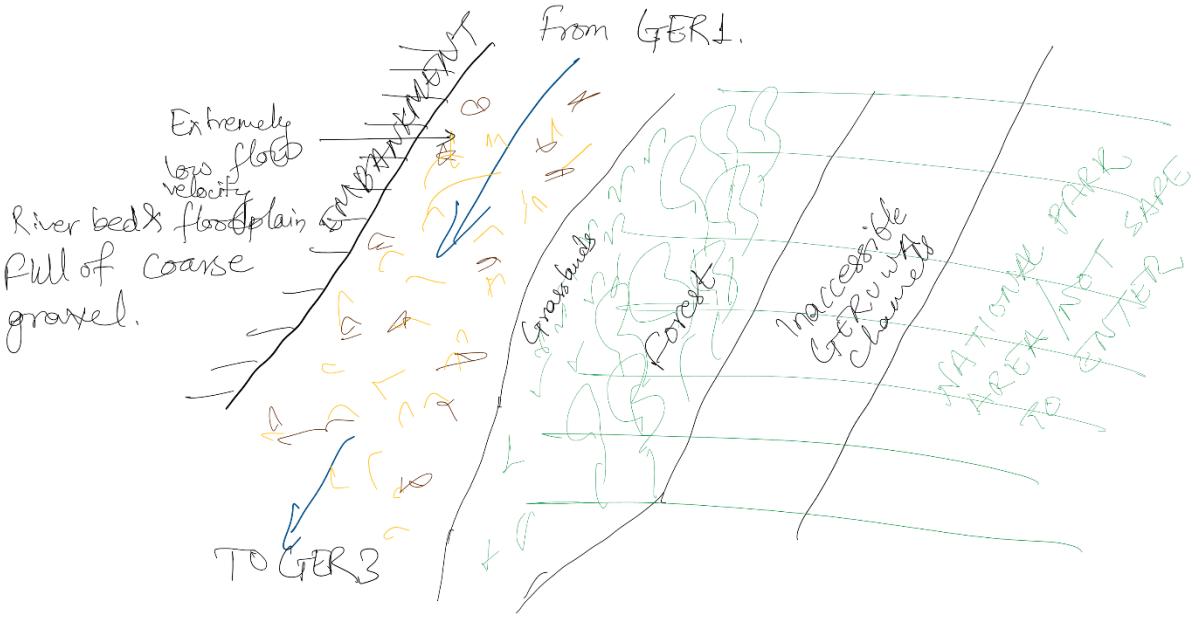

Cross-section

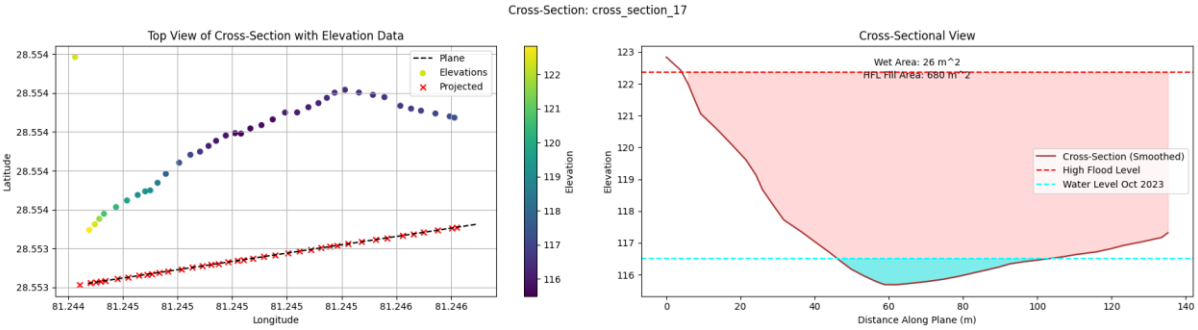

GER3

Elehpant tracks

Overview

Sediment images	Waterlevel	Highflood level	Cross-section	Width
14	112.0	-	RTK GPS	170 m

Observations

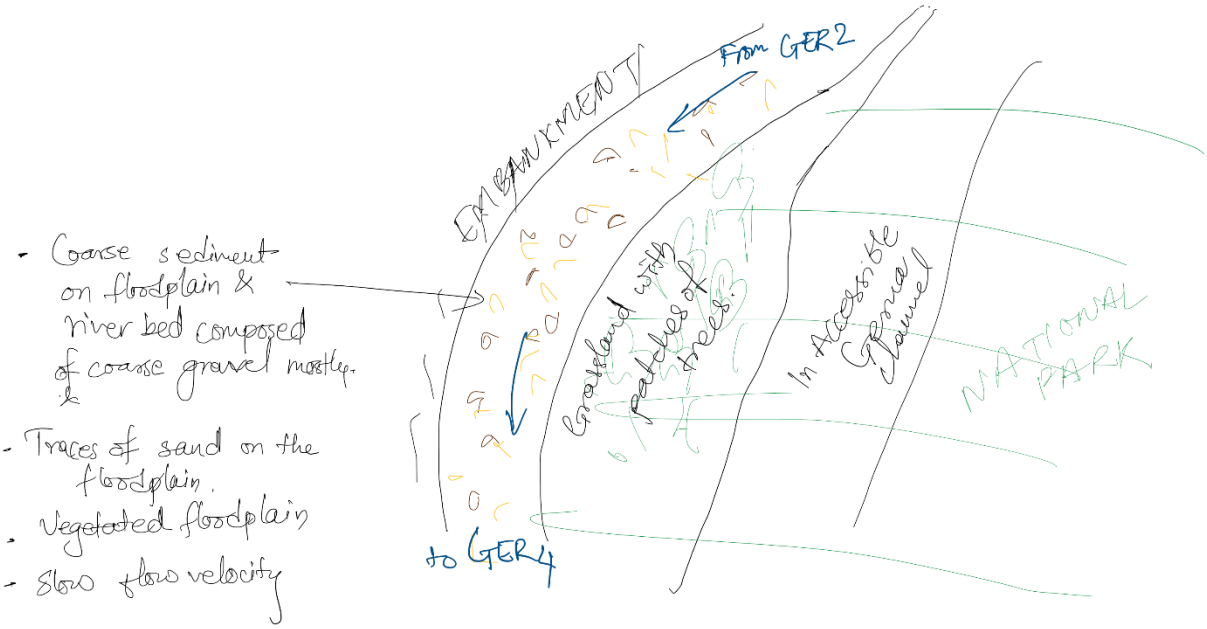

Cross-section

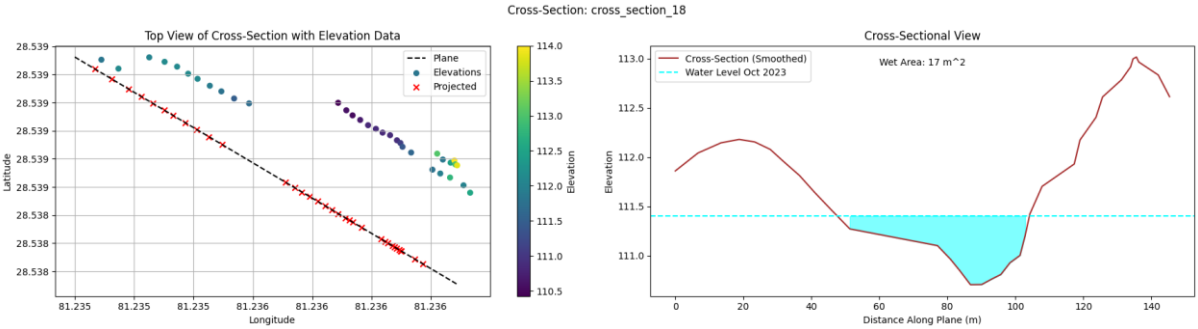

GER4

Overview

Sediment images	Waterlevel	Highflood level	Cross-section	Width
10	105.1	108-109	RTK GPS	600 m

Observations

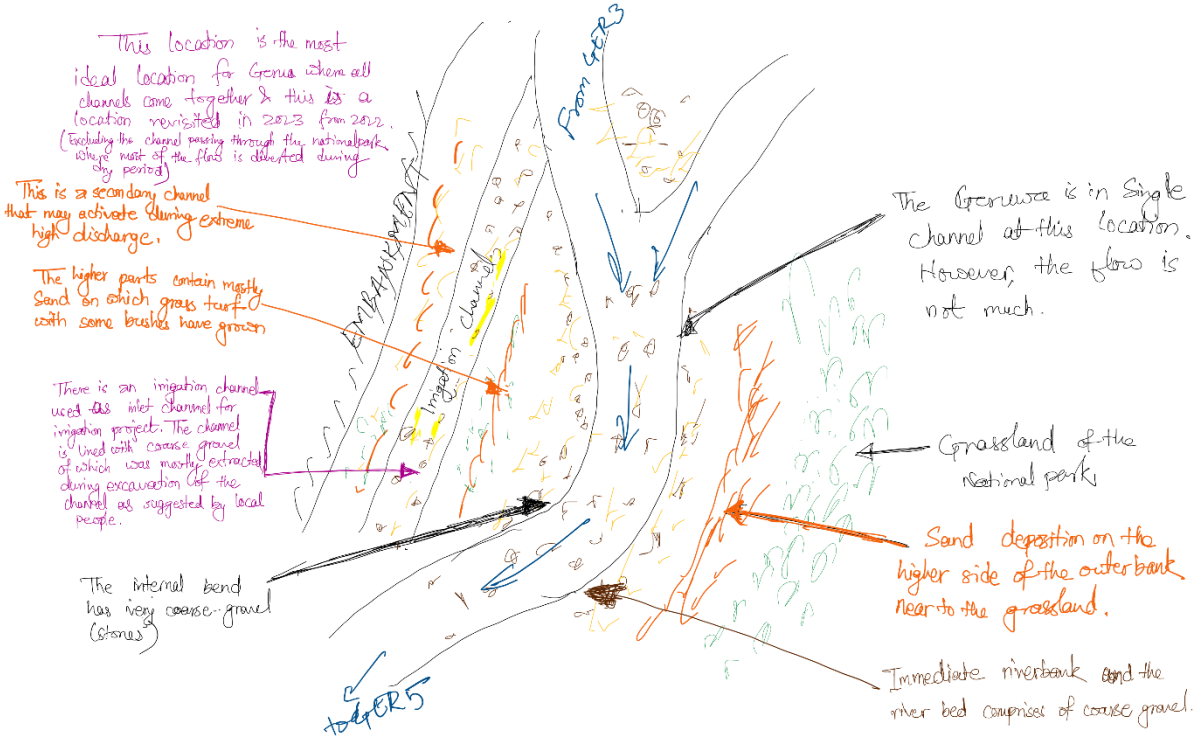

Cross-section

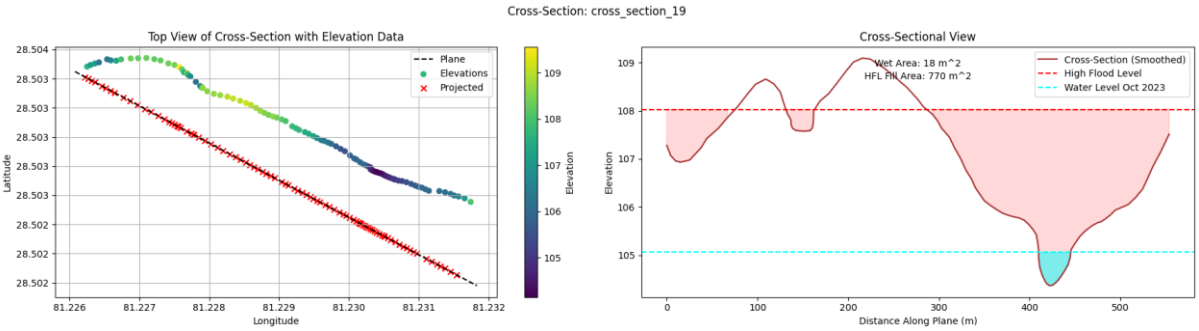

GER5

Overview

Sediment images	Waterlevel	Highflood level	Cross-section	Width
19	100.5	104.2	CHIRP+RTK GPS	250 m

Observations

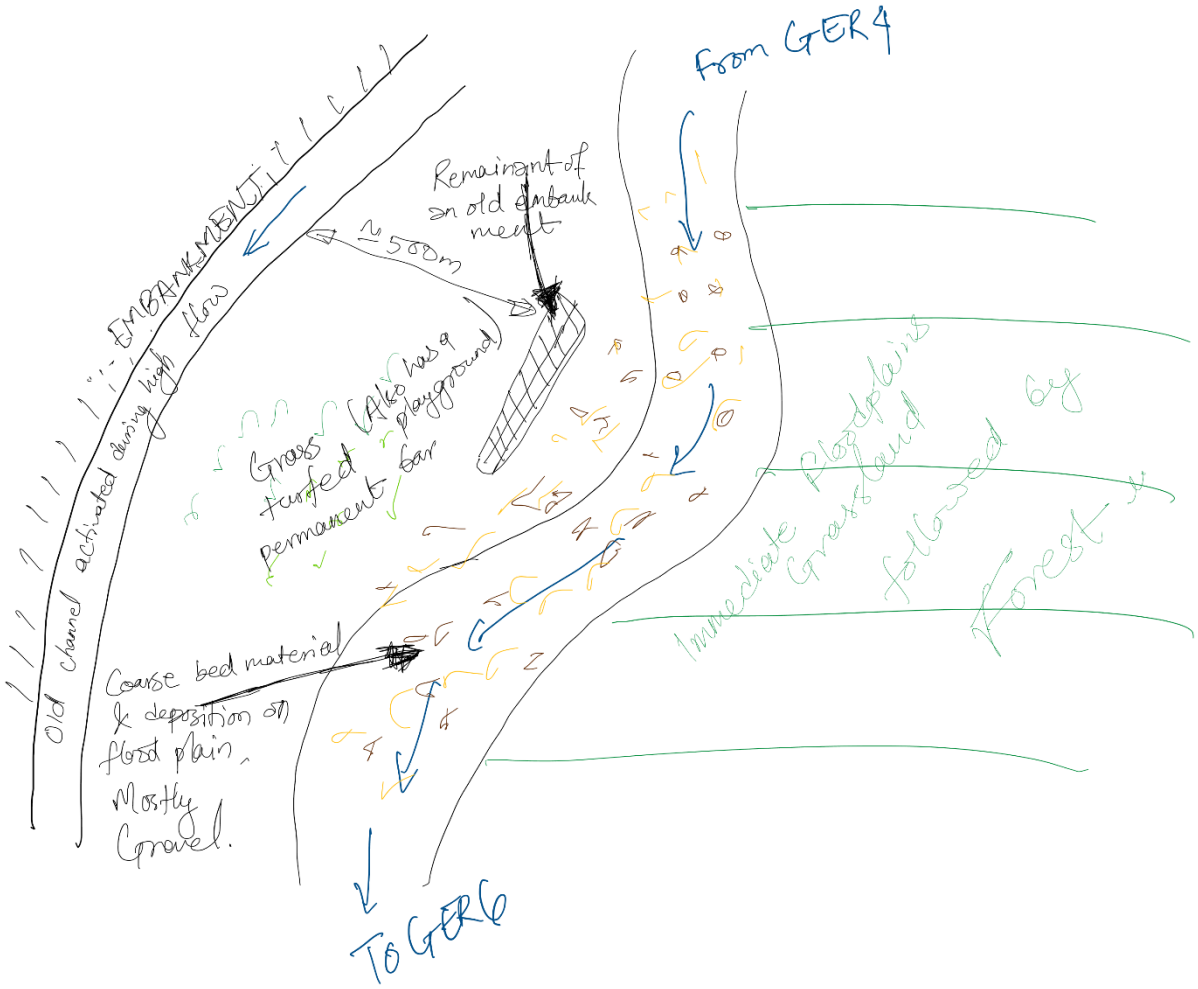

Cross-section

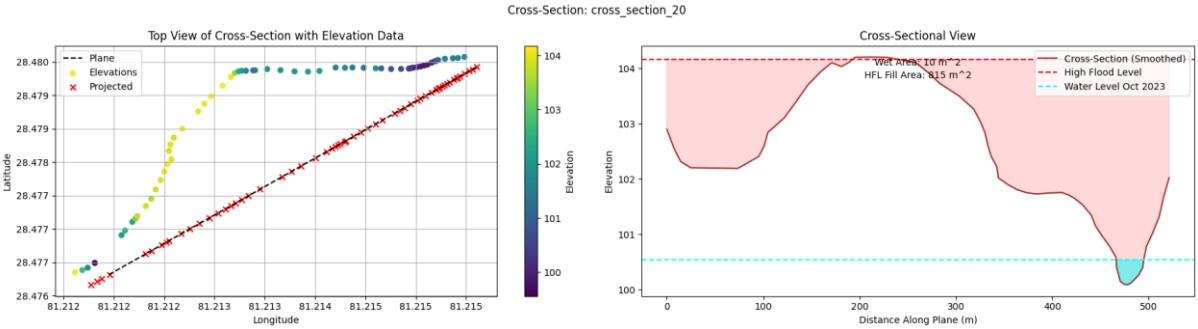

GER6

Overview

Sediment images	Waterlevel	Highflood level	Cross-section	Width
19	96.3	98.9	RTK GPS	350 m

Observations

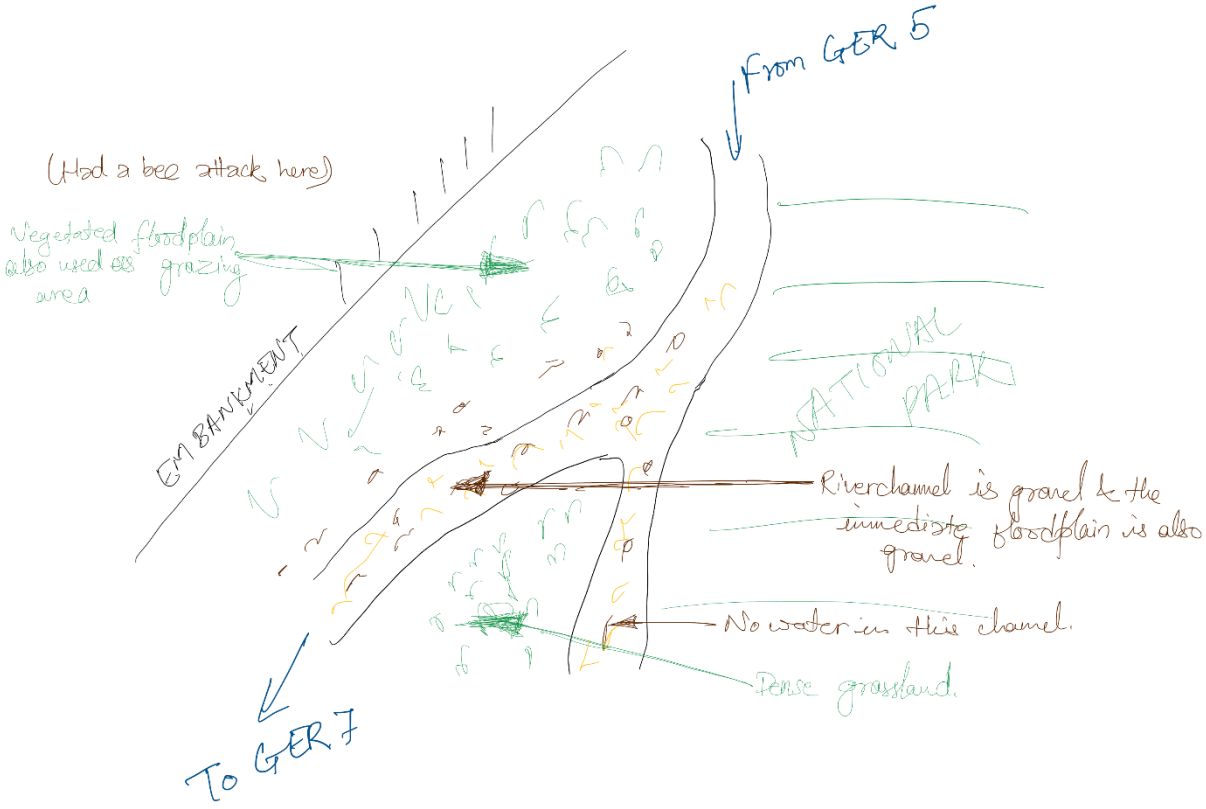

Cross-section

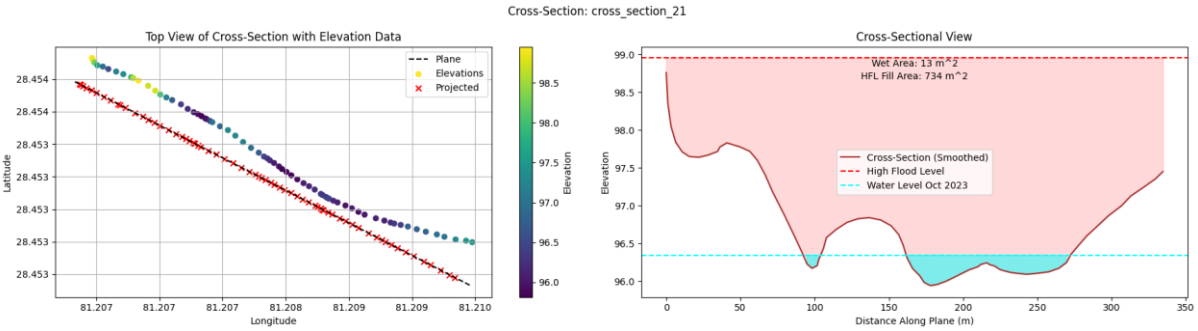

GER7

Overview

Sediment images	Waterlevel	Highflood level	Cross-section	Width
9	86.1	-	RTK GPS	210 m

Observations

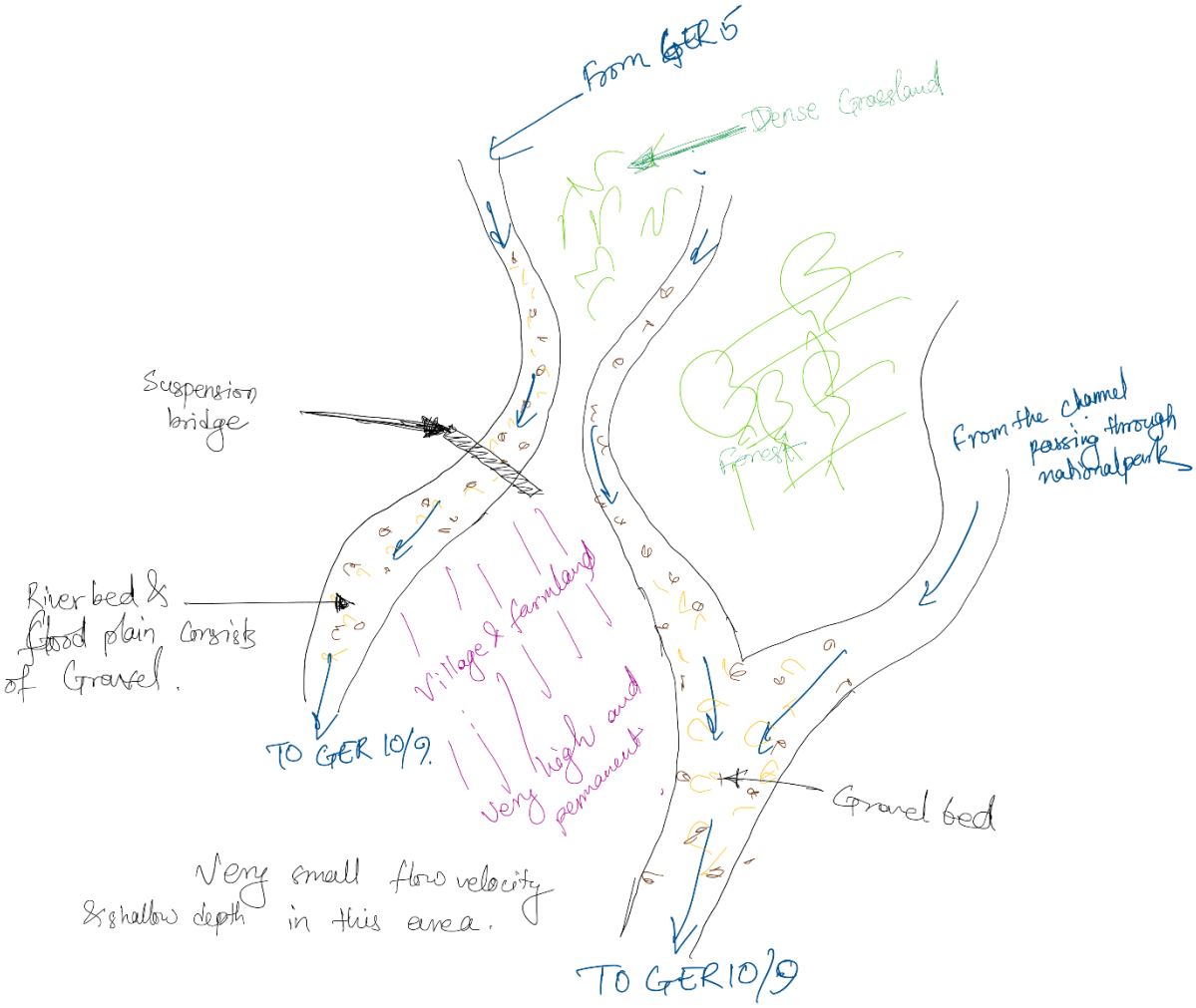

Cross-section

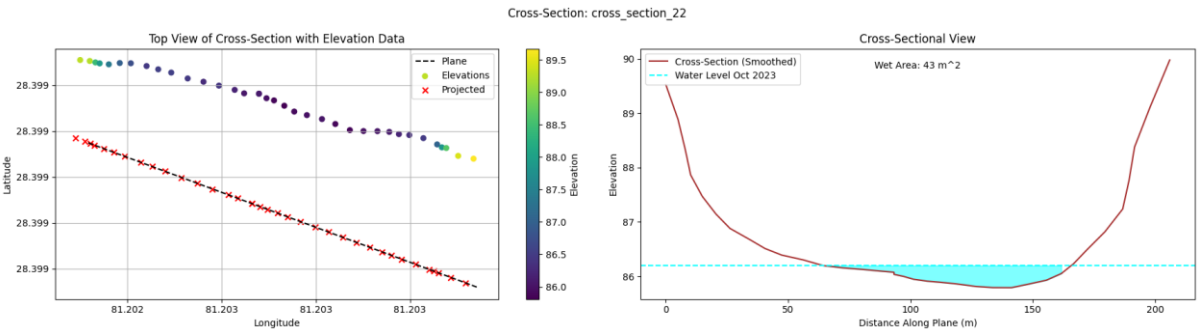

GER8

Overview

Sediment images	Waterlevel	Highflood level	Cross-section	Width
9	84.4	-	RTK GPS	180 m

Observations

Included in previous drawing.

Cross-section

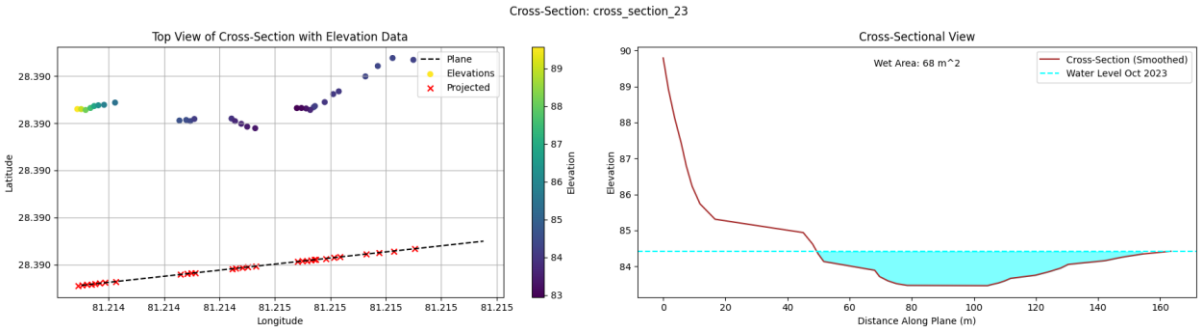

GER9

Overview

Sediment images	Waterlevel	Highflood level	Cross-section	Width
10	-	87.5	RTK GPS	280 m

GER10

Overview

Sediment images	Waterlevel	Highflood level	Cross-section	Width
0	83.0	85.6	CHIRP+RTK GPS	200 m

Observations

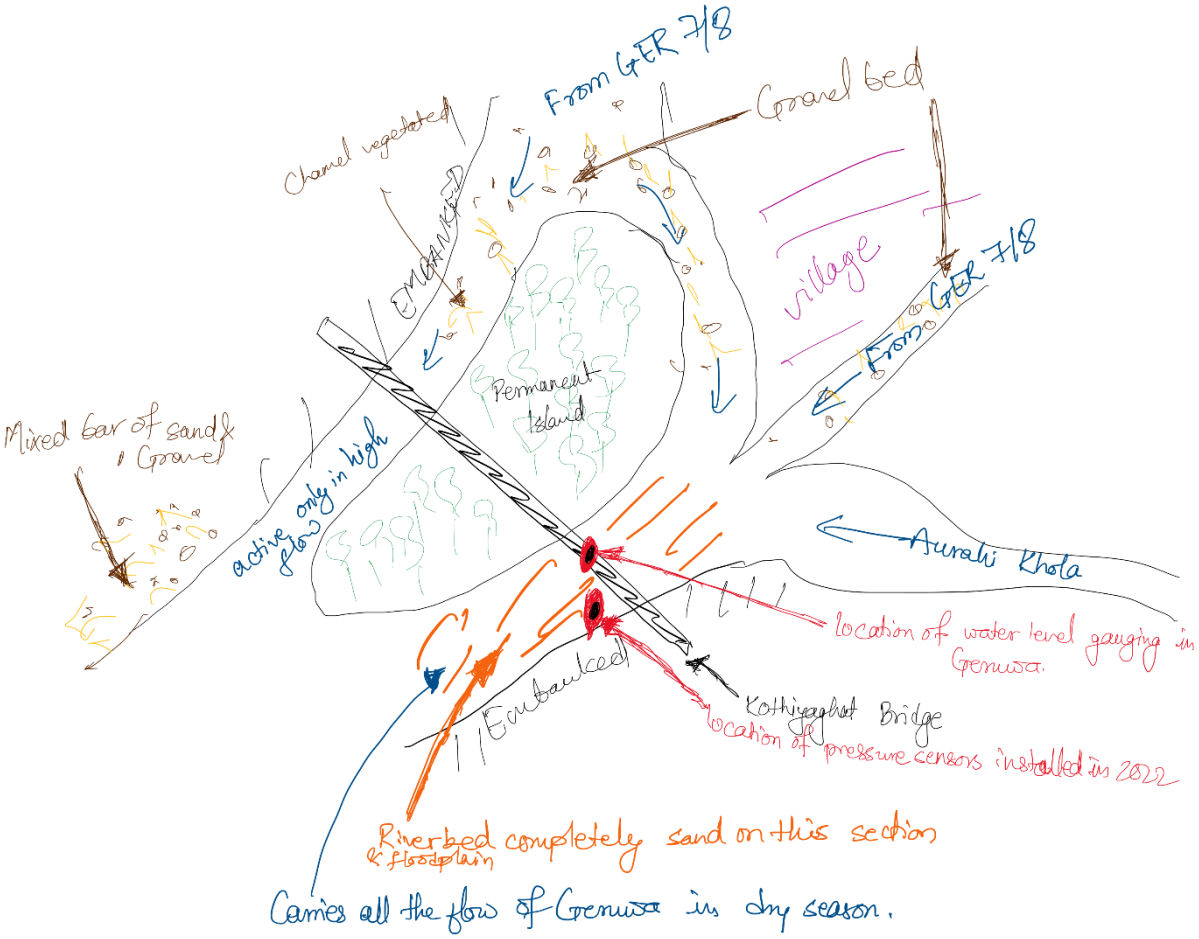

Cross-section

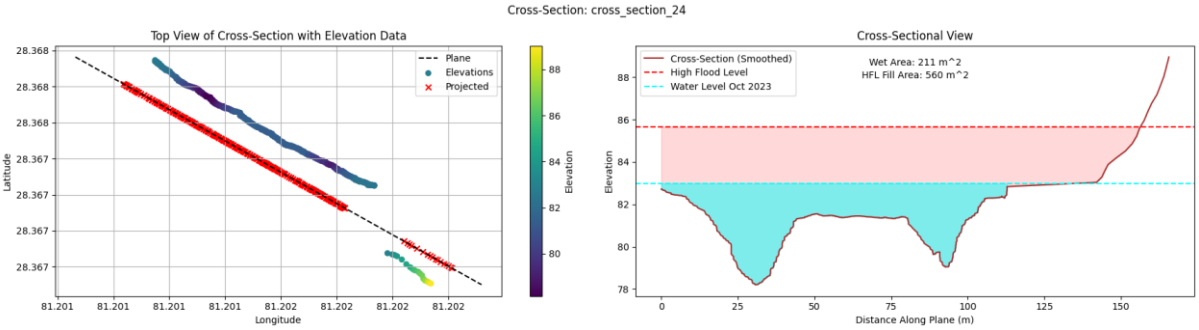

7.2 Sediment Photographs from the Fieldwork

KAR1

None

BIF1



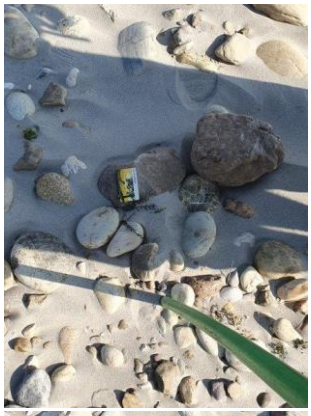








BIF2

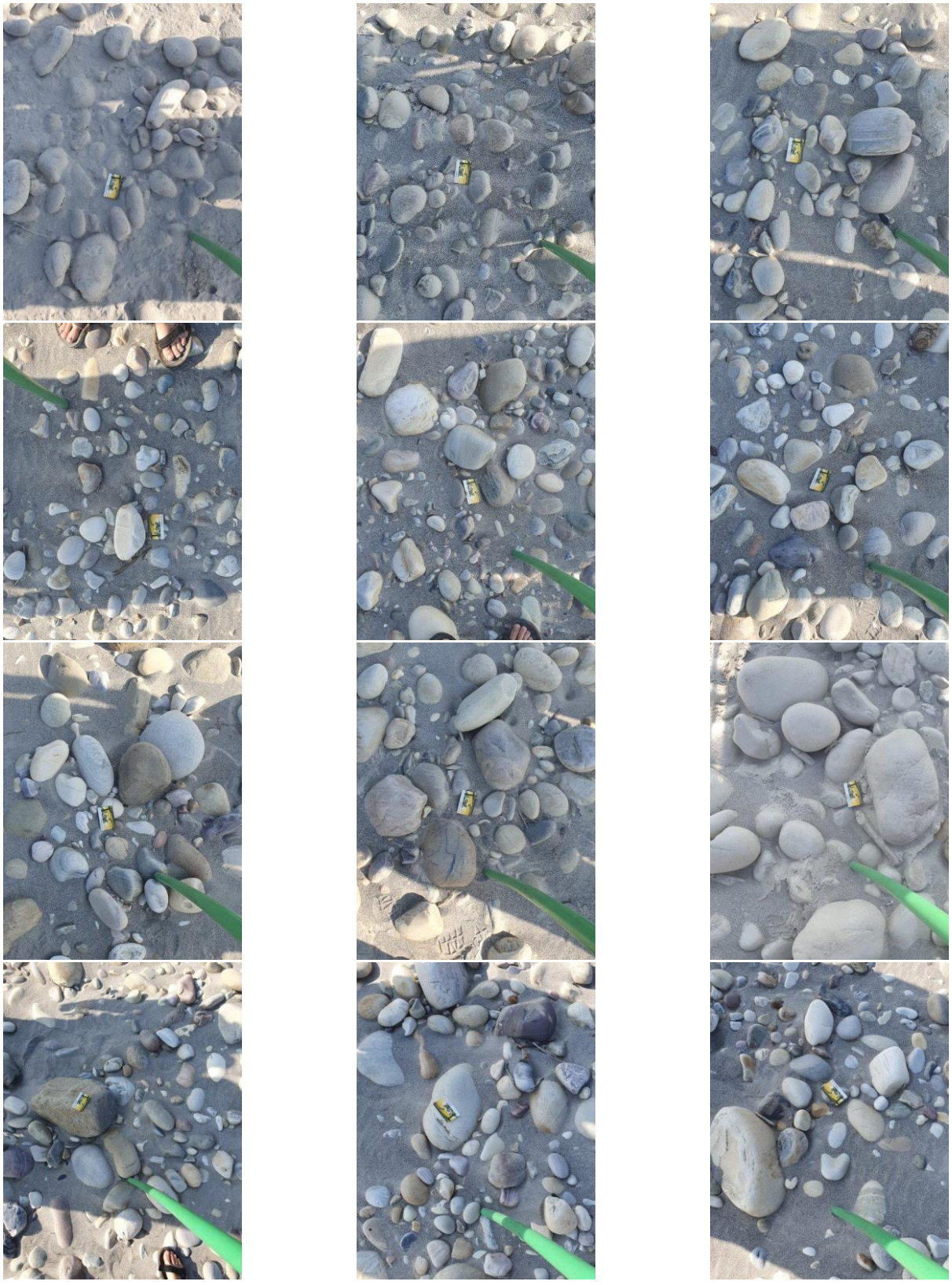






BIF3











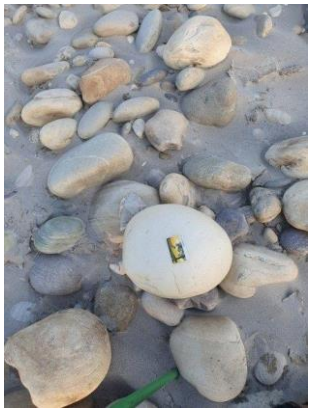
























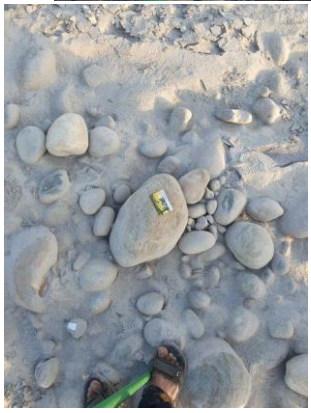











KAU1





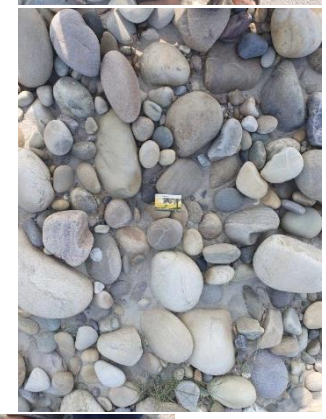



KAU2











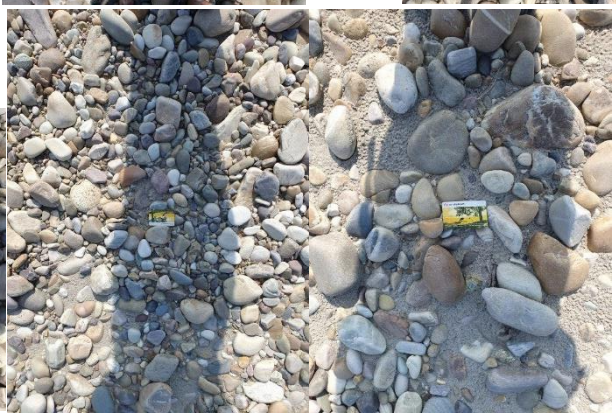

KAU3

-

KAU4


















KAU5





KAU6



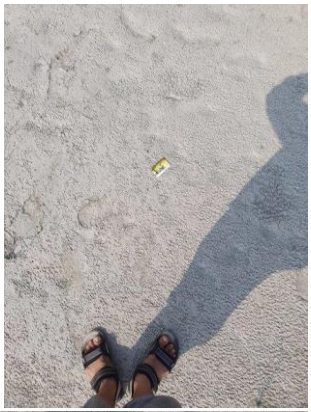


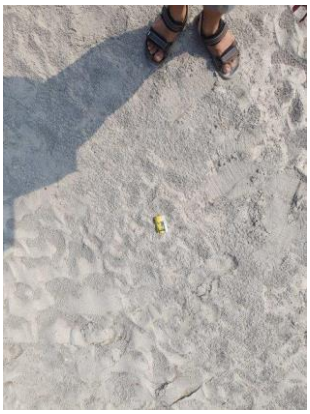


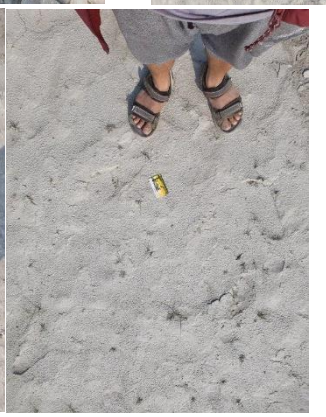




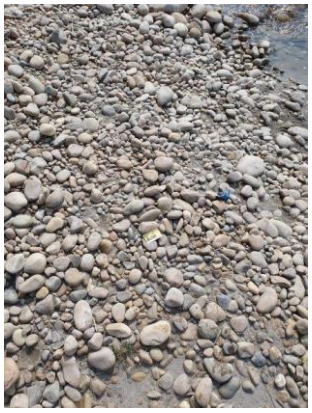



GER1












GER2



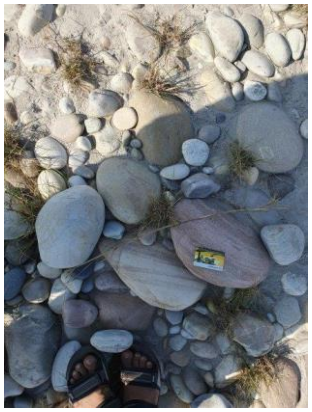



GER3













GER4









GER5














GER6








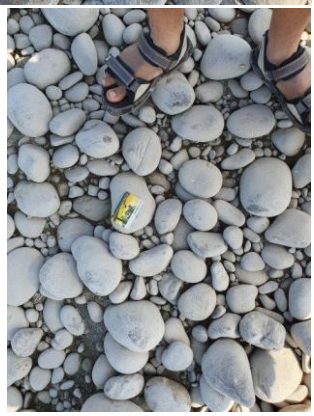









GER7







GER8


GER9




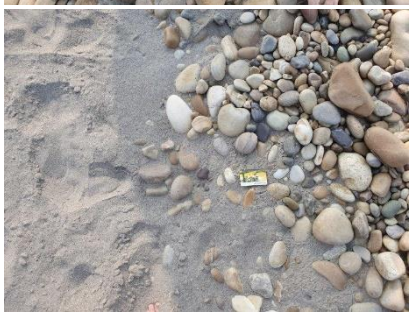





GER10

None

7.3 Additional tables

Table photos, name + coordinates

Name	Latitude	Longitude	Name	Latitude	Longitude
20231106_144722.jpg	28.3796887	81.1997716	**20231122_153713.jpg**	28.479382	81.2144672
20231106_144803.jpg	28.3799838	81.1996104	**20231122_153732.jpg**	28.479421	81.2143578
20231106_144836.jpg	28.3799838	81.1996104	**20231122_153814.jpg**	28.479533	81.2141205
20231106_144934.jpg	28.3798593	81.1995399	**20231122_153832.jpg**	28.479446	81.2140311
20231106_145014.jpg	28.3797701	81.1994376	**20231122_153846.jpg**	28.479514	81.2139944
20231106_145034.jpg	28.3797066	81.1993688	**20231122_153908.jpg**	28.479465	81.2138217
20231106_150656.jpg	28.3797541	81.200659	**20231122_153932.jpg**	28.479459	81.2137309
20231106_151034.jpg	28.382011	81.2097104	**20231122_153945.jpg**	28.479459	81.2137309
20231106_151101.jpg	28.3798545	81.2007407	**20231122_153959.jpg**	28.479459	81.2137309
20231106_151159.jpg	28.3798545	81.2007407	**20231122_154011.jpg**	28.479459	81.2137309
20231106_151242.jpg	28.379662	81.2004084	**20231122_154034.jpg**	28.479411	81.213359
20231107_110720.jpg	28.4330045	81.0734069	**20231123_101829.jpg**	28.453456	81.2077472
20231107_110752.jpg	28.432942	81.0735115	**20231123_101847.jpg**	28.453349	81.2077368
20231107_110820.jpg	28.432942	81.0735115	**20231123_101901.jpg**	28.453399	81.2076659
20231107_110902.jpg	28.4325381	81.0737542	**20231123_101914.jpg**	28.453399	81.2076659
20231107_110919.jpg	28.4325381	81.0737542	**20231123_101926.jpg**	28.453399	81.2076659
20231107_111256.jpg	28.4318495	81.0747775	**20231123_101936.jpg**	28.453478	81.2075864
20231107_111322.jpg	28.4318495	81.0747775	**20231123_101946.jpg**	28.453509	81.2075714
20231107_111736.jpg	28.4318804	81.0748889	**20231123_101957.jpg**	28.453591	81.2074457
20231107_111836.jpg	28.4317758	81.0752446	**20231123_102013.jpg**	28.453571	81.2074357
20231107_111913.jpg	28.4317758	81.0752446	**20231123_102031.jpg**	28.453583	81.2073878
20231107_111918.jpg	28.4317758	81.0752446	**20231123_102138.jpg**	28.453247	81.2073422
20231107_112000.jpg	28.432036	81.075635	**20231123_102149.jpg**	28.453247	81.2073422
20231107_112051.jpg	28.4321067	81.0757046	**20231123_102157.jpg**	28.453222	81.2072219
20231107_112111.jpg	28.4321067	81.0757046	**20231123_102208.jpg**	28.453222	81.2072219
20231107_112150.jpg	28.4324476	81.0755361	**20231123_102243.jpg**	28.453302	81.2072202
20231107_112215.jpg	28.4328351	81.0750888	**20231123_102259.jpg**	28.453302	81.2072202
20231107_112343.jpg	28.4333565	81.0745807	**20231123_102310.jpg**	28.453302	81.2072202
20231107_112405.jpg	28.4333565	81.0745807	**20231123_102340.jpg**	28.45325	81.2071479
20231107_152445.jpg	28.5170728	81.1643545	**20231123_102557.jpg**	28.4535	81.2073658
20231107_152522.jpg	28.5170728	81.1643545	**20231123_114931.jpg**	28.399216	81.2026138
20231107_152545.jpg	28.5171224	81.1647212	**20231123_114940.jpg**	28.399216	81.2026138
20231107_152644.jpg	28.5173288	81.1648385	**20231123_114949.jpg**	28.399216	81.2026138
20231107_152755.jpg	28.5173355	81.1650175	**20231123_114958.jpg**	28.399165	81.2024297
20231107_152841.jpg	28.5176537	81.1654118	**20231123_115006.jpg**	28.399245	81.2024622
20231107_152921.jpg	28.5179019	81.1654356	**20231123_115146.jpg**	28.398949	81.2024228
20231107_153007.jpg	28.5179019	81.1654356	**20231123_115201.jpg**	28.399323	81.2022863
20231107_153047.jpg	28.5181075	81.1657724	**20231123_115241.jpg**	28.399323	81.2022863
20231107_153112.jpg	28.5181075	81.1657724	**20231123_115258.jpg**	28.399162	81.2021136
20231107_153149.jpg	28.5178907	81.1659724	**20231123_121817.jpg**	28.389751	81.2140579
20231107_153939.jpg	28.5174284	81.1671225	**20231123_121826.jpg**	28.389751	81.2140579
20231107_154007.jpg	28.5174354	81.1670354	**20231123_121836.jpg**	28.389751	81.2140579

20231107_154011.jpg	28.5174354	81.1670354	**20231123_121848.jpg**	28.389751	81.2140579
20231107_154034.jpg	28.5174354	81.1670354	**20231123_121850.jpg**	28.389751	81.2140579
20231107_154046.jpg	28.5174897	81.1671664	**20231123_121900.jpg**	28.389751	81.2140579
20231107_154113.jpg	28.5174321	81.16718	**20231123_121909.jpg**	28.389751	81.2140579
20231107_154132.jpg	28.5174321	81.16718	**20231123_121919.jpg**	28.389758	81.2138964
20231107_154159.jpg	28.5173028	81.1674156	**20231125_134047.jpg**	28.630865	81.2743431
20231107_154223.jpg	28.517255	81.1675156	**20231125_134124.jpg**	28.630865	81.2743439
20231108_122735.jpg	28.4695475	81.1128981	**20231125_134147.jpg**	28.630887	81.274269
20231108_122836.jpg	28.4692702	81.1129135	**20231125_134150.jpg**	28.630887	81.2742692
20231108_122909.jpg	28.4694673	81.1126952	**20231125_134215.jpg**	28.630933	81.2741765
20231108_122936.jpg	28.469441	81.1125964	**20231125_134301.jpg**	28.630805	81.274018
20231108_123109.jpg	28.4692395	81.113091	**20231125_134319.jpg**	28.630768	81.2740167
20231109_130341.jpg	28.5776865	81.2002621	**20231125_134348.jpg**	28.630757	81.273916
20231109_130415.jpg	28.577994	81.2004182	**20231125_135826.jpg**	28.63355	81.2713069
20231109_130443.jpg	28.578102	81.2004084	**20231125_135857.jpg**	28.633526	81.2714612
20231109_130501.jpg	28.5781538	81.2004813	**20231125_135944.jpg**	28.633257	81.2717296
20231109_130633.jpg	28.5784578	81.200493	**20231125_140019.jpg**	28.633115	81.2718988
20231109_130655.jpg	28.5784578	81.200493	**20231125_140129.jpg**	28.632731	81.272349
20231109_130721.jpg	28.5785324	81.2006978	**20231125_140158.jpg**	28.632565	81.2725365
20231109_130739.jpg	28.5785324	81.2006978	**20231125_141548.jpg**	28.62765	81.2713361
20231109_130815.jpg	28.5787252	81.2007458	**20231125_141636.jpg**	28.627701	81.2713093
20231109_130909.jpg	28.5787252	81.2007458	**20231125_141700.jpg**	28.627775	81.2712523
20231109_153119.jpg	28.5791057	81.2006426	**20231125_141718.jpg**	28.627822	81.2711975
20231110_104410.jpg	28.5691415	81.2218294	**20231125_141741.jpg**	28.627934	81.2711414
20231110_104501.jpg	28.5691055	81.2215649	**20231125_141804.jpg**	28.628017	81.2710959
20231110_104530.jpg	28.5691055	81.2215649	**20231125_141900.jpg**	28.628316	81.2710396
20231110_104548.jpg	28.5691055	81.2215649	**20231125_141947.jpg**	28.62865	81.2709508
20231110_104609.jpg	28.5689233	81.2214827	**20231125_142013.jpg**	28.62881	81.2709317
20231110_104626.jpg	28.5688901	81.2215024	**20231125_142032.jpg**	28.628913	81.2709266
20231110_104646.jpg	28.5688099	81.2215753	**20231125_144113.jpg**	28.627835	81.2674674
20231110_104706.jpg	28.5687661	81.2216211	**20231125_144131.jpg**	28.627796	81.2675252
20231110_104722.jpg	28.5687099	81.2216732	**20231125_144155.jpg**	28.627716	81.2676307
20231110_131109.jpg	28.5387168	81.2362565	**20231125_144221.jpg**	28.627632	81.2677486
20231110_131119.jpg	28.5387168	81.2362565	**20231125_144246.jpg**	28.627558	81.2678731
20231110_131133.jpg	28.5387168	81.2362565	**20231125_144319.jpg**	28.627467	81.2680436
20231110_131152.jpg	28.5387888	81.2360725	**20231125_144352.jpg**	28.627395	81.268185
20231110_131641.jpg	28.5391072	81.2364143	**20231125_144425.jpg**	28.62733	81.2683405
20231110_131725.jpg	28.5391072	81.2364143	**20231125_144443.jpg**	28.62731	81.2684031
20231110_131749.jpg	28.5396746	81.2362467	**20231125_144510.jpg**	28.627281	81.2685285
20231110_131803.jpg	28.5396746	81.2362467	**20231126_154004.jpg**	28.605366	81.2696644
20231110_131816.jpg	28.5396746	81.2362467	**20231126_154038.jpg**	28.605165	81.2698134
20231110_131832.jpg	28.5399701	81.2359918	**20231126_154059.jpg**	28.605126	81.2699195
20231110_131901.jpg	28.5399308	81.2359769	**20231126_154128.jpg**	28.605085	81.2700654
20231110_131905.jpg	28.5399308	81.2359769	**20231126_154154.jpg**	28.605024	81.2702176
20231110_132117.jpg	28.5397285	81.2361833	**20231126_154219.jpg**	28.604973	81.2703355
20231110_132559.jpg	28.5395243	81.235934	**20231126_154246.jpg**	28.6049	81.270484

20231110_132621.jpg	28.5395243	81.235934	**20231126_154310.jpg**	28.604831	81.2706141
20231110_132637.jpg	28.5395243	81.235934	**20231126_154333.jpg**	28.604763	81.2707228
20231122_095057.jpg	28.5031576	81.2294084	**20231126_154402.jpg**	28.604681	81.270935
20231122_095133.jpg	28.5029803	81.2294501	**20231126_154420.jpg**	28.604655	81.2710444
20231122_095221.jpg	28.5030306	81.2295258	**20231126_160124.jpg**	28.603494	81.2649381
20231122_095255.jpg	28.5030306	81.2295258	**20231126_160141.jpg**	28.603494	81.2649381
20231122_095325.jpg	28.5029374	81.2297466	**20231126_160154.jpg**	28.603494	81.2649381
20231122_095420.jpg	28.5028848	81.229989	**20231126_160256.jpg**	28.603582	81.2646302
20231122_095532.jpg	28.502791	81.2302006	**20231126_160313.jpg**	28.603571	81.2644787
20231122_102021.jpg	28.5031346	81.2294121	**20231126_160342.jpg**	28.603462	81.2643442
20231122_102527.jpg	28.5033977	81.2286161	**20231126_162634.jpg**	28.600894	81.261752
20231122_102925.jpg	28.5038559	81.2275788	**20231126_162654.jpg**	28.600995	81.261921
20231122_121755.jpg	28.553517	81.2447047	**20231126_162711.jpg**	28.600967	81.2619906
20231122_121814.jpg	28.553517	81.2447047	**20231126_162727.jpg**	28.600949	81.262057
20231122_121845.jpg	28.5536012	81.2447683	**20231126_162747.jpg**	28.600907	81.2621141
20231122_121908.jpg	28.5535861	81.2447757	**20231126_162808.jpg**	28.600856	81.2623488
20231122_121910.jpg	28.5535861	81.2447757	**20231126_162822.jpg**	28.600856	81.2623488
20231122_121943.jpg	28.5534586	81.2446996	**20231126_162836.jpg**	28.60084	81.2624287
20231122_121945.jpg	28.5534603	81.2447005	**20231126_162853.jpg**	28.600796	81.262518
20231122_122015.jpg	28.5534179	81.2448063	**20231126_162910.jpg**	28.600747	81.2626154
20231122_125011.jpg	28.5686144	81.2490165	**20231126_162931.jpg**	28.600612	81.262707
20231122_125038.jpg	28.5686144	81.2490165	**20231126_162953.jpg**	28.600569	81.2628355
20231122_125053.jpg	28.5686144	81.2490165	**20231126_163009.jpg**	28.600556	81.2629271
20231122_125111.jpg	28.5686007	81.2487888	**20231126_163359.jpg**	28.601851	81.2647615
20231122_125128.jpg	28.5687552	81.2488721	**20231126_163558.jpg**	28.601904	81.2647768
20231122_125148.jpg	28.5687552	81.2488721	**20231126_163627.jpg**	28.601873	81.2649175
20231122_125200.jpg	28.5687552	81.2488721	**20231126_163703.jpg**	28.601958	81.2652756
20231122_125214.jpg	28.5687552	81.2488721	**20231126_163735.jpg**	28.601989	81.2654674
20231122_125229.jpg	28.5685397	81.2484028	**20231126_163821.jpg**	28.602067	81.2657022
20231122_125247.jpg	28.5685397	81.2484028	**20231126_163855.jpg**	28.601993	81.265966
20231122_125304.jpg	28.5685397	81.2484028	**20231126_163932.jpg**	28.602087	81.2661327
20231122_125331.jpg	28.5685544	81.2481071	**20231126_163948.jpg**	28.602082	81.2661724
20231122_130128.jpg	28.5685803	81.247978	**20231126_164010.jpg**	28.601989	81.2663263
20231122_130154.jpg	28.568654	81.247878	**20231126_164058.jpg**	28.602027	81.2667017
20231122_153402.jpg	28.4795	81.2149421	**20231126_164143.jpg**	28.602043	81.2667405
20231122_153419.jpg	28.4795	81.2149421	**20231126_164154.jpg**	28.602043	81.2667405
20231122_153433.jpg	28.4795	81.2149421	**20231126_164239.jpg**	28.602182	81.2671851
20231122_153443.jpg	28.4795	81.2149421	**20231126_164308.jpg**	28.60221	81.2675174
20231122_153458.jpg	28.4793861	81.2146489	**20231126_164754.jpg**	28.602221	81.2681256
20231122_153521.jpg	28.4793996	81.214555	**20231126_164825.jpg**	28.602327	81.2683659
20231122_153539.jpg	28.4793708	81.214523	**20231126_165107.jpg**	28.602679	81.2697915